CANCER-ASSOCIATED FIBROBLAST HETEROGENEITY AND IMMUNE CELL INTERACTION IN PANCREATIC DUCTAL ADENOCARCINOMA

by

FOUZIA ZAYOU



UNIVERSITY OF BIRMINGHAM

A Thesis submitted to
The University of Birmingham
For the degree of
DOCTOR OF PHILOSOPHY

School of Immunology and Immunotherapy
College of Medical and Dental Sciences
The University of Birmingham
August 2024

UNIVERSITY OF
BIRMINGHAM

University of Birmingham Research Archive

e-theses repository

This unpublished thesis/dissertation is copyright of the author and/or third parties. The intellectual property rights of the author or third parties in respect of this work are as defined by The Copyright Designs and Patents Act 1988 or as modified by any successor legislation.

Any use made of information contained in this thesis/dissertation must be in accordance with that legislation and must be properly acknowledged. Further distribution or reproduction in any format is prohibited without the permission of the copyright holder.

ABSTRACT

Pancreatic ductal adenocarcinoma (PDAC) represents one of the greatest unmet needs in oncology with suboptimal clinical outcome for most patients. An important factor is the complex tumour microenvironment (TME) in PDAC that serves to support tumour growth whilst suppressing potential immune control. Cancer-associated fibroblasts (CAFs) play a pivotal role within the TME and may represent an important target for future immune therapies.

This thesis investigates the diversity of fibroblast populations within PDAC tumours, comparing them to adjacent normal fibroblasts (ANFs), with a focus on the predominant subtypes: myofibroblasts (myCAFs) and inflammatory fibroblasts (iCAFs). Flow cytometry identified iCAFs as the dominant CAF subtype within the tumour stroma, in contrast to their lower prevalence in ANFs. Functional assays demonstrated that co-culturing patient-derived fibroblasts with healthy donor NK and T cells led to distinct effects on T cell phenotype. Specifically, CAF co-culture selectively induced proliferation in unstimulated NK and T cells, along with increased expression of activation markers CD69 and NKG2D, and the checkpoint inhibitor PD-1 on T cells, suggesting a role in either T cell activation or exhaustion and immune evasion within the tumour microenvironment.

Furthermore, unstimulated CAFs enhanced lymphocyte adhesion and migration, while an inhibitory effect was observed on activated cells. Stimulation of CAFs with the inflammatory cytokines TNF-α/IFN-γ, which elicits an iCAF phenotype, further promoted lymphocyte migration. In contrast, incubation with TGF-β, which develops a myCAF profile, suppressed migration, indicating opposing effects of cytokine polarization on lymphocyte dynamics. Co-culture of cytokine-polarised CAF populations revealed that TGF-β incubation led to decrease in $CD56^{bright}$ NK cell adhesion and an increase in $CD56^{dim}$ stimulated NK cell migration. CAFs also upregulated KIRs and NKp46 on NK cells, indicating potential alterations in NK cell activation and recognition capabilities.

Spatial analysis revealed that tumour-proximal fibroblasts have a myCAF phenotype and express markers that form barriers to lymphocyte migration, while distal fibroblasts display characteristics of iCAF and likely contribute to an inflammatory environment through cytokine secretion.

My findings contribute to studies showing the profound diversity of the CAF population in PDAC. Together, the findings indicate that the PDAC environment is enriched with the presence of inflammatory CAF that are located relatively distant from the tumour, most likely in the lymphoid follicles and tertiary lymphoid structures that develop during PDAC development. These populations appear to support the transmigration of lymphoid cells and may help to support the recruitment of populations that initiate a tumour-specific immune response. In contrast, the myofibroblast populations encase the tumour, and my work indicates that these are also likely to suppress the migration of lymphoid cells into the tumour bed.

These findings highlight the significant heterogeneity and functional diversity of CAFs in PDAC, underscoring their critical roles in modulating immune cell behaviour and suggesting potential targets for enhancing immune surveillance and improving therapeutic outcomes in pancreatic cancer.

ACKNOWLEDGMENTS

Firstly, I would like to express my deepest gratitude to my supervisor, Professor Paul Moss, for giving me the opportunity to work on this project. I am immensely thankful to my co-supervisors, Dr Hayden Pearce, Dr Helen McGettrick, and Dr Jianmin Zuo, whose combined effort, dedication, and support were crucial to the completion of this work. I extend my heartfelt thanks to all the colleagues and friends in Professor Moss's Laboratory at the School of Immunology and Immunotherapy for their invaluable help and advice.

Special thanks to Dr Rachel Bruton for her tireless efforts, including dedicating her weekends and after-hours time to help me navigate the complexities of my thesis. I am also deeply grateful to my friend Samantha Nicol for the fantastic scientific discussions, advice, and support, and for always bringing chocolate and shortbread biscuits to fuel my brain during late nights in the lab. Thanks to Dr Sandra Margielewska-Davies for her scientific advice, support and for being such a great friend. My appreciation also extends to Dr Wayne Croft for his assistance with NanoString and sequencing experiment with analysis, and to Natalie, Megan, Nahla and Maggie for being such wonderful friends. I extend heartfelt thanks to my dear colleague Juliet, who was a cherished friend. Her spirit and support are deeply missed. May her soul rest in peace.

I would like to acknowledge the members of the Pancreas Unit at Queen Elizabeth Hospital, UHB NHS Foundation Trust, including the theatre staff, for their essential role in collecting the samples for this project. My heartfelt thanks go to the patients who donated samples, without whom this research would not have been possible.

I am deeply appreciative of the continuous support and prayers from my parents and little sister. This accomplishment is dedicated to them and to PDAC patients.

Lastly, I am grateful to the Marie Curie Fellowship for funding this research.

TABLE OF CONTENTS

ABSTRACT *1*

ACKNOWLEDGMENTS *3*

Chapter 1: Introduction *24*

1.1 Pancreatic ductal adenocarcinoma (PDAC) **25**

1.1.1 Epidemiology and risk factors 29

1.1.2 Clinical aspects 30

1.2 Cancer Associated Fibroblasts **31**

1.2.1 What are fibroblasts? 31

1.2.2 What is the origin of fibroblast? 32

1.2.3 What is the origin of CAF? 35

1.2.4 CAF function 36

1.2.5 CAF markers 41

1.3 CAF and T cells **52**

1.4 CAF and NK cells **58**

1.5 Effect of CAF on lymphocyte migration **63**

1.6 Targeting CAFs for clinical benefit and future perspectives **67**

1.7 Hypothesis **68**

Chapter 2: Material & Methods *69*

2.1 Ethics and recruitment **70**

2.2 Isolation of Adjacent Normal Fibroblasts (ANFs) and Cancer associated fibroblasts (CAFs) from PDAC patients. **72**

2.3 Culture of primary ANFs and CAFs **74**

2.4 Primary ANFs and CAFs immortalisation using SV40 and hTERT vectors. 76

2.4.1 Plasmid extraction 77

2.4.2 Virus culture 83

2.4.3 Viral transfection 84

2.4.4 Antibiotic killing Curve 85

2.4.5 Transduction 87

2.5 FACS analysis of freshly digested ANFs and CAFs 88

2.5.1 Surface staining 89

2.5.2 Nuclear staining 91

2.5.3 Live and dead gating strategy 91

2.5.4 Statistical analysis 92

2.6 Conditioned-Media (CM) collection from ANFs and CAFs 94

2.7 PBMCs isolation 96

2.7.1 T cells isolation 98

2.7.2 NK cells isolation 98

2.7.3 Co-culture of fibroblasts with T cells and NK cells 98

2.7.4 ANF / CAF Conditioned media (ANF-CM & CAF-CM) 103

2.7.5 T and NK cells gating strategy 104

2.7.6 Statistical analysis 105

2.8 Pseudo-Emperipolesis assay 107

2.8.1 Fibroblast seeding 107

2.8.2 PBL isolation 108

2.8.3 ANF/CAF monolayer co-culture 108

2.8.4 How to use the Phase contrast microscopy 109

2.8.5 Analysis of cell behaviour from video recordings 109

2.9 Trans-well assay 111

2.10 Sandwich ELISA 114

2.10.1 ELISA 114

2.10.2 Statistical analysis 116

2.11 NanoString Spatial RNA Profiling (DSP) 118

2.11.1 Sample Processing 118

2.11.2 NanoString nCounter Data Analysis 118

2.12 scRNA-Seq data analysis 120

Chapter 3: Fibroblast Heterogeneity in PDAC *122*

3.1 Introduction 123

3.2 Results 125

3.2.1 Characterising Cellular Composition in Pancreatic Ductal Adenocarcinoma: Insights from Treatment-Naive and Neo-Adjuvant Chemotherapy Patients 125

3.2.2 Exploring iCAF and myCAF Fibroblast Subtypes in Adjacent Normal and Tumour Tissues: Impact of Neo-Adjuvant Chemotherapy on Fibroblast Phenotype. 131

3.2.3 Assessment of individual protein expression in total Fibroblasts, and iCAF, and myCAF subtypes, within Adjacent Normal and Tumour Tissues: Impact of Neo-Adjuvant Chemotherapy on Fibroblast Phenotype. 135

3.3 Discussion 163

3.4 Conclusion 168

Chapter 4: Interaction of Fibroblasts with immune cells *169*

4.1 Introduction 170

4.2 Results 171

4.2.1 Effect of fibroblasts on T and NK cells proliferation and IFN-□ production 171

4.2.2 Effect of fibroblasts on T cells phenotyping 184

4.2.3 Effect of fibroblasts on NK cells phenotyping 202

4.3 Discussion 216

4.4 Conclusion 224

Chapter 5: Adhesion and migration of lymphocytes to Cancer Associated Fibroblasts ***225***

5.1 Introduction **226**

5.2 Results **233**

5.2.1 The impact of incubation period on functional behaviour of lymphocytes in co-culture with fibroblasts 233

5.2.2 The impact of stimulated fibroblasts on functional behaviour of lymphocytes in co-cultures. 237

5.2.3 How do ANF and CAF influence the phenotype of adhered and migrated T cell lymphocytes in the absence of close contact? 247

5.2.4 Impact of ANF and CAF on adherence and migration of NK cell subsets 264

5.2.5 Spatial determination and impact of fibroblast transcriptome in PDAC 270

5.3 Discussion **276**

5.4 Conclusion **283**

5.5 Limitations **284**

Summative discussion ***285***

References ***292***

LISTS OF FIGURES

Figure 1.1. The endocrine and exocrine pancreas (Pandol., 2010). 26

Figure 1.2. Genetic progression model of pancreatic carcinogenesis development (Guo et al., 2016). 27

Figure 1.3. Molecular classifications of PDAC (Orth et al., 2019). 29

Figure 1.4. Developmental origin of fibroblasts (LeBleu & Neilson, 2020). 34

Figure 1.5. The origin of CAF (Ping et al., 2021). 35

Figure 1.6. Mechanisms of CAF mediated T cell inhibition (Koppensteiner et al., 2022) 57

Figure 1.7. Illustration of the known effects of fibroblast subpopulations on NK cell activity (Malchiodi & Weiner, 2021). 62

Figure 2.2. Developed Colonies on a Petri Dish. 79

Figure 2.3. Experimental design for virus transduction. 87

Figure 2.4. Gating strategy for fibroblasts flow cytometry analysis. 92

Figure 2.5. Protocol Design for fibroblasts isolation and phenotyping using BioRender program. 93

Figure 2.6. Protocol Design fibroblasts Conditioned Media (CM) collection using BioRender program. 95

Figure 2.7. Protocol Design for Co-Culture of T/NK cells with fibroblasts (direct contact) using BioRender program. 102

Figure 2.8. Gating strategy for T cell flow cytometry analysis. 104

Figure 2.9. Gating strategy for NK cell flow cytometry analysis. 104

Figure 2.10. Protocol Design for Co-Culture of T cells with fibroblasts Conditioned Media (CM) using BioRender program. 106

Figure 2.11. Protocol Design for Pseudo- Emperipolesis Assay using BioRender program. 110

Figure 2.12. Protocol Design for Trans-well Assay using BioRender program. 113

Figure 3.1. Gating strategy to identify fibroblasts by flow cytometry 128

Figure 3.2. Comparison of the cellular composition within PDAC tumour tissue and adjacent normal pancreatic tissue from individual patients using flow cytometry. 129

Figure 3.3. Comparison of cell type percentage and ratio in Naïve PDAC and Neo-adjuvant chemotherapy patients using flow cytometry. 130

Figure 3.4. Comparison of the percentages of the two fibroblast subtypes, iCAF and myCAF, within adjacent normal and tumour tissues in Naïve PDAC and Neo-adjuvant chemotherapy patients using flow cytometry. 133

Figure 3.5. Comparison of the percentages of the iCAF and myCAF fibroblast subtypes in treatment-naïve PDAC and Neo-adjuvant chemotherapy patients within adjacent normal and tumour tissues using flow cytometry. 134

Figure 3.6. Comparison of C3 Expression in Fibroblast Subtypes in Pancreatic Cancer Patients with and without Neo-adj3uvant Chemotherapy. 137

Figure 3.7. Comparison of Cadherin-11 Expression in Fibroblast Subtypes in Pancreatic Cancer Patients with and without Neo-adjuvant Chemotherapy... 139

Figure 3.8. Comparison of CD26 Expression in Fibroblast Subtypes in Pancreatic Cancer Patients with and without Neo-adjuvant Chemotherapy... 141

Figure 3.9. Comparison of CD29 Expression in Fibroblast Subtypes in Pancreatic Cancer Patients with and without Neo-adjuvant Chemotherapy... 143

Figure 3.10. Comparison of C34 Expression in Fibroblast Subtypes in Pancreatic Cancer Patients with and without Neo-adjuvant Chemotherapy. 145

Figure 3.11. Comparison of CD90 Expression in Fibroblast Subtypes in Pancreatic Cancer Patients with and without Neo-adjuvant Chemotherapy... 147

Figure 3.12. Comparison of CD74 Expression in Fibroblast Subtypes in Pancreatic Cancer Patients with and without Neo-adjuvant Chemotherapy... 149

Figure 3.13. Comparison of MHC-II Expression in Fibroblast Subtypes in Pancreatic Cancer Patients with and without Neo-adjuvant Chemotherapy... 151

Figure 3.14. Comparison of CD105 Expression in Fibroblast Subtypes in Pancreatic Cancer Patients with and without Neo-adjuvant Chemotherapy... 153

Figure 3.15. Comparison of Ki-67 Expression in Fibroblast Subtypes in Pancreatic Cancer Patients with and without Neo-adjuvant Chemotherapy... 156

Figure 3.16. Comparison of PDGFR-α Expression in Fibroblast Subtypes in Pancreatic Cancer Patients with and without Neo-adjuvant Chemotherapy... 158

Figure 3.17. Comparison of PDGFR- Expression in Fibroblast Subtypes in Pancreatic Cancer Patients with and without Neo-adjuvant Chemotherapy... 160

Figure 3.18. Comparison of PDPN Expression in Fibroblast Subtypes in Pancreatic Cancer Patients with and without Neo-adjuvant Chemotherapy... 162

Figure 4.1. Comparison in T cells proliferation ability between T cells co-cultured with primary ANFs and CAFs using CFSE assay (direct contact). 172

Figure 4.2. Comparison of T cell proliferation ability between T cell co-cultured with primary ANFs and CAFs using CFSE assay (direct contact). 173

Figure 4.3. Comparison in NK cells proliferation ability between NK cells co-cultured with primary ANFs and CAFs using CFSE assay (direct contact). **174**

Figure 4.4. Comparison in NK cell proliferation ability between NK cell co-cultured with primary ANFs and CAFs using CFSE assay (direct contact). **175**

Figure 4.5. Comparison of T cells proliferation ability between T cells co-cultured with immortalised ANF (ImANF) and CAF (ImCAF) cells using CFSE assay (direct contact). **177**

Figure 4.6. Comparison in NK cell proliferation activity between NK cell co-cultured with immortalised ANF (ImANF) and CAF (ImCAF) cells from 4 different PDAC donors was made by CFSE assay (direct contact). **178**

Figure 4.7. T cell proliferation can be enhanced by primary (ANF & CAF) and Immortalised (ImANF & ImCAF) Conditioned media (CM). **180**

Figure 4.8. Increased NK cell proliferation by primary (ANF & CAF) and Immortalised (ImANF & ImCAF) Conditioned media (CM). **181**

Figure 4.9. IFN-γ production from unstimulated and stimulated T cells culture with conditioned media (CM) from primary and immortalised fibroblasts. **183**

Figure 4.10. Flow cytometry gating strategy of unstimulated versus stimulated T cells. **185**

Figure 4.11. The effect of co-culture with primary ANF and CAF on the percentage of stimulated CD4+ and CD8+ T cells and mean fluorescence intensity (MFI) of CD4 and CD8. **186**

Figure 4.12. Flow cytometry histograms comparing the percentage of co-stimulatory (CD69, NKG2D and DNAM1) and inhibitory (PD-1) molecules expression in CD4+ T cells between those co-cultured with ANF and CAF. 189

Figure 4.13. The effect of co-culture with primary ANF and CAF on the percentage and mean fluorescence intensity (MFI) of stimulated CD4+ T cells marked by activating and inhibitory molecules. 190

Figure 4.14. Flow cytometry histograms comparing the percentage of co-stimulatory (CD69, NKG2D and DNAM1) and inhibitory (PD-1) molecules expression in CD8+ T cells between those co-cultured with ANF and CAF. 191

Figure 4.15. The effect of co-culture with primary ANF and CAF on the percentage and mean fluorescence intensity (MFI) of stimulated CD8+ T cells marked by activating and inhibitory molecules. 192

Figure 4.16. The effect of co-culture with primary ANF and CAF on the percentage of unstimulated CD4+ and CD8+ T cells and mean fluorescence intensity (MFI) of CD4 and CD8. 195

Figure 4.17. The effect of co-culture with primary ANF and CAF on the percentage and mean fluorescence intensity (MFI) of unstimulated CD4+ T cells marked by activating and inhibitory molecules. 196

Figure 4.18. The effect of co-culture with primary ANF and CAF on the percentage and mean fluorescence intensity (MFI) of unstimulated CD8+ T cells marked by activating and inhibitory molecules. 197

Figure 4.19. The effect of co-culture with primary ANF and CAF on the percentage of stimulated CD4+ T cells subtypes, central memory (CM), effector memory (EM), Naïve and Temra. 199

Figure 4.20. The effect of co-culture with primary ANF and CAF on the percentage of stimulated CD8+ T cells subtypes, central memory (CM), effector memory (EM), Naïve and Temra. 200

Figure 4.21. Graphical Abstract- Role of CAFs in modulating T cell responses within the PDAC-TME. 201

Figure 4.22. Flow cytometry gating strategy of unstimulated versus stimulated NK cells. 204

Figure 4.23. The effect of co-culture with primary ANF and CAF on the percentage of $CD56^{bright}$ and $CD56^{dim}$ unstimulated and stimulated NK cells. 205

Figure 4.24. Flow cytometry gating strategy of unstimulated versus stimulated NK cells to identify. 208

Figure 4.25. The effect of co-culture with primary ANF and CAF on the percentage of stimulated total NK cell subpopulations. 209

Figure 4.26. The effect of co-culture with primary ANF and CAF on the percentage of unstimulated NK cells subtypes. 210

Figure 4.27. The effect of co-culture with primary ANF and CAF on the percentage of stimulated total NK cell markers. 213

Figure 4.28. The effect of co-culture with primary ANF and CAF on the percentage of unstimulated total NK cell markers. 214

Figure 4.29. Graphical Abstract- Role of CAFs in modulating NK cell responses within the PDAC-TME. 215

Figure 5.1. Sequential Events in Leukocyte Extravasation. 228

Figure 5.2. Illustration of the principles of the Pseudo-emperipolesis and Transwell Assays. 231

Figure 5.3. illustration of Pseudo-emperipolesis counting strategy. 232

Figure 5.4. Kinetics of adhesion of lymphocytes to fibroblast subsets during co-culture using Pseudo-emperipolesis assay. 235

Figure 5.5. Kinetics of adhesion of lymphocytes to fibroblast subsets during co-culture using Pseudo-emperipolesis assay. 236

Figure 5.6. Effect of cytokine-stimulated CAF and ANF on lymphocyte total adhesion in co-culture at two-point times using Pseudo-emperipolesis assay. 239

Figure 5.7. Effect of stimulated CAFs and ANFs on lymphocyte firm adhesion and transmigration in co-culture at two-point times using Pseudo-emperipolesis assay. 242

Figure 5.8. Representative gating strategy of lymphocyte number using CountBright™ Absolute counting beads. 245

Figure 5.9. Effect of stimulated CAFs and ANFs on lymphocyte adhesion and migration in co-culture at two-point times using Transwell assay. 246

Figure 5.10. Flow cytometry gating strategy of T cell subsets. 248

Figure 5.11. Effect of stimulated CAFs and ANFs on CD4+ T cell migration in co-culture at two-point times using Transwell assay. 251

Figure 5.12. Effect of stimulated CAFs and ANFs on CD8+ T cell migration in co-culture at two-point times using Transwell assay. 252

Figure 5.13. Effect of stimulated CAFs and ANFs on the migration of naïve CD4+ and CD8+ T cell subset (CD45RA+CCR7+) in co-culture at two-point times using Transwell assay. 253

Figure 5.14. Effect of stimulated CAFs and ANFs on the migration of central memory (CM) CD4+ and CD8+ T cell subset (CD45RA−CCR7+) in co-culture at two-point times using Transwell assay. 255

Figure 5.15. Effect of stimulated CAFs and ANFs on the migration of effector memory (EM) CD4+ and CD8+ T cell subset ($CD45RA^{-}CCR7^{-}$) in co-culture at two-point times using Transwell assay. 257

Figure 5.16. Effect of stimulated CAFs and ANFs on the migration of TEMRA CD4+ and CD8+ T cell subset ($CD45RA^{+}CDR7^{-}$) in co-culture at two-point times using Transwell assay. 259

Figure 5.17. Effect of stimulated CAFs and ANFs on the expression of PD-1 on CD4+ and CD8+ T cell in co-culture at two-point times using Transwell assay. 262

Figure 5.18. Effect of stimulated CAFs and ANFs on the expression of CD69 on CD4+ and CD8+ T cell in co-culture at two-point times using Transwell assay. 263

Figure 5.19. Flow cytometry gating strategy of total NK cell and its subsets: $CD56^{Bright}$ and $CD56^{dim}$ from CD3- lymphocytes population. 265

Figure 5.20. Effect of stimulated CAFs and ANFs on migrated $CD56^{Bright}$ and $CD56^{dim}$ NK cell at two-point times using Transwell assay. 267

Figure 5.21. Effect of stimulated CAFs and ANFs on migrated Total NK cell examining the expression of inhibitory molecule PD-1 and co-stimulatory molecule CD69 at two-point times using Transwell assay. 269

Figure 5.22. Identification of gene expression data from spatially defined stromal two regions within the PDAC tumour microenvironment using NanoString GeoMx DSP. 272

Figure 5.23. Proximal, Distal, and unknown Fibroblast populations identified in PDAC single cell transcriptome data. 274

Figure 5.24. Graphical Abstract-Dynamic interplay of iCAF and myCAF within the PDAC-TME. 275

LISTS OF TABLES

Table 1.1. The heterogeneity of CAF subtypes in cancers. 40

Table 2.1. Clinical data of samples used in phenotyping. 71

Table 2.2. Used Reagents with Catalogue Numbers and Companies 73

Table 2.3. Used Reagents with Catalogue Numbers and Companies 75

Table 2.4. Used Reagents with Catalogue Numbers and Companies. 77

Table 2.5. Used Reagents with Catalogue Numbers and Companies. 78

Table 2.6. Used Reagents with Catalogue Numbers and Companies. 80

Table 2.7. Used Reagents with Catalogue Numbers and Companies. 82

Table 2.8. Used Reagents with Catalogue Numbers and Companies. 83

Table 2.9. Used Reagents with Catalogue Numbers and Companies. 84

Table 2.10. Antibiotic Killing curve for 3 antibiotics, Puromycin, G418 and Hygromycin. 85

Table 2.11. Used Reagents with Catalogue Numbers and Companies. 86

Table 2.12. Used Reagents with Catalogue Numbers and Companies. 88

Table 2.13. Fibroblasts flow cytometry panel. 90

Table 2.14. Used Reagents with Catalogue Numbers and Companies. 94

Table 2.15. Used Reagents with Catalogue Numbers and Companies. 97

Table 2.16. T-cell flow cytometry panel. 101

Table 2.17. NK-cell flow cytometry panel. 101

Table 2.18. Used Reagents with Catalogue Numbers and Companies. 102

Table 2.19. Experimental conditions. 103

Table 2.20. Used Reagents with Catalogue Numbers and Companies. 107

Table 2.21. T and NK-cell flow cytometry panel. 112

Table 2.22. Used Reagents with Catalogue Numbers and Companies. 112

Table 2.23. Used Reagents with Catalogue Numbers and Companies. 116

LIST OF ABREVIATIONS

aPSCs: Activated pancreatic stellate cells

AN: Adjacent Normal

ANF: Adjacent Normal Fibroblast

apCAF: Antigen presenting CAFs

BCP: Breast cancer patients

BRCA2: Breast Cancer gene 2

BSA: Bovine Serum Albumin

CAF: Cancer associated fibroblast

CAF: Cancer-Associated-Fibroblast

C1R/S: Complement 1R/S

C3: Complement 3

C7: Complement 7

CCL3/6/8: Chemokine (C-C motif) ligand 3/6/8

CCR1: Chemokine receptor type 1

CD69: Cluster of Differentiation 69

CD74: Cluster of Differentiation 74

CDKN2A: Cyclin-dependent kinase inhibitor 2A

CFD : Complement factor D

CFSE : Carboxyfluorescein diacetate succinimidyl ester

CM: Central memory

CTL: Cytotoxic T lymphocytes

CTLA4: Cytotoxic T-lymphocyte–associated antigen 4

CXCL-12: C-X-C motif chemokine ligand 12

CXCL1/3: C-X-C motif chemokine ligand 1/3

CXCL13: C-X-C motif chemokine ligand 13

CXCL14: C-X-C motif chemokine ligand 14

CXCR4: C-X-C motif chemokine receptor 4

DPP4: Dipeptidyl peptidase 4

DNAM-1: DNAX Accessory Molecule-1

EGF: Epidermal growth factor

ECM: Extracellular matrix

EM: Effector memory

EMT: Epithelial mesenchymal transition

EnC: Endothelial cells

EpC: Epithelial cells

FAP: Fibroblast activation protein

FBLN2: Fibulin-2a

FcR: Fc receptor

FLS: Fibroblast-like synoviocytes

FSP: Fibroblast-specific proteins

GM-CSF: Granulocyte-macrophage colony-stimulating factor

HER2: Human epidermal growth factor receptor 2

HGSOC: High-grade serous ovarian cancer

IC: Immune cells

ICAM-1: Intercellular adhesion molecule-1

IDO: Indoleamine 2,3-dioxygenase

IFN-γ: Interferon gamma

IL-1: Interleukin-1

IL-6: Interleukin-6

IL-21: Interleukin-21

ImANFs: Immortalized Adjacent Normal Fibroblasts

ImCAFs: Immortalized Cancer-Associated Fibroblasts

KIRs: Killer Ig-Like Receptors

Kras: Kirsten rat sarcoma viral oncogene

LAG-3: Lymphocyte activation gene 3

LIF: Leukemia inhibitory factor

MDSCs: Myeloid-derived suppressor cells

meCAFs: Metabolic cancer-associated fibroblasts

MFI: Mean fluorescence intensity

MHC-I: Major histocompatibility complex class I molecule

MHC-II: Major histocompatibility complex class II molecule

MIF: Microphage migration inhibitory factor

Mins: Minutes

MMPs: Matrix metalloproteinases

myCAF: Myo-fibroblastic cancer-associated fibroblasts

Naive PDAC: Naïve pancreatic adenocarcinoma

Neo-Adj-Chemo: Neo-adjuvant-chemotherapy

NK: Natural Killer

NKp30: Natural killer protein 30

NKp44: Natural killer protein 44

NKG2D: Natural killer group 2 member D

NKG2D: Natural killer group 2 member D

OC: Other cancer

OSCC: Oral squamous cell carcinoma

PBL: Peripheral blood lymphocyte

PBMC: Peripheral blood mononuclear cell

PD-1: Programmed Cell Death Protein 1

PD-L1: Programmed Cell Death Protein-Ligand 1

PDAC: Pancreatic Cancer Adenocarcinoma

PDGF: Platelet-derived growth factor

PDGF-α: Platelet derived growth factor receptor alpha

PDGFR-β: Platelet derived growth factor receptor beta

PDPN: Podoplanin

PGE2: Prostaglandin E2

PI3K/AKT: Phosphatidylinositol 3-kinase/protein kinase B

PKN2: Rho effector protein kinase N2

PSC: Pancreatic Stellate cells

PTEN: Phosphatase and TENsin homolog

QM: Quasi-mesenchymal

RA: Rheumatoid arthritis

RQF: Resident quiescent fibroblasts

SMAD4: Mothers against decapentaplegic homolog 4

T : Tumour

T-D : Tumour Distal

T-P: Tumour proximal fibroblast

TCR: T-cell receptor

TEMRA: Terminally differentiated

TF: Total Fibroblast

TGF-α: Transforming growth factor-alpha

TGF-β: Transforming growth factor-beta

Thy-1: Thymus cell antigen 1

TIGIT: T cell immunoreceptor with Ig and ITIM domains

TIL: Tumour-infiltrating lymphocytes

TIM-3: T cell Ig- and mucin-domain-containing molecule-3

TNF: Tumour necrosis factor

TNF-α: Tumour necrosis factor alpha

TP53: Tumour protein p53

VCAM-1: Vascular cell adhesion molecule-1

Wnt: Wingless-related integration site

α-SMA: Alpha-Smooth Muscle Actin

Chapter 1: Introduction

1.1 Pancreatic ductal adenocarcinoma (PDAC)

Pancreatic ductal adenocarcinoma (PDAC) is a highly aggressive disease with poor prognosis and rising incidence (Rawla et al., 2019). To date, PDAC is the fourth most frequent cause of cancer-related deaths worldwide with a 5-year following diagnosis with overall survival fewer than 6% (Y. Noda et al., 2022). By 2030, PDAC is predicted to become the second leading cause of cancer-related death (Hur et al., 2016). Late detection and a particularly rapid metastasis are the major challenges which determine therapeutic failure. PDAC is a highly chemo-resistant disease and has one of the worst prognoses of all tumour subtypes (Eibl, 2014). The most effective treatment is early resection of the pancreas, but this is not always possible because of late presentation and aggressive metastasis with chemo-resistance (Sarantis et al., 2020).

The pancreas is composed of exocrine and endocrine cells, the latter of which contribute <2% of mass but play an important role in blood sugar regulation by secreting hormones into blood stream (Wang et al., 2016). Exocrine cells comprise >95% of cells, and predominantly comprise acinar cells that play an essential role in the digestive process by producing digestive enzymes such as trypsin and chymotrypsin into the duodenum **(Figure 1)** (Pandol., 2010). Pancreas cells are known for their plasticity which is considered to support pancreas homeostasis and regeneration (Backx et al., 2022).

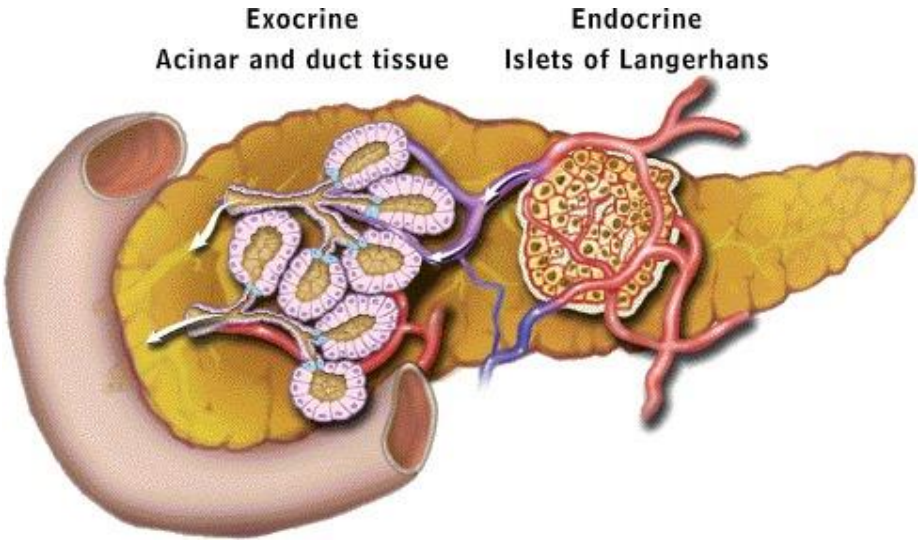


Figure 1.1. The endocrine and exocrine pancreas (Pandol., 2010).

PDAC originates within the exocrine pancreas and is believed to arise from ductal cells (Backx et al., 2022) (Eibl, 2014). A distinctive feature of PDAC is its marked desmoplasia that is composed of extracellular matrix ECM proteins such as type I and V collagen and fibronectin, myo-fibroblastic pancreatic stellate cells, and immune cells associated with a multitude of cytokines and growth factors. Desmoplasia is believed to play a key role in promoting the resistance of this cancer to treatment and progression of disease (Thomas Kolodecik, 2014).

The progression of pancreatic lesions, starting with precursor lesions such as pancreatic intra-epithelial neoplasia (PanINs), leads to adenocarcinoma with invasion beyond the basement membrane. Early genetic events such as telomere shortening, Kras mutation (present in over 90% of human pancreatic cancers), and the inactivation of the tumour-suppressor genes such as *CDKN2A, TP53, SMAD4* (in approximately

50% of pancreatic cancers) and *BRCA2* contribute to this progression (Guo et al., 2016).

Oncogenic *Kras* mutations activate important signalling proteins such as PI3K/AKT, PTEN and Wnt that drive PDAC development. The complex anatomical relationship that pancreas displays with other organs and major vessels may contribute to early dissemination of tumour cells in distant organs (**Figure 2**) (Eibl, 2014; Guo et al., 2016).

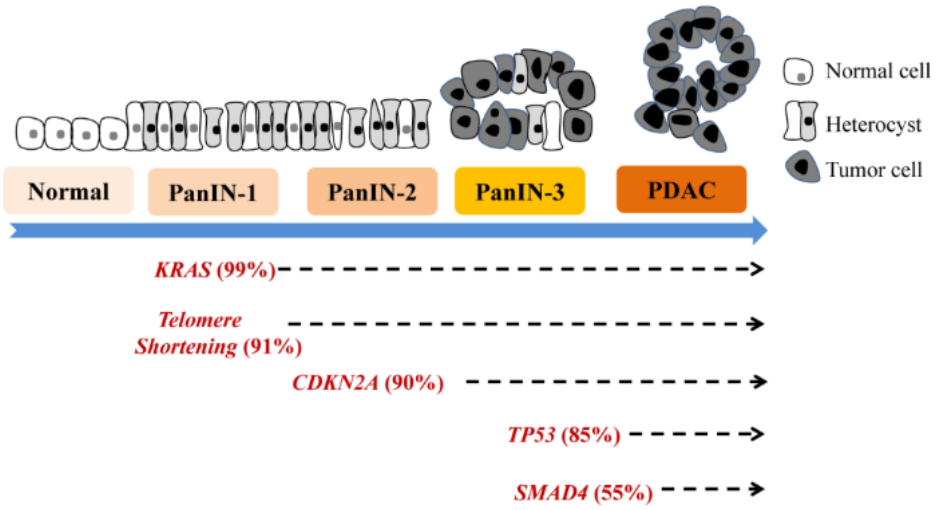


Figure 1.2. Genetic progression model of pancreatic carcinogenesis development (Guo et al., 2016).

The emergence of PDAC subtypes is attributed to both inter-tumoral heterogeneity and tumour cell plasticity, influencing PDAC classification (Orth et al., 2019). Baley et al. identified four PDAC subgroups using RNA-seq: pancreatic progenitor, squamous, aberrantly differentiated endocrine exocrine (ADEX), and immunogenic. ADEX was defined by gene expression pathways associated with exocrine and β cell development. The squamous subtype exhibited activation of inflammatory and hypoxic genes expression, along with upregulation of ECM, TGF-β and WNT signalling proteins. Additionally, the immunogenic subtype was distinguished by substantial immune infiltrate, which correlated with better overall survival compared to other groups (Orth et al., 2019).

Conversely, Moffitt and colleagues identified two PDAC subtypes, classical subtype, and basal subtype. In addition, Collison at al. classified PDAC into three subtypes, classical, quasi-mesenchymal (QM) and exocrine-like. The classical subtype exhibited upregulation of the adhesion and epithelial genes, whilst the QM subtype is defined by a high expression of mesenchymal genes and was associated with poor prognosis. Finally, the exocrine subtype was characterized by the expression of digestive enzymes genes **(Figure 3)** (Veenstra et al., 2018).

Basal-like tumours are often associated with a greater prevalence of TP53 mutations, contributing to their aggressive nature and diminished genomic stability. In contrast, the classical subtype is defined by elevated expression of GATA6, a transcription factor integral to maintaining epithelial identity, and a pronounced reliance on KRAS signalling pathways for tumour progression. Clinically, basal-like tumours exhibit higher pathological grades and are linked to significantly poorer overall survival outcomes compared to their classical counterparts (Collisson et al., 2011; S. Wang et al., 2021).

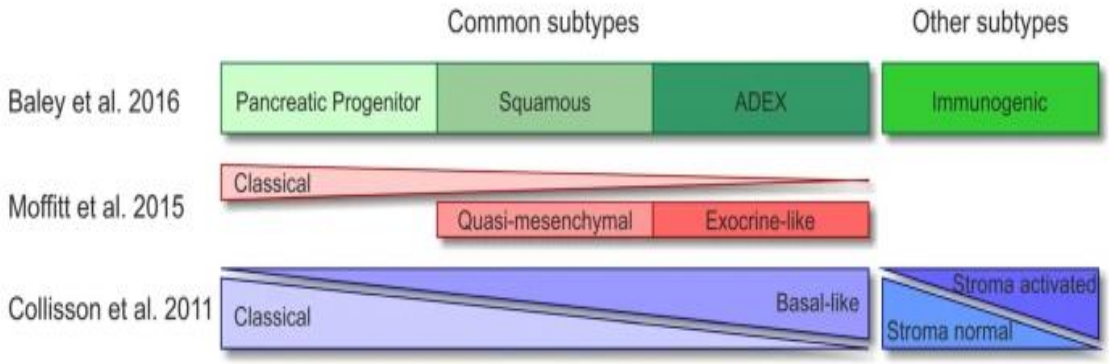


Figure 1.3. Molecular classifications of PDAC (Orth et al., 2019).

1.1.1 Epidemiology and risk factors

By 2030 it is estimated that PDAC will become the second leading cause of death with a median age of onset 70 years (Noor L. et al, 2017). A GLOBOCAN survey in 2020 revealed a continuing increase in the incidence of new PDAC cases, reaching a cumulative global total of 495,773 cases, ranking it as the fourteenth most prevalent malignancy among other cancers. Despite this, PDAC stands out for its considerable impact on mortality, contributing to 466,003 deaths annually and securing its place as the seventh leading cause of cancer deaths (Ushio et al., 2021).

The mortality caused by PDAC exhibits geographical disparities, with Europe and North America exhibiting the highest age-standardised incidence rates, whilst in Africa and central Asia the rates are comparatively low. In addition, PDAC displays a slight predilection for males over females, with incidence rates of 5.7 per 100,000 for males (262,865 cases) and 4.1 per 100,000 for females (232,908 cases) (Ushio et al., 2021).

1.1.2 Clinical aspects

The need of early diagnosis remains crucial for enhancing patient survival in PDAC, although this ambition remains challenging. Complications include low incidence and the absence of safe and cost-effective tests (Noor L. et al, 2017). Adopting healthy lifestyle habits is pivotal in reducing the risk of PDAC, give the well-established association between alcohol and tobacco abuse and PDAC susceptibility. Additionally, conditions such as diabetes, chronic pancreatitis, and obesity are known as contributors to the heightened incidence of PDAC (Ushio et al., 2021).

While early pancreatic resection is identified as the most effective treatment, its feasibility is often hindered by late presentations and aggressive metastasis associated with chemo-resistance. The major challenge in treating pancreatic cancer is the occurrence of new mutational changes in pancreatic tumours that generate genome instability (Sarantis et al., 2020).

The selection of treatment approach for pancreatic cancer depends on disease stage, location, and underlying patient health status. Treatment modalities may include surgery, radiation, chemotherapy, immunotherapy, or a combination of these treatments. Notably, the tumour microenvironment stands out as a primary factor contributing to cancer resistance, impacting the effectiveness of cancer treatment (Lambin et al., 2022). This is notable as the objective of my doctoral research was to investigate the phenotype and function of fibroblasts, the most prevalent stromal cells, and their potential contribution to pancreatic cancer progression.

1.2 Cancer Associated Fibroblasts

The PDAC tumour microenvironment (TME) is extremely heterogenous, with key elements deriving from cancer-associated fibroblasts (CAFs), endothelial cells and immune cell subsets including T cells subtypes, NK cells, macrophages, myeloid-derived suppressor cells (MDSCs) and neutrophils (Rubin et al., 2022). The stroma is now acknowledged as a defining feature of PDAC playing a pivotal role in promoting and regulating tumour growth, evasion, and dissemination (Huber et al., 2020). The importance of CAF in PDAC progression, especially in the induction of immunosuppression, is uncertain with a range of conflicting studies. This is frustrating as greater insight could lead to targeted therapies that may act, for instance, to limit desmoplastic expansion and enhance immune cell and chemotherapy access to tumour (Koyama et al., 2008).

1.2.1 What are fibroblasts?

Fibroblasts were first described in the late 19th century by German pathologist Rudolf Virchow based on their location and morphological criteria (Plikus et al., 2021). They produce the necessary elements to maintain the structural integrity of the body's connective tissue by secreting precursors of extracellular matrix (ECM) and collagen (Dick, 2022; Gorchs & Kaipe, 2021). This function is modified over time and may contribute to ageing disorders (E. Sahai et al., 2020). Fibroblasts have many additional roles including regulation of epithelial differentiation and wound repair during inflammation. This is mediated through the synthesis of proteins such as collagen, fibronectin, and laminin that maintain structural homeostasis. During wound healing, secretion of soluble mediators such as cytokines and growth factors is important to

maintain the crosstalk homeostasis of cell interactions with adjacent epithelia (Kalluri & Zeisberg, 2006; E. Sahai et al., 2020). Of note, under pathological conditions excessive production of ECM and collagen can cause functional dysregulation (Dick, 2022). Many pro-inflammatory cytokines and growth factors regulate fibroblast function, and this includes growth factor-alpha and beta (TGF-α and TGF-β), platelet-derived growth factor (PDGF), granulocyte-macrophage colony-stimulating factor (GM-CSF), epidermal growth factor (EGF), and tumour necrosis factor (TNF) (Dick, 2022; Gorchs & Kaipe, 2021).

Fibroblasts are notably dynamic and morphologically heterogeneous and have a variety of roles depending on their location and activity (Chang et al., 2014). The ability of fibroblasts to recognise environmental cues and change phenotype is partly due to the expression of a wide range of cell surface adhesion receptors such as integrins and cadherins that support the interaction of fibroblasts with their environments. This ‘plasticity’ is seen in many settings and an example is that observed in the transformation of fibroblasts into myo-fibroblasts that express alpha-SMA (Dick, 2022).

1.2.2 What is the origin of fibroblast?

Answering the question “what is the origin of fibroblasts” is challenging and relates primarily to their remarkable heterogeneity, particularly during pathological conditions (LeBleu & Neilson, 2020).

Most studies support the concept that fibroblasts originate from primitive mesenchymal cells that populate fibroblasts and fibrocytes throughout body tissues. During embryonic and early development fibroblasts are derived from primary mesenchyme as epiblasts and undergo epithelial mesenchymal transition (EMT) to mesoderm. Then, the mesoderm gives rise to mesenchyme, endothelial cells, epithelial cells, pericytes, adipocytes, and bone marrow. The mesenchyme constitutes the adult mature resident quiescent fibroblasts (RQF) (non-proliferative) along with connective tissue, bones, cartilage, and lymphatic systems. RQF are believed to maintain ECM and structural homeostasis (LeBleu & Neilson, 2020).Fibroblast-like cells may also be derived from epithelial, endothelial, perivascular or adipocytes through mesenchymal transition. EMT is characterised by loss of epithelial markers such as E-cadherin and expression of fibroblast-specific proteins (FSP). Conversely, in situations such as wound healing and tumorigenesis, fibroblasts may give rise to epithelia by undergoing Mesenchymal to epithelial transition (MET) (Chang et al., 2014). Because of these properties, fibroblasts have recently given a very high attention.

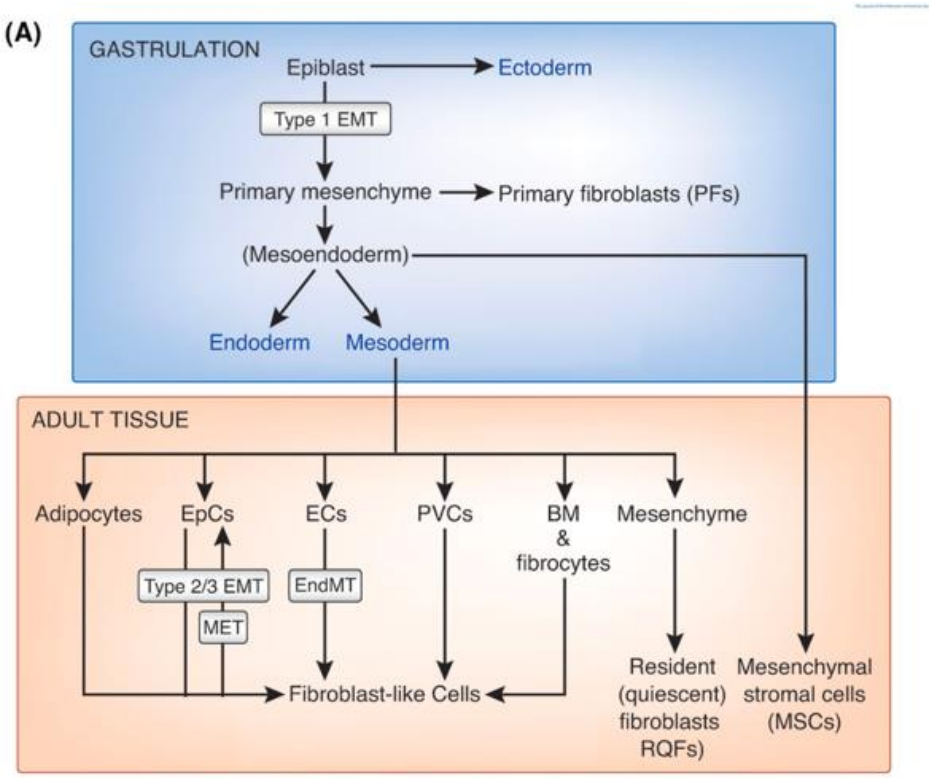


Figure 1.4. Developmental origin of fibroblasts (LeBleu & Neilson, 2020).

1.2.3 What is the origin of CAF?

Fibroblasts respond to injury with enhanced production of growth factors, transcription factors and chemokines (Erik Sahai et al., 2020). This can lead to increased fibrosis and it is possible that the CAF phenotype develops as a response to sensing of 'chronic injury' within the TME. Indeed, CAF appear to differentiate from activated mature fibroblasts in a range of anatomical settings.

The phenotype and function of CAF differs greatly between patients and tumour subtype. These dynamic characteristics demonstrate the plasticity and heterogeneity of CAF. Due to the lack of specific markers, the origin of CAF is hard to determine and remains a challenge (Öhlund et al., 2014; Ping et al., 2021). The TME changes during tumour development and the role of the CAF differentiation in driving, or responding, to this is uncertain.

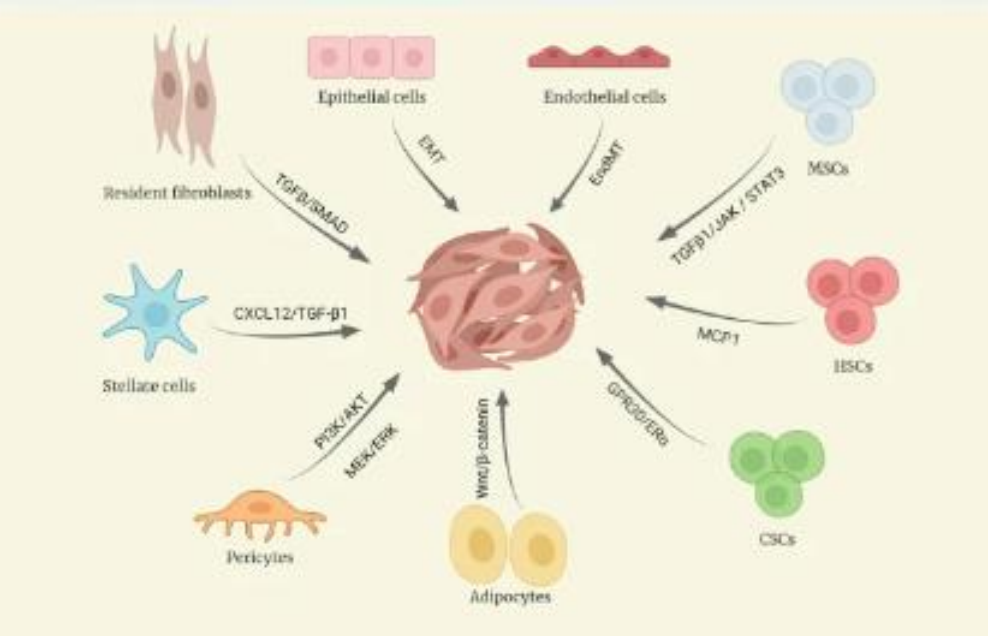


Figure 1.5. The origin of CAF (Ping et al., 2021).

1.2.4 CAF function

It has been shown that CAF exhibit dual function pro-tumorigenic and suppressive properties. Tumour-promoting CAF support proliferative, pro-inflammatory, immune-suppressive, angiogenic, pro-invasive and pro-metastatic environments that are required for aggressive tumorigenesis. In contrast, CAF may have a tumour suppressive function in the early stage of tumours. However, the biological programmes that determine this balance remain unknown with emerging data indicating that age is an important determinant (Erik Sahai et al., 2020).

The approach of targeting tumour stroma has become very attractive over the last decade. However, results are variable, and the underlying pathophysiology is uncertain. A plausible explanation for these divergent results is the existence of subpopulations of fibroblasts in the tumour stroma with pro- and anti-tumorigenic traits. Understanding the phenotype, spatial location, and function of these CAF subsets can be a key factor for the development of successful combinatorial immunotherapies (Han et al., 2020; Ping et al., 2021; Erik Sahai et al., 2020).

1.2.4.1 CAF heterogeneity and plasticity

Several studies have shown that the spatial distribution of CAF is an important determinant of function. Öhlund et al. identified two distinct CAF subpopulations within PDAC. The first was described as myo-fibroblastic CAFs (myCAF) in close apposition to cancer cells which respond to elevated amount of tumour cell-secreted TGF-β and display a high level of alpha-smooth muscle actin (α-SMA) expression and collagen genes. In addition, myCAF lack the expression of inflammatory cytokines distinguishing them from the second dominant population, inflammatory CAF (iCAF).

myCAF shows an activated phenotype with contractile properties (Belle & DeNardo, 2019; Ohlund et al., 2017) whilst iCAF are located more distantly from tumour cells in the desmoplastic stroma. iCAF express high level of IL-6 protein and other inflammatory cytokines and chemokines such as IL-1, IL-21, LIF, CXCL-12 and CXCL1/3. iCAF have lower α-SMA levels compared to myCAF and are characterized by immune-modulating properties.

Importantly, quiescent PSCs can differentiate into both iCAF and myCAF and can dynamically reverse from one cell state to the other (Ohlund et al., 2017). The trans-differentiation of PSC into iCAF phenotype is mediated by IL-1α-induced JAK/STAT activation signalling pathway via LIF induction. The TGF-beta signalling pathway is thought to further promote differentiation of CAF into myCAF phenotype by downregulation of IL1-R1 expression (Biffi et al., 2019).

The tumour distribution and secretory potential of CAF subtypes has led to suggestions of a potential role of iCAF in promoting tumour progression, chemoresistance and immune suppression whilst myCAF may restrain tumour progression. iCAF and myCAF are also interconvertible, dependent on location within the tumour (Biffi et al., 2019), and insights into potential mechanisms are being defined. Rho effector protein kinase N2 (PKN2) is critical for PSC myofibroblast differentiation, and its depletion promotes a myofibroblast to inflammatory CAF switch both in vitro and in vivo (Murray et al., 2022). Recently a new CAF subtype that expresses MHC class II and CD74, and lacks costimulatory molecules such as CD80 or CD86, has been defined by Tuveson and colleagues (Elyada et al., 2019), termed as antigen presenting CAFs (apCAF). The same group found that apCAF subpopulations activate CD4+ T cells in an antigen-specific fashion ex vivo suggesting

their role in modulating the PDAC immune system capacities and progression. It currently remains unclear whether apCAF induce T-cell anergy in vivo or not, due to their lack of co-stimulatory molecule expression needed to induce T cell proliferation and suggesting that MHC-II expression by apCAF acts as a decoy receptor to deactivate CD4+ T cells by promoting either anergy or differentiation into Tregs. Thus, apCAF might contribute to PDAC immune suppression. ApCAFs are also dynamic and can differentiate into myCAFs (Elyada et al., 2019). Huang et al. Reported that apCAFs are originated from mesothelial cells and induce naïve CD4+ T cells into Treg cells in an antigen-specific manner (Huang et al., 2022). As a result, CAFs heterogeneity and plasticity might potentially guide the design of treatment strategies by shifting tumour promoting CAFs into anti-tumorigenic populations.

In line with these studies, Collagen type I (col-I) depletion in α-SMA+ myofibroblasts aggravates PDAC progression and tumour immunosuppression (Y. Chen et al., 2021; Madsen, 2021). MyCAF populations in PDAC mouse models were found to suppress immune surveillance through increasing CD4+Foxp3+ Tregs phenotype expression leading to aggressive tumours with low survival (Hosein et al., 2019; Ozdemir et al., 2014). However, myCAF depletion can also result in decreased type I collagen, altered ECM, and suppression of angiogenesis and EMT (Ozdemir et al., 2014).

Two novel CAF subtypes were recently found in PDAC, metabolic cancer-associated fibroblasts (meCAFs) (Y. Wang et al., 2021) and complement-secreting CAF (csCAFs) (K. Chen et al., 2021). meCAF are characterized by a high metabolic activity and are found in loose-type PDAC. In addition, PDAC patients with elevated meCAFs phenotype were associated with increased metastasis and poor overall survival (K. Chen et al., 2021; Y. Wang et al., 2021). Accordingly, csCAFs have been identified by

the expression of complement system components such as C3, C7, C1R/S and were in the tissue stroma adjacent to tumour cells in early stage PDAC (K. Chen et al., 2021). Complement system components are not only important effectors of innate immunity but also play a crucial role in the modulation of cell interaction within the tumour (Kolev et al., 2022).

Using single-cell analysis Hutton et al. described two CAF population in PDAC based on CD105 expression, CD105+ and CD105- CAFs. CD105+ fibroblasts were strongly tumour promoting whilst CD105-negative fibroblasts had a negative impact on tumour development in a manner dependent on adaptive immunity. CD105- and CD105+ CAF respond differently to signals including TGF-β, LIF and IL-1. However, both populations express myCAF and iCAF signature genes. High expression of apCAF and mesothelial cells markers such as MHC-II and CD74 have been seen in CD105- fibroblasts (Hutton et al., 2021). Interestingly, CD105+ and CD105-normal fibroblasts were discretely distributed in the inflamed pancreas, with CD105+ fibroblasts observed in the intra-acinar regions and CD105- fibroblasts in the inter-acinar regions (Hutton et al., 2021). These findings provide insights into the remarkable profile of CAF heterogeneity and dynamic plasticity during PDAC development (Y. Chen et al., 2021; Costa et al., 2018; Davidson et al., 2020; Green et al., 2016; Pelon et al., 2020; Venning et al., 2021). Taken together, these data indicate that research studies focusing on the crosstalk between CAF and immune cells might lead to the development of new effective strategies.

Table 1.1. The heterogeneity of CAF subtypes in cancers.

References	CAF supbtypes	Details	Disease	Study models	Study type
Hutton et al., 2021	**CAD105+**	Tumour promotor/ Abundant in PDA/enhance TGF-response and suppress mesothelial gene expression/ express myCAF and iCAF markers AND NOT apCAF	KPC mice	different studies on tumours and Primary pancreatic fibroblasts (PaFs)	Mass cytometry, Bulk RNA & scRNA-seq
	CD105-	Tumour suppressive/ less abundant in PDA/express myCAF, iCAF and apCAF markers (MHCII+CD74+)			
Wang et al., 2021	**meCAF: metabolic CAF**	Found in loose-type PDAC/ highly active glycolytic ativity/ higher risk of metastasis and a poor prognosis	Human PDAC	loose-, moderate-, or dense-type PDAC	scRNA-seq
Huang et la., 2022	**apCAF: PDPN+MHCII+**	mesothelial cells are the origin of apCAF. apCAF induce Treg formation in PDAC	KPC mice model	normal & different stage of cancer (low to high)	Flow-cytometry,
	myCAF: PDPN+ MHCII- aSMA+	iCAF and myCAF lineages are derived from resident fibroblasts			
	iCAF: PDPN+ MHCII-IL6+				
Davidson et al., 2020	**$PDPN^{h}$ $PDGFRa^{h}CD34^{h}$ $aSMA^{low}$ (S1)**	S1 = Immune-early tumours. Engage in immune talk upregulating genes involved the recruitment and regulation of immune cells including cytokine genes, receptors and COMPLEMENT. C3 is high in S1 (C3 is upregulated in CD34h population).	Mainly Melanoma Tumour	Orthotopic mice (N vs T) and human	scRNA- seq, Flow cytometry in normal skin and within tumours of mice models (No gating for C3)
	$PDPN^{h}$ $PDGFRa^{h}CD34^{low}aSMA^{bw}$ (S2)	S2= Desmoplastic-early tumours= encodes for ECM components and implicated in immune exclusion			
	$PDPN^{low}$ $PDGFRa^{bw}$ $CD34^{bw}aSMA^{h}$ (S3)	S3= contractile- late tumour stage= express genes involved in regulation and rearrangement of the actin cytoskeleton.			
K. Chen et al., 2021	**cCAFs: classical CAF**	expressed high levels of ECM related components, MMP11 (matrix remodeling molecular), FAP (stromal fibroblast activeted pro- tein) and SFRP2 (modulators of Wnt signaling), which are involved in extracellular matrix deposition	PDAC	Human PDAC	Single cell RNA-seq, RNA ISH, IF and RT-qPCR
	csCAFs: (complement-secreting CAFs)	showed highly activated transcription of complement system, including C3, C7, CFB, CFD, CFH, CFI, which may regulate immune and inflammation response within the tumor;			
	PSCs (pancreatic stellate cells)	were distinct from both cCAF and csCAF, and expressed marker genes of stellate cells, such as RGS5, ADIRF, CRIP1, NDUFA4L2, NOTCH3 and PDGFa.			
Pelon et al., 2020	**CAF-S1: FAPHigh CD29Med-High αSMAHigh PDPNHigh PDGFRβHigh;**	Dominant in LN/Myofibroblast characteristic. accumulate in LN and stimulate cancer cell migration & initiate EMT through CXCL12 and TGFb pathways	BC metastatic axillary LNs	Fresh human breast Primary tumours & matched LN	Flow cytometry, IHC, RAN seq on CAF-S1 & CAF-S4
	CAF-S2: FAPNeg CD29Low αSMANeg-Low PDPNLow PDGFRβLow;	Dominant in NON invaded auxilary LN/ detected in healthy breast tissues			
	CAF-S3: FAPNeg-Low CD29Med αSMANeg-Low PDPNLow PDGFRβLow-Med;	Dominant in NON invaded auxilary LN/ detected in healthy breast tissues			
	CAF-S4: FAPLow-Med CD29High αSMAHigh	Dominant in LN/highly contractile and exert a pro-invasive effect on cancer cells via NOTCH signaling			
Costa et al., 2018	**CAF-S1: CD29Med FAPHi FSP1Low-Hi aSMAHi PDGFRbMed-Hi CAV1Low**	myofibro characterestic/ Proximity of tumour/ promote immunosuppression. Attract CD4+CD25+ T cells by secreting CXCL12 and retain them by OXX40L, PD-L2 & JAM2	Human Breast cancer	Fresh human BC tumors and juxta-tumors	Flow cytometry, IHC, RNA-seq for CAF-S1 &S4
		increases T lymphocyte survival and promotes their differentiation into CD25HighFOXP3High, through B7H3, CD73, and DPP4.			
		enhances the regulatory T cell capacity to inhibit T effector proliferation.			
	CAF-S2: CD29Low FAPNeg FSP1Neg-Low aSMANeg PDGFRbNeg CAV1Neg;	equally distributed in the two compartment/LumA tumors			
	CAF-S3: CD29Med FAPNeg FSP1Med-Hi aSMANeg-Lo PDGFRbMed CAV1Neg-Lov	Juxta-tumours/negative for FAP and aSMA suggesting their expression on normal cells			
	CAF-S4: CD29Hi FAPNeg FSP1Low-Med aSMAHi PDGFRbLow-Med CAV1Neg-Low	distributed in Lum, HER2, and TNBC/ Lack of CAF-S1 activities			
Venning et al., 2021	**CD26+ CAF**	highly expressed on tumour comapred to normal	Breast cancer	static) and poorly/non-metastatic tumour mouse m	Flow Cytometry
Elayda et al., 2019	**myCAF = myofibroblastic CAF = High aSMA, MHCII-**	adjacent to cancer cells	PDAC	Human and KPC (T vs N)	Flow cytometry on KPC tissues
		high expression of the smooth muscle genes Acta2 and Tagln, as well as Igfbp3, Thy1, Col12a1 and Thbs2			
	iCAF =inflammatory CAF = low aSMA, high cytokines & chemokines, MHCII-	located in the desmoplastic areas of the tumor, farther away from the cancer cells			
	apCAF = Antigen Presenting CAF = MHCII+CD74+	apCAFs can convert into myCAF==>apCAF are dynamic and interconvertible states.			
		Present Ag to CD4+Tcells (decoy receptors)/ lack the costimulatory molecules needed to stimulate T cells proliferation			
Biffi et al., 2019	**iCAF = PDPN+PDGFRa+ Ly6C+**	IL-1a induces the iCAFs phenotype	PDAC	KPC mouse model	Flow cytometry on KPC
	myCAF = PDPN+PDGFRa+ Ly6C-	TGF-b promote myCAF generation			
Y. Chen et al., 2021	**aSMA+ myofibroblasts**	are major contributors of Collagen1 in the PDAC stroma	PDAC	Mice models	Not flow
		Collagenl deletion in aSMA+myfibro increased immune suppression in PDAC			
Ohlund et la., 2017	**myCAF : FAP+ aSMAhigh IL6low**	**jacent to neo- plastic cells in mouse and human PdA tissue/ lack the ex- pression of inflammatory cytokin**	PDAC	Mouse and human cultured cells	Flow on cultured PSC
	iCAF = IL6+ aSMALow	source of IL-6 and IL-11 and LIF in the PDA microenvironment/ located more distantly from neoplastic cells			
Green et al., 2015	**PDGFRa+CD29+**	Myofibrolast chracterestics	Lung cancer	Mice models	Flow cytometry
	PDGFRa+ CD34+	Matrix and/or lipofibroblast characteristics			

1.2.5 CAF markers

- **CD90**

Thy1 or CD90 is a glycoprotein expressed on the surface of many cells, including fibroblasts and endothelial cells, (Haeryfar & Hoskin, 2004), whilst being absent from most mature T cells (Bradley et al., 2009).

Thy1 is involved in a range of physiological and pathological processes (Haeryfar & Hoskin, 2004; Rege & Hagood, 2006) and engagement induces apoptosis, cell-cell interaction, tumour growth, migration, and promotion of T cell activation. Moreover, interactions between Thy-1 and integrins are necessary for the migration of leukocytes and melanoma cells across an endothelial cell monolayer, suggesting Thy-1 may be important for melanoma metastasis and leukocyte recruitment. Thy1 modulates fibroblast phenotype relevant to wound healing and fibrosis: Thy-1 (+) splenic fibroblasts produce greater levels of interleukin 6 (IL-6), whereas only Thy-1 (-) fibroblasts express class II major histocompatibility complex (MHC) antigens after IFN-gamma treatment. Absence of Thy-1 in lung and synovial fibroblasts indicates a more fibrotic myofibroblast phenotype (Rege & Hagood, 2006). As such, the exact biological role(s) of Thy-1 has remained controversial and is context dependant.

- **Alpha-SMA**

α-SMA is an actin protein that forms the microfilaments in the cytoskeleton. ACTA2 is one of 6 different actin isoforms and is involved in the contractile apparatus of smooth muscle. It is expressed widely and plays a role in regulating cell shape, movement, and contraction of cells during cell division and in the establishment and maintenances of cell junctions. More importantly, α-SMA expression is altered during cancer or

inflammation, and it is used as a marker of myofibroblast phenotype (Chaponnier, 2001; Rockey et al., 2013).

- **Cadherin11**

Cadherin11 is a member of the calcium-dependent adherent protein family which are cell adhesion molecules that form adherent junctions that help cells to adhere to each other and to regulate cytoskeletal complexes. Cadherins require calcium for their activity and the removal of calcium abolishes their function. Their expression is restricted to mesenchymal tissues and found in osteoblasts and synovial fibroblasts. Cadherin-11 regulates cell proliferation via PDGFR-β in human Mesenchymal stem cells (Chang et al., 2017). A recent study showed that the cadherin-11 and PDGFR-β complex in fibroblasts enhances proliferation and tissue regeneration via the PDGFR-AKT signalling axis (Passanha et al., 2022) and mediates activation of synovial fibroblasts resulting in synovial inflammation by producing pro-inflammatory cytokines including IL-6 (Chang et al., 2011).

- **CD26**

CD26 is a glycoprotein encoded by the DPP4 gene, also known as adenosine deaminase complexing protein 2. It is an enzyme expressed on the surface of most cell types such as T cells and epithelial cells. CD26 is strongly expressed on subsets of both activated CD4+ and CD8+ T cells and plays a crucial role in both T cell activation and in enhancing T cell cytotoxic activity when crosslinked via their Fc receptor (FcR) on the surface of accessory or target cells (Morimoto & Schlossman, 1998). Worthen et al. found that CD26+CD90+ subpopulation express relatively high levels of COL1A1 (Worthen et al., 2020).

- **CD34**

CD34, initially identified on hematopoietic stem cells, is also expressed on vascular endothelial cells and fibroblasts across different organs. Its functions include cellular adhesion, T lymphocyte homing, and haematopoietic cell trafficking (Simmons & Torok-Storb, 1991). CD34+ fibroblasts, found in various organs and believed to secrete cytokines, regulate stromal collagen content, facilitate angiogenesis, and cell migration, and change phenotype into myofibroblasts upon activation. In cancer, CD34 expression is lost in cancer-associated fibroblasts (CAFs), which are implicated as adverse prognostic factors (Radu et al., 2023). Notably, CD34+ fibroblasts are absent in the stroma of most carcinomas, replaced by α-SMA+ myofibroblasts, as observed in ductal carcinoma in situ and IBC-NST cases (Barth et al., 2002). The absence of CD34+ fibroblasts in tumour stroma associated with the presence of α-SMA+ myofibroblasts, metastases, and reduced survival indicating CAF transformation (Westhoff et al., 2020). Research conducted on synovial fibroblasts indicated that the CD34+THY1+ subset exhibited significant potential for osteogenic and chondrogenic differentiation. Additionally, this subset displayed the highest expression levels of MSC-positive surface markers, including CD73, CD271, and THY1, at the protein level (S. Noda et al., 2022).

- **Ki-67**

Ki-67, also known as MKI67 (marker of proliferation Ki67), is a nuclear antigen expressed during the growth and synthesis phases of the cell cycle, but not during the resting phase. It serves as a well-established marker for predicting clinical outcomes in various types of cancer (Kim et al., 2014). Elevated Ki-67 levels in cancerous tissue are typically associated with a poorer prognosis, yet they also indicate a positive response to chemotherapy. Beyond traditional parameters, Ki-67 has been proposed as a crucial factor in guiding tumour treatment decisions (Jing et al., 2018; Kim et al., 2014). A study found that increased Ki-67 expression in fibroblast-like cells at the invasive front of tumours correlates with improved clinical outcomes for patients with oral squamous cell carcinoma (OSCC) (Jing et al., 2018).

- **PDGFR-α**

PDGFs, comprising PDGF-α and PDGF-β, are a growth factor family implicated in tumour pathogenesis and angiogenesis. Tumour growth can be facilitated via PDGF through autocrine stimulation, overexpression, or angiogenesis induction. PDGFR blockade potentially reduces interstitial fluid pressure, enhancing drug delivery within solid tumours (Board & Jayson, 2005).

Elevated PDGFR-α signalling is associated with increased proliferation but a delayed fibroblast-to-myofibroblast transition, emphasizing the necessity of PDGFR-α downregulation for the transition to myofibroblasts (Yao et al., 2022). Conversely, PDGFR-α deletion impedes both proliferation and differentiation (Yao et al., 2022). Lineage-tracing studies have shown that many PDGF-activated progenitors evolve into α-SMA+ myofibroblasts (Li et al., 2018; Shook et al., 2018). Additionally, Contreras and his colleagues revealed that fibro–adipogenic progenitors (FAPs) numbers

correlate with TGF-β levels and extracellular matrix deposition during regeneration (Contreras et al., 2019). Interestingly, post-injury, PDGFR-α expression dynamically changes in the fibroblast lineage. TGF-β signalling reduces PDGFR-α levels in FAPs, mouse dermal fibroblasts, and related mesenchymal cell lines, while promoting myofibroblast differentiation and inhibiting adipogenicity (Contreras et al., 2019). However, in hepatocytes, scleroderma fibroblasts, and tumour cells, TGF-β upregulates PDGFR-α, while it downregulates its expression in human lung fibroblasts and smooth muscle cells (By Akio Yamakage, 1992; James C. Bonner, 1995).

- **PDGFR- β**

PDGFR-β, a receptor for platelet-derived growth factor, plays a pivotal role in guiding cell differentiation towards specific mesenchymal lineages and enhancing fibroblast function. Additionally, it facilitates the transformation of fibroblasts into myofibroblasts, crucial for bolstering the production of extracellular matrix proteins essential for tissue repair (Gao et al., 2005; Hewitt et al., 2012). Interruption of PDGFR-β pathways in PDGFR-β deficient dermal fibroblasts impede their proliferation, survival, and migratory capabilities (Gao et al., 2005).

- **CD105**

CD105, also known as Endoglin, is a cell surface glycoprotein integral to the TGF-β receptor complex and serving as an accessory receptor for TGF-β (Bastos et al., 2022; FARSHAD NASSIRI, 2011). CD105 is a prominent marker for various endothelial cell subtypes, pericytes, and mesenchymal stem cells. Additionally, it has been observed in the stroma of human prostate and colorectal tumours, as well as in healthy human breast tissue (Hutton et al., 2021). Research indicates that 90%–95% of human bone marrow-derived mesenchymal stem cells (MSCs) express CD105 (endoglin), while

approximately 50% of cancer-associated fibroblasts (CAFs) within the tumour stroma of breast cancer patients (BCPs) also express CD105 (Pasanen et al., 2016).

As discussed previously, Hutton and colleagues delineated how CD105 (Endoglin) expression distinguishes two pancreatic fibroblast subsets with opposing functions (Hutton et al., 2021). Another study found that high CD105 expression in cancer-associated fibroblasts correlates with increased metastatic risk, especially for bone metastasis, and shorter survival rate (Giorello et al., 2023).

- **C3**

Complement, a key component of innate immunity, acts as an initial defence against foreign and abnormal cells. Infections activate complement, leading to inflammation, opsonization, phagocytosis, pathogen destruction, and activation of adaptive immunity (Merle et al., 2015). Cells within the tumour microenvironment, both immune and non-immune, and including fibroblasts, possess the capability to express and release C3 and various other complement proteins (Kolev et al., 2022). In patients with breast cancer, fibroblasts emerged as a significant supplier of C3 and C3a, thereby facilitating breast cancer metastasis (Shu et al., 2020). Davidson et al. classified three stromal populations: immune (S1), desmoplastic (S2), and contractile (S3). The complement component C3 is expressed in the immune population, mainly found in early tumours. However, 'contractile' cells dominate in later stages. C3's cleavage product, C3a, recruits C3aR+ macrophages, vital for immune infiltration. Disruption of C3a and C3aR impedes immune infiltration, hindering tumour growth (Davidson et al., 2020). Chen et al. introduced a novel subset of CAFs in PDAC termed complement secreting CAFs (csCAFs), characterized by their expression of complement system components such as C3 and C7 (K. Chen et al., 2021). These csCAFs were specifically located in the

tissue stroma adjacent to malignant ductal cells, particularly in early pancreatic ductal adenocarcinoma (PDAC). Interestingly, although the study did not find iCAFs or apCAFs, there appeared to be some similarity between csCAFs and previously reported iCAFs. Both subsets exhibited enriched expression of complement system components such as C3 and complement factor D (CFD) (K. Chen et al., 2021). In addition, iCAFs were prevalent in tumour-distal subsets and exhibited expression of complement components (Croft et al., 2023).

- **PDPN**

Podoplanin, a mucin-type transmembrane protein, derives its name from its expression on kidney podocytes. Found in various tissues during development and adulthood, including the brain, heart, kidney, lungs, osteoblasts, and lymphoid organs, it plays a pivotal role in lung, heart, and lymphatic system development. Podoplanin serves as a marker for lymphatic endothelial cells, fibroblastic reticular cells of lymphoid organs, and lymphatics in the skin and tumour microenvironment (Astarita et al., 2012). In terms of cancer, PDPN is upregulated by CAF in the stroma surrounding various tumours, including adenocarcinomas and colorectal cancers (Kitano et al., 2010) and its expression on CAFs is associated with poor prognosis (Kubouchi et al., 2018). In PDAC, PDPN exhibited a significant increase on cells proximal to the tumour and displayed a robust enhancement on CAFs. High expression levels of PDPN are associated with poor prognosis (Croft et al., 2023).

- **CD29**

The CD29 or integrin β1, a subset of integrin proteins, plays a crucial role in mediating cell-ECM interactions with proteins such as collagen, laminin, and fibronectin. Widely expressed across various cell types and tissues such as blood, skin, and mammary glands, CD29 holds significant functional importance in cell adhesion, organ development, tissue repair, and homeostasis (Togarrati et al., 2018). Five different isoforms of CD29 have been identified, including β1A, β1B, β1C, β1C-2, and β1D (Togarrati et al., 2018). These variants exhibit differential effects on cell proliferation, receptor localization, adhesion, migration, and downstream signalling pathways, with β1D notably inhibiting cell proliferation and reduced protein expression observed in various cell types, including fibroblast (Belkin & Retta, 1998; Togarrati et al., 2018). Zeltz and colleagues observed an upregulation of integrin α11 expression in pancreatic cancer, with myCAFs displaying a moderate level of α11 positivity linked to PC tumours (Zeltz et al., 2019). Costa et al. conducted an extensive study to classify four distinct subpopulations of CAFs in breast cancer, primarily based on CD29 expression levels. Notably, the CAF-S1 ($CD29^{med}$) and CAF-S4 ($CD29^{high}$) subsets were predominantly present in aggressive breast cancer subtypes like HER2-positive and triple-negative, emphasizing their role as prognostic indicators. The CAF-S4 subset showed widespread distribution across Luminal, HER2-positive, and triple-negative breast cancer subtypes, with HER2-positive breast cancer exhibiting the highest enrichment (Costa et al., 2018). Further investigations by the same group explored ovarian and lymph node fibroblasts, identifying four CAF subtypes based on CD29 expression. This work revealed that CAF-S1 ($CD29^{med}$) promotes cancer cell migration and initiates epithelial-to-mesenchymal transition through CXCL12 and TGF-β pathways, while highly contractile CAF-S4 ($CD29^{high}$) induces cancer cell invasion via NOTCH

signalling (Pelon et al., 2020). Patients with elevated CAF levels, particularly CAF-S4, at diagnosis are more prone to develop late distant metastases. Moreover, mesenchymal high-grade serous ovarian cancer (HGSOC) demonstrates a high content of CAF-S1 fibroblasts, which exhibit immunosuppressive effects by enhancing attraction, survival, and differentiation of CD25+FOXP3+ T lymphocytes. CXCL12β expression in CAF-S1 cells significantly influences their immunosuppressive activity and serves as a reliable prognostic factor in HGSOC, contrasting with CXCL12α (Givel et al., 2018).

- **FAP**

Fibroblast activation protein-α (FAP) is a type-II transmembrane serine protease prominently expressed in pathological conditions such as fibrosis, arthritis, and cancer, with detrimental implications for patient outcomes across diverse cancer types, including breast, colorectal, pancreatic, lung, bladder, and ovarian cancers (Fitzgerald & Weiner, 2020). FAP induction on fibroblasts was observed upon exposure to conditioned media from the HO-8910PM ovarian cell line (Chen et al., 2009). Furthermore, myofibroblasts exhibit heightened FAP expression upon TNF-α and TGF-β exposure, indicating a requirement for pre-existing cell reprogramming for FAP induction (Truffi et al., 2018). FAP expression is seen on in both malignant and adjacent stromal cells in colorectal cancer, including myofibroblasts, fibroblasts, and endothelial cells (Iwasa et al., 2003). Co-culturing gastric cancer cells with FAP-expressing fibroblasts augmented proliferation and migration in vitro and promoted tumour growth and resistance to anti-PD-1 therapy in vivo (Wen et al., 2017). Additionally, co-culturing pancreatic ductal adenocarcinoma (PDAC) cell lines with FAP-expressing fibroblasts heightened Rb phosphorylation, prompting cell cycle progression and increased proliferation (Kawase et al., 2015). Feig et al. identified

FAP+ cancer-associated fibroblasts (CAFs) as the primary source of tumour CXCL12, with inhibition of the CXCL12 receptor, CXCR4, resulting in reduced tumour growth and enhanced efficacy of anti-PD-1 therapy (Feig et al., 2013).

- **MHC-II**

While tumour cells commonly express MHC-I, certain tumours also express MHC-II, traditionally associated with professional antigen-presenting cells. MHC-II is pivotal for antigen presentation to CD4+ T lymphocytes which, in addition to their role as T regulatory cells, are recognized increasingly for an additional protective effect in cancer immunity. Indeed, evidence suggests that tumour-specific MHC-II expression correlates with favourable outcome in cancer patients, including enhanced response to immunotherapies and tumour rejection in murine models. Effective immune checkpoint inhibition relies on T cell recognition of tumour antigens mediated by MHC:T-cell receptor (TCR) interactions. MHC-I presents endogenously derived peptides to CD8+ T cells, while MHC-II, primarily expressed by professional antigen-presenting cells like dendritic cells, presents exogenously derived peptides to CD4+ T cells. Tumour-specific MHC-II expression enhances tumour recognition by the immune system, potentially influencing immunotherapy outcomes positively (Axelrod et al., 2019).

MHC-II+ antigen-presenting cancer-associated fibroblasts (apCAFs) were discovered in pancreatic adenocarcinoma and breast cancer, with elevated HLA class II gene expression correlating with longer-term survival, suggesting a vital role for HLA-DR+ antigen-presenting CAF (ApCAF) populations (Elyada et al., 2019; Friedman et al., 2020). Recently, Kerdidani et al. identified apCAFs in non-small-cell lung cancers, highlighting their potential in promoting anti-tumour immunity (Kerdidani et al., 2022).

Notably, apCAFs were concentrated in lung cancer, with abundant CD4+ T cells in closer proximity to apCAFs compared to MHC-II+ hematopoietic antigen-presenting cells. Additionally, apCAFs (MHC-II+) partially mediate their beneficial effect through complement protein expression, rescuing intra-tumoral T cells from exhaustion (Kerdidani et al., 2022).

- **CD74**

The invariant chain CD74 is pivotal in antigen presentation, facilitating MHC-II assembly and trafficking (Farr et al., 2020; Schroder, 2016). Additionally, it regulates endosomal trafficking, cell migration, and cellular signalling as a surface receptor for the pro-inflammatory cytokine macrophage migration inhibitory factor (MIF). Upregulation of CD74 is observed in several cancers, where it correlates with increased immune checkpoint activity, cytokine secretion, and infiltration of immune cells such as macrophages, dendritic cells, and neutrophils (Xu et al., 2021). CD74 involvement in cancer development suggests its significance in shaping the tumour microenvironment and influencing the activities of infiltrating cells. As a polypeptide of the human lymphocyte antigen (HLA) class II, CD74 contributes to antigen presentation and the activation of CD4+ T cells (Xu et al., 2021; Yang et al., 2018). Knockdown of CD74 expression resulted in decreased cell proliferation, migration, and invasion, whilst promoting apoptosis in PDAC cells (Hong et al., 2023). However, the exact molecular mechanism of CD74 in PDAC remains poorly elucidated.

Fibroblasts exposed to CD74 knockdown cell-conditioned media in an indirect co-culture with tumour cells showed decreased expression of inflammatory cytokines, indicating CD74's role in modulating cytokine secretion in the tumour

microenvironment (Hong et al., 2023). Recently Elyada et al. identified a novel subset of CAFs termed "antigen presenting CAFs" (apCAFs) and characterized by the expression of MHC class II and CD74 rather than traditional costimulatory molecules (Elyada et al., 2019).

1.3 CAF and T cells

T cells can be divided into different functional subsets based on markers including CD45RA, CCR7, and CD28. Naïve T cells co-express all three markers and are antigen-inexperienced, requiring co-stimulation for activation. Central memory (CM) T cells express CD45R0, CCR7, and CD62L, residing primarily in secondary lymphoid organs where they mount rapid recall responses upon antigen stimulation. CM cells exhibit limited immediate effector function but quickly differentiate into effector T cells when activated. Effector memory (EM) T cells, which lack CCR7 and CD62L, are primarily found in peripheral tissues and respond rapidly to antigenic challenges, typically through production of inflammatory cytokines. Terminally differentiated effector memory T cells (TEMRA) re-express CD45RA and are highly cytotoxic. Together, these subsets ensure a robust immune response tailored to specific environments (Martinez, 2010; Nielsen et al., 2017).

T cells are a major effector population of the adaptive immune system (Humphrey, 2023) and recent research highlights bidirectional crosstalk between T cells and CAFs. Here I will review various mechanisms through which CAF/T cell crosstalk may impede effective anti-cancer immunity.

The immune landscape within tumours is typically categorized into distinct immunophenotypes in relation to immune infiltrate. ‘Inflamed’ or ‘hot’ tumours are characterized by T cell infiltration and are associated with an improved response to checkpoint inhibition. ‘Cold’ tumours show little or no immune infiltrate and here immune cells may be absent, in ‘deserted’ tumours, or they may be restricted to invasive margins or stromal regions, preventing direct contact with cancer cells, hence labelled as ‘excluded’.

CAF impact T cell function through several mechanisms, including enhancement of extracellular matrix (ECM) density with elevated interstitial fluid pressure within CAF-rich stroma leading to T cell exclusion from tumour cells. Numerous studies have reported diminished cytotoxic T lymphocyte infiltration in tumours enriched with CAF compared to those with low CAF content (reviewed in (Koppensteiner et al., 2022). For instance, Kato et al. observed CD8+ T cells predominantly in peritumoral rather than intra-tumoral areas in CAF-rich oesophageal cancer, contrasting with CAF-low tumours where CD8+ T cells were distributed throughout both sites (Kato et al., 2018; Ozdemir et al., 2014). An inverse correlation between T cell counts and ECM density has been reported and regions abundant in fibronectin, particularly those surrounding tumour islets, have been identified as hindrances to T cell motility (Salmon et al., 2012). Targeting CAFs to mitigate ECM density holds promise for enhancing T cell trafficking to the tumour nest, potentially improving the effectiveness of checkpoint inhibition therapy.

CD8+ T cells are cytotoxic and recognize and attack target cells that express the antigen in association with MHC class I molecules. Activated fibroblasts, particularly FAP+ CAFs, have been implicated in impeding CD8+ T cell migration to access cancer

cells through the secretion of CXCL12 cytokine. Inhibition of CXCL12, however, results in rapid T cell accumulation in cancer cells, indicating an antitumour effect (Carstens et al., 2017; Ene-Obong et al., 2013).

T regulatory cells (Treg) are a class of immunosuppressive T cells which play a pivotal role in regulating or suppressing other immune cells and maintaining self-tolerance. Treg are the predominant source of TGF-β that drives CAF differentiation into α-SMA+ myofibroblasts (myCAF) (Biffi et al., 2019), a subpopulation that has been described as tumour restraining. In addition, Treg depletion led to reprogramming of pancreatic α-SMA+ myCAF into a tumour-promoting phenotype that accelerated tumour progression (Biffi et al., 2019; Y. Zhang et al., 2020). Neo-adjuvant therapy reduces the level of intra-tumoral Tregs and MDSC cells, which were accompanied by lower myCAF numbers and increased CD8+ cytotoxic T cells infiltration (Mota Reyes et al., 2022). Further, Treg depletion increased CCL3/6/8 chemokines expression promoting myeloid cell recruitment in a CCR1-dependent manner (Y. Zhang et al., 2020).

Moreover, CAFs secrete soluble factors which directly influence T cell migration and function in the tumour microenvironment (reviewed in (Koppensteiner et al., 2022). One of the most well-defined mechanisms involves the CXCL12-CXCR4 chemokine axis, which contributes to the exclusion of cytotoxic T lymphocytes (CTL). In the tumour microenvironment (TME) FAP+CAFs produce CXCL12, which binds to its receptor CXCR4 expressed by T cells. This interaction traps tumour-infiltrating lymphocytes (TIL) in the tumour stroma, limiting their access to areas containing cancer cells (Fearon, 2014). Feig et al. revealed that inhibiting CXCR4 caused a redistribution of T cells within the tumour tissue, enhanced CTL activity, and slowed tumour growth in PDAC (Feig et al., 2013). Initial clinical data also indicates that

CXCR4 inhibition in PDAC increases CD8+ T cell infiltration into the tumour (Bockorny et al., 2020). Remarkably, it has been observed that the pharmacological degradation of stromal hyaluronan led to an augmentation of effector memory CD8+ tumour-infiltrating lymphocytes (TIL) and enhanced antitumour immunity in a murine model of PDAC (Blair et al., 2019). Intriguingly, a substantial secretion of IL-6 is significantly correlated with an immunosuppressive FAP+CAF phenotype (CAF S1) in breast cancer and is a predominant feature of an inflammatory CAF phenotype in PDAC (Costa et al., 2018; Ohlund et al., 2017).

CAFs expressing elevated levels of FAP and α-SMA are notably implicated in the exclusion of CD8+ T cells. Additionally, NOX4 inhibition in CAF-rich murine tumours attenuated TGF-β-induced myofibroblast differentiation, downregulated α-SMA and collagen 1 and transitioning CAFs to a quiescent state. This resulted in a transition to a more "quiescent" state, rescuing CD8+ TIL response by redistributing CD8+ T cells in the tumour microenvironment (Ford et al., 2020). Desbois et al. recently demonstrated that T cell-excluding tumours exhibit a key hallmark of upregulated TGF-β and activated stroma (Desbois et al., 2020). This finding resonates in urothelial cancer, where TGF-β blockade facilitated T cell entry into the tumour centre, leading to subsequent tumour regression (Mariathasan et al., 2018). TGF-β, IL-6, and IL-10 produced by CAFs contribute to T cell dysfunction and immune evasion (Kalluri & Zeisberg, 2006; Ozdemir et al., 2014). Mariathasan et al. demonstrated that Cancer-Associated Fibroblasts (CAFs) play a multifaceted role in immunosuppression within the tumour microenvironment. CAFs enhance the recruitment of immunosuppressive cell types, including regulatory T cells (Tregs) and myeloid-derived suppressor cells

(MDSCs), further dampening T cell function. Additionally, CAFs modulate the extracellular matrix (ECM) composition, influencing T cell infiltration and function.

PDAC tissue displays a desmoplastic reaction mediated by the activation of quiescent pancreatic stellate cells (PSC). PSC are myofibroblast-like cells in the exocrine gland of the pancreas and act to modulate T cell function (Li et al., 2020; Ren et al., 2018). Activated PSC reduces CD8+ T cells infiltration to juxta-tumoral stromal region and may suppress CD8+ activity (Ene-Obong et al., 2013). Understanding these dynamics is essential for developing targeted therapies that modulate CAF behaviour to enhance T cell-mediated anti-tumour immunity.

The impact of CAFs extends to the expression of immune checkpoint molecules, such as programmed death-ligand 1 (PD-L1), which engages with programmed cell death protein 1 (PD-1) on T cells, resulting in T cell exhaustion and impaired anti-tumour responses (Mariathasan et al., 2018). Conversely, some studies suggest that CAFs might also support T cell responses in certain contexts. The dual role of CAFs in either promoting or suppressing T cell activity highlights the complexity of their interactions within the TME. T cell exhaustion describes a state in which T cells show impaired functional response following target recognition. A key mechanism is thought to be the presence of chronic antigen. Exhausted T cells are mainly characterized by low proliferative capacity, low to moderate effector functions, loss of cytotoxic function and increased susceptibility to apoptosis. Phenotypically these cells demonstrate increased expression of inhibitory receptors known as immune checkpoint receptors such as PD-1, CTLA4, TIM-3, LAG-3 and TIGIT (Goulart et al., 2021).

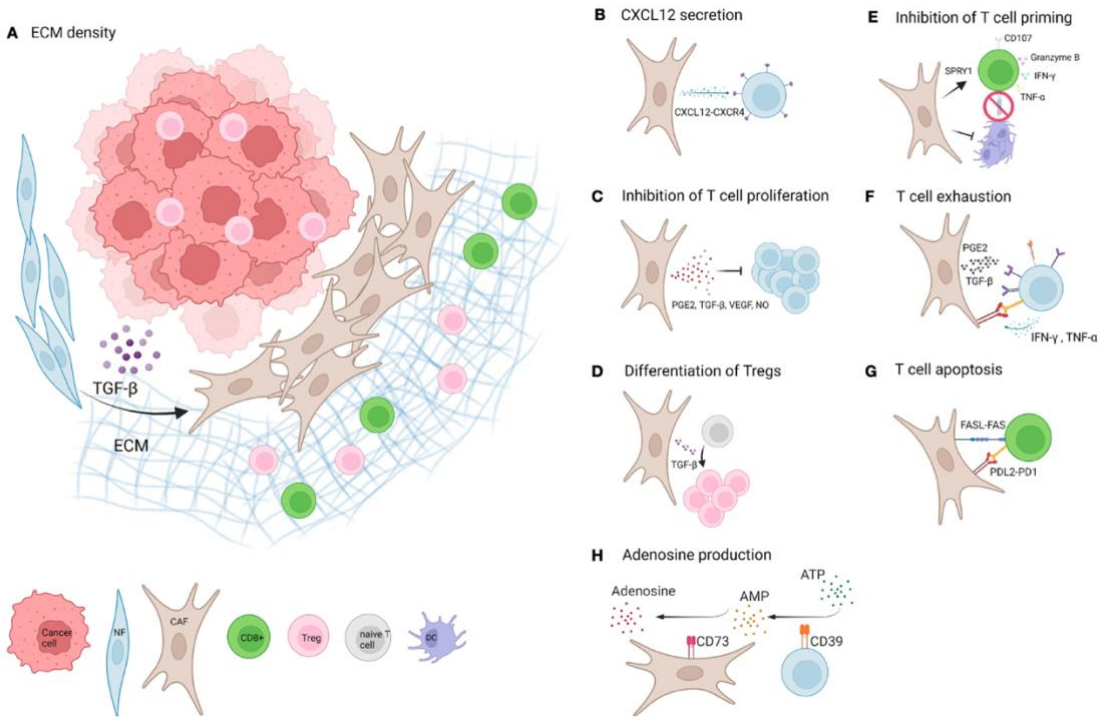


Figure 1.6. Mechanisms of CAF mediated T cell inhibition (Koppensteiner et al., 2022)

1.4 CAF and NK cells

Natural Killer (NK) cells possess a unique ability to target and lyse cells, including cancer cells, without prior sensitization. These cells originate from the common lymphoid progenitor cells in the bone marrow and undergo a series of differentiation stages to acquire their unique functional characteristics. The process involves interactions with specific cytokines, such as interleukin-15 (IL-15), which drives NK cell development, survival, and homeostasis (Vivier et al., 2008). Following maturation in the bone marrow, NK cells migrate to peripheral tissues, including the spleen, liver, and lymph nodes, where they remain poised for rapid responses. The intricate interplay of activating and inhibitory signalling pathways governs NK cell function. This nuanced understanding of NK cell biology has paved the way for their exploitation in various cancer therapies. Approaches such as cytokine therapies, chimeric antigen receptor (CAR)-NK cell therapy, and immune checkpoint inhibitors targeting CTLA-4, PD-1, and PD-L1 showcase the versatility of NK cells in cancer treatment. Notably, emerging evidence suggests that NK cells can also engage with and target cancer-associated fibroblasts, indicating a broader role in the tumour microenvironment (reviewed in (Malchiodi & Weiner, 2021; Megan A. Cooper, 2001)

NK cells exhibit heterogeneity, with CD56dimCD16bright populations representing mature NK cells known for heightened cytotoxicity compared to CD56brightCD16dim counterparts (Megan A. Cooper, 2001). Understanding the diverse functions and interactions of NK cells holds significant promise for advancing cancer immunotherapies.

Pancreatic stellate cells (PSCs) contribute to suppression of natural killer (NK) cell function in pancreatic cancer. In particular, PSCs reduce the levels of CD107a, IFN-gamma, and granzyme B in NK cells, compromising their cytotoxic activity (Huang et al., 2019). Patients with PDAC exhibited a diminished NK cell function, highlighting the potential of therapies involving reactivated or highly active NK cells. (K. Funa, 1984). Furthermore, NK cells within the pancreatic tumour microenvironment exhibit reduced cytotoxicity and adopt a regulatory phenotype marked by interleukin-10 (IL-10) expression, indicative of immunosuppressive properties (Marcon et al., 2020). This underscores the impact of the pancreatic tumour microenvironment on NK cell functionality, potentially contributing to immune evasion and disease progression. Moreover, high NK cell densities in peripheral blood correlate with poor overall survival in advanced PDAC, especially with a high neutrophil: lymphocyte ratio (Fincham et al., 2021; Yang et al., 2018).

The interaction between natural killer (NK) cells and stromal cells has been demonstrated to induce substantial cellular dysfunction and the exclusion of NK cells from tumour tissues, indicating the educational impact of the tumour microenvironment (TME) on NK cells. In the context of pancreatic ductal adenocarcinoma (PDAC), the intricate interplay between NK cells and various stromal and tumour cells plays a pivotal role in determining the cytotoxic efficacy of NK cells. The release of immunosuppressive factors such as transforming growth factor-beta (TGF-β), interleukin (IL)-10, IL-6, IL-23, and IL-1β significantly impairs NK cell cytotoxicity and functionality, ultimately inhibiting the intertumoral proliferation of NK cells. Furthermore, the immunosuppressive TME hinders NK cell-mediated cytokine release, and the release of chemokines may contribute to the sequestration of NK

cells in the pan-stromal compartment, limiting their interaction with tumour cells. These intricate interactions underscore the formidable challenges associated with harnessing NK cell-mediated antitumour responses in the context of PDAC.

There is limited understanding regarding the interactions and impact of cancer-associated fibroblasts (CAFs) on natural killer (NK) cells within the tumour microenvironment (TME). The cytokines and chemokines secreted by CAFs have the potential to influence various immune cell populations, including NK cells. In endometrial cancer models CAFs have been observed to induce greater suppression of the killing activity of allogeneic NK cells compared to normal fibroblasts. This suppression is associated with a reduction in the expression of the cell surface poliovirus receptor (PVR/CD155) when cultured with CAFs, which serves as a ligand for the activating NK receptor DNAM-1 (Inoue et al., 2016).

A study found that NK92 cells co-cultured with tumour-derived aPSCs exhibited a marked decrease in IFN-γ, granzyme B, and CD107a production compared to those co-cultured with nPSCs or without co-culture suggesting that aPSCs potentially suppress NK cell function and cytotoxicity (Huang et al., 2019). Research on melanoma, hepatocellular, and colorectal carcinoma-derived fibroblasts have revealed that CAFs possess the capability to reduce the expression of various NK activating receptors, such as NKp30, NKp44, and NKG2D, on the surface of NK cells. This suppression is mediated through the secretion of prostaglandin E2 (PGE2) and/or indoleamine-2,3-dioxygenase (IDO), resulting in diminished cytotoxic activity of NK cells against tumour target cells (Linda Ziani, 2017; Mirna Balsamo, 2009; Zhang et al., 2019).

IL-6 production by iCAFs suggests their involvement in immune suppression, as IL-6 inhibits NK cell function. Moreover, NK cells are attracted to cells secreting CXCL12, potentially diverting them from PDAC cells to FAP+ CAFs, thus supporting the hypothesis that FAP+ CAFs contribute to immune evasion. RO6874281 targets FAP+ CAFs and enhances NK cell activation via an IL-2 variant, indicating therapeutic interest in targeting NK cell-CAF interactions. Additionally, myCAFs, characterized by high α-SMA levels driven by increased TGF-β expression, inhibit IFN-γ and TNF-α production from NK cells. MDSCs, recruited by CCL2 from FAP+ CAFs, inhibit NK cells via membrane-bound TGF-β, reviewed in (Malchiodi & Weiner, 2021). Activated CAFs, comprising myCAFs, iCAFs, and apCAFs, release cytokines, chemokines, and MMPs to impede immune cell function, particularly suppressing NK cell cytotoxicity against malignant epithelial cells. CAF subpopulations exhibit variable expression of markers such as α-SMA, IL-6, and FAP, offering potential targets to counter CAF-mediated NK cell immunosuppression as shown un figure 1.7 (Malchiodi & Weiner, 2021).

While there is much to learn about the interplay between NK cells and PSCs, previous studies have not adequately addressed key aspects. These include specifying the molecular mechanism of NK cell-CAF interactions, identifying the responsible fibroblasts subpopulation, and evaluating changes in NK cell cytotoxicity following CAF coculture. Moreover, the expression of NK cell ligands on CAFs has been overlooked, impeding potential strategies to improve NK cell targeting of malignant cells.

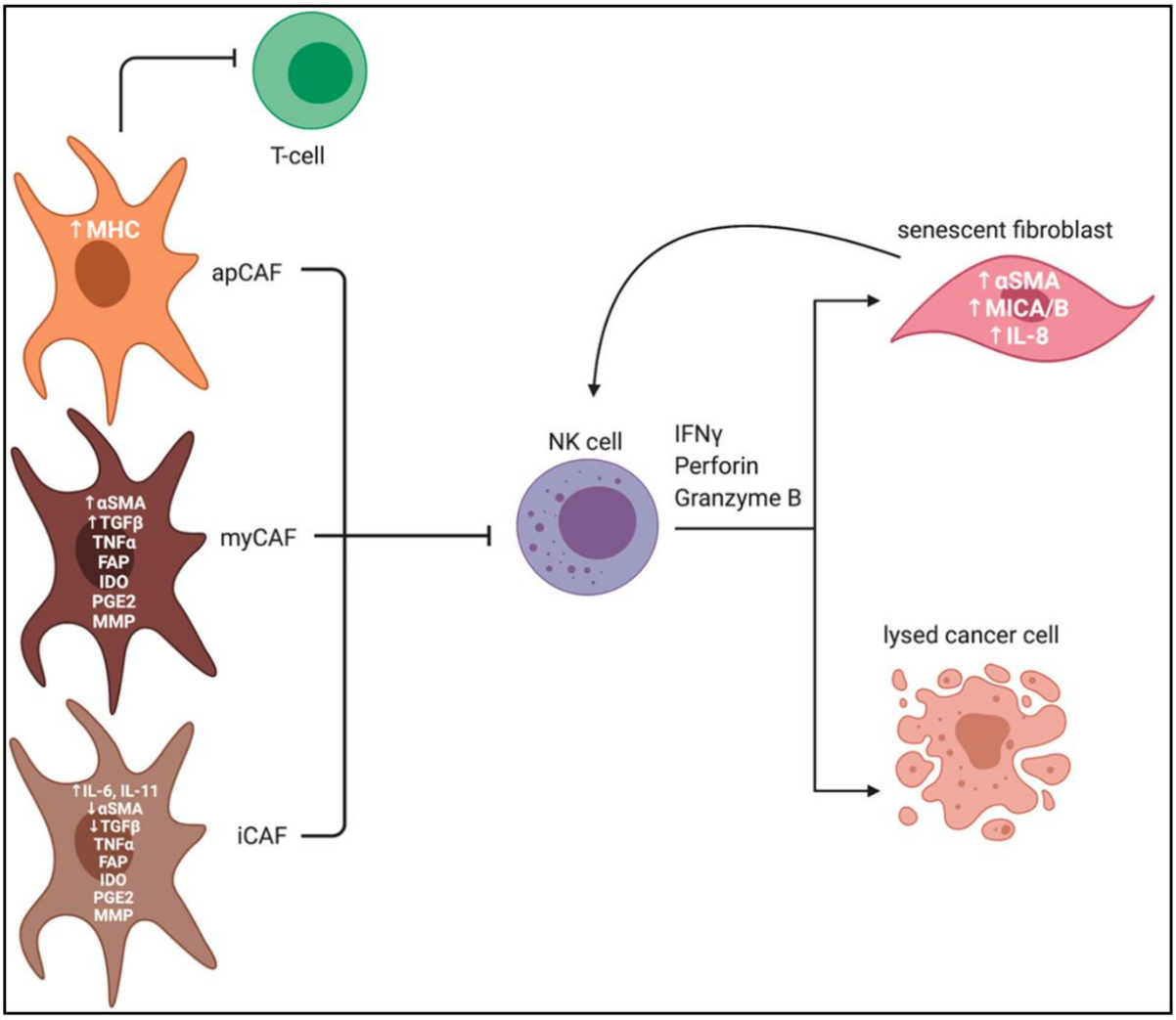


Figure 1.7. Illustration of the known effects of fibroblast subpopulations on NK cell activity (Malchiodi & Weiner, 2021).

1.5 Effect of CAF on lymphocyte migration

Cancer-associated fibroblasts (CAFs) have a profound impact on the adhesion and migration of lymphocytes within the TME, influencing the dynamics of the anti-tumour immune response. The complex interplay between CAFs and lymphocytes involves various signalling pathways, chemokines, and adhesion molecules that regulate immune cell trafficking.

The multistep adhesion cascade is a highly coordinated process that regulates leukocyte recruitment to sites of inflammation. It begins with the selectin family of adhesion molecules, which mediate the initial tethering and rolling of leukocytes on the endothelial surface under shear stress. Selectins, such as L-selectin on leukocytes and P- and E-selectins on activated endothelial cells, facilitate transient and labile interactions, allowing leukocytes to roll along the vessel wall. This rolling slows the leukocytes and positions them for the next steps in the cascade (Ley et al., 2007; Springer, 1994).

A critical step in firm leukocyte adhesion is the activation of integrins, driven by chemokines and their receptors. Chemokines bind to G-protein-coupled receptors (GPCRs) on leukocytes, triggering "inside-out" signalling pathways. This leads to conformational changes in integrins, transitioning them from a low-affinity bent state to a high-affinity extended state. Integrins such as LFA-1 (αLβ2) and VLA-4 (α4β1) can then bind tightly to their ligands, such as ICAM-1 and VCAM-1, expressed on endothelial cells. Chemokines also regulate integrin clustering and spatial organization, ensuring firm adhesion and leukocyte arrest. This interplay between

chemokines, GPCRs, and integrins enables efficient leukocyte recruitment and migration, highlighting their pivotal role in immune surveillance and inflammatory responses (Ley et al., 2007; Springer, 1994).

CAFs contribute to the remodelling of the ECM by secreting factors such as fibronectin, collagens, and proteoglycans. These alterations in the ECM composition affect lymphocyte adhesion and migration. CAF-derived fibronectin, for example, serves as a substrate for lymphocyte adhesion, promoting their interaction with the stromal compartment (Kalluri & Zeisberg, 2006; Öhlund et al., 2014). Additionally, CAFs produce chemokines like CCL2, CXCL12, and CXCL14, which act as chemoattractant for lymphocytes, guiding their migration towards specific areas within the TME (Kalluri & Zeisberg, 2006; Shiga et al., 2015).

The expression of adhesion molecules on CAFs further modulates lymphocyte behaviour. Intercellular adhesion molecule-1 (ICAM-1) and vascular cell adhesion molecule-1 (VCAM-1) expressed by CAFs can interact with lymphocyte integrins, facilitating adhesion and subsequent migration (Mhaidly & Mechta-Grigoriou, 2020; Öhlund et al., 2014). The engagement of these adhesion molecules contributes to the formation of immunological synapses between lymphocytes and CAFs, influencing immune cell activation and function (Kalluri & Zeisberg, 2006). It is important to note that the impact of CAFs on lymphocytes is context-dependent, as different CAF subsets and states may have divergent effects on immune cell behaviour. While some studies highlight the immunosuppressive role of CAFs in impeding lymphocyte infiltration, others suggest that certain CAF populations may support anti-tumour immunity by promoting lymphocyte adhesion and activation (Kalluri & Zeisberg, 2006;

Mhaidly & Mechta-Grigoriou, 2020). Understanding the intricate crosstalk between CAFs and lymphocytes in the TME is critical for devising therapeutic strategies that modulate these interactions to enhance anti-tumour immune responses.

In arthritis, the interplay between fibroblasts and lymphocytes significantly influences the inflammatory microenvironment, contributing to disease progression. Fibroblasts, particularly synovial fibroblasts, play a pivotal role in modulating lymphocyte adhesion and migration within the affected joints. These interactions are orchestrated by various adhesion molecules, chemokines, and cytokines. Synovial fibroblasts, activated during inflammation, express adhesion molecules like ICAM-1 and VCAM-1, promoting the adhesion of lymphocytes to the synovial lining (Bartok & Firestein, 2010; Croft et al., 2019). Additionally, fibroblasts secrete chemokines such as CXCL12, which attract lymphocytes to the synovium (Lefevre et al., 2009). This adhesion and recruitment contribute to the infiltration of lymphocytes, particularly T cells, into the synovial tissue.

Fibroblasts also influence lymphocyte migration within the synovium through the secretion of chemotactic factors. The chemokine CXCL13, produced by synovial fibroblasts, plays a crucial role in organizing lymphoid structures within the synovium and facilitating lymphocyte movement (Croft et al., 2019; Lefevre et al., 2009) Additionally, fibroblasts contribute to the production of matrix metalloproteinases (MMPs), which can degrade the extracellular matrix and create pathways for lymphocyte migration (Bartok & Firestein, 2010). In pancreatic adenocarcinoma, dense collagen networks act as physical barriers, hindering the migration of activated

T cells and potentially impeding the effectiveness of T-cell-based immunotherapies (Hartmann et al., 2014; Jiang et al., 2016).

In rheumatoid arthritis (RA), fibroblast-like synoviocytes (FLS), a subtype of fibroblasts in the synovial lining, contribute to lymphocyte recruitment and retention in the synovium. McGettrick's work emphasizes the active participation of FLS in facilitating lymphocyte adhesion to the endothelium and guiding their migration into the joint (McGettrick et al., 2009). FLS express adhesion molecules such as ICAM-1 and VCAM-1, creating a permissive environment for lymphocyte adhesion lymphocyte adhesion to the endothelium and guiding their migration into the joint (Filer et al., 2017; McGettrick et al., 2009). Moreover, McGettrick's research sheds light on the dynamic interactions between fibroblasts and lymphocytes during the formation of lymphoid-like structures within the inflamed synovium, known as ectopic lymphoid follicles. These structures contribute to the perpetuation of chronic inflammation in RA (McGettrick et al., 2012).

The influence of fibroblasts extends beyond adhesion, as they modulate lymphocyte migration within the joint. McGettrick has highlighted the role of chemokines, particularly CXCL12, produced by FLS, in guiding lymphocyte movement (Filer et al., 2017; McGettrick et al., 2012). This chemotactic axis contributes to the positioning of lymphocytes within the synovium, fostering the inflammatory milieu characteristic of arthritis. Understanding the intricate crosstalk between fibroblasts and lymphocytes in arthritis provides valuable insights for developing targeted therapeutic strategies aimed at disrupting these interactions and mitigating the inflammatory processes underlying rheumatic diseases.

1.6 Targeting CAFs for clinical benefit and future perspectives

Targeting CAFs holds significant promise for clinical benefit and future therapeutic interventions. Despite ongoing efforts, there remains a considerable need to comprehensively delineate CAF subpopulations across various human cancers beyond pancreatic and breast carcinomas. A deeper understanding of CAF plasticity, origins, and interactions is imperative. Nonetheless, with the substantial volume of data amassed thus far, the field is poised to translate these evolving CAF atlases into actionable therapeutic targets. Rather than focusing solely on specific CAF subtypes or cell origins, targeting key signalling molecules and pathways within the heterogeneous mesenchymal tumour microenvironment may offer a more effective therapeutic approach. Moreover, directing interventions towards the cellular sources of CAFs presents another avenue for precision treatment strategies. This shift towards a nuanced understanding of CAF biology holds great potential for advancing cancer therapy.

1.7 Hypothesis

The hypothesis of this thesis is that fibroblasts modulate T and NK cell phenotype, adhesion, and migration within the tumour microenvironment. Fibroblasts, as key stromal cells, interact with immune cells through direct contact and secretion of cytokines and chemokines. These interactions may alter the activation state, surface marker expression, and functional capabilities of T and NK cells, influencing their ability to adhere to and migrate through the extracellular matrix. By understanding the mechanisms of fibroblast-mediated modulation, we can gain insights into immune evasion strategies employed by tumours and identify potential therapeutic targets to enhance anti-tumour immune responses.

To test this hypothesis, I undertook the following three Aims and Objectives:

- **Aim 1 (Chapter 3): Explore the phenotype and heterogeneity of CAFs in human PDAC**

  Objectives

  - To assess the expression of a range of fibroblast-associated proteins on primary fibroblast cells isolated from primary PDAC tumours
  - To assess the interrelationship of these proteins and their potential role in functional responses
    Relate PDAC fibroblast expression to the clinical status of patients

- **Aim 2 (Chapter 4): Determine the functional impact of interaction of CAFs/ANFs with NK and T cells**

  - To assess the impact of CAF engagement with T cell and NK cells on the profile of immune cell proliferation
  - To assess the impact of CAF engagement with T cell and NK cells on the profile of immune cell profile and cytokine production

- **Aim 3 (Chapter 5): Determine the effect of CAFs/ANFs on lymphocytes Adhesion & migration**

  - To incubate CAF with cytokines to generate polarised functional subsets that mimic those seen within the tumour microenvironment
  - To assess the ability of these cells to modulate the pattern of immune cell migration in vitro

Chapter 2: Material & Methods

2.1 Ethics and recruitment

This project is part of a larger study on pancreatic adenocarcinoma, titled "*A nonvaccine approach for the treatment of pancreatic cancer*". Ethical approval by Birmingham Local Research Ethics Committee for this study was REC 16/WM/0214). Patients with primary PDAC were recruited at University Hospitals Birmingham NHS Foundation Trust, Queen Elizabeth Hospital (Birmingham, United Kingdom). Patients are identified from the central specialist pancreatic MDT, to which all potential patients are referred to for clinical discussion. If surgery is the chosen option, patient is asked to attend clinic, where consent for surgery is taken. At this point, the HPB Consultant informs the patient on the possibility to take part into the research study and provide the Patient Information Sheet (PIS). Consent for taking part into the research is then signed on the day of the procedure studies were conducted in accordance with the Declaration of Helsinki.

The clinical data for the samples used in phenotyping are presented in Table 2.1.

CAF/ANF	Patient	TISSUE PATHOLOGY	ChemoT_regimen	Description	Gender, M=0, F=1,	Age at consent	Date of consent	Date surgery or consent if no surg	Size tumour Max diameter (mm)	Differentiation 1=Well, 2=Well-Mod, 3= Mod, 4=Mod-Poor, 5=Poor	T stage (AJCC 8th Edition)	N stage (AJCC 8th Edition)
T/N	S359	PDAC	No		0	61	13/06/2022	13/06/2022	25	1	2	1
T/N	S361	PDAC	No		0	70	30/06/2022	30/06/2022	22	3	2	0
T/N	S362	PDAC	No		0	75	01/07/2022	01/07/2022	32	3	2	2
T/N	S368	PDAC	Yes	Folfirinox	0	63	04/08/2022	13/09/2022	17	N/A	2	1
T/N	S369	PDAC	No		1	49	05/08/2022	05/08/2022	37	3	2	1
T/N	S377	PDAC	No		0	76	03/10/2022	03/10/2022	22	5	2	0
T/N	S378	PDAC	No		1	82	06/10/2022	06/10/2022	22	3	2	0
T/N	S380	PDAC	No		0	58	20/10/2022	20/10/2022	23	3	2	1
T/N	S381	PDAC	No		1	55	21/10/2022	21/10/2022	32	3	2	2
T/N	S382	PDAC	No		1	63	24/10/2022	24/10/2022	37	3	2	2
T/N	S391	PDAC	No		0	81	30/11/2022	30/11/2022	24	3	2	1
T/N	S401	different cancer	No	Ampullary adeno	0	75	16/02/2023	06/03/2023	39	3	3a	1a
T/N	S405	PDAC	No		1	78	09/03/2023	09/03/2023	21	4	2	0
T/N	S413	PDAC	Yes	6 cycles FOLFIRIN	1	68	05/04/2023	06/04/2023	18	N/A	1c	0
T/N	S415	PDAC	YES	YES (Neo adjuver	0	63		25/04/2023	30	N/A	2	1
T/N	S418	PDAC	YES	YES (Neo adjuver	1	70		03/05/2023	21	N/A	2	1
T/N	S338	PDAC	YES	Yes (8 cycles FO	1	55	24/01/2022	01/02/2022	35	N/A	2	1
T/N	S340	PDAC	No		0	64	11/02/2022	11/02/2022	32	3	2	2
T/N	S342	PDAC	No		1	75	03/03/2022	11/03/2022	23	3	2	1
T/N	S344	PDAC	No		1	51	08/03/2022	10/03/2022	24	5	2	2
T/N	S350	PDAC	YES	Yes (6 cycles FO	1	60	06/09/2023	25/04/2022	27	N/A	2	1
T/N	S351	PDAC	NO		0	74	08/08/2023	27/04/2022	12	3	1	2
T/N	S352	different cancer	YES	Yes (8 cycles FO	0	73	12/09/2023	03/05/2022	19	N/A	2	0

Table 2.1. Clinical data of samples used in phenotyping.

2.2 Isolation of Adjacent Normal Fibroblasts (ANFs) and Cancer associated fibroblasts (CAFs) from PDAC patients.

The surgical specimen was sent fresh from the operating theatres to Pathology, where a dedicated PDAC Pathologist processed the specimen and provided the adjacent normal and tumour pancreatic tissue. The two tissues were then placed in 1 ml of MACS tissue storage solution overnight at 4 °C, to which I added Primocin (200 µl) and PenStrep (P/S) (1 ml) antibiotics. The storage solution allowed optimized preservation of fresh tissue samples without altering or losing the functional capacities of cells.

The next day, the two tissues were cut into small pieces, approximately 2–3 mm, and placed in 5 ml of filtered prewarmed media (DMEM + 10 % FCS + 1 % P/S) using a 0.2 µm filter. Collagenase/Hyaluronidase (1X), Liberase TL (1X), and Benzonase (50 U/ml) were added to break down the native collagen and hyaluronan that held the tissue together, enhance the quality, viability, functionality, and reproducibility of isolated cells, and limit cell clumping during the preparation of cell mixtures. Both tissues were added to gentleMACS tubes, agitated on the gentleMACS dissociator using the “Human Tumour 1 Programme,” and incubated in a 37 °C water bath for 30 minutes. This step was repeated twice with the “Human Tumour 1, 2, and 3 Programmes. The digested cells were passed through a prewetted 70 µm filter into a new 50 ml falcon tube, and the filter was washed with 2–3 ml of media to ensure complete cell collection. A total of 15 ml of DMEM was added, and the suspension was centrifuged at 475 g for 5 minutes to pellet the cells. The cells were then counted using a hemacytometer. The two digested tissues were either used for phenotyping via flow cytometry (FACS), fibroblast culture, or cryopreservation. Cryovials in 1 ml of 90 % FBS + 10 % DMSO in liquid nitrogen for future use.

Reagents	Catalogue number	Company
MACS Tissue Storage solution	130-100-008	Miltenyl Biotec
Primocin	Ant-pm-1	InvivoGen
PenStrep (P/S)	P4458-100ML	Sigma
DMEM	D6429-500ML	Sigma
FCS	A5256801	Gibco
0.2uM filter	16534-K	Sartorium
Collagenase/Hyaluronidase	07919	Stemcell
LiberaseTL	05401020001	Merck
Benzonase	E1014-25KU	Merck
gentleMACS C Tubes	130-093-237	Miltenyl Biotec
gentleMACS Dissociator	130-093-235	Miltenyl Biotec
70uM Easy strainer	542070	Greiner Bio-One
50ml Falcon	62559001	Strarstedt
haemocytometer	390497	SLS
FBS	A5256801	Gibco
DMSO	D2650-100ML	Sigma
Cryovials	17190	ThermoFisher
Centrifuge 5810R	5811000065	Eppendorf

Table 2.2. Used Reagents with Catalogue Numbers and Companies

2.3 Culture of primary ANFs and CAFs

Between 0.2 and 1 × 10^6 digested primary ANFs and CAFs cells were cultured in a 12-well plate and incubated at 37 °C in 20 ml of tissue culture media (DMEM + Sodium Pyruvate [1X] + 10 % FCS + 1 % GlutaMAX + 1 % P/S + 1 ml Primocin) for a period of 1 to 3 weeks until they became 70–80 % confluent. They were then transferred to 6-well plates, 25 cm dishes, and subsequently 75 cm dishes. Culturing the primary cells initially in 12-well plates ensured that the cells were close enough to send and receive chemical messages, supporting their growth and proliferation. The proliferation rate varied between ANFs and CAFs from the same patient as well as between patients.

The confluent primary cells in 75 cm dishes were washed with 10 ml of PBS, then trypsinzed with Trypsin (1X) to dissociate and detach the cells from the flasks. Fifteen millilitres of DMEM were added, and the cells were centrifuged at 475 g for 5 minutes to pellet the ANFs or CAFs. Cells were then counted on a hemacytometer and used for immortalization, phenotyping, or cryopreserved in 1 ml of 90 % FBS + 10 % DMSO in liquid nitrogen for future use.

Reagents	Catalogue number	Company
12 well plate	3513	Costar
DMEM	D6429-500ML	Sigma
Sodium pyruvate (100X)	11360-070	Gibco
GlutaMAX (100X)	35050-038	Gibco
PenStrep (P/S)	P4458-100ML	sigma
Primocin	Ant-pm-1	InvivoGen
6 well plate	3516	Costar
25cm flask	430168	Corning
75cm flask	430720U	Corning
Trypsin (1X)	12605-010	Gibco
Centrifuge 5810R	5811000065	Eppendorf
DMSO	D2650-100ML	Sigma
Primocin	Ant-pm-1	Invivogen
PenStrep (P/S)	P4458-100ML	Sigma
FCS	A5256801	Gibco
PBS	D8537-500ml	Sigma-Aldrich

Table 2.3. Used Reagents with Catalogue Numbers and Companies

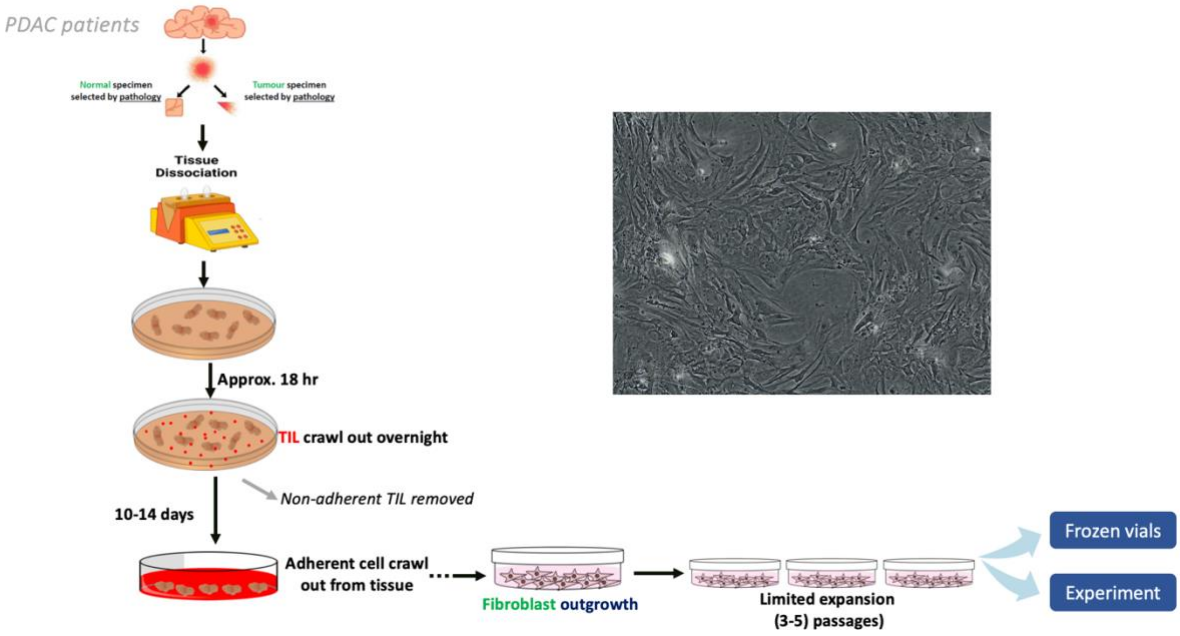


Figure 2.3. Protocol design for fibroblasts culture using BioRender program.

2.4 Primary ANFs and CAFs immortalisation using SV40 and hTERT vectors.

Immortalized cells are cells that have acquired mutations in a manner that renders them immune to senescence; thus, they can divide and proliferate indefinitely and cultured for generations without changing their phenotype or genotype. The common immortalisation methods include the transfection of Telomerase reverse transcriptase (hTERT), the Simian virus T-antigen (SV40) or combination of both into human primary cells:

- **Expression of (hTERT) protein:** in normal physiological cell division, telomeres shorten after each division until the cell dye. Expressing the human hTERT protein leads to lengthen telomeres and promote cell survival and indefinite proliferation.
- **Expression of SV40 T-antigen:** The inactivation of Retinoblastoma (Rb) and p53 proteins prevent cell senescence and apoptosis; thus, promotion of cell immortalization.
- **Combined approach:** However, these processes are not always effective when manipulating them separately for some cells. Combining the two methods produce best results. In this project we used both methods separately and they work perfectly.

The subsequent sections outline the procedures I undertook to immortalize fibroblasts.

2.4.1 Plasmid extraction

We used four vectors: pBABE-puro-hTERT, pBABE-hygro-hTERT, pBABE-neo-hTERT and pCL-Amp.

Reagents	Bacterial resistance	Catalogue number	Company
pBABE-puro-hTERT	Ampicillin	1771	Addgene
pBABE-hygro-hTERT	Ampicillin	1773	Addgene
pBABE-neo-hTERT	Ampicillin	1774	Addgene
pCL-Amp	Ampicillin	NBP229541	Fischer scientific

Table 2.4. Used Reagents with Catalogue Numbers and Companies.

a. LB and Agar culture media preparation

Eight tablets of LB and four tablets of Agar were added to 400 ml and 200 ml of distilled water respectively, and then sterilized by autoclaving at 121 °C (250°F) for a period of 2 hours. The molten agar was cooled in the water bath prior to adding the Ampicillin antibiotic.

In sterile condition using the hood, 150 μl of ampicillin antibiotic was added in 150 ml of the cooled Agar (1 μl per 1 ml) to allow the selection of bacteria with resistance to Ampicillin. The Agar-Ampicillin mixture was poured into 4 Petri dishes and then swirled to remove bubbles and ensure an equal distribution of agar over the plates. The 4 Petri dishes were capped and placed on bench at room temperature to dry. After overnight

drying, the plates were wrapped with parafilm to reduce condensation and then stored at 4 °C until use.

Reagents	Catalogue number	Company
LB tablets	L7275-500TAB	Sigma
Agar tablets	BR0014G	Oxoid
Ampicillin antibiotic	A9518-5G	Sigma
Petri dish	821473	Sarstedt
Parafilm	PM-992	Bemis

Table 2.5. Used Reagents with Catalogue Numbers and Companies.

b. Plasmid culture

The Petri dishes prepared according to the procedure described in section 2.4.1.a. were labelled with the plasmid names and the date in the bottom of each plate. A small portion of pBABE-puro-hTERT, pBABE-hygro-hTERT, pBABE-neo-hTERT and pCL-Amp plasmids were taken from the original vials with a pipette tip and were stripped and spread carefully over a section of the plate without digging into the agar, then were incubated at 37 °C overnight for the development of colonies This step was done under sterile conditions. The next day, single colonies were observed growing on the solid medium, as shown in the images below, and were then used for plasmid extraction.

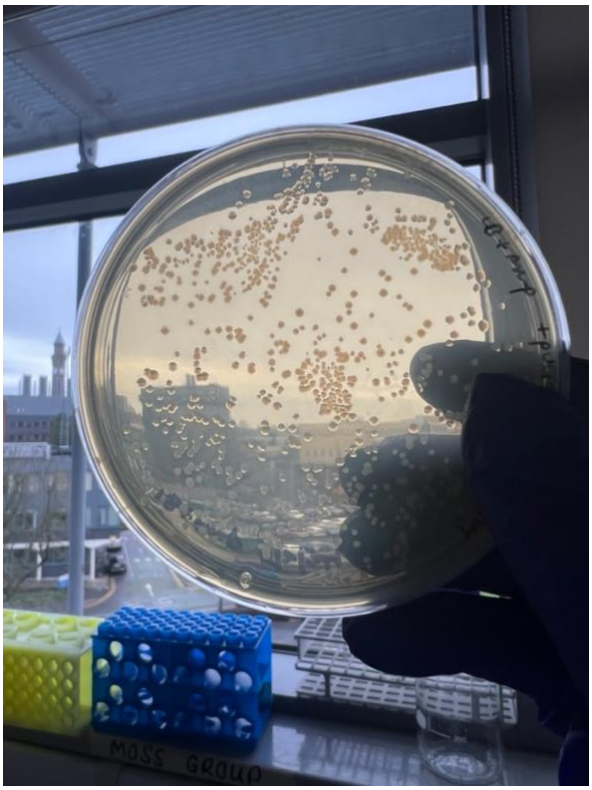


Figure 2.1. Developed Colonies on a Petri Dish.

c. Starter culture preparation

New tube containing 5 ml of LB media were prepared and then a single colony was picked from freshly streaked plate and inoculate a starter culture with 5 μl of the Ampicillin antibiotic. The tubes were chook at 37 °C, 150 rotation per minute (RPM) for almost 6 hours.

5 ml of each grown vector “Start Culture” were added to an Erlenmeyer with 200 ml LB and 200 μl Ampicillin, then shook at 37 °C, 150RPM overnight. The media in the Erlenmeyer was cloudy which proof the bacterial growth. and the resulted grown bacteria were used for plasmid purification and a very small portion (-700 ul) were stocked in 300 μl of glycerol in -80 °C. The addition of glycerol stabilizes the frozen bacteria, preventing damage to the cell membranes and keeping the cells alive.
This procedure was repeated for all the 4 vectors.

Reagents	Catalogue number	Company
pCL-Amp	NBP229541	Fischer scientific
Shaker (INR-201)	A060175	Sigma Aldrich
Glycerol	G9012-100ML	Sigma
Tube for plasmid	SLE7520	SLS

Table 2.6. Used Reagents with Catalogue Numbers and Companies.

d. Plasmid extraction using Endo-Free Maxi kit.

The LB cultures prepared in section 2.4.1.c were harvested and centrifuged at 6000 x g for 15 mins at 4 °C and the pellet was resuspended in 10 ml Buffer P1 (included in the kit). 10 ml Buffer P2 were added and mixed thoroughly by inverting 4-6 times and incubated at room temperature (RT) for 5minutes. The colour turned blue. Next, 10 ml of chilled buffer P3 were added and mixed until it is completely colourless. The lysate was poured into the barrel of the QIAfilter Cartidge and incubated again at room temperature (RT) for 10 minutes. The cell lysate was filtered into a 50 ml tubes and 2.5 ml of Buffer ER were added to the filtered lysate and mixed by inverting the tube and then incubated on ice for 30 mins. After that, a QIAGEN-tip 500 was equilibrated by applying 10 ml of Buffer QBT and allowed the column to empty by gravity and washed with 2 x 30 ml Buffer QC. The DNA was eluted with 15 ml Buffer QN into a 30 ml endotoxin-free tube, precipitated by adding 10.5 ml RT isopropanol to the eluted DNA and centrifuged at ≥ 15,000 x g for 30 minutes at 4°C. Finally, the DNA pellet was washed with 5 ml of endotoxin-free RT 70% ethanol and centrifuge again at 15,000 x g for 10 minutes and the pellet was air dried and dissolved in 200 μl of endotoxin-free Buffer TE. DNA concentration was detected and quantified with Nanodrop Spectrophotometer (v1.8, ThermoFischer Scientific, USA) and recorded.

Reagents	Catalogue number	Company
Centrifuge (S0RVALLRCZLT)	9903426	Sorvall
Endo-Free Maxi kit	12362	Qiagen
Isopropanol	200-661-7	Fisher chemical
Ethanol	20821.330	VWR chemical
Nanodrop Spectrophotometer	v1.8	ThermoFischer

Table 2.7. Used Reagents with Catalogue Numbers and Companies.

2.4.2 Virus culture

At first, 2.5 x 10^6 of frozen Phoenix cells were thawed and cultured in DMEM (10 %FCS + 1% P/S) in a 150 cm^2 flask for 48 hours until they become no more than 60% confluent. Afterward, the Phoenix cells were trypsinized with 5 ml Trypsin (1X) and seeded at 3 x 10^6 in 75 cm^2 flask in antibiotic free DMEM. Next day, Phoenix cells were transfected using FugeneHD (See next section 2.4.3).

Reagents	Catalogue number	Company
Phoenix cells	18324012	Thermo Fisher
PenStrep (P/S)	P4458-100ML	Sigma
DMEM	D6429-500ML	Sigma
FCS	A5256801	Gibco
150 cm^2 flask	430724U	Corning
Trypsin (1X)	12605-010	Gibco
75cm^2 flask	430720U	Corning

Table 2.8. Used Reagents with Catalogue Numbers and Companies.

2.4.3 Viral transfection

In an Eppendorf tube, 4.5 μg of purified pCL-Amph DNA and 3 μl of Fugene per 1 μg of DNA of interest (pBABE-puro-hTERT, pBABE-hygro-hTERT, pBABE-neo-hTERT) was added to 500 μl of OptiMEM and then incubated at room temperature for 15mins. Next, Phoenix cells media was removed and replaced with fresh 6 ml of antibiotic free DMEM and then the DNA/Fugene mixture was added and incubated at 37 °C overnight.

The following day, 6 ml of media containing the secreted virus was collected and centrifuged at 845 x g for 5 mins then filtered using 0.45 μM filter and froze in 4°C.

For more virus collection, the media in the same flasks was replaced with fresh DMEM medium antibiotic deprived antibiotic and incubated at 37 °C overnight. 24 hours later, the same procedure was followed for virus collection and then mixed with the frozen media in 4 °C and frozen in -80°C for future use.

Reagents	Catalogue number	Company
pCL-Amph DNA	NBP229541	Fischer scientific
FugeneHD	72050	Promega
DMEM	D6429-500ML	Sigma
0.45uM filter	E4780-1456	Star lab

Table 2.9. Used Reagents with Catalogue Numbers and Companies.

2.4.4 Antibiotic killing Curve

Before proceeding to fibroblast transduction step, 500,000 PDAC fibroblasts were cultured into 24 well plate. After a 60-80% confluency rate, fibroblasts were subjected to increasing concentration of selection antibiotic as shown in the table below to determine the minimum concentration that can kill the cells in a specific period.

Upon testing various concentrations, I determined the optimal concentrations for Puromycin to be 0.5 μg/ml, G418 to be 100 μg/ml, and Hygromycin B to be 50 μg/ml. All three antibiotics conferred resistance within 5-6 days.

Antibiotic	Resistance gene	Concentration range (ug/ml)	Killing curve concentration (ug/ml)	Selection time
Puromycin	Puromycin	0.5, 1, 2, 4 and 8μg/ml	0.5	5-6 days
G418 (Geneticin)	Neomycin	50, 100, 200, 400 & 800 μg/ml	100	5-6 days
Hygromycin B	Hygromycin B	50, 100, 200, 400 μg/ml	50	5-6 days

Table 2.10. Antibiotic Killing curve for 3 antibiotics, Puromycin, G418 and Hygromycin.

Reagents	Catalogue number	Company
24 well plate	3526	Costar
OptiMEM	31985-047	Gibco
Puromycin	P9620-10ml	Sigma
G418 (Geneticin)	10131-035	Gibco
Hygromycin	10687010	Thermo Fisher
Hexadimethrine Bromide (Polybrene)	H9268-5G	Sigma aldrich

Table 2.11. Used Reagents with Catalogue Numbers and Companies.

2.4.5 Transduction

250,000 ANFs and CAFs fibroblasts were seeded into a 6-well plate and divided into 5 conditions: control with fibroblasts only, Mock with OptiMEM + Fugene, Neo-hTERT, Puro-hTERT, and Hygro-hTERT. After 24 hours of incubation, 1 ml of prepared virus from section 2.4.3 was added to each well, along with 1 ml of DMEM (10 % FCS + 1 % P/S + 1 % Glutamax + 1 ml Primocin) and 1.6 μl of fresh Polybrene per 1 ml of virus. The plate was spun down at 32 °C, 845 x g for 30 minutes to facilitate virus transduction and then further incubated for 48 hours. Antibiotic selection reagent was introduced to the fibroblasts, followed by additional incubation for several days. Cell viability and resistance were assessed every two days under a microscope.

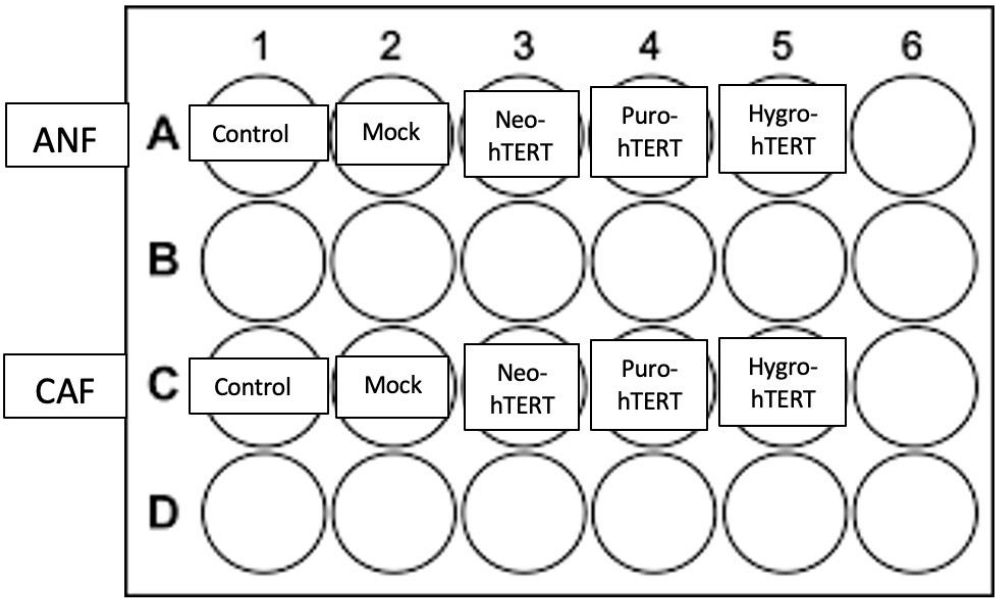


Figure 2.2. Experimental design for virus transduction.

2.5 FACS analysis of freshly digested ANFs and CAFs

The single colour compensation control was prepared by adding ½ test antibody conjugate to each tube, 50 μl of BSB and 1 drop of compensation beads. Mixed well by vortexing and then incubated at 4 °C for 30 min in the dark. Washed with 3 ml PBS and centrifuged at 450 x g for 5 mins and then the supernatant was removed and 300 μl of PBS was added to each tube and finally run Symphony flow cytometry (BD Bioscience, USA) or kept at 4 °C for up to 1 week.

Reagents	Catalogue number	Company
Brilliant stain buffer (BSB)	563794	BD Horizon
PBS	D8537-500ML	Sigma-Aldrich
FACS tubes	352058	Falcon
Fixable Viability Stain FVS575V	565694	BD
FcR block	422302	Biolegend
PBS	D8537-500ml	Sigma-Aldrich
BSA	A7906-100G	Sigma-Aldrich
EDTA	T2601-100ML	Merck
True-NuclearTM 1X Fix	424401	Biolegend
True-Nuclear™ 1X Perm buffer		
FACS flow cytometry	BD FACS Symphony A3	BD
Heater block	Accublock	LabNet

Table 2.12. Used Reagents with Catalogue Numbers and Companies.

2.5.1 Surface staining

Approximately 0.2 x 10^6 to 0.5 2 x 10^6 freshly digested ANFs and CAFs cells were collected as described in section 2.2 and transferred to FACS tubes. Then washed with PBS and centrifuged at 611 x g for 10 min. 1 μl of Fixable Viability Stain (FVS575V) and 5μl of FcR block were added and then incubated for 10 minutes. The surface staining antibodies were prepared in 50 μl BSB and added to each ANF and CAF samples. Details of used antibodies and their fluorochromes can be found in the table 2.12. 30 mins later, the cells were washed with 4ml MACS buffer (PBS + 0.5% BSA + 2 mM EDTA) and centrifuged at 611 x g for 5 mins then washed twice with PBS before moving to nuclear staining step.

Marker/Antibodies	Clone	Fluorescence channel	Catalogue number	Company	Concentration (µl)
CD90	5E10	BUV395	566219	BD Biosciences	2
HLA-ABC	G46-2.6	BUV496	741156	BD Biosciences	2
CD26	M-A261	BUV615	751490	BD Biosciences	2
CD34	581	BUV661	749902	BD Biosciences	2
CD106 (VCAM-1)	51-10C9	BUV737	749672	BD Biosciences	2
CD45	HI30	BUV805	612891	BD Biosciences	1
a-SMA	1A4	BV421	IC1420V-100	R&D	2
HLA-DR, DP, DQ	Tu39	BV480	746360	BD Biosciences	2
Viability	---	575V	565694	BD Biosciences	1
Ki-67	B56	BV650	563757	BD Biosciences	2
CD74	LN2	BV711	743735	BD Biosciences	2
PDGFR-a(CD140a)	aR1	BV750	747232	BD Biosciences	2
PDGFR-b (CD140b)	28D4	BV876	743038	BD Biosciences	2
Pan-Cytokeratin	REA831	FITC	130-112-743	Miltenyi	2
CD105	266	BB700	566529	BD Biosciences	2
C3	6C9	PE	567667	BD Biosciences	2
PDPN	NC-08	PD/Dazzle594	337028	BioLegend	2
CD29	TS2/16	PE/Cy7	303026	BioLegend	2
Cadherin-11	16G5	APC	368706	BioLegend	2
FAP	427819	AF700	FAB3715N	R&D	2
CD31	WM59	APC-Cy7	563653	BD Biosciences	2

Table 2.13. Fibroblasts flow cytometry panel.

2.5.2 Nuclear staining

1 ml of True-Nuclear™ 1X Fix was added to each tube, vortexed and incubated at RT in the dark. After 45 minutes incubation, 2 ml of True-Nuclear™ 1X Perm buffer was added and then centrifuged at 685 x g at RT for 5 min. This step was repeated twice. Then, the pellet was resuspended in 100 μl of the True-Nuclear™ 1X Perm buffer and intracellular antibody mix was added, vortexed and incubated at RT for at least 30 minutes. Intracellular master antibody mix was prepared in 50 μl 1X Perm Buffer. Next, the cells were washed with 2 ml True-Nuclear™ 1X Perm buffer and then with 4ml MACS buffer and centrifuged at 685 x g for 5min after each wash. Finally, the cells were resuspended in 200 μl MACS buffer and acquired on FACS flow cytometry. At least 30,000 events were acquired per sample and analysed offline using Flowjo v5.0 software. Figure 2.4 in section 2.5.3 illustrates the gating strategies used to select live cells and Fibroblasts.

2.5.3 Live and dead gating strategy

Fresh isolated ANFs and CAFs cells as described in section 2.2 were split into equal volumes in two Eppendorf tubes, Live and dead cells. Dead cells were heated in heater block for 20 minutes at 60 degrees then mixed with live cells and stained with Viability dye (BV575V). The mixture was run in FACS flow cytometry and gated on live and dead cells control for control samples.

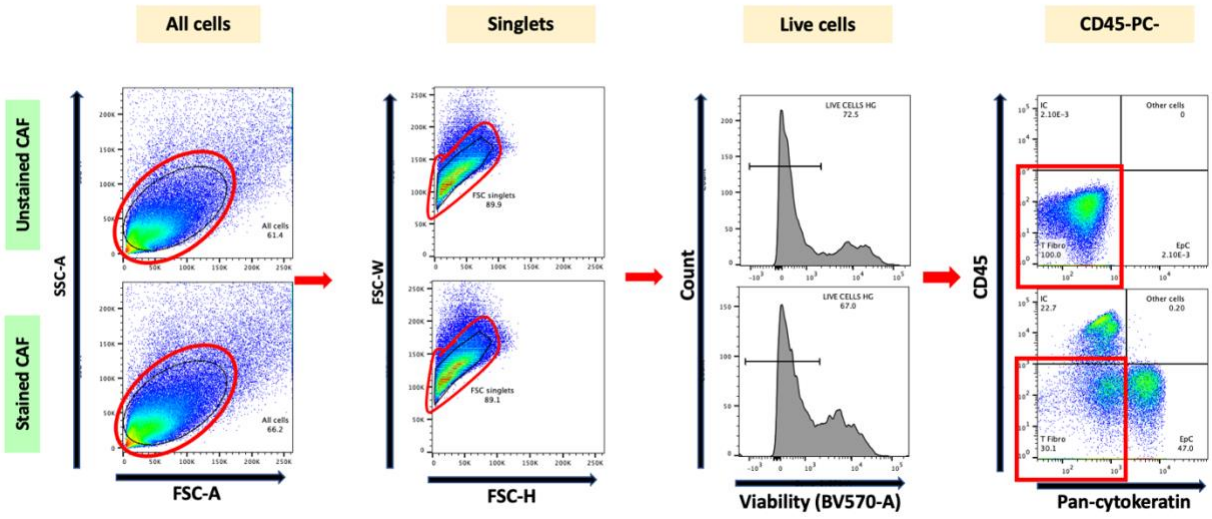


Figure 2.3. **Gating strategy for fibroblasts flow cytometry analysis.**

Gating strategies shown for the detection of fibroblasts ($CD45^{neg}$ Pan-$cytokeratin^{neg}$). At first, all cells were gated and subsequently Singlets were selected using SSC-W versus FSC-H. Live cells were gated using viability dye marker ($BV570\text{-}A^{neg}$). Then, Immune cells and epithelial cells were eliminated using $CD45^{pos}$ and Pan-$cytokeratin^{pos}$ respectively. The negative population ($CD45^{neg}$ Pan-$cytokeratin^{neg}$) are Fibroblasts.

2.5.4 Statistical analysis

Statistical analysis was performed with Flowjo™10.8.1 software and Prism 8 (GraphPad, California USA), both for Mac OS X operating system.

I used “Shapiro-Wilk tests” and “QQ plots” to assess the normal distribution of the data. Following this, for normally distributed data, I performed “t-tests” for pairwise comparisons, while for non-normally distributed data, I applied “non-parametric equivalents”, such as the “Mann-Whitney U test”.

When analysing multiple groups, I used “One-Way ANOVA” for normally distributed data, followed by “Tukey’s post-hoc test” to account for multiple comparisons. For non-parametric data, I utilized the “Kruskal-Wallis test” followed by “Dunn’s post-hoc test”. Additionally, when comparing data across two factors or independent variables, I used “Two-Way ANOVA”. This test allows for the evaluation of interactions between the two factors while considering their individual effects on the outcome variable. Post-hoc analysis following Two-Way ANOVA was performed using “Tukey’s test” for pairwise comparisons.

These methods were chosen to ensure that the appropriate statistical tests were applied depending on the distribution of the data.

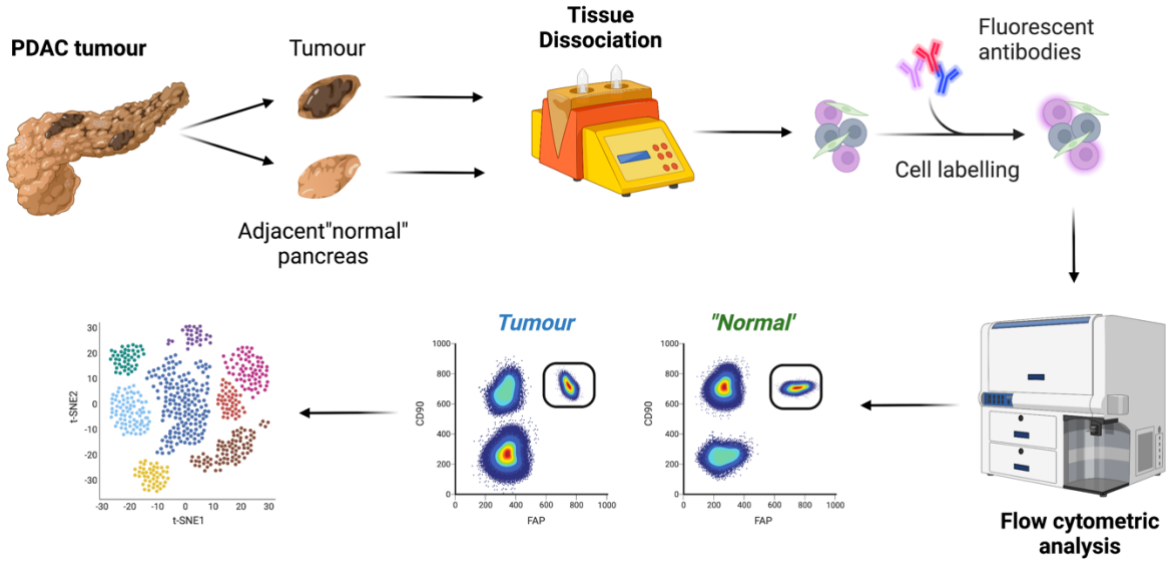


Figure 2.4. Protocol Design for fibroblasts isolation and phenotyping using BioRender program.

2.6 Conditioned-Media (CM) collection from ANFs and CAFs

2.5 x 10^6 CAFs and ANFs were cultured in 75cm^2 flasks with DMEM (10 % FBS + 1% P/S + 1 ml Primocin). Fibroblasts were utilized at lower passages (P3-P6). When the cells are almost 70-80 % confluent, they were washed three time with PBS to remove all debris and the high amounts of protein supplements in the culture media and then 8ml of DMEM deprived serum (only with 1 % P/S + 1 ml Primocin) were added and incubated at 37 °C for 48 hours. The supernatant was collected and centrifuged at 300 x g for 10minutes at 4°C and filtered using 0.2 □M filter. The conditioned media was kept at -80 °C until future use.

Reagents	Catalogue number	Company
75cm^2 flasks	430720U	Corning
DMEM	*D6429-500ML*	Sigma
FBS	A5256801	Gibco
Pen/Strip (P/S)	P4458-100ML	Sigma
Primocin	Ant-pm-1	InvivoGen
PBS	D8537-500ml	Sigma-Aldrich
Red Blood Lysis buffer (RBC)	158904	Qiagen
0.2 uM filter	16534-K	Sartorium

Table 2.14. Used Reagents with Catalogue Numbers and Companies.

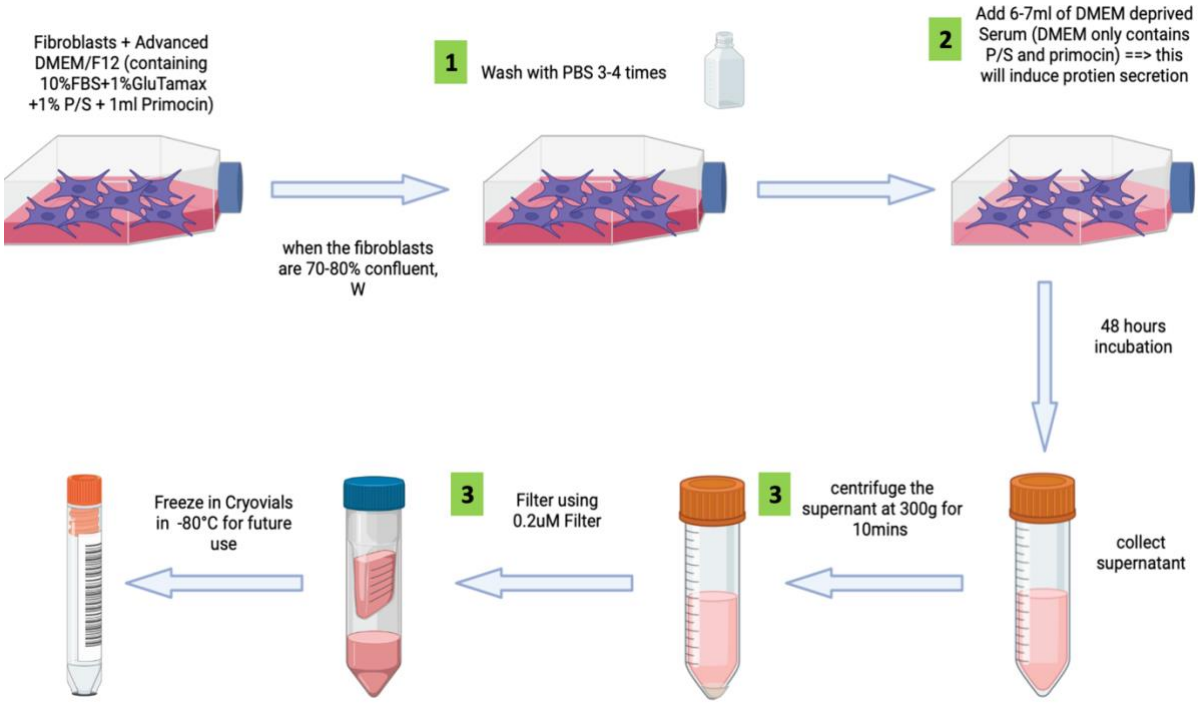


Figure 2.5. Protocol Design fibroblasts Conditioned Media (CM) collection using BioRender program.

2.7 PBMCs isolation

Blood samples were obtained from healthy donors using lithium heparin cones. Up to 30 mL of fresh blood was collected from cones buffy and transferred into a 75 cm flask containing 90 mL of RPMI 1640 without FCS or P/S. The blood was gently mixed to prevent clotting. Subsequently, 33 mL of the blood-media mixture was overlaid onto 15 mL of lymphoprep solution and centrifuged at 845 x g for 30 minutes.

Similarly, blood samples were collected from healthy donors using lithium heparin cones, with up to 10 mL of fresh blood collected and transferred into a 50 mL Falcon tube containing 15 mL of RPMI 1640 without FCS or P/S. Thirty millilitres of the blood-media mixture were overlaid onto 15 mL of lymphoprep solution and centrifuged at 845 x g for 30 minutes.

Decelerated slowly with no brake to prevent disruption of cones layers. The interface layer was transferred to a new 50 ml falcon tube and topped up to 40 ml of RPMI 1640 and then centrifuged for 10 min to pellet PBMCs. Supernatant was discarded and the pellet was resuspended in 40 ml of RPMI 1640 and centrifuge again at 475 x g for 10 minutes to pellet the PBMCs. The cells were counted at 1:10 dilution of original stock on a haemocytometer. The cells were either used for flow cytometric staining or co-culture. The remainder was centrifuged at 370 x g for 10 min to pellet PBMC and then cryopreserved in freezing media (90 % FBS + 10 % DMSO) at approximately 20 – 50 million per cryovial.

Reagents	Catalogue number	Company
lithium heparin cones	367526	BD Vacutainer
RPMI 1640	R8758-500ML	Sigma-Aldrich
lymphoprep solution	CL5020	CedaRlane
FBS	A5256801	Gibco
DMSO	D2650-100ML	Sigma
Cryovials	171901	ThermoFisher
EasySep™ Human T Cell	17951	StemCell Tech
a polystyrene round-bottom tube	352063	FAlcon
EasySep™ magnet	18000	StemCell Tech
EasySep™ Human NK Cell	17955	StemCell Tech

Table 2.15. Used Reagents with Catalogue Numbers and Companies.

2.7.1 T cells isolation

T cells were isolated from PBMCs of healthy donors using EasySep™ Human T Cell Isolation Kit-negative selection (StemCell Technologies, Canada; Catalogue number #17951). 20 x 10^6 to 50 x 10^6 of PBMCs were added to a polystyrene round-bottom tube and 50 μl of Isolation Cocktail were added to sample, mixed, and incubated at RT for 5 minutes. RapidSphere™ was added to sample and topped up with medium to 2.5 ml then the tube placed into the EasySep™ magnet (Catalog # 18000) and incubated at RT for 3 minutes. In one continuous motion, the enriched cell suspension was poured by inverting the tube and magnet into new tube and Isolated T cells are ready for use.

2.7.2 NK cells isolation

NK cells were isolated from PBMCs of healthy donors using EasySep™ Human NK Cell Isolation Kit (StemCell Technologies, Canada; Catalogue #17955). The same procedure was followed up as in section 2.7.1. using NK cells isolation kits-negative selection.

2.7.3 Co-culture of fibroblasts with T cells and NK cells

On the first day, fibroblasts were trypsinized from a T75 flask, centrifuged at 475 x g, and the resulting pellet was resuspended in 2 ml of DMEM media. The cells were then

counted using a haemocytometer, and 30,000 cells were added to each well of a 96-well plate. The cells were allowed to attach overnight at 37 °C. On the following day, T or NK cells were isolated according to the procedures outlined in sections 2.7.1 and 2.7.2. Following the enrichment of T and NK cells, the cells were resuspended in PBS and counted. Subsequently, 200,000 cells were aliquoted for the "Unstimulated unlabelled control" into a new FACS tube and supplemented with T or NK media specifically TEXMACS and RPMI medium respectively. The cells were centrifuged at 300 x g for 10 min. After centrifugation, the cell pellet was resuspended in the residual volume and transferred to a well of a 96-well flat-bottom plate for incubation.

For the proliferation assay, T and NK cells are stained with CFSE before co-culturing with fibroblasts. For T and NK phenotyping, the cells are stimulated according to the procedure outlined below. Subsequently, they are added to fibroblasts for incubation, after which they are stained with markers of interest.

To prepare for the proliferation assay, 1 µL of 5 mM CFSE stock solution is diluted in 2 mL of PBS to create a 2.5 µM working solution, which is then warmed up. Next, 250 µL of the warm CFSE working solution was added to the enriched cells and incubated for 20 minutes at 37 °C. Staining was quenched by adding 4 mL of T or NK cells media containing 2 % human serum and incubating for an additional 10 minutes at 37°C. After cell counting, a specific number of T and NK cells were transferred to a new FACS tube, topped up with media, and centrifuged at 300 x g for 5 min. The resulting cell pellet was resuspended in T or NK media and transferred to the plate along with the 200 µl of conditioned media. Next, T or NK cells were stimulated with 5 µl of ImmunoCult Human CD3/CD28 T Cell Activator reagent and IL-2 (100 U/ml) for T cells, and IL-2 (1000 U/ml) for NK cells per condition then the stimulated cells were

transferred to a 96-well flat-bottom plate on top of the cultured fibroblasts (ANF and CAF) with a number of 70,000 per condition. The plate was then incubated for 4 days at 37°C. After the 4-day incubation period, the plate was centrifuged at 300 ×g for 5 minutes. Subsequently, 100 µl of supernatant was gently removed from each well without disturbing the cell pellet and stored at -80°C for cytokine/chemokine analysis. To each well, 100 µl of MACS buffer was added, thoroughly pipetted, and transferred to flow cytometry tubes. CFSE fluorescence was detected on the FITC (FL-1) channel.

For T and NK phenotyping, T or NK cells were stained using a panel of antibodies, with detailed specifications available in table 2.15 and 2.16. Following staining, cells were then incubated for 30 minutes at 4 °C in the dark. Tubes were subsequently washed with 3 ml of MACS buffer (consisting of 500 mL PBS, 0.5 % BSA, and 2 mM EDTA) and centrifuged at 300 x g for 5 minutes. Finally, 1 µl of Propidium Iodide (PI) was added to each tube to identify and exclude dead cells in both CFSE assay and phenotyping, and the samples were analysed using a Gallios flow cytometer, with PI fluorescence detected on the PE-Texas Red (FL-3) channel.

T cells panel	Clone	Catalogue number	Company	FC colour	Concentration (μl)
CCR7	G043H7	353216	BioLegend	FITC (FL1)	2.5
DNAM-1	11A8	338306	BioLegend	PE (FL2)	2.5
Live/Dump (Propidium Iodide)	---	130-093-233	Mitenyi Biotec	PE-Texas Red (FL3)	1
CD8	RPA-T8	301032	BioLegend	PerCP-Cy5.5 (FL4)	2.5
PD-1	EH12.2H7	329918	BioLegend	PE-Cy7 (FL5)	2.5
CD45RA	HI100	304112	BioLegend	APC (FL6)	2.5
CD3	HIT3a	300324	BioLegend	AF700 (FL7)	2.5
CD4	RPA-T4	300518	BioLegend	APC-Cy7 (FL8)	2.5
NKG2D	1D11	320822	BioLegend	BV421 (FL9)	2.5
CD69	FN50	310936	BioLegend	BV510 (FL10)	2.5

Table 2.16. T-cell flow cytometry panel.

NK cells panel	Clone	Catalogue number	Company	FC colour	Concentration (μl)
KIR2LD1S1/S3/S5	HP-MA4	339504	BioLegend	FITC	2.5
KIR3LD1, NKB1	DX9	312706			
KIR2LD2/L3, NKAT2	DX27	312604			
DNAM-1	11A8	338306	BioLegend	PE	2.5
Live/Dump (Propidium Iodide)	---	130-093-233	Mitenyi Biotec	PE-Texas Red (FL3)	1
CD56	MEM-188	304628	BioLegend	PE-Cy7	2.5
NKP46	9E2	17-3359-42	ThermoFisher	APC	2.5
CD3	HIT3a	300324	BioLegend	AF700	2.5
CD16	3G8	302018	BioLegend	APC-Cy7	2.5
NKG2D	1D11	320822	BioLegend	BV421	2.5
CD69	FN50	310936	BioLegend	BV510	2.5

Table 2.17. NK-cell flow cytometry panel.

Reagents	Catalogue number	Company
polystyrene round-bottom tube	352063	FAlcon
TEXMACS	130-097-196	Miltenyi Biotec
RPMI	R8758-500ML	Sigma-Aldrich
96-well flat-bottom plate	3596	Costar
CFSE	65-0850-84	Invitrogen
human serum	H4522-100ML	Sigma-Aldrich
of ImmunoCult Human CD3/CD28 T Cell Activator	10971	StemCell
IL-2	200-02	Peprotech
Propidium Iodide (PI)	130-093-233	Miltenyi Biotec
Flow cytometry	4016589	Beckman Coulter

Table 2.18. Used Reagents with Catalogue Numbers and Companies.

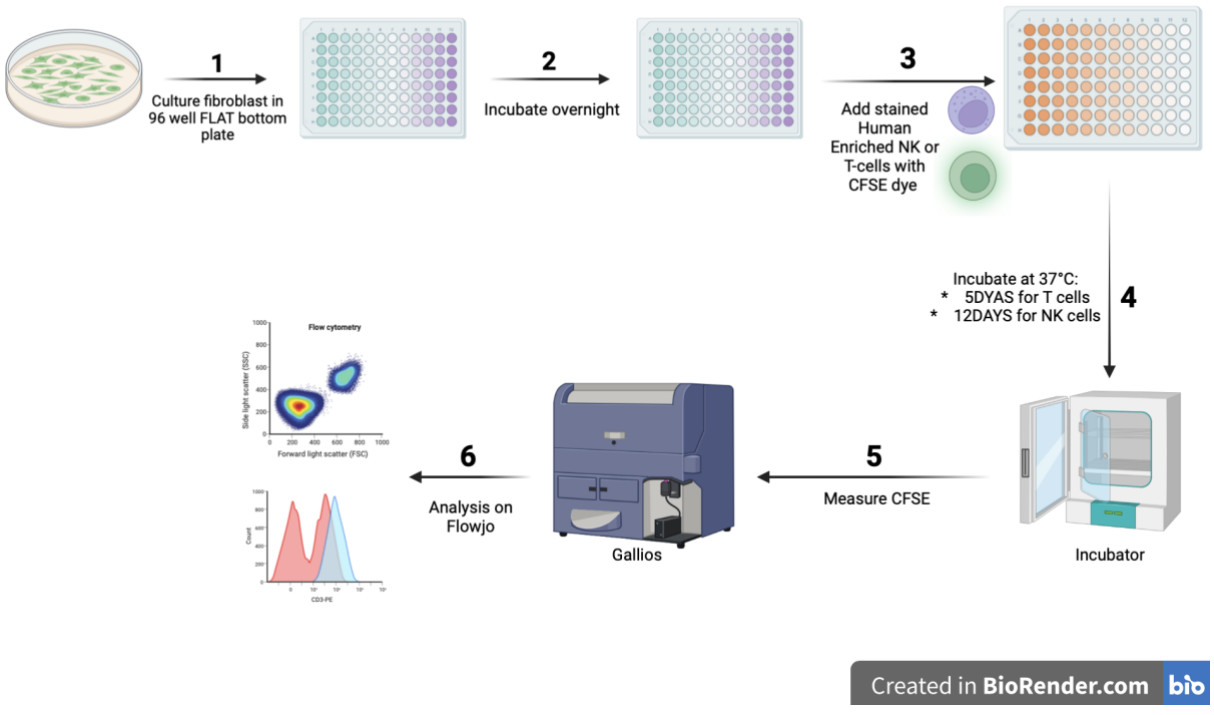


Figure 2.6. Protocol Design for Co-Culture of T/NK cells with fibroblasts (direct contact) using BioRender program.

2.7.4 ANF / CAF Conditioned media (ANF-CM & CAF-CM)

After staining T and NK cells with CFSE according to the procedure outlined in section 2.7.3, the enriched cells were stimulated with 5 µl of ImmunoCult Human CD3/CD28 T Cell Activator reagent and IL-2 (100 U/ml) for T cells and IL-2 (1000 U/ml) for NK cells. then the stimulated cells were transferred to a 96-well flat-bottom plate along with fibroblast-conditioned media and the contents were mixed thoroughly by pipetting with a P200 set to 150 µl without introducing air bubbles. The plate was then incubated for 4 days at 37 °C. After the 4-day incubation period, the plate was centrifuged at 300 ×g for 5 minutes. Subsequently, 100 µl of supernatant was gently removed from each well without disturbing the cell pellet and stored at -80 °C for cytokine/chemokine analysis. To each well, 100 µl of MACS buffer was added, thoroughly pipetted, and transferred to flow cytometry tubes. Finally, 1 µl of Propidium Iodide (PI) was added to each tube to gate out dead cells, and the samples were analysed using a Gallios flow cytometer. CFSE fluorescence was detected on the FITC (FL-1) channel, while PI fluorescence was detected on the PE-Texas Red (FL-3) channel.

Conditions	Unstimulated			Stimulated			ANF-CM	CAF-CM
	NKs alone	+ANF-CM	+CAF-CM	NKs alone	+ANF-CM	+CAF-CM	Alone	Alone
#Volume	100 µl NKs media + 100 µl DMEM	10 µl NKs media + 100µl CM	100µl NKs media + 100µl CM	100µl NKs media + 100µl DMEM	100µl NKs media + 100µl CM	100 µl NKs media + 100 µl CM	200 µl CM	200 µl CM

Table 2.19. Experimental conditions.

2.7.5 T and NK cells gating strategy

Antibodies-stained samples were run on a Beckman Coulter Gallio's flow cytometry. at least 50,000 events were acquired per sample and analysed using flowjo software. Figure 2.8 and 2.9 shows the gating strategies used to select different T and NK cells. Flowjo^{TM}10.8.1 software and Prism 8 (GraphPad, California USA), both for Mac OS X operating system.

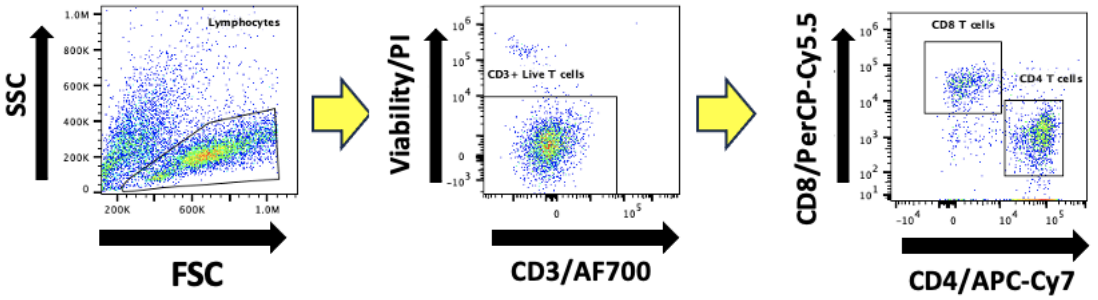


Figure 2.7. Gating strategy for T cell flow cytometry analysis.

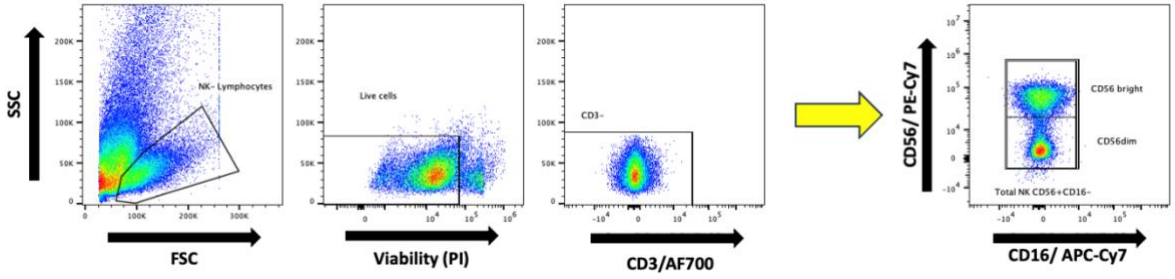


Figure 2.8. Gating strategy for NK cell flow cytometry analysis.

2.7.6 Statistical analysis

Statistical analysis was performed with Flowjo™10.8.1 software and Prism 8 (GraphPad, California USA), both for Mac OS X operating system.

I used “Shapiro-Wilk tests” and “QQ plots” to assess the normal distribution of the data. Following this, for normally distributed data, I performed “t-tests” for pairwise comparisons, while for non-normally distributed data, I applied “non-parametric equivalents”, such as the “Mann-Whitney U test”.

When analysing multiple groups, I used “One-Way ANOVA” for normally distributed data, followed by “Tukey’s post-hoc test” to account for multiple comparisons. For non-parametric data, I utilized the “Kruskal-Wallis test” followed by “Dunn’s post-hoc test”. Additionally, when comparing data across two factors or independent variables, I used “Two-Way ANOVA”. This test allows for the evaluation of interactions between the two factors while considering their individual effects on the outcome variable. Post-hoc analysis following Two-Way ANOVA was performed using “Tukey’s test” for pairwise comparisons.

These methods were chosen to ensure that the appropriate statistical tests were applied depending on the distribution of the data.

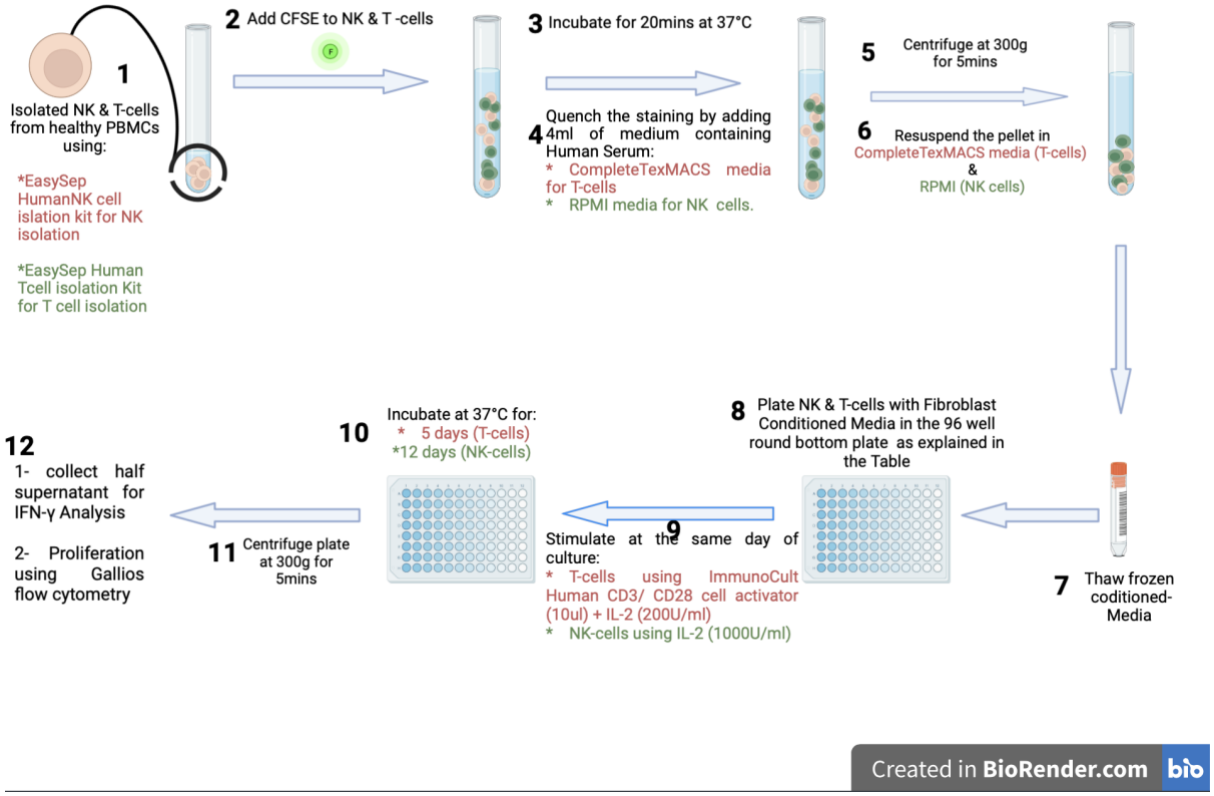


Figure 2.9. Protocol Design for Co-Culture of T cells with fibroblasts Conditioned Media (CM) using BioRender program.

2.8 Pseudo-Emperipolesis assay

2.8.1 Fibroblast seeding

ANF and CAF were trypsinized and resuspended in 8 ml DMEM medium containing (10 % FBS, 1 % P/S, 1 % GlutaMAX and 1 ml Primocin). The cells were counted and seeded into 12 well plate at a density of 150.000 cells /ml in each well. Incubated at 37 °C for 24 hours to ensure confluency.

In the stimulation experiment, fibroblasts were seeded overnight and subsequently treated with cytokines (TNF-α: 100 U/ml, IFN-γ: 10 ng/ml, and TGF-β: 10 ng/ml), followed by overnight incubation at 37°C. After the allotted time, the culture medium was carefully washed off twice with before adding lymphocytes 1ml DMEM medium containing (10 % FBS, 1 % P/S, 1 % GlutaMAX and 1 ml Primocin).

Reagents	Catalogue number	Company
Trypsin (1X)	12605-010	Gibco
DMEM	D6429-500ML	Sigma
FBS	A5256801	Gibco
P/S	P4458-100ML	Sigma
GlutaMAX (100X)	35050-038	Gibco
Primocin	Ant-pm-1	InvivoGen
T25 flask	430168	Corning
PBS	D8537-500ml	Sigma-Aldrich
BSA	A7906-100G	Sigma-Aldrich
M199	31150-022-500ML	Gibco
TNF-α	210-TA	R&D
IFN-γ	RIFNG100	Thermo scientific
TGF-β	T7039	Sigma-Aldrich

Table 2.20. Used Reagents with Catalogue Numbers and Companies.

2.8.2 PBL isolation

PBMCs were isolated from 20-100 ml of fresh blood from healthy donors as described in section 2.7. Mononuclear cells of monocytes were depleted by placing PBMCs in T25 plastic culture dish for 10-30 minutes in 5ml of standard PBS with 2 % BSA (5ml) at 37 °C for monocytes to sediment and adhere. Gently washed off enriched peripheral blood lymphocytes using 5 ml of PBS- 2 %BSA. PBLs were counted and then diluted to the desired concentration, adjusted according to the number of conditions present in M199BSA medium supplemented with 0.15 % (w/v) bovine albumin. I used 1million of isolated PBL per condition.

2.8.3 ANF/CAF monolayer co-culture

Confluent fibroblasts layer was washed with 1ml of pre-warmed M199/BSA before adding the isolated PBLs. PBL cells were resuspended in M199/BSA at concentrations of $1x10^6$/ml. 1 million/ml of PBLs was then added to each well and incubated for 20mins, 1hour, 2 hours, 3hours, and 24hours at 37 °C, 5 % CO_2. Ratio of (150.000 CAF or ANF: 1M PBLs). After the designated time-period, the culture medium was washed off with warm M199/BSA to remove any remaining non-adherent cells. The cells were then imaged using an inverted phase contrast microscope, and phase bright, grey, and dark cells were counted.

2.8.4 How to use the Phase contrast microscopy

To begin, the temperature-controlled chamber (heating box) was turned on at least 3-4 hours prior to use, ensuring it reached 37 °C, with both the light and camera deactivated during the heating process. Subsequently, a series of video recordings were made capturing fields along the centreline of the chamber, with 6 fields recorded for 10 seconds each during the final minute of the bolus. These recordings were intended for subsequent offline analysis of cell behaviour, such as stationary adhesion and migration. Data analysis is conducted offline using software such as Image-Pro or ImageJ.

2.8.5 Analysis of cell behaviour from video recordings

First, a recording was made using a microscope stage-micrometre positioned parallel and perpendicular to the flow, which served to calibrate the size of the video field observed on the monitor during playback and within the image analysis software. Subsequently, the number of adherent cells and their behaviour was quantified by digitizing a sequence of images, taken at 1-second intervals, from recordings made at specific time points of interest. The cells were categorized as follows:

a. Bright phase: Adherent cells representing total PBLs on the fibroblast surface, typically exhibiting a bright phase with a distorted outline and slow migration on the surface.

b. Grey phase: Other cells observed alongside adherent cells.

c. Dark phase: Migrated cells located beneath the fibroblast cells, characterized by a distorted shape resulting from prior adherence.

The counts of total adherent cells (Bright + Grey + migrated) were converted to number per square millimetre (cells/mm^2) using the known field dimension.

To calculate the number of adherent cells per square millimetre per 10^6 cells added, we divided the cells/mm^2 by the total number of cells added. The counts of cells that are stationary adherent or transmigrated were expressed as percentages of the total adherent cell population.

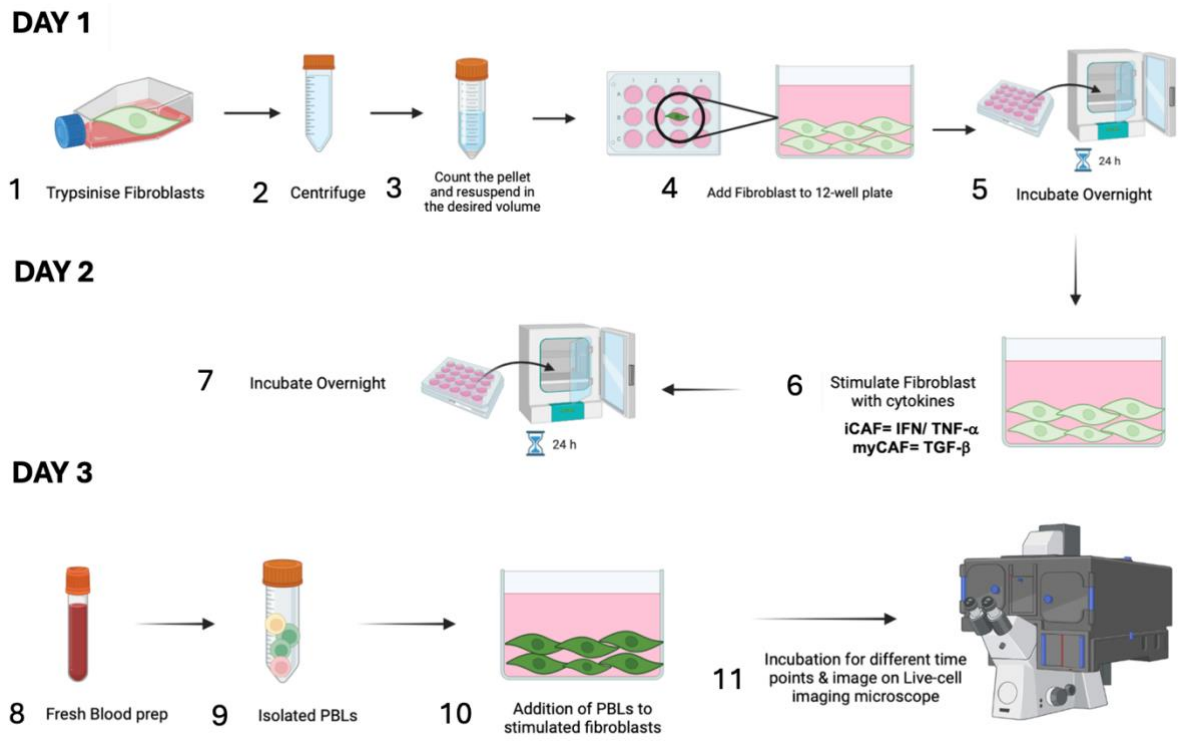


Figure 2.10. Protocol Design for Pseudo- Emperipolesis Assay using BioRender program.

2.9 Trans-well assay

First, fibroblast cells from a single T75 flask were trypsinized using 3 mL of trypsin and incubated for 3-5 minutes. The cells were then suspended in 8 mL of DMEM media. Following this, the cells were centrifuged at 475 x g for 5 minutes, and the resulting pellet was resuspended in 2 mL of media before cell counting. For static assays, a sterile box with an inverted filter was prepared, and 50 x 10^4 fibroblast cells were carefully seeded onto the outer surface of the inverted filter, with 350 µL in a 12-well filter. The cells were then incubated at 37 °C for 1 hour, after which the filter was re-inverted and placed into wells containing culture medium. The fibroblasts were treated with cytokines (TNF-α: 100 U/ml, IFN-γ: 10 ng/ml, and TGF-β: 10 ng/ml), and incubated overnight at 37 °C. The following day, the medium containing cytokines from both the upper and lower chambers was removed. Subsequently, 700 µL of fresh M199+BSA was added to the lower chamber, and 200 µL of lymphocytes was added to the upper chamber. The lymphocytes were allowed to settle, adhere, and migrate at 37 °C for 6 and 24 hours, after which the experiment was stopped by transferring the filter into a fresh well. Lymphocytes from the upper chamber were transferred to a fresh well, and the upper chamber was washed twice with 200 µL of warm M199+BSA, which served as the non-adherent cell fraction. Cells from the original lower chamber were retrieved, rinsed with 300 µL of M199+BSA, and pooled with the retrieved cells. Microscopic examination was conducted to ensure the removal of all cells, followed by further washing. The non-adherent and migrated cells were then stained using T and NK cell markers as shown in the table below and then counted using counting beads. The staining procedure followed the guidelines outlined in section 2.7.3.

Following the staining of adhered and migrated lymphocytes, 50 µl of the counting bead suspension was added to each sample. The initial volume of each sample was recorded before the addition of beads, and the final volume was adjusted to at least 300 µl. Subsequently, the samples were analysed using flow cytometry.

The sample calculations were performed as follows:

Absolute count (Cell/ul) = ((cell count*counting beads)/(counting beads*cell volume)).

T & NK cells panel	Clone	Catalogue number	Company	FC colour	Concentration (ul)
CCR7	G043H7	353216	BioLegend	FITC (FL1)	2.5
PD-1	EH12.2H7	329918	BioLegend	PE-Cy7 (FL-2)	2.5
Live/Dump (Propidium Iodide)	---	130-093-233	Mitenyi Biotec	PE-Texas Red (FL3)	1
CD8	RPA-T8	301032	BioLegend	PerCP-Cy5.5 (FL4)	2.5
CD56	MEM-188	304628	BioLegend	PE-Cy7 (FL5)	2.5
CD45RA	HI100	304112	BioLegend	APC (FL6)	2.5
CD3	HIT3a	300324	BioLegend	AF700 (FL7)	2.5
CD4	RPA-T4	300518	BioLegend	APC-Cy7 (FL8)	2.5
CD69	FN50	310936	BioLegend	BV510 (FL10)	2.5

Table 2.21. T and NK-cell flow cytometry panel.

Reagents	Catalogue number	Company
Trans-well filters (3uM pore)	353181	Falcon
TNF-α	210-TA	R&D
IFN-γ	RIFNG100	Thermo scientific
TGF-β	T7039	Sigma-Aldrich
counting bead	C36950	Invitrogen

Table 2.22. Used Reagents with Catalogue Numbers and Companies.

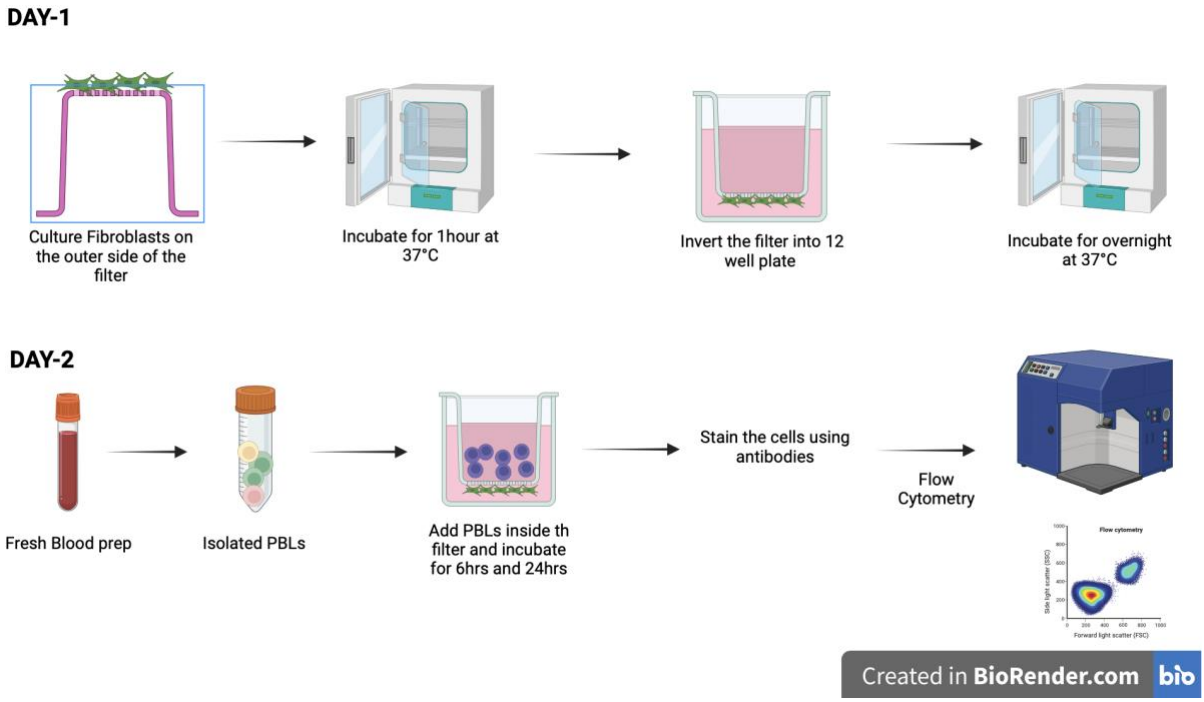


Figure 2.11. Protocol Design for Trans-well Assay using BioRender program.

2.10 Sandwich ELISA

The conditioned media from fibroblasts was collected following the procedure outlined in section 2.6. Subsequently, it was centrifuged at 300 x g for 10 minutes at 4°C and then filtered using a 0.2 µm filter. The resulting soluble conditioned media were then tested for IFN-gamma.

2.10.1 ELISA

ELISA was performed in duplicate for all samples using a 96-well plate according to the manufacturer's instructions. Wells were coated with 50 µl of a coating buffer containing 0.75 µg/ml of anti-human IFN-γ monoclonal antibody and incubated overnight at 4°C. The following day, the coating buffer was removed, and 200 µl of blocking buffer was added to each well and incubated at room temperature for 1 hour. The wells were then washed 3-4 times with wash buffer (PBS containing 1% Tween 20).

After blocking, 50 µl of sample or an 8-fold standard dilution series was added to each well and incubated at room temperature for 2 hours. Wells were washed six times with PBS/Tween, followed by the addition of 50 µl of a secondary detection antibody. The plate was incubated for 1 hour at room temperature, washed again six times with PBS/Tween, and then 50 µl of Streptavidin-HRP complex was added. After a 30-minute incubation at room temperature, 50 µl of TMB substrate solution was added to each well and incubated for 2-3 minutes to allow colour development. Positive wells displayed a blue coloration, proportional to the concentration of the target analyte.

The reaction was stopped by adding 50 µl of 1M HCl, converting the blue colour to bright yellow. Optical density (OD) readings were taken immediately at 450 nm using a microplate reader, with a wavelength correction set at 655 nm to account for plate optical imperfections.

To prepare the ELISA reagents, the following methods were employed:

1. Blocking Solution:

We combined 5 g of BSA with 500 ml of PBS to create a blocking solution. Additionally, we added 250 µl of tween to this mixture Wash Buffer.

2. Wash Buffer

For the wash buffer, we dissolved 20 PBS tablets in 2 litters of water. To this solution, we added 1 ml of tween.

3. Coating Buffer

In 450ml of H_2O, we dissolved 2.65 g of Na_2CO_3, 2.1g of $NaHCO_3$, and 0.5 g of sodium azide. Adjusting the pH to 9.6 with NaOH, we then brought the volume up to 500 ml.

4. 1M HCl Preparation

To prepare 1M HCl, we mixed 41.5 ml of 37% HCl with 458.5 ml of H_2O

Reagents	Catalogue number	Company
ELISA 96 well plate	MSBVN1250	Millipore
Sodium Carbonate (Na2CO3)	S7795-500G	Sigma-Aldrich
Sodium Bicarbonate (NaHCO3)	S5761-500G	Sigma-Aldrich
sodium azide	71290-100G	Sigma-Aldrich
Anti-human IFN-γ monoclonal antibody	M700A	Invitrogen
IFN-γ antibody	M700-A	Invitrogen
BSA	A79906	Sigma-Aldrich
PBS tablets	BR0014G	Oxoid
Tween	21079-500ML	Sigma-Aldrich
IFN-γ standard	29-8319-65	Thermo Fischer
Biotinylated anti human IFN-γ antibody	M701B	Invitrogen
ExtrAvidin peroxidise	E2886-1ML	Sigma-Aldrich
TMB substrate	34029	ThermoFisher
HCl	12364889	Fischer Scientific
Plate reader	(iMark)	Bio-Rad

Table 2.23. Used Reagents with Catalogue Numbers and Companies.

2.10.2 Statistical analysis

Statistical analysis was performed using Prism 8 (GraphPad, California USA), for iMac. All variables were checked for normal distribution.

I used “Shapiro-Wilk tests” and “QQ plots” to assess the normal distribution of the data. Following this, for normally distributed data, I performed “t-tests” for pairwise comparisons, while for non-normally distributed data, I applied “non-parametric equivalents”, such as the “Mann-Whitney U test”.

When analysing multiple groups, I used “One-Way ANOVA” for normally distributed data, followed by “Tukey’s post-hoc test” to account for multiple comparisons. For non-parametric data, I utilized the “Kruskal-Wallis test” followed by “Dunn’s post-hoc test”. Additionally, when comparing data across two factors or independent variables, I used “Two-Way ANOVA”. This test allows for the evaluation of interactions between the two factors while considering their individual effects on the outcome variable. Post-hoc analysis following Two-Way ANOVA was performed using “Tukey’s test” for pairwise comparisons.

These methods were chosen to ensure that the appropriate statistical tests were applied depending on the distribution of the data.

2.11 NanoString Spatial RNA Profiling (DSP)

2.11.1 Sample Processing

FFPE tissue blocks were sectioned at 5-µm thickness, deparaffinized, and rehydrated using standard methods. Slides were profiled using the NanoString GeoMx Digital Spatial RNA Profiling (DSP) platform through the Technology Access Program (TAP) by NanoString (Seattle, WA, USA). Immunofluorescent antibody staining was performed with tissue morphology markers (Pan-CK, CD45, α-SMA, and DAPI). Concurrently, slides were stained with a panel of photocleavable RNA probes. Custom regions of interest (ROI) were selected based on these markers to generate specific domains, including ‘tumour-proximal stroma,’ ‘tumour-distant stroma,’ and ‘immune-enriched’ areas. Four ROIs were selected for each domain per slide. RNA probes within each ROI were liberated by UV light, hybridized to optical fluorescent barcodes, and counted on the nCounter to determine the absolute number of mRNA transcripts.

2.11.2 NanoString nCounter Data Analysis

Raw NanoString nCounter data expression matrix was processed following normalization and quality control procedures. Due to redundancy in the tags used for both IFNG and ACTA2, data from these probes were removed. Correlations of housekeeping gene expression across all ROIs were assessed to select the most correlated housekeeping probes, H3F3A and UBB, for downstream normalization (Supp. Fig. S2A). Unwanted variation was removed using the R package RUVSeq.

Firstly, distributional differences were scaled between lanes using upper-quartile normalization. Then, unwanted technical factors were estimated in the resulting gene expression data with the RUVs function, selecting H3F3A and UBB as the negative control genes and setting the number of dimensions of unwanted variation to remove to 1. A variance-stabilizing transformation of the original count data was computed using DESeq2, and estimated unwanted variation was removed using the remove Batch Effects function from limma. RLE plots were used to detect potential outliers before and after normalization.

Differential expression analysis was conducted to compare immune vs. stromal regions, and tumour-proximal vs. tumour-distant stromal regions using DESeq2, adjusting for multiple testing with the Benjamini-Hochberg (BH) procedure. Differentially expressed genes were determined by BH-adjusted $p < 0.05$ and absolute log2FC > 0.25. Dimensionality reduction by Uniform Manifold Approximation and Projection (UMAP) was performed on the normalized counts matrix using the UMAP R package, with ggplot2 utilized for plotting. Heatmap visualizations were generated using the ComplexHeatmap package. Pearson correlation was calculated, and plots were generated using ggpairs and ggcorr functions from the R package GGally.

2.12 scRNA-Seq data analysis

Genes of Interest Exploration:

Genes of interest identified from the nCounter data analysis were further explored for their expression profiles in single-cell RNA sequencing data (GEO accession GSE210199) from the tumour microenvironment of 3 PDAC patients.

Raw Read Data Processing:

Raw reads were processed using CellRanger (10X Genomics, v3) with the mkfastq and count functions. Raw bcl files were converted to fastq and aligned to the human reference genome GRCh38. Gene expression matrices for each patient were analysed using R software (v3.6). Data pre-processing, quality control, dimensionality reduction, clustering, and subsequent downstream analysis were performed using the Seurat package (v3.1.1).

Data Integration and Clustering:

Data from the 3 PDAC patient samples were integrated using the Seurat SCTransform Integrate workflow, with the top 3000 most variable genes as integration features. Principal Component Analysis (PCA) was applied, and Uniform Manifold Approximation and Projection (UMAP) embedding was determined using PCs 1:20. For unsupervised clustering, a shared nearest neighbour graph based on Euclidean distance in PCA space was constructed using the Seurat Find Neighbours function,

and clusters were identified using the Louvain algorithm with Seurat Find Clusters. High-level cell type annotation was performed by assessing canonical cell type marker gene expression levels.

scRNA-Seq Fibroblast Data Analysis:

The transcriptome data was subset to include only Fibroblast cells, and unsupervised clustering was re-applied. The expression profile of stromal genes identified from the nCounter dataset, associated with tumour-proximal or tumour-distant regions, was assessed within the Fibroblast scRNA-Seq data. These gene signatures were scored using GSVA to identify likely tumour-proximal and tumour-distant fibroblasts. Expression profiling and GSVA signature scoring were used to annotate fibroblast subpopulations as "Proximal-like" and "Distant-like." To expand the pool of possible transcriptional markers for these fibroblasts, differential expression analysis was conducted comparing Proximal-like and Distant-like clusters using findMarkers with the MAST option (test.use = "MAST"). MAST is a two-part GLM that models both the proportion of cells expressing a gene (logistic regression) and the expression level (Gaussian distribution). Differential expression testing was performed using the likelihood ratio test, with differentially expressed genes determined by Benjamini-Hochberg adjusted $p < 0.05$ and absolute log2FC > 0.5.

Chapter 3: Fibroblast Heterogeneity in PDAC

3.1 Introduction

Fibroblasts perform a wide variety of roles including tissue repair and production of the ECM found in the skin, lung heart, kidney, eye, liver, and other organs (Dick, 2020; Gorchs & Kaipe, 2021). Fibroblasts are notably dynamic and morphologically heterogeneous and have a variety of roles depending on their location and activity (Chang et al., 2014). The ability of fibroblasts to recognise environmental cues and change phenotype is partly due to the expression of a wide range of cell surface adhesion receptors such as integrins and cadherins that support the interaction of fibroblasts with their environments. This 'plasticity' is seen in many settings and an example is that observed in the transformation of fibroblasts into myo-fibroblasts that express α-SMA (Dick, 2022). Several studies have shown that the spatial distribution of CAF is an important determinant of function. Öhlund et al. identified two distinct CAF subpopulations within PDAC. The first was described as myo-fibroblastic CAFs (myCAF) in close apposition to cancer cells which respond to elevated amount of tumour cell-secreted TGF-β and display a high level of alpha-smooth muscle actin (α-SMA) expression and collagen genes. In addition, myCAF lack the expression of inflammatory cytokines distinguishing them from the second dominant population, inflammatory CAF (iCAF). myCAF shows an activated phenotype with contractile properties (Belle & DeNardo, 2019; Ohlund et al., 2017) whilst iCAF are located more distantly from tumour cells in the desmoplastic stroma. iCAF express high level of IL-6 protein and other inflammatory cytokines and chemokines such as IL-1, IL-21, LIF, CXCL-12 and CXCL1/3. iCAF have lower α-SMA levels compared to myCAF and are characterized by immune-modulating properties. Recently a new CAF subtype that expresses MHC class II and CD74, and lacks costimulatory molecules such as CD80

or CD86, has been defined by Tuveson and colleagues (Elyada et al., 2019), termed as antigen presenting CAFs (apCAF). The same group found that apCAF subpopulations activate CD4+ T cells in an antigen-specific fashion *ex vivo* suggesting their role in modulating the PDAC immune system capacities and progression. In line with these studies, collagen type I (col-I) depletion in α-SMA+ myofibroblasts aggravates PDAC progression and tumour immunosuppression (Y. Chen et al., 2021; Madsen, 2021). Two novel CAF subtypes were recently found in PDAC and termed metabolic cancer-associated fibroblasts (meCAFs) (Y. Wang et al., 2021) and complement-secreting CAF (csCAFs) (K. Chen et al., 2021). meCAF are characterized by a high metabolic activity and are found in loose-type PDAC. In addition, PDAC patients with elevated meCAFs phenotype were associated with increased metastasis and poor overall survival (K. Chen et al., 2021; Y. Wang et al., 2021). Using single-cell analysis Hutton et al. described two CAF populations in PDAC based on CD105 expression, CD105+ and CD105- CAFs. CD105+ fibroblasts were strongly tumour promoting whilst CD105-negative fibroblasts had a negative impact on tumour development in a manner dependent on adaptive immunity (Hutton et al., 2021).

These data demonstrate the considerable diversity and heterogeneity of fibroblast populations in the tumour microenvironment of pancreatic cancer. Importantly, almost all this work has taken place through the use of immunohistochemistry or transcriptional analysis. In addition, short term fibroblast culture leads to rapid acquisition of phenotypic modifications that support *in vitro* survival. In contrast, there is little information regarding the phenotype of fibroblasts isolated directly from the tumour microenvironment.

3.2 Results

3.2.1 Characterising Cellular Composition in Pancreatic Ductal Adenocarcinoma: Insights from Treatment-Naive and Neo-Adjuvant Chemotherapy Patients

The tumour microenvironment (TME) plays a crucial role in cancer progression, treatment response, and immune evasion. Understanding the cellular components of tumour tissue can help to provide insights into the complex architecture of the TME. Comparison with adjacent normal tissue serves as a baseline reference for cellular composition in the absence of cancer and can be used to highlight specific alterations associated with tumorigenesis. The stromal cell compartment, including fibroblasts, play a significant role in shaping the TME and influencing disease progression. The plasticity and heterogeneity of fibroblasts pose challenges in their precise identification using specific markers, often sharing markers with epithelial and endothelial cells (Elyada et al., 2019; Lavie et al., 2022). In this study, I employed pan-cytokeratin, CD45, and CD31 to quantify epithelial, immune, and endothelial cells, respectively. Following the exclusion of these cell types, positive expression of FAP and/or α-SMA served as specific markers for identifying fibroblasts (as depicted in figure 3.1).

Using flow cytometric analysis of primary PDAC tissue I aimed to characterise the cellular compositions within paired tumour (T) and adjacent normal pancreatic (AN) tissues. The proportion of each cell subset was represented on a per-patient basis (Figure 3.2) and collectively (Figures 3.3 and 3.4). In addition, I extended the analysis to determine differences between untreated PDAC patients (Naive PDAC) and those who underwent neo-adjuvant chemotherapy prior to surgery (Neo-Adj-Chemo). Significant variability was observed in the cellular composition among patients within

naïve PDAC, neo-adjuvant chemotherapy, and other cancer (OC) groups, in both AN and tumour tissues (Figure 3.2). This highlights the inherent cellular heterogeneity between patients regardless of tissue type and treatment regimen.

An in-depth analysis was conducted to compare the proportions of each cell type between matched adjacent normal (AN) and tumour tissues in both untreated and neo-adjuvant chemotherapy-treated PDAC patients (Figure 3.3A&B). The percentages of IC, EpC, and other cell subsets in Figure 3.3 are based on the percentage of live cells gated according to FSC/SSC parameters. However, for EpC and FAP+, these subsets were gated from the percentage of total fibroblasts, which includes fibroblasts along with other cell types. For total fibroblasts, the gating was based on the FAP+ subset.

In the untreated group, tumour tissues exhibited a significantly higher proportion of epithelial cells (EpC) with a mean of 29.5 ($p = 0.04$) and total fibroblasts (TF) with a mean of 29.5 ($p = 0.03$), while showing a lower proportion of other cell types (Other) with a mean of 17.1 ($p = 0.01$) compared to AN tissue (Figure 3.3A). No significant differences were found in the percentage of immune cells (IC) ($p = 0.9$) or endothelial cells (EnC) ($p = 0.3$) (Figure 3.3A). In the Neo-Adj-Chemo group, no significant differences in cell composition were observed (Figure 3.3B). However, when comparing AN to tumour tissues on a per-patient basis, an inverse relationship was noted between the abundance of epithelial cells (mean = 14.4) or immune cells (mean = 35.6) in the tumour and their corresponding presence in the AN (mean of EpC = 4.71, mean of IC = 19.2). Additionally, there was a discernible difference in fibroblast abundance between AN and tumour tissues within the same patients.

Furthermore, the relative abundance of different cellular subsets was determined by comparing ratios to gain further insight into the dynamic interactions and relationships between different cell populations within the TME. A higher ratio of TF:IC with a mean of 12.8 ($p = 0.01$) and TF:EpC with a mean of 13.2 ($p = 0.01$) in AN tissue compared to tumour tissue was observed (mean of TF:IC = 3, mean of TF:EpC = 1.46), suggesting a greater density of immune cells per fibroblast and a higher proportion of epithelial cells per fibroblast in tumour samples from treatment-naive patients (Figure 3.3C&D). Interestingly, no significant differences in cellular subset ratios were observed in patients treated with neo-adjuvant chemotherapy (Figure 3.3E&F). Although statistical significance was not reached in figure 3.3G when comparing TF:IC ratio, there was a clear trend towards a greater ratio of immune cells per fibroblast ($p=0.05$) and a reduced ratio of epithelial cells per fibroblast ($p=0.02$) in tumour tissue from the Neo-Adj-Chemo group compared to the untreated group (Figure 3.3G&H).

Specifically, the mean ratio of fibroblasts to immune cells (Fibro:IC) in the tumour (T) was 0.92 compared to 19.6 in adjacent normal tissue (AN), while the mean ratio of fibroblasts to epithelial cells (Fibro:EpC) was 14.1 in tumour tissue compared to 14.1 in adjacent normal tissue.

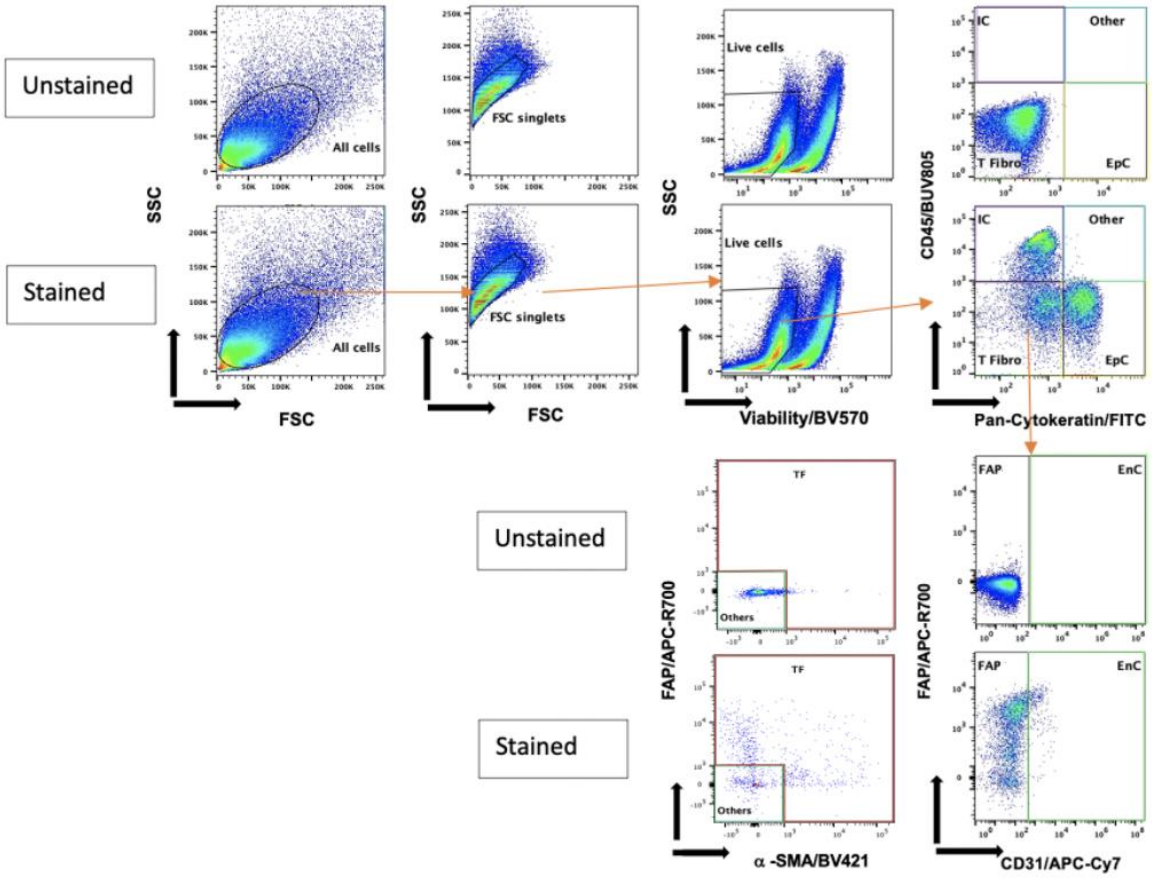


Figure 3.1. Gating strategy to identify fibroblasts by flow cytometry
Enzymatic digestion and staining with fibroblast markers were conducted on PDAC tumour single cell suspensions. Data was collected using flow cytometry and analysed using FlowJo software. Initially, tumour cells were gated based on forward scatter (FSC) and side scatter (FSC) properties. Viability dye (BV570) was used to exclude dead cells, then CD45/BUV805, pan-cytokeratin/FITC and CD31/APC-Cy7 were used to exclude immune cells, epithelial cells, and endothelial cells, respectively. FAP/APC-R700 and α-SMA/BV421 were employed to identify fibroblasts.

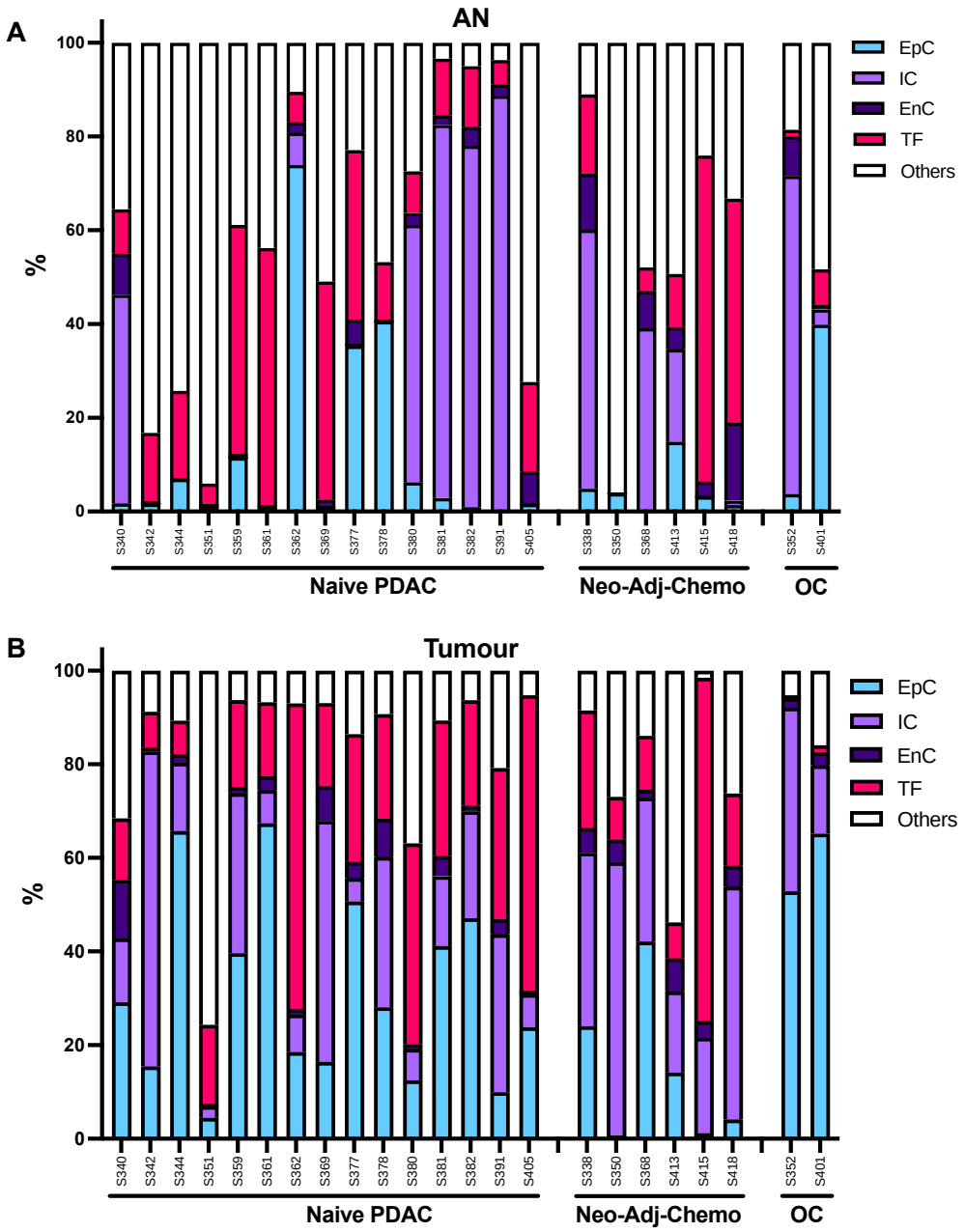


Figure 3.2. Comparison of the cellular composition within PDAC tumour tissue and adjacent normal pancreatic tissue from individual patients using flow cytometry.

Adjacent normal (AN) and tumour (T) tissue were enzymatically digested, stained with markers to identify epithelial cells (EpC), immune cells (IC), endothelial cells (EnC), total fibroblasts (TF) and other undefined cell types (Other), then evaluated via flow cytometry. **A-B**, Percentage of each cell subset of total gated cells in AN tissue (A) and tumour tissue (B) for Naïve PDAC patients (n=15), Neo-Adj-Chemo PDAC patients (n=6) and patients with other pancreatic cancer types (OC) (n=2). Each bar represents a single patient.

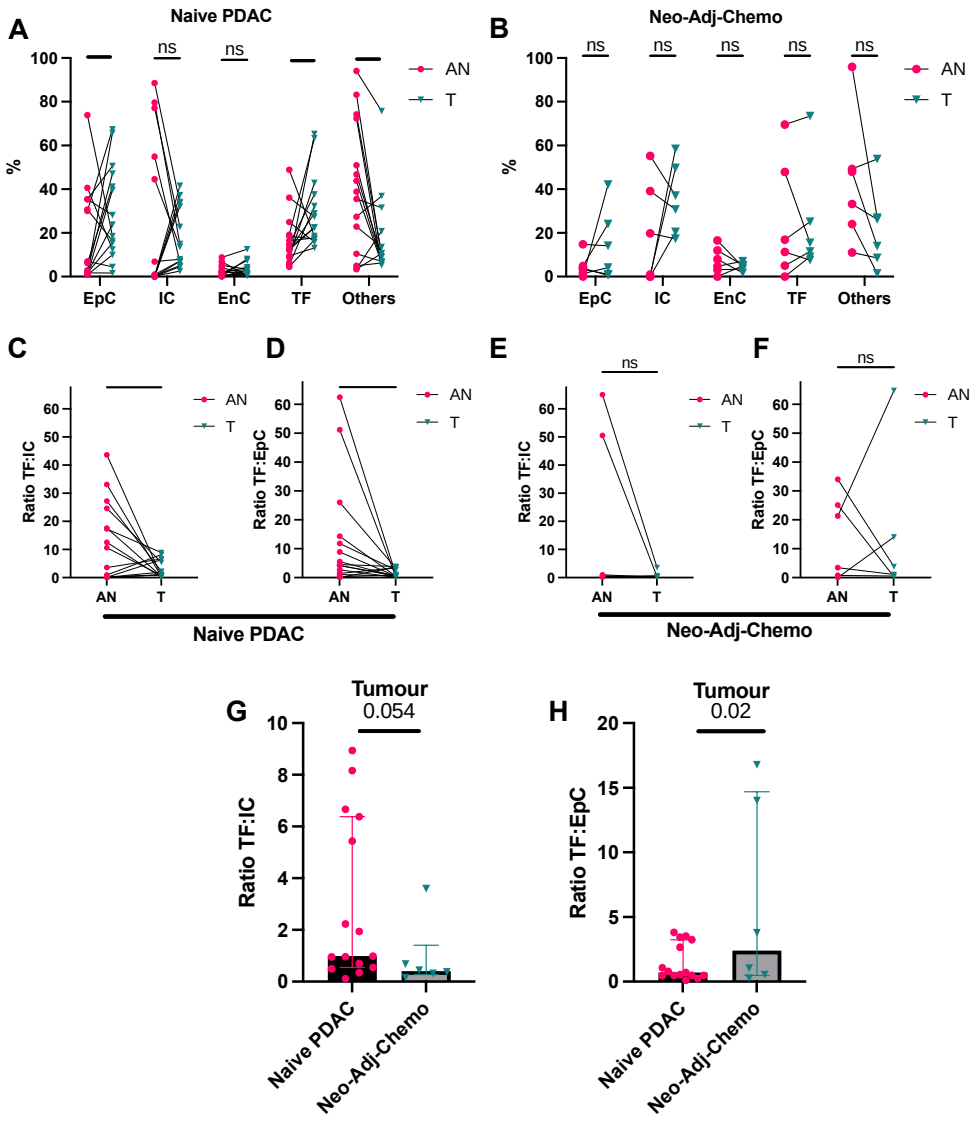


Figure 3.3. Comparison of cell type percentage and ratio in Naïve PDAC and Neo-adjuvant chemotherapy patients using flow cytometry.

Adjacent normal (AN) and tumour (T) tissue were enzymatically digested, stained with markers to identify epithelial cells (EpC), immune cells (IC), endothelial cells (EnC), total fibroblasts (TF) and other undefined cell types (Other), then evaluated via flow cytometry. **A-B**, percentages of each cell subset of total gated cells in Naïve PDAC patients (A), Neo-Adj-Chemo PDAC patient groups (B) for AN and Tumour samples. Each dot represents a single patient. **C-D-E-F**, percentage of ratios of both TF:IC and TF:EpC within the Naïve PDAC (C, D) and Neo-Adj-Chemo group (E, F) from AN and tumour tissues. G-H, percentage of TF:IC and TF:EpC ratios within the tumour tissues from Naive PDAC and Neo-adjuvant chemotherapy patients utilizing flow cytometry. Data are from 15 Naïve PDAC and 6 Neo-Adjuvant chemotherapy (Neo-Adj-Chemo). Statistical analysis was carried out using Wilcoxon matched-pairs signed rank test or Mann-Whitney test with * ≤0.05; ** ≤0.01.

3.2.2 Exploring iCAF and myCAF Fibroblast Subtypes in Adjacent Normal and Tumour Tissues: Impact of Neo-Adjuvant Chemotherapy on Fibroblast Phenotype.

Cancer-associated fibroblasts (CAFs) play a crucial role as stromal cells within tumours, exhibiting significant plasticity, heterogeneity, and spatial distribution. Various subtypes of CAFs have been identified in human PDAC, including myCAF and iCAF. The myofibroblast (myCAF) subset typically resides proximal to the tumour, characterized by α-SMA expression and TGF-β signalling, while inflammatory (iCAF) CAFs are found more distally from the tumour and exhibit a cytokine and chemokine secretory phenotype (Belle & DeNardo, 2019; Biffi et al., 2019; Elyada et al., 2019). In this section, I aimed to investigate the prevalence of iCAF and myCAF subtypes within both AN and tumour tissues and assess the impact of neoadjuvant chemotherapy on fibroblast phenotype, as depicted in figures 3.4 and 3.5.

A gating strategy for iCAF and myCAF was devised using FAP and α-SMA markers, as illustrated in figure 3.4A. Between 10,000 and 100,000 cells were analysed per sample. The cell count varied among patients based on tissue size. iCAF are characterized by FAP expression and lack of α-SMA, whereas myCAF express both FAP and α-SMA (Figure 3.4A). Figures B and C display the expression of iCAF and myCAF per patient within AN (B) and tumour tissues (C). myCAF are seen to be the dominant subtype within AN tissue compared to iCAF (Figure 3.4B). In contrast, this profile within tumour tissue is reversed, with a higher percentage of iCAF and fewer myCAF in almost all patients (Figure 3.4C).

As such I next investigated the expression of iCAF and myCAF between AN and tumour tissues in relation to treatment-naïve PDAC or the Neo-Adj-chemo group. Within the former group I found that tumours have a higher proportion of iCAF and lower myCAF compared to AN (Figure 3.4D & E). However, no significant effects were observed in the Neo-Adj-Chemo group (Figure 3.4F & G).

Subsequently, the impact of neo-adjuvant chemotherapy on CAF subtypes was examined, as depicted in figure 3.5. Within the AN tissue, I observed that the Neo-adjuvant group exhibited a higher proportion of iCAF compared to the treatment-naïve PDAC group. Conversely, the Naïve PDAC group showed a greater prevalence of myCAF compared to the Neo-adjuvant group, although this difference was not statistically significant. No significant effects were observed within the tumour tissues.

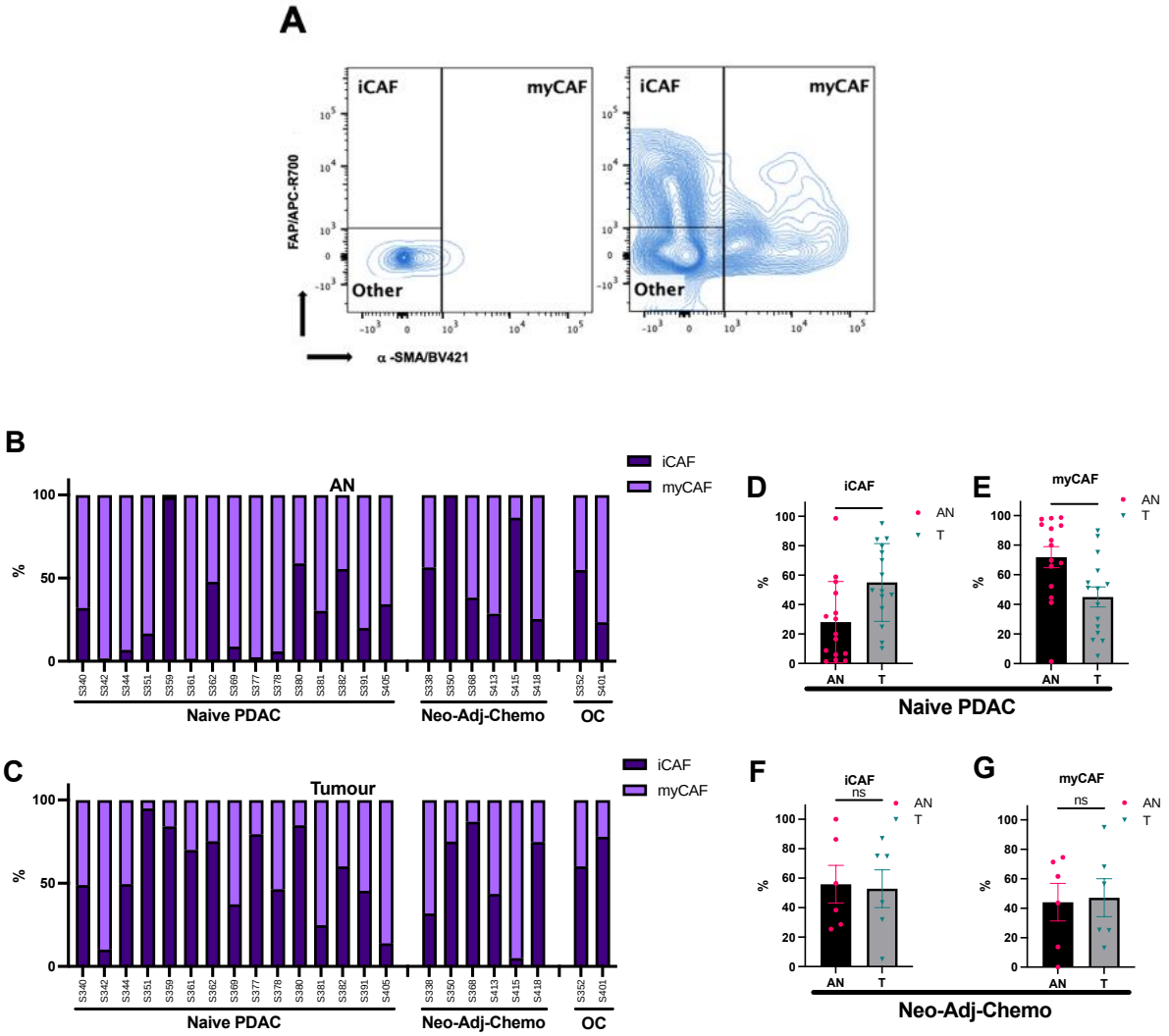


Figure 3.4. Comparison of the percentages of the two fibroblast subtypes, iCAF and myCAF, within adjacent normal and tumour tissues in Naïve PDAC and Neo-adjuvant chemotherapy patients using flow cytometry.

Enzymatic digestion and staining with markers for iCAF and myCAF fibroblasts was performed on AN and tumour cells, followed by evaluation via flow cytometry.

A. gating strategy of iCAF and myCAF subtypes in PDAC.

B-C-D-E-F-G. percentage of total fibroblasts and of each fibroblast subtype, iCAF and myCAF, within both the adjacent normal (AN) (B) and tumour tissues (T) (C) is assessed for each patient individually, as well as across all Naïve PDAC (D, E) and Neo-Adjuvant chemotherapy (Neo-Adj-Chemo) (F, G) PDAC patients. Data are from 15 Naïve PDAC and 6 Neo- Neo-Adj-Chemo. Statistical analysis was carried out using Wilcoxon matched-pairs signed rank test or Mann-Whitney test with * ≤0.05; ** ≤0.01.

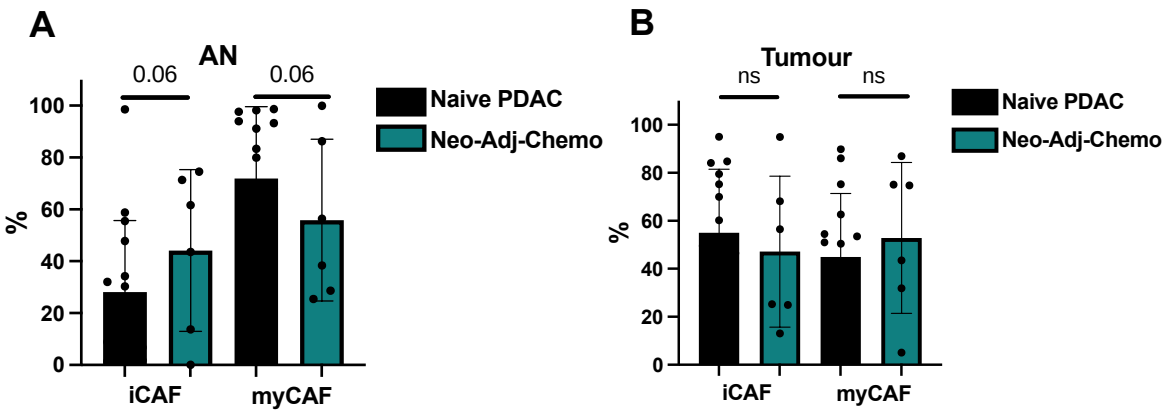


Figure 3.5. Comparison of the percentages of the iCAF and myCAF fibroblast subtypes in treatment-naïve PDAC and Neo-adjuvant chemotherapy patients within adjacent normal and tumour tissues using flow cytometry.
Enzymatic digestion and staining with markers for iCAF and myCAF fibroblasts were performed on AN and tumour cells, followed by evaluation via flow cytometry. **A-B** percentage of iCAF and myCAF, within naïve PDAC and Neo-Adj-Chemo in both the adjacent normal (AN) (A) and tumour tissues (B) is assessed. Data are from 15 Naïve PDAC (C, D) and 6 Neo- Neo-Adj-Chemo (E, F). Statistical analysis was carried out using Wilcoxon matched-pairs signed rank test or Mann-Whitney test with * ≤0.05.

3.2.3 Assessment of individual protein expression in total Fibroblasts, and iCAF, and myCAF subtypes, within Adjacent Normal and Tumour Tissues: Impact of Neo-Adjuvant Chemotherapy on Fibroblast Phenotype.

Fibroblasts, essential components of the tumour microenvironment, exhibit diverse surface marker expression profiles. Given my observation that the proportion of many fibroblast subtypes differs in relation to tumour site and treatment stage, I next went on to characterize expression of a range of fibroblast-associated proteins on these subset proteins. This comprehensive examination is presented and elucidated from figure 3.6 to figure 3.18. Through this exploration, I aimed to gain insight into the dynamic interplay of fibroblast populations and their associated marker expressions within the context of PDAC progression and treatment response.

The first protein of interest was the complement component C3. The results from figure 3.6 illustrate the expression levels of C3 within total fibroblasts (TF), inflammatory CAFs (iCAF), and myofibroblasts (myCAF). Notably, tumour tissues tend to show elevated percentage C3 expression on fibroblasts compared to AN tissue in the treatment-naïve PDAC group, although this difference lacks statistical significance (Figure 3.6A). Conversely, normal tissues tend to exhibit elevated C3 expression levels compared to tumour tissue in the neo-adj-chemo group as indicated by MFI, although this difference also lacks statistical significance (Figure 3.6B). Further comparisons between the Naïve PDAC and Neo-Adj-Chemo groups were also explored.

The most striking observation was the proportion of fibroblasts that expressed C3 was increased on myCAF in the tumour tissue. This was seen both in comparison between iCAF and myCAF, and on myCAF in tumour as compared to normal tissue. The expression of C3 on fibroblasts is currently of considerable interest in oncology and these serve to focus this on to the myCAF subsets. It is noteworthy that this expression pattern was attenuated following neo-adjuvant. It is tempting to speculate that some of the therapeutic value of this treatment may relate to the ability to normalise stromal tissue composition. However, whether this is a primary effect or simply reflects a reduction in tumour burden is not clear.

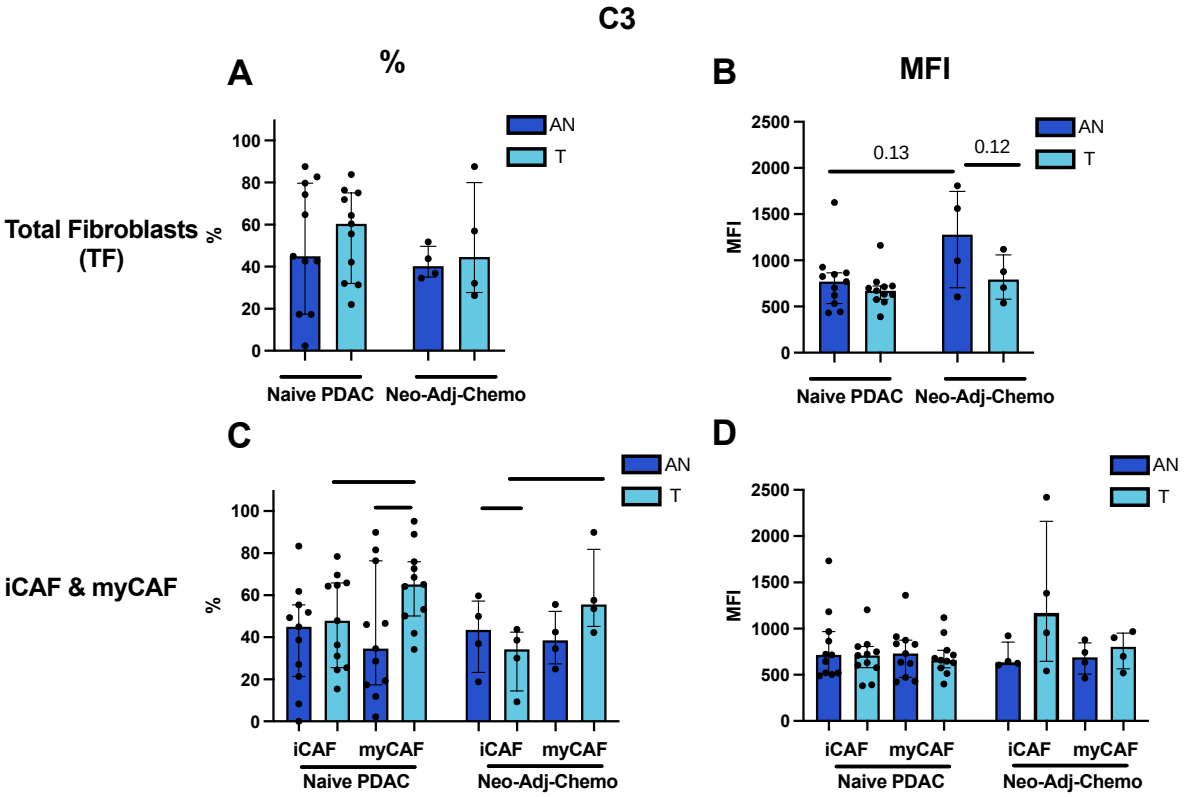


Figure 3.6. Comparison of C3 Expression in Fibroblast Subtypes in Pancreatic Cancer Patients with and without Neo-adj3uvant Chemotherapy.
Fibroblasts from adjacent normal (AN) and tumour (T) tissues were analysed using flow cytometry after enzymatic digestion and staining with a 21-marker panel. Data from n=11 untreated pancreatic ductal adenocarcinoma (Naïve PDAC) patients and n=4 PDAC patients who received neo-adjuvant chemotherapy (Neo-Adj-Chemo) were assessed. **A-B-C-D**, comparison of C3 expression within total fibroblasts (A, B) and iCAF/myCAF (C, D). The comparison includes the percentage (A & C) and Median Fluorescence Intensity (MFI) (B & D) of total fibroblasts (TF) (A, B) and of iCAF/myCAF (C, D). Statistical analysis was carried out using Wilcoxon matched-pairs signed rank test or Mann-Whitney test with * ≤0.05.

I next assessed the impact of expression of the inflammatory regulator Cadherin-11 on fibroblast subsets (Figure 3.7). The profile of expression here displayed a different pattern. Notably, a striking feature was the impact of chemotherapy on reducing the expression of Cadherin-11 on fibroblasts within the adjacent normal tissue. In contrast, there was relatively little impact of treatment on the tumour population.

Using my gating strategy, I was then able to address this observation further by focussing on iCAF and myCAF populations. Here I saw a very marked decrease of Cadherin-11 expression on the iCAF population in normal tissue following treatment. In contrast, less impact of chemotherapy was observed within tumour populations.

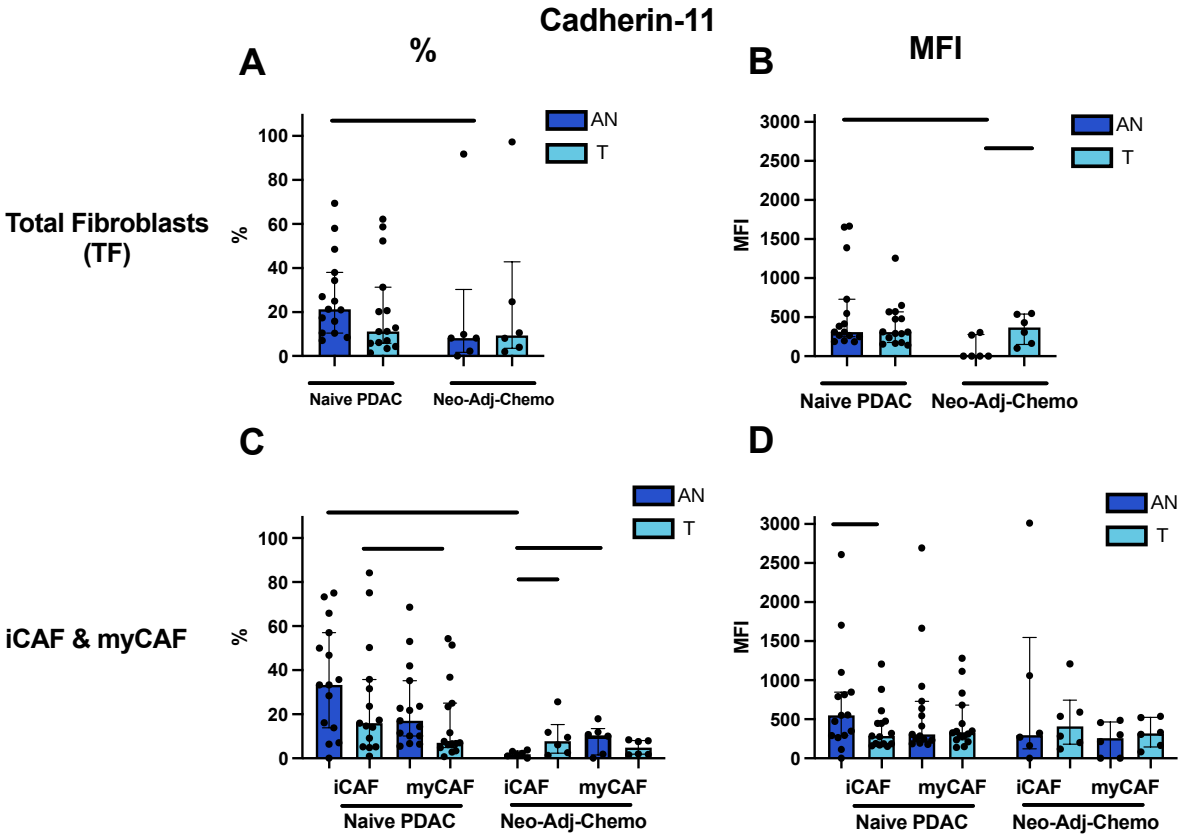


Figure 3.7. Comparison of Cadherin-11 Expression in Fibroblast Subtypes in Pancreatic Cancer Patients with and without Neo-adjuvant Chemotherapy.
Fibroblasts from adjacent normal (AN) and tumour (T) tissues were analysed using flow cytometry after enzymatic digestion and staining with a 21-marker panel. Data from *n=11* untreated pancreatic ductal adenocarcinoma (Naïve PDAC) patients and *n=4* PDAC patients who received neo-adjuvant chemotherapy (Neo-Adj-Chemo) were assessed. **A-B-C-D,** comparison of Cadherin-11 expression within total fibroblasts (A, B) and iCAF/myCAF (C, D). The comparison includes the percentage (A & C) and Median Fluorescence Intensity (MFI) (B & D) of total fibroblasts (TF) (A, B) and of iCAF/myCAF (C, D). Statistical analysis was carried out using Wilcoxon matched-pairs signed rank test or Mann-Whitney test with * ≤0.05, *** ≤0.001.

I next assessed the expression of CD26 on fibroblast subsets, a molecule associated with collagen production during wound healing (Figure 3.8). A comparison of AN versus tumour in the Naïve PDAC group reveals no significant difference in CD26 expression (Figure 3.8A and B). However, tumour tissues in the neo-adj-chemo group tend to display elevated CD26 expression compared to AN tissue, as indicated by MFI (Figure 3.8B). Further comparisons between the Naïve PDAC and Neo-Adj-Chemo groups have been conducted. A significantly higher MFI of CD26 expression in the AN tissue from the Naïve group compared to the Neo-Adj-Chemo group was observed (Figure 3.8A and B), with no significant effect observed within the tumour tissues from both groups (Figure 3.8A and B). Regarding the iCAF subtype, the expression of CD26 (MFI) showed no significant difference when comparing AN versus tumour from both the Naïve PDAC and Neo-Adj-Chemo groups (Figure 3.8D). CD26 was elevated in both the Naïve PDAC and Neo-Adj-Chemo groups within both AN and tumour tissues, as expressed by MFI (Figure 3.8D). Moving to the myCAF subtype, the expression of CD26 showed no significant difference when comparing AN to tumour from both the Naïve PDAC and Neo-Adj-Chemo groups (Figure 3.8C and D). The comparison of Naïve PDAC versus Neo-Adj-Chemo groups shows that there is higher CD26 expression within the Naïve PDAC group compared to the Neo-Adj group in the AN tissue, as indicated by percentage and MFI (Figure 3.8C and D). A similar trend was observed when comparing the percentage of Naïve PDAC to Neo-Adj-Chemo groups within tumour tissues (Figure 3.8C and D). Finally, the comparison of iCAF versus myCAF reveals that there is no significant difference between iCAF and myCAF within AN and tumour tissues from both the Naïve PDAC and Neo-Adj-Chemo groups, exhibiting no significant difference in expressing CD26 (Figure 3.8C and D).

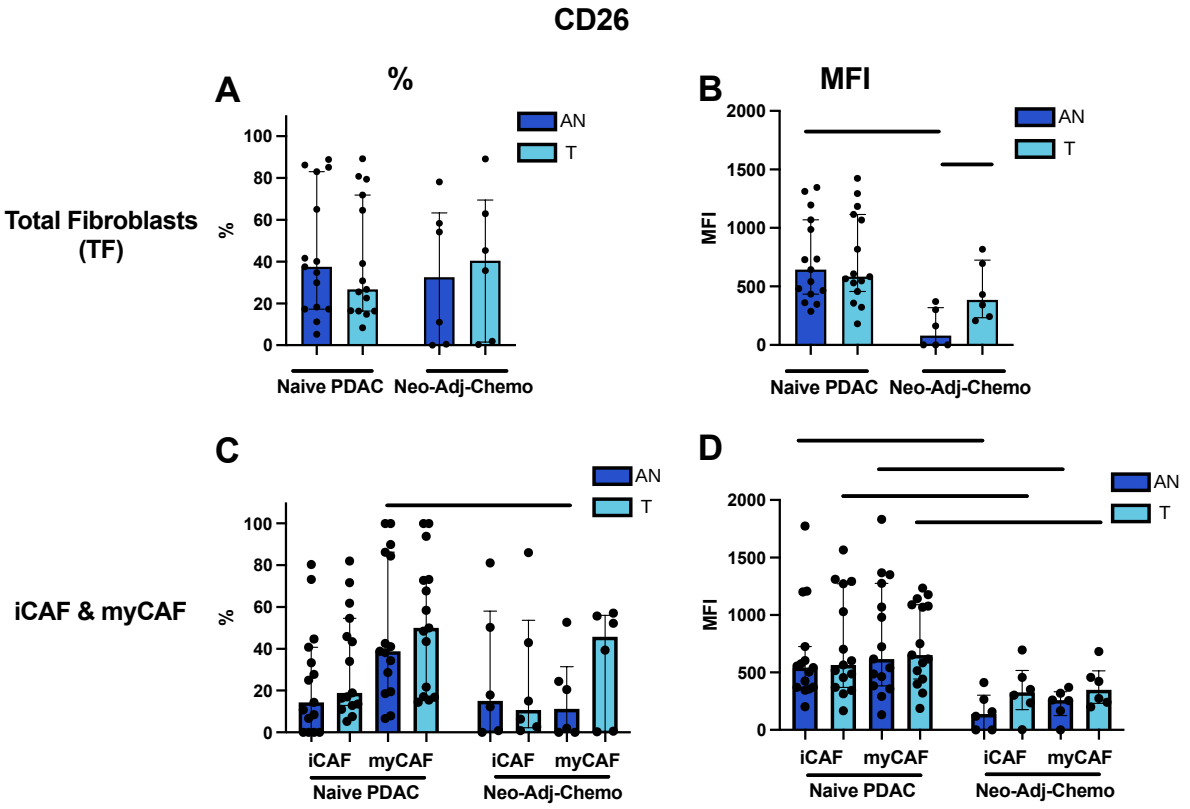


Figure 3.8. Comparison of CD26 Expression in Fibroblast Subtypes in Pancreatic Cancer Patients with and without Neo-adjuvant Chemotherapy.
Fibroblasts from adjacent normal (AN) and tumour (T) tissues were analysed using flow cytometry after enzymatic digestion and staining with a 21-marker panel. Data from *n=11* untreated pancreatic ductal adenocarcinoma (Naïve PDAC) patients and *n=4* PDAC patients who received neo-adjuvant chemotherapy (Neo-Adj-Chemo) were assessed. **A-B-C-D**, comparison of CD26 expression within total fibroblasts (A, B) and iCAF/myCAF (C, D). The comparison includes the percentage (A & C) and Median Fluorescence Intensity (MFI) (B & D) of total fibroblasts (TF) (A, B) and of iCAF/myCAF (C, D). Statistical analysis was carried out using Wilcoxon matched-pairs signed rank test or Mann-Whitney test with * ≤0.05; ** ≤0.01; *** ≤0.001.

CD29 is expressed on populations of mesenchymal stem cells and was also considered an interesting molecule to assess on CAF populations.

An important initial observation was that both the percentage of CD29+ fibroblasts and CD29 expression intensity were increased on fibroblasts within the tumour. Chemotherapy had some effect on reducing the relative expression within the tumour. Of interest, this dual pattern of increased expression was seen on both the iCAF and myCAF populations. As I observed in several of my biomarker panels, these relative differences in CD29 expression were relatively attenuated following delivery of neo-adjuvant treatment.

These data suggest that the expression and intensity of CD29 may represent a valuable marker for identifying CAF populations. Moreover, it is possible that CD29 may play an important role in CAF function and as such may represent a therapeutic target.

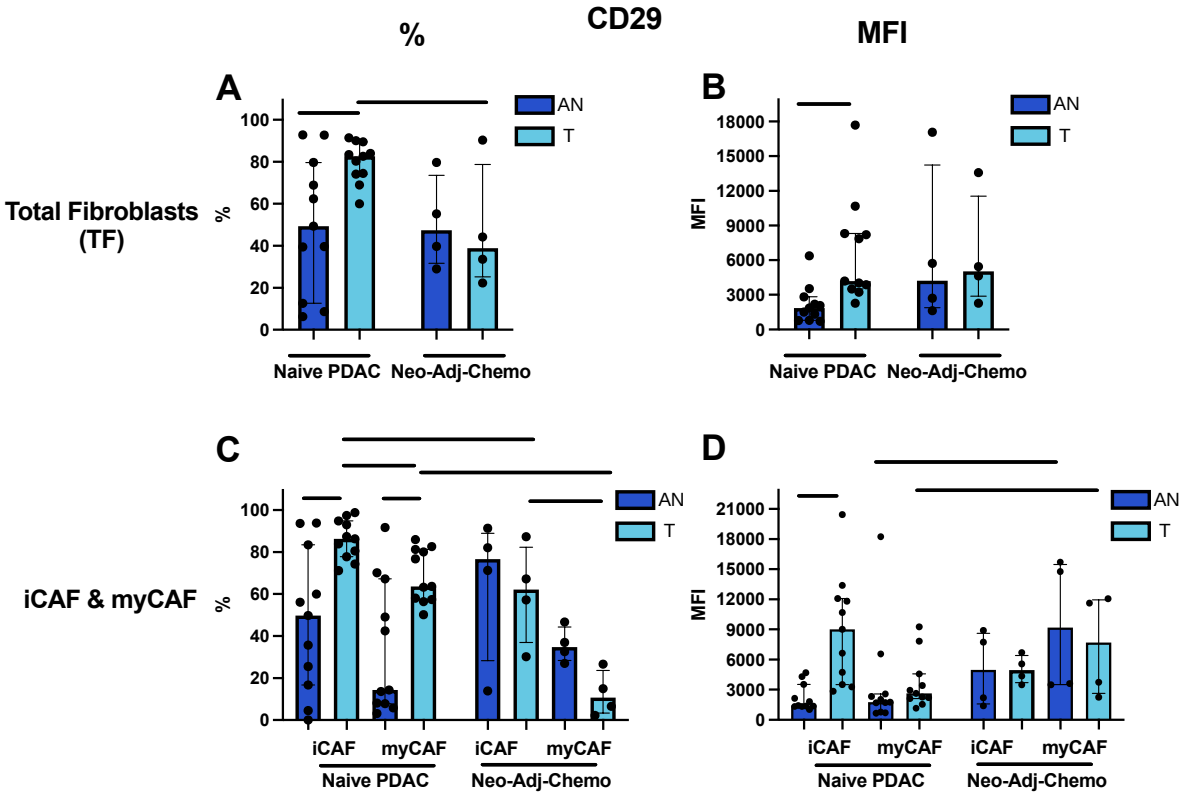


Figure 3.9. Comparison of CD29 Expression in Fibroblast Subtypes in Pancreatic Cancer Patients with and without Neo-adjuvant Chemotherapy.
Fibroblasts from adjacent normal (AN) and tumour (T) tissues were analysed using flow cytometry after enzymatic digestion and staining with a 21-marker panel. Data from *n=11* untreated pancreatic ductal adenocarcinoma (Naïve PDAC) patients and *n=4* PDAC patients who received neo-adjuvant chemotherapy (Neo-Adj-Chemo) were assessed. **A-B-C-D**, comparison of CD29 expression within total fibroblasts (A, B) and iCAF/myCAF (C, D). The comparison includes the percentage (A & C) and Median Fluorescence Intensity (MFI) (B & D) of total fibroblasts (TF) (A, B) and of iCAF/myCAF (C, D). Statistical analysis was carried out using Wilcoxon matched-pairs signed rank test or Mann-Whitney test with * ≤0.05; ** ≤0.01.

The next marker that I interrogated was CD34, a protein that has been described on pro-regenerative subsets (Figure 3.10).

A trend towards a higher relative expression and intensity was seen within adjacent normal tissue but this pattern did not reach statistical significance ($p = 0.38$). However, a striking observation was a markedly increased intensity of expression on both fibroblast subsets, and in both normal and tumour tissue, following neo-adjuvant chemotherapy ($p = 0.03$). It is not entirely clear why this should be, but it may represent an increase in regenerative fibroblast subsets following systemic chemotherapy.

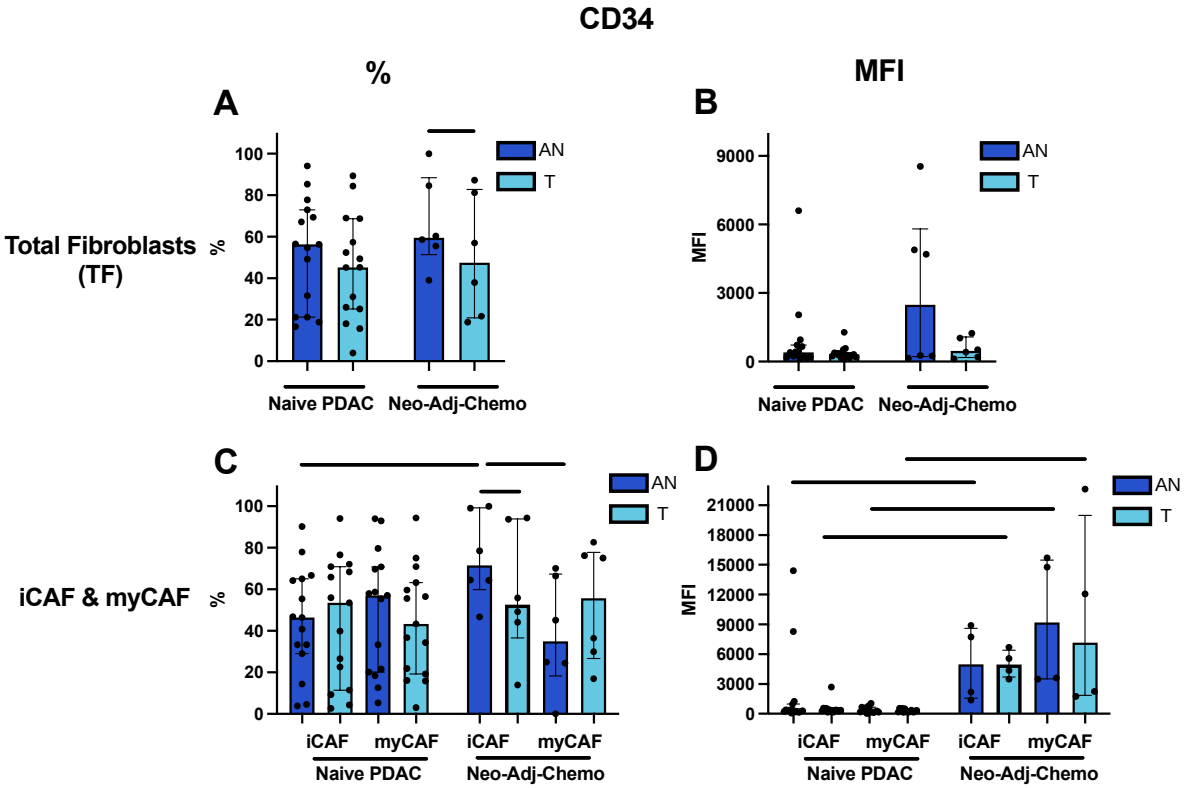


Figure 3.10. Comparison of C34 Expression in Fibroblast Subtypes in Pancreatic Cancer Patients with and without Neo-adjuvant Chemotherapy.

Fibroblasts from adjacent normal (AN) and tumour (T) tissues were analysed using flow cytometry after enzymatic digestion and staining with a 21-marker panel. Data from *n=11* untreated pancreatic ductal adenocarcinoma (Naïve PDAC) patients and *n=4* PDAC patients who received neo-adjuvant chemotherapy (Neo-Adj-Chemo) were assessed. **A-B-C-D**, comparison of CD34 expression within total fibroblasts (A, B) and iCAF/myCAF (C, D). The comparison includes the percentage (A & C) and Median Fluorescence Intensity (MFI) (B & D) of total fibroblasts (TF) (A, B) and of iCAF/myCAF (C, D). Statistical analysis was carried out using Wilcoxon matched-pairs signed rank test or Mann-Whitney test with * ≤0.05; *** ≤0.001.

I next assessed the relative expression of CD90 on the sample set. CD90 expression has typically been associated with inflammatory fibroblasts in cancer and inflammation.

Expression of CD90 was broadly similar between tumour and adjacent normal tissue, with subset analysis revealing that CD90 was expressed on a larger population of myofibroblasts compared to inflammatory fibroblasts in the tumour tissues ($p = 0.04$). This suggests a potential subset-specific role for CD90 in the fibroblast populations. Interestingly, CD90 expression was somewhat higher in CAF populations, indicating that CAFs may play a distinct role in CD90-mediated signalling within the tumour microenvironment. Additionally, the mean fluorescence intensity (MFI) of CD90 expression was somewhat higher following neoadjuvant chemotherapy, which may suggest an increased presence or activation of CD90+ fibroblast subsets post-treatment. This observation warrants further investigation to better understand the functional implications of CD90 in the context of cancer therapy and its potential involvement in the regenerative processes following chemotherapy.

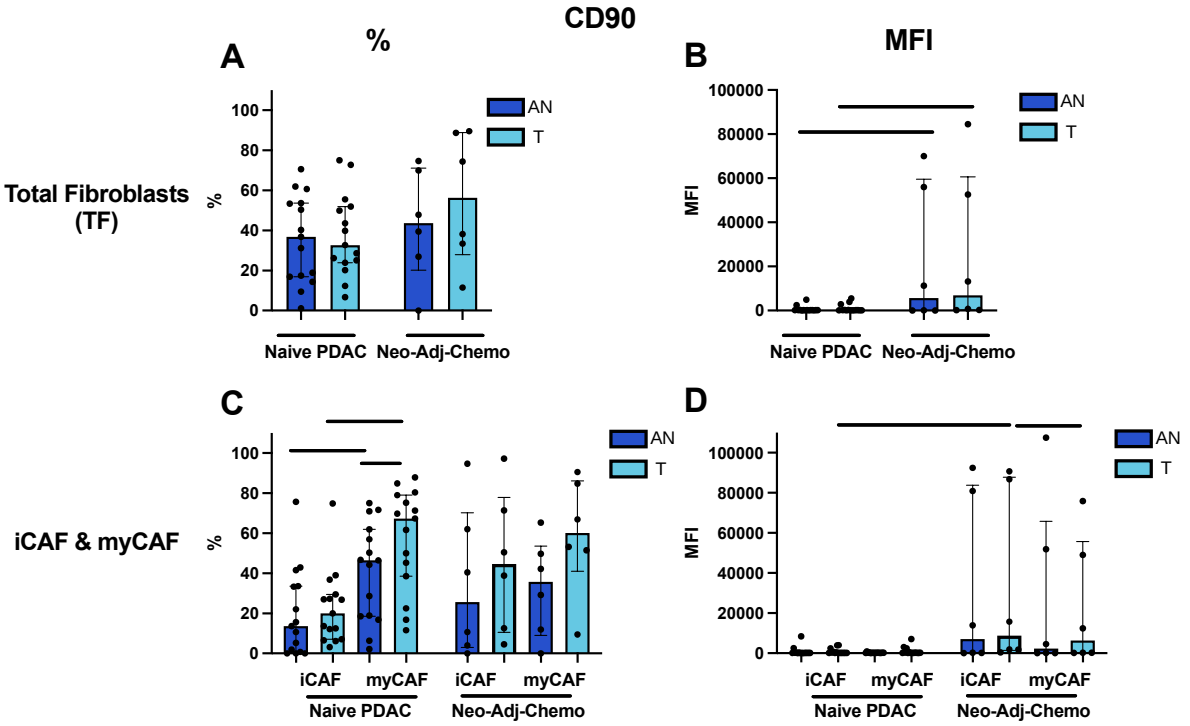


Figure 3.11. Comparison of CD90 Expression in Fibroblast Subtypes in Pancreatic Cancer Patients with and without Neo-adjuvant Chemotherapy.
Fibroblasts from adjacent normal (AN) and tumour (T) tissues were analysed using flow cytometry after enzymatic digestion and staining with a 21-marker panel. Data from *n=11* untreated pancreatic ductal adenocarcinoma (Naïve PDAC) patients and *n=4* PDAC patients who received neo-adjuvant chemotherapy (Neo-Adj-Chemo) were assessed. **A-B-C-D**, comparison of CD90 expression within total fibroblasts (A, B) and iCAF/myCAF (C, D). The comparison includes the percentage (A & C) and Median Fluorescence Intensity (MFI) (B & D) of total fibroblasts (TF) (A, B) and of iCAF/myCAF (C, D). Statistical analysis was carried out using Wilcoxon matched-pairs signed rank test or Mann-Whitney test with * ≤0.05; ** ≤0.01.

CD74 is the receptor for macrophage migration inhibitory factor (MIF) and elevated expression has been observed on fibroblasts in fibrotic conditions such as systemic sclerosis. As such I was interested to assess the relative expression of CD74 on fresh fibroblasts isolated from patient samples.

The relative expression of CD90 on fibroblasts within tumour did not differ from adjacent normal tissue although the relative intensity of expression was somewhat reduced on CAF. Analysis of fibroblast subsets showed a differential pattern. Relative CD74 expression was increased on iCAF populations in tumour but decreased on the myCAF subset. The intensity of expression was also notably high on myCAF cells in adjacent normal tissue. Relatively little differences were seen after neo-adjuvant chemotherapy.

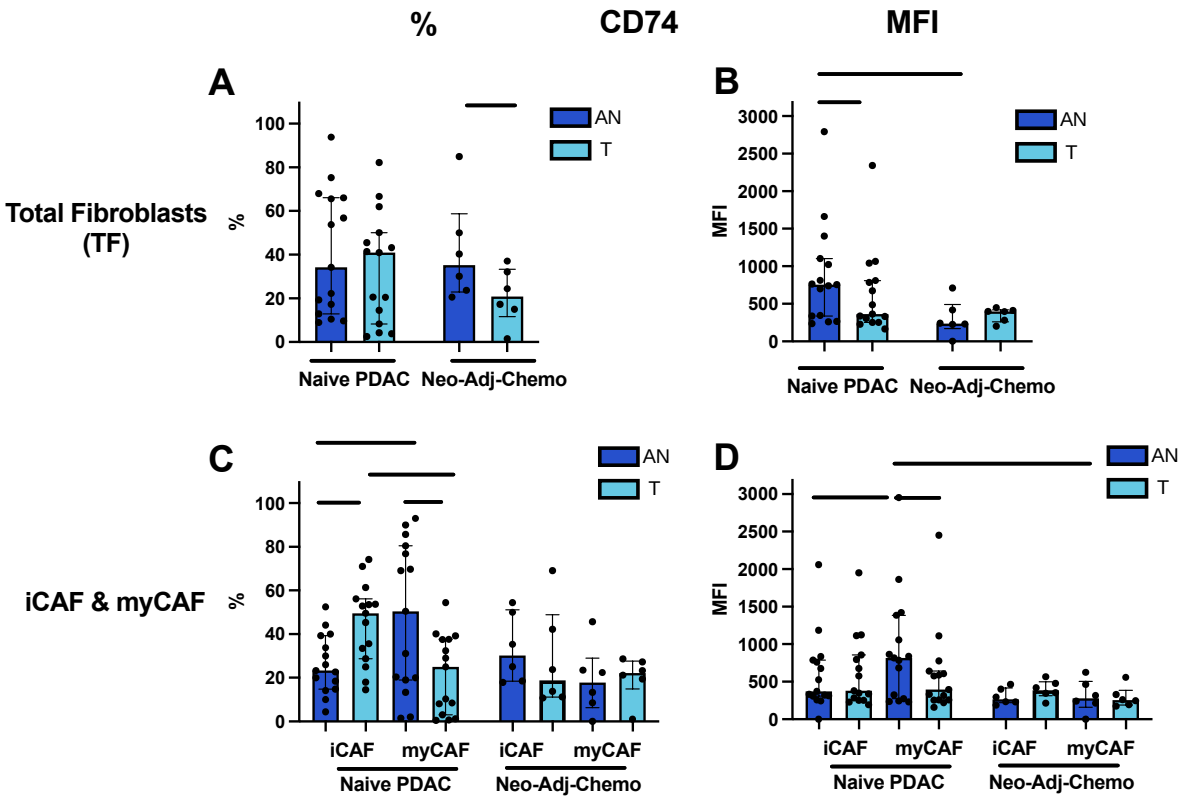


Figure 3.12. Comparison of CD74 Expression in Fibroblast Subtypes in Pancreatic Cancer Patients with and without Neo-adjuvant Chemotherapy.
Fibroblasts from adjacent normal (AN) and tumour (T) tissues were analysed using flow cytometry after enzymatic digestion and staining with a 21-marker panel. Data from *n=11* untreated pancreatic ductal adenocarcinoma (Naïve PDAC) patients and *n=4* PDAC patients who received neo-adjuvant chemotherapy (Neo-Adj-Chemo) were assessed. **A-B-C-D**, comparison of CD74 expression within total fibroblasts (A, B) and iCAF/myCAF (C, D). The comparison includes the percentage (A & C) and Median Fluorescence Intensity (MFI) (B & D) of total fibroblasts (TF) (A, B) and of iCAF/myCAF (C, D). Statistical analysis was carried out using Wilcoxon matched-pairs signed rank test or Mann-Whitney test with * ≤0.05; ** ≤0.01.

My flow cytometry panel also included an antibody against MHS class II (MHC-II; Figure 3.13). This was of interest as MHC-II is involved in antigen presentation and this functional profile has been seen on certain CAF subsets. As such this work could offer insight into the expression levels of MHC-II across total fibroblasts (TF), iCAF, and myCAF. Comparison of adjacent normal (AN) tissue to tumour tissue in both the Naïve PDAC and Neo-Adj-Chemo groups reveals no significant difference in MHC-II expression (see Figure 3.13A and B), reflecting similar observations between Naïve PDAC versus Neo-Adj-Chemo groups in both AN and tumour tissues (Figure 3.13A and B). In terms of the iCAF subtype, a notable increase in MHC-II expression is observed in tumour tissues compared to AN tissue within the Naïve PDAC group, as indicated by percentage and MFI (Figure 3.13C and D), with no significant effect observed in the Neo-Adj-Chemo group (see Figure 3.13C and D). Moreover, no significant difference is noted when comparing Naïve PDAC to Neo-Adj-Chemo groups in AN tissue (Figure 3.13C and D). However, an increase is observed in the Naïve PDAC group compared to the Neo-Adj-Chemo group in tumour tissue, as shown by percentage (Figure 3.13C). Regarding the myCAF subtype, AN tissue exhibits no significant difference in MHC-II expression when comparing AN versus tumour tissues within both Naïve PDAC and Neo-Adj-Chemo groups, as well as when comparing Naïve versus Neo-Adj-Chemo within both AN and tumour tissues (Figure 3.13C and D). Lastly, comparison of iCAF versus myCAF reveals that within AN tissue, myCAF demonstrate a higher level of MHC-II expression compared to iCAF, as shown by MFI. Moreover, no significant difference is observed in tumour tissues, as well as when comparing iCAF and myCAF within both AN and tumour tissues in the Neo-Adj-Chemo group (Figure 3.13C and D).

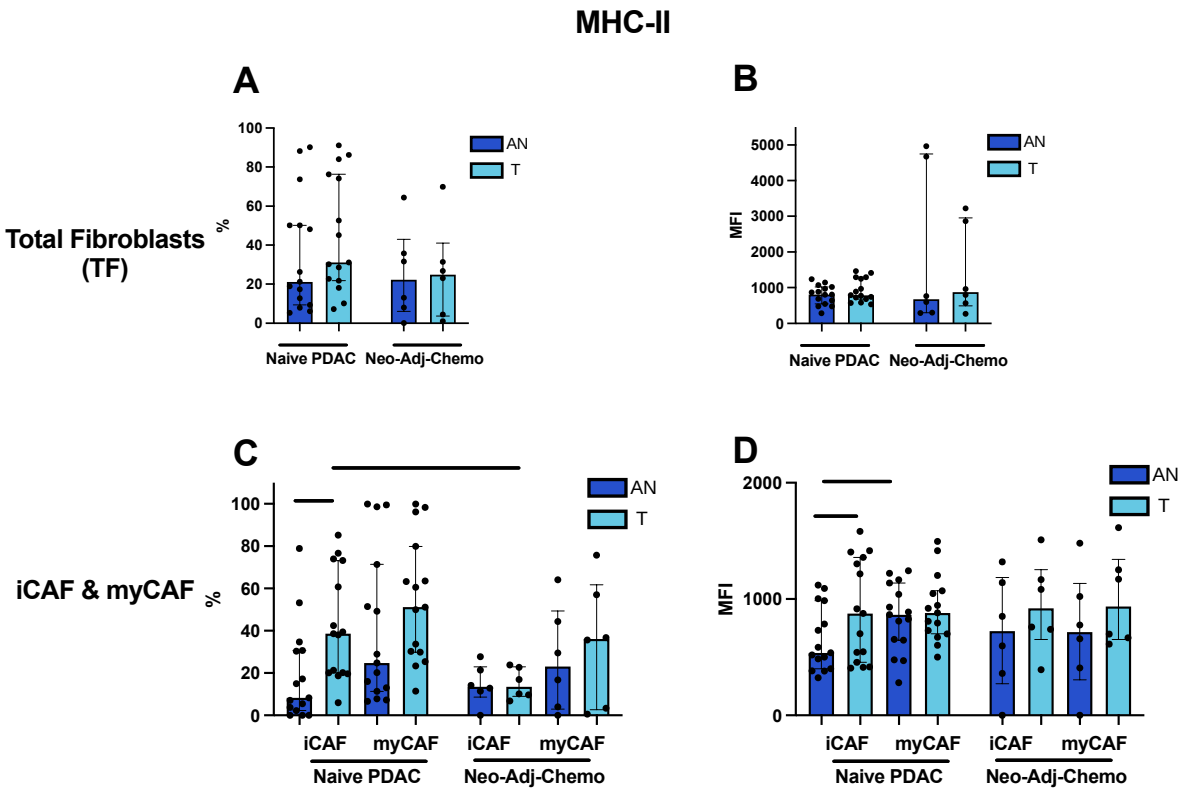


Figure 3.13. Comparison of MHC-II Expression in Fibroblast Subtypes in Pancreatic Cancer Patients with and without Neo-adjuvant Chemotherapy.
Fibroblasts from adjacent normal (AN) and tumour (T) tissues were analysed using flow cytometry after enzymatic digestion and staining with a 21-marker panel. Data from *n=11* untreated pancreatic ductal adenocarcinoma (Naïve PDAC) patients and *n=4* PDAC patients who received neo-adjuvant chemotherapy (Neo-Adj-Chemo) were assessed. **A-B-C-D**, comparison of MHC-II expression within total fibroblasts (A, B) and iCAF/myCAF (C, D). The comparison includes the percentage (A & C) and Median Fluorescence Intensity (MFI) (B & D) of total fibroblasts (TF) (A, B) and of iCAF/myCAF (C, D). Statistical analysis was carried out using Wilcoxon matched-pairs signed rank test or Mann-Whitney test with * ≤0.05; *** ≤0.001.

Expression of CD105 was of particular interest to me as CD105-positive pancreatic fibroblasts have been shown to be permissive for tumour growth whilst CD105-negative subsets can be tumour suppressive (Hutton et al., 2021).

Somewhat surprisingly, very little differences were seen in relation to CD105 expression within the sample set. Somewhat higher levels of expression were seen on myCAF subsets within tumour but little else of note was observed.

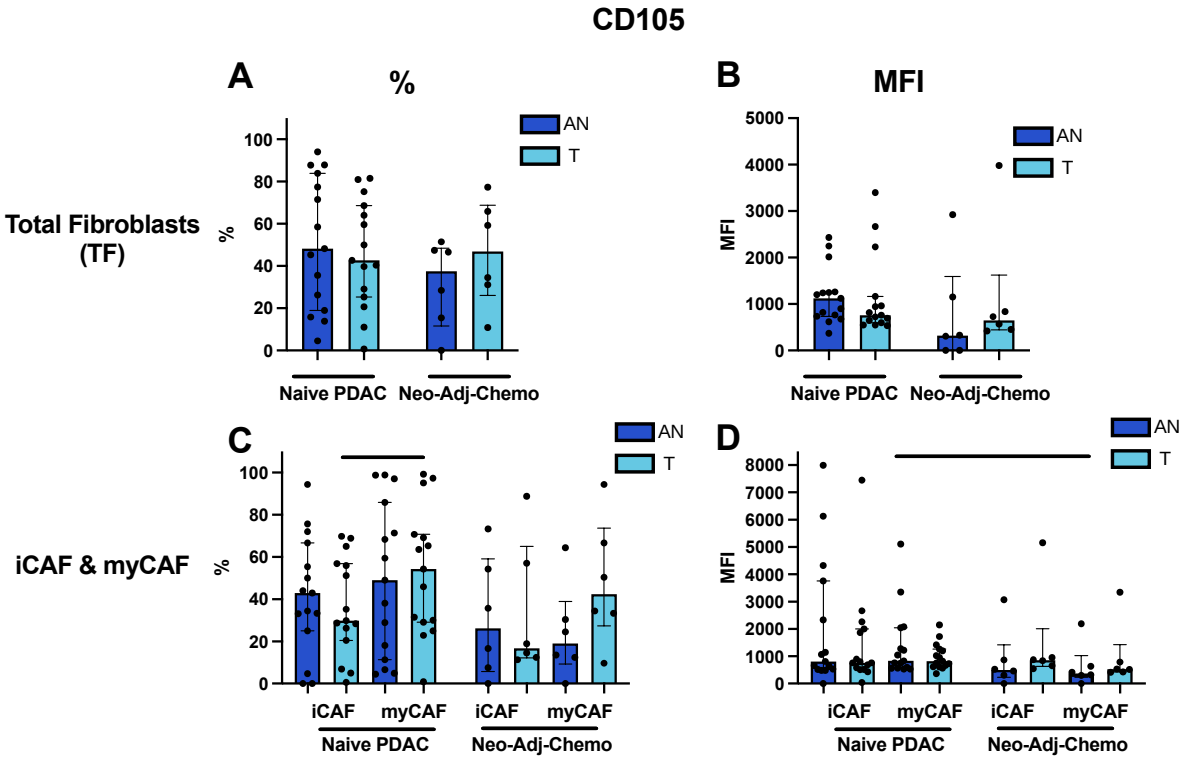
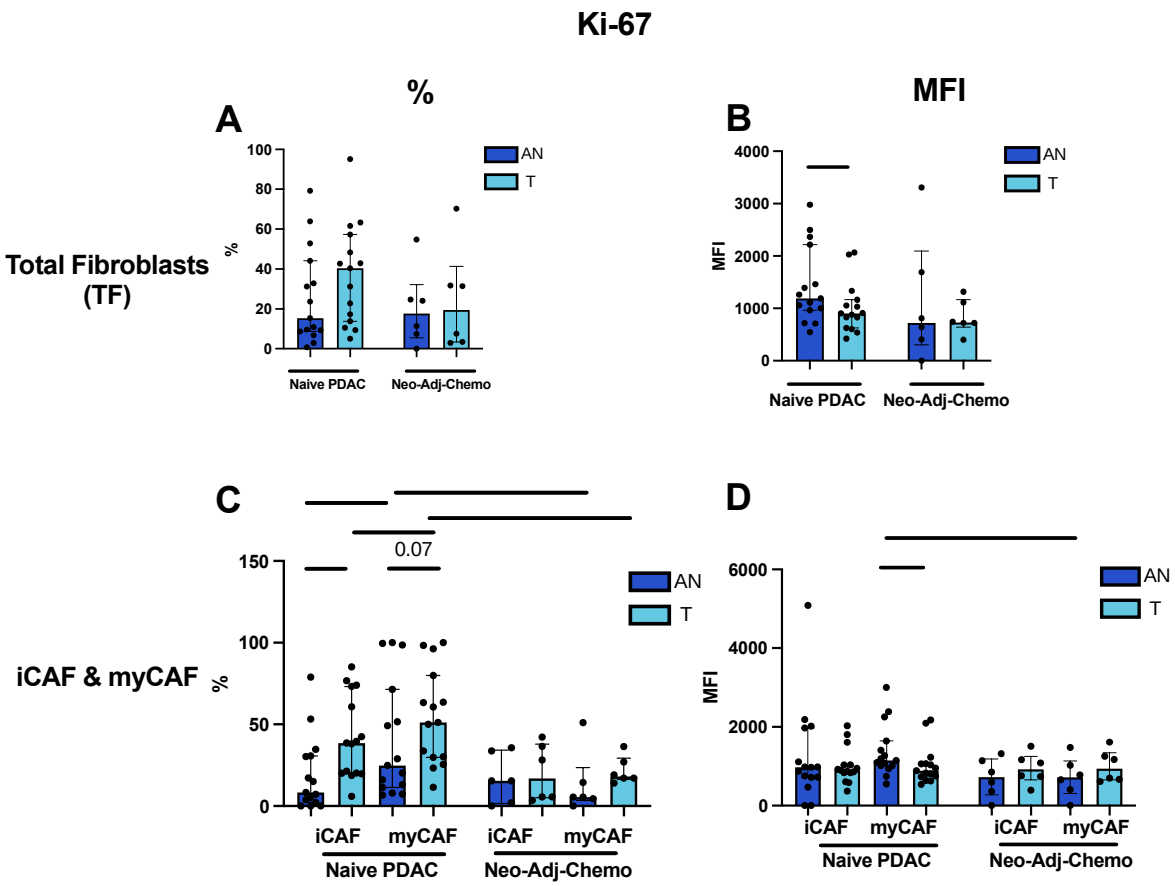


Figure 3.14. Comparison of CD105 Expression in Fibroblast Subtypes in Pancreatic Cancer Patients with and without Neo-adjuvant Chemotherapy.
Fibroblasts from adjacent normal (AN) and tumour (T) tissues were analysed using flow cytometry after enzymatic digestion and staining with a 21-marker panel. Data from n=11 untreated pancreatic ductal adenocarcinoma (Naïve PDAC) patients and n=4 PDAC patients who received neo-adjuvant chemotherapy (Neo-Adj-Chemo) were assessed. **A-B-C-D**, comparison of CD105 expression within total fibroblasts (A, B) and iCAF/myCAF (C, D). The comparison includes the percentage (A & C) and Median Fluorescence Intensity (MFI) (B & D) of total fibroblasts (TF) (A, B) and of iCAF/myCAF (C, D). Statistical analysis was carried out using Wilcoxon matched-pairs signed rank test or Mann-Whitney test with * ≤0.05.

Ki67 is a valuable marker of cellular proliferation and as such I had included this in the flow cytometry panel in order to see if there were any differences in relative cell division between samples.

The data depicted in Figure 3.15 provide insights into the expression levels of Ki-67 among different fibroblast subtypes, including total fibroblasts (TF), iCAF and myCAF. When comparing AN tissue to tumour tissue in both the Naïve PDAC and Neo-Adj-Chemo groups, a significant difference is observed in AN compared to tumour in the Naïve PDAC group, evidenced by the MFI, while no significant difference is observed in the Neo-Adj-Chemo group (Figure 3.15). Furthermore, comparing the Naïve PDAC group to the Neo-Adj-Chemo group in both AN and tumour tissues reveals non-significant differences (see Figure 3.15A and B). Regarding the iCAF subtype, a significant increase in Ki-67 expression is observed in tumour tissues compared to AN tissue in the Naïve PDAC group, as indicated by percentage (Figure 3.15C), with no significant effect observed in the Neo-Adj-Chemo group (see Figure 3.15C and D). Additionally, no significant difference is noted when comparing Naïve PDAC to Neo-Adj-Chemo groups in both AN and tumour tissues (see Figure 3.15C and D). In the case of the myCAF subtype, AN tissue showcases low level of Ki-67 expression compared to tumour tissues in the Naïve PDAC group as demonstrated by the MFI, albeit the results did not achieve significance in the percentage ($p=0.07$), with no notable impact observed in the Neo-Adj-Chemo groups (Figure 3.15C and D). Conversely, when comparing Naïve PDAC and Neo-Adj-Chemo groups, a higher expression of Ki-67 is observed in the Naïve PDAC group in both AN and tumour tissues, as indicated by both percentage and MFI (Figure 3.15C and D). Lastly, comparing iCAF versus myCAF reveals that within AN tissue, myCAF demonstrate a higher level of Ki-67 expression compared to iCAF in both AN and tumour tissues, as

shown by percentage. Moreover, no significant difference is observed between iCAF and myCAF within both AN and tumour tissues in the Neo-Adj-Chemo group (Figure 3.15C and D).



test

Figure 3.15. Comparison of Ki-67 Expression in Fibroblast Subtypes in Pancreatic Cancer Patients with and without Neo-adjuvant Chemotherapy.
Fibroblasts from adjacent normal (AN) and tumour (T) tissues were analysed using flow cytometry after enzymatic digestion and staining with a 21-marker panel. Data from *n=11* untreated pancreatic ductal adenocarcinoma (Naïve PDAC) patients and *n=4* PDAC patients who received neo-adjuvant chemotherapy (Neo-Adj-Chemo) were assessed. **A-B-C-D,** comparison of Ki-67 expression within total fibroblasts (A, B) and iCAF/myCAF (C, D). The comparison includes the percentage (A & C) and Median Fluorescence Intensity (MFI) (B & D) of total fibroblasts (TF) (A, B) and of iCAF/myCAF (C, D). Statistical analysis was carried out using Wilcoxon matched-pairs signed rank test or Mann-Whitney test with * ≤0.05; ** ≤0.01; *** ≤0.001.

I next went on assess the relative expression of PDGF-R proteins within tumour tissue. This is a cell surface tyrosine kinase receptor for the platelet derived growth factor (PDGF) molecules that regulate many aspects of cell and tissue regulation. There are two forms of PDGF-R and these may form homo- or heterodimers based on which ligand they bind.

I initially started by assessment of PDGFR-α expression. Murine data have shown that PDGFR-α signalling can support fibroblast progenitor expansion whilst its downregulation may facilitate differentiation into myofibroblasts (Yao et al., 2022). Interestingly, both the relative expression and the expression level of PDGF-Ra were reduced on CAF populations. Furthermore, this pattern was seen on both iCAF and myCAF populations.

I next assessed the impact of protein expression on fibroblasts from neo-adjuvant samples. Here it was noteworthy that chemotherapy attenuated the suppression of PDGF-Ra expression in relation to both expression levels and protein staining intensity.

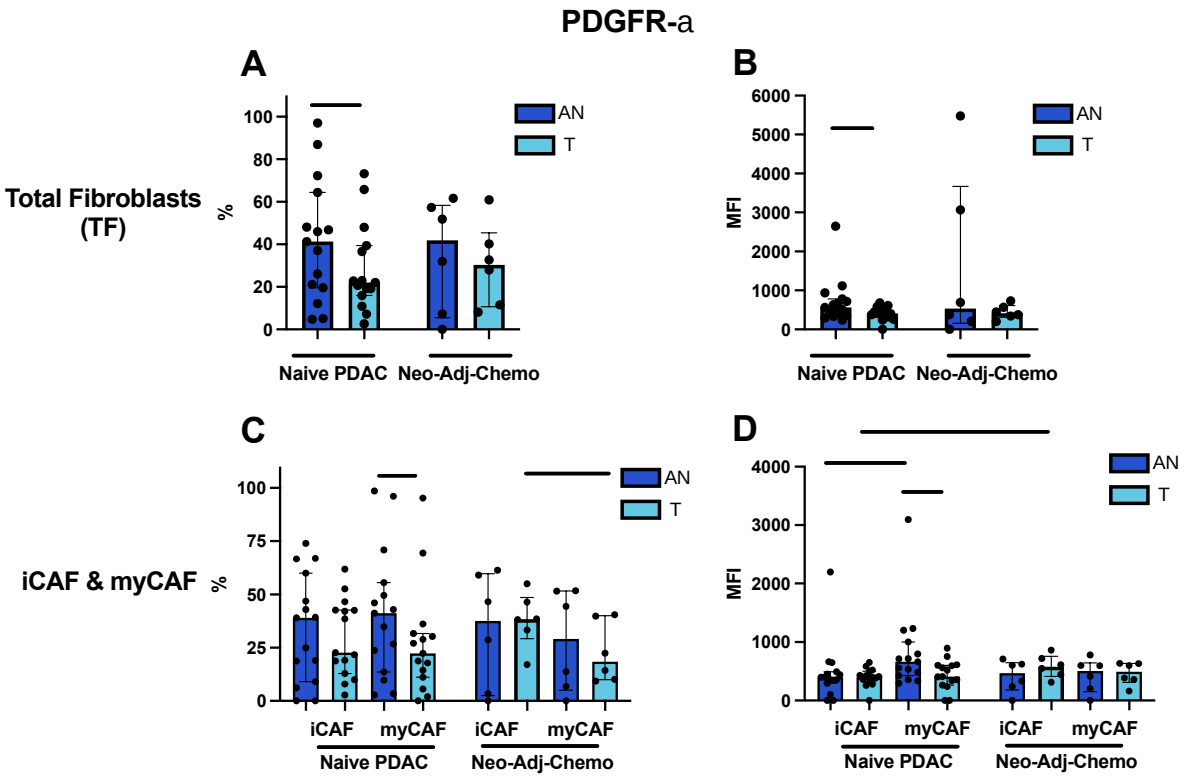


Figure 3.16. Comparison of PDGFR-α Expression in Fibroblast Subtypes in Pancreatic Cancer Patients with and without Neo-adjuvant Chemotherapy.
Fibroblasts from adjacent normal (AN) and tumour (T) tissues were analysed using flow cytometry after enzymatic digestion and staining with a 21-marker panel. Data from *n=11* untreated pancreatic ductal adenocarcinoma (Naïve PDAC) patients and *n=4* PDAC patients who received neo-adjuvant chemotherapy (Neo-Adj-Chemo) were assessed. **A-B-C-D**, comparison of PDGFR-α expression within total fibroblasts (A, B) and iCAF/myCAF (C, D). The comparison includes the percentage (A & C) and Median Fluorescence Intensity (MFI) (B & D) of total fibroblasts (TF) (A, B) and of iCAF/myCAF (C, D). Statistical analysis was carried out using Wilcoxon matched-pairs signed rank test or Mann-Whitney test with * ≤0.05, ** ≤0.01.

A trend towards a decrease in expression of PDGFR-α was also seen on CAF although this pattern was less pronounced than that seen with PDGFR-α (Fig. 3.17) Indeed, the intensity of protein expression was enhanced on myCAF subsets within tumour. No significant impact of neo-adjuvant chemotherapy was observed.

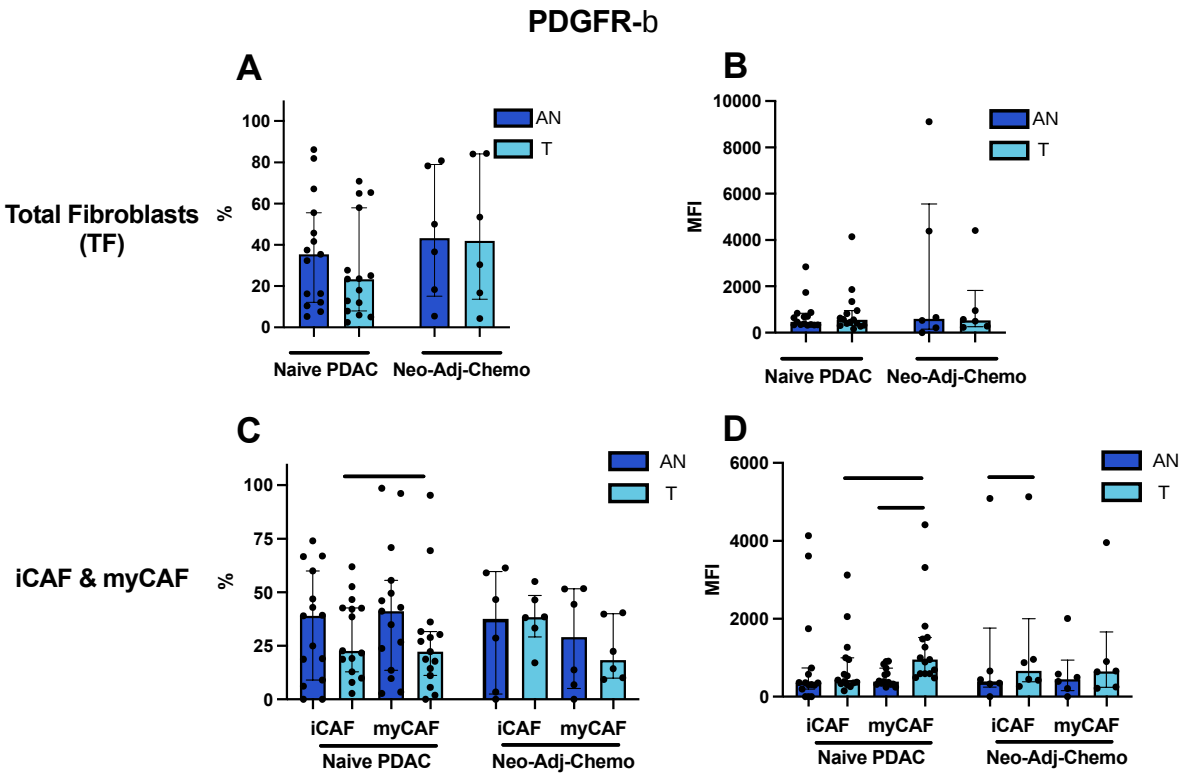


Figure 3.17. Comparison of PDGFR-β Expression in Fibroblast Subtypes in Pancreatic Cancer Patients with and without Neo-adjuvant Chemotherapy.
Fibroblasts from adjacent normal (AN) and tumour (T) tissues were analysed using flow cytometry after enzymatic digestion and staining with a 21-marker panel. Data from *n=11* untreated pancreatic ductal adenocarcinoma (Naïve PDAC) patients and *n=4* PDAC patients who received neo-adjuvant chemotherapy (Neo-Adj-Chemo) were assessed. **A-B-C-D**, comparison of PDGFR-β expression within total fibroblasts (A, B) and iCAF/myCAF (C, D). The comparison includes the percentage (A & C) and Median Fluorescence Intensity (MFI) (B & D) of total fibroblasts (TF) (A, B) and of iCAF/myCAF (C, D). Statistical analysis was carried out using Wilcoxon matched-pairs signed rank test or Mann-Whitney test with * ≤0.05; *** ≤0.001.

The data provided in figure 3.18 illuminate the expression levels of PDPN among total fibroblasts (TF), as well as distinct fibroblast subtypes including iCAF and myCAF. Comparison of adjacent normal (AN) tissue to tumour tissue in both the Naïve PDAC and Neo-Adj-Chemo groups reveals no significant difference in PDPN expression (Figure 3.18A and B). However, upon closer examination between the Naïve PDAC and Neo-Adj-Chemo groups, a noteworthy increase in PDPN expression is observed in the Naïve PDAC group compared to the Neo-Adj-Chemo group within both AN and tumour tissues, as emphasized by the mean fluorescence intensity (MFI) (Figure 3.18B). Regarding the iCAF subtype, a non-significant difference is noted when comparing AN versus tumour tissue in the Naïve PDAC groups. However, within the Neo-Adj-Chemo group, AN tissue exhibits lower PDPN expression compared to tumour tissue, as indicated by MFI (Figure 3.18D). Nonetheless, upon further analysis between the Naïve PDAC and Neo-Adj-Chemo groups, no significant difference in PDPN expression is observed in both AN and tumour tissues (Figure 3.18C and D). For the myCAF subtype, comparison of AN to tumour tissue in both the Naïve PDAC and Neo-Adj-Chemo groups reveals no significant difference in PDPN expression (Figure 3.18C and D), echoing similar observations between Naïve PDAC versus Neo-Adj-Chemo groups in both AN and tumour tissues (Figure 3.18C and D). Lastly, comparing iCAF versus myCAF reveals that within AN tissue, iCAF demonstrate a higher level of PDPN expression compared to myCAF, as shown by percentage, with no significant difference observed in tumour tissues. Moreover, no significant difference is observed between iCAF and myCAF within both AN and tumour tissues in the Neo-Adj-Chemo group (see Figure 3.18C and D).

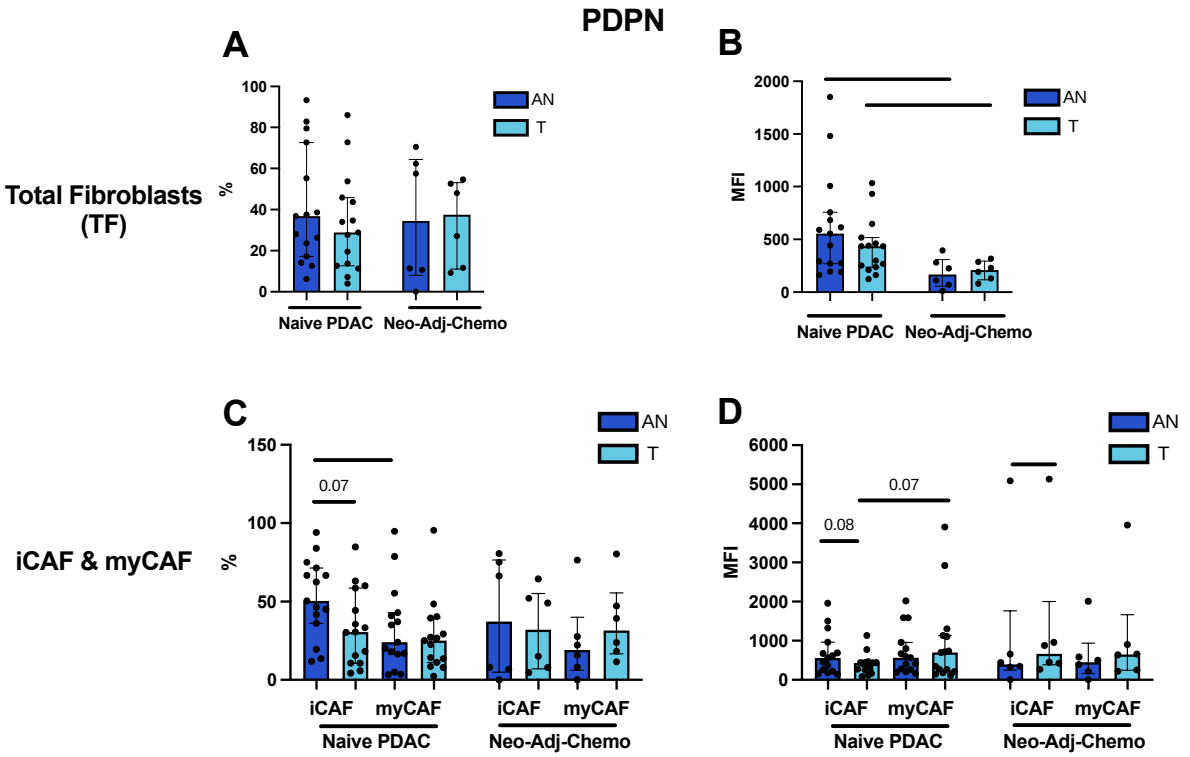


Figure 3.18. Comparison of PDPN Expression in Fibroblast Subtypes in Pancreatic Cancer Patients with and without Neo-adjuvant Chemotherapy.
Fibroblasts from adjacent normal (AN) and tumour (T) tissues were analysed using flow cytometry after enzymatic digestion and staining with a 21-marker panel. Data from *n=11* untreated pancreatic ductal adenocarcinoma (Naïve PDAC) patients and *n=4* PDAC patients who received neo-adjuvant chemotherapy (Neo-Adj-Chemo) were assessed. **A-B-C-D**, comparison of PDPN expression within total fibroblasts (A, B) and iCAF/myCAF (C, D). The comparison includes the percentage (A & C) and Median Fluorescence Intensity (MFI) (B & D) of total fibroblasts (TF) (A, B) and of iCAF/myCAF (C, D). Statistical analysis was carried out using Wilcoxon matched-pairs signed rank test or Mann-Whitney test with * ≤0.05.

3.3 Discussion

The work in this chapter underscores the pivotal role of fibroblasts in PDAC progression and therapeutic response, focusing on three specific aims: characterizing cellular composition in PDAC, investigating the distinct roles of iCAF and myCAF, and exploring fibroblast marker expression profiles in response to chemotherapy. Through these aims, this study aims to enhance the understanding of the dynamic interactions between fibroblasts and PDAC, potentially improving therapeutic strategies and patient outcomes.

The TME of PDAC is a complex assembly of various cell types, including extracellular matrix (ECM), cancer-associated fibroblasts (CAFs), endothelial cells (EnCs), pericytes, nerves, and immune cells (Falcomata et al., 2023). My findings support prior observations of substantial heterogeneity in cellular composition among PDAC patients, revealing an inverse correlation between the abundance of endothelial cells, immune cells, and fibroblasts in tumour tissues compared to adjacent normal (AN) regions. This heterogeneity may arise from tumour-intrinsic characteristics like genomic instability and epigenetic modifications, as well as external influences from the TME, such as hypoxia, endothelial remodelling, and immune responses. Additionally, factors like treatment history, host genetics, nutrition, obesity, microbiome, and environmental influences further contribute to this complexity. PDAC is characterized by a highly desmoplastic and stroma-rich phenotype, yet the extent to which this fibrotic environment drives tumour progression remains debated (Moustakas et al., 2022). The presence of frequent mutations in genes such as KRAS, CDKN2A, SMAD4, and TP53 adds to the complexity of PDAC biology and its impact

on cellular composition and function (Sun et al., 2020). The balance between effector and tolerogenic immune responses also plays a crucial role in tumour fate (Gonzalez et al., 2018).

Chemotherapy significantly influences the cellular composition of PDAC. It targets rapidly proliferating cancer cells and affects the TME (Liu et al., 2017). Agents like gemcitabine can induce stromal depletion and may promote resistance to immunotherapy (Werba et al., 2023). Ozdemir et al. demonstrated that myofibroblast depletion leads to more invasive tumours with poor response to gemcitabine but improved response to anti-CTLA4 immunotherapy (Ozdemir et al., 2014). Understanding the interplay between chemotherapy and cellular components of PDAC is crucial for optimizing therapeutic strategies. This study compared cell type proportions in matched AN and tumour tissues from untreated and neo-adjuvant chemotherapy treated PDAC patients. In untreated patients, tumour tissues exhibited higher proportions of epithelial cells (EpC), and fibroblasts compared to AN tissue. However, no significant differences were observed in the chemo-treated group, suggesting chemotherapy-induced alterations in TME dynamics. This observation aligns with findings that tumours are characterized by a predominance of EpC and fibroblasts, with epithelial-to-mesenchymal transition (EMT) contributing to tumour progression (J P Thiery, 1999; Kalluri & Neilson, 2003).

Various subtypes of CAFs, including myCAF and iCAF, have been identified in PDAC (Belle & DeNardo, 2019; Biffi et al., 2019; Elyada et al., 2019). MyCAF, characterized by α-SMA expression and TGF-β signalling, typically reside proximal to the tumour, while iCAF, with a cytokine and chemokine secretory phenotype, are found more

distally. My study found a differential distribution of fibroblasts within the TME, with myCAF predominating in AN tissue and iCAF in tumour tissues. This suggests myCAF's role in maintaining tissue homeostasis or supporting early tumour development, while iCAF may promote tumour progression and immunosuppression. The higher proportion of iCAF in the neo-adjuvant group compared to the Naïve PDAC group suggests a chemotherapy-induced shift towards a pro-inflammatory microenvironment. Conversely, the greater prevalence of myCAF in the Naïve PDAC group indicates a relatively quiescent or less inflammatory state. However, some of these differences were not statistically significant, highlighting the need for larger sample sizes to understand the effects of chemotherapy on CAF subtypes in the TME.

Elevated C3 expression in total fibroblasts and myCAF of tumour tissues in the Naïve PDAC group suggests C3's role in promoting tumour growth through inflammation, angiogenesis, or immunosuppression. In contrast, higher C3 expression in AN tissue of the neo-adj-chemo group may indicate a protective role against tumour development, potentially through C3-mediated immune surveillance enhanced by chemotherapy (K. Chen et al., 2021; Davidson et al., 2020; Shu et al., 2020).

Higher Cadherin-11 expression in total fibroblasts and iCAF in tumour tissues of the neo-adj-chemo group suggests its role in tumour-stromal interactions and tumour progression. Differential expression of Cadherin-11 between iCAF and myCAF indicates distinct functional roles within the tumour stroma, with iCAF potentially contributing more to tumour-promoting processes (Chang et al., 2011; Passanha et al., 2022).

Elevated CD26 expression in iCAF within PDAC tumour tissues suggests its involvement in the inflammatory milieu of PDAC, shaping the TME by fostering

inflammation and recruiting immune cells. The significance of CD26 elevation post-chemotherapy remains ambiguous, possibly reflecting treatment response or microenvironmental adjustments (Worthen et al., 2020).

Higher CD29 expression in total fibroblasts, iCAF and myCAF of tumour tissues in the Naïve PDAC group suggests its role in tumour progression and microenvironmental remodelling. CD29, or integrin beta 1, promotes interactions between cancer cells and the ECM, facilitating invasive behaviour and metastatic potential. The modulation of CD29 expression by chemotherapy indicates its potential as a biomarker for treatment response (Costa et al., 2018; Pelon et al., 2020; Zeltz et al., 2019).

Elevated CD34 expression in total fibroblasts within AN tissue from the neo-adj-chemo group suggests a role in supporting tumour suppression or tissue homeostasis. CD34 presence on CAFs implies additional roles in tumour biology, with higher expression in iCAF suggesting involvement in angiogenesis and immune regulation (Barth et al., 2002; S. Noda et al., 2022; Radu et al., 2023; Westhoff et al., 2020).

The elevation of CD90 expression in the neo-adj-chemo group suggests its significance in chemotherapy response and TME modulation in PDAC. CD90, or Thy-1, plays roles in cell adhesion, migration, and signalling. Its association with tumorigenesis, metastasis, and drug resistance suggests its potential involvement in PDAC progression and response to chemotherapy (Rege & Hagood, 2006).

Higher CD74 levels in AN tissue within the Naïve PDAC group suggest a protective role against tumour development. However, lower expression in tumour tissues within the same group indicates a loss of CD74-mediated protection during tumour progression. Chemotherapy-induced changes in CD74 expression patterns highlight its complex, context-dependent role in PDAC development and response to treatment (Elyada et al., 2019; Hong et al., 2023; Xu et al., 2021).

Elevated MHC-II expression in iCAF within tumour tissues of the Naïve PDAC group indicates enhanced immune activation or antigen presentation capacity, potentially contributing to anti-tumour immunity. The lack of significant effects in myCAF suggests differential responses of fibroblast subtypes to tumour progression and chemotherapy (Elyada et al., 2019; Friedman et al., 2020; Kerdidani et al., 2022).

Elevated CD105 levels in myCAF from the Naïve PDAC group suggest enhanced angiogenic potential, promoting tumour vascularization and progression. Conversely, lower CD105 expression in myCAF from the neo-adj-chemo group indicates chemotherapy-induced alterations in angiogenic signalling pathways (Hutton et al., 2021).

Higher Ki-67 expression in myCAF than iCAF within AN tissue implies a more proliferative myCAF phenotype involved in tissue repair or remodelling. In tumour tissues, elevated Ki-67 in the Naïve PDAC group suggests heightened proliferative activity, influencing tumour progression and treatment response (Jing et al., 2018; Kim et al., 2014).

PDGFR-α and PDGFR-β are essential in fibroblast activation, with differential expression patterns indicating distinct roles in tumour progression. Higher PDGFR-α in AN tissue suggests less activated fibroblasts, while elevated PDGFR-β in iCAF post-chemotherapy suggests a role in tumour progression. The differential expression highlights the heterogeneity of fibroblasts and their implications in tumour biology and therapeutic response (Gao et al., 2005; Hewitt et al., 2012; Li et al., 2018; Shook et al., 2018; Yao et al., 2022).

3.4 Conclusion

This study highlights the critical role of fibroblasts in PDAC progression and therapeutic response, revealing the complex interplay between fibroblast subtypes, the TME, and chemotherapy. The differential expression of markers and the distinct roles of iCAF and myCAF emphasize the need for targeted therapeutic strategies to modulate fibroblast activity and enhance treatment efficacy. Understanding the dynamic interactions within the TME can pave the way for improved therapeutic approaches and better patient outcomes in PDAC.

Chapter 4: Interaction of Fibroblasts with immune cells

4.1 Introduction

Fibroblasts play a crucial role in modulating the function of immune cells, including T and NK cells, in various cancers through the secretion of cytokines, chemokines, and other signalling molecules (Lavie et al., 2022). Studies have demonstrated that CAF strongly suppress the proliferation of T and NK cells in contact-independent models across different cancer types (Gorchs et al., 2019; Gorchs & Kaipe, 2021; Yang et al., 2020). This leads to the conclusion that depleting CAFs may enhance the activity of T and NK cells and promote their infiltration into tumours, thereby overcoming the immune-suppressive and tumour-promoting effects of CAFs. There has been limited research dedicated to understanding the influence of fibroblasts on the phenotypes of T and NK cells, encompassing factors such as proliferation, activation, and effector functions. This chapter delves into the evaluation of T and NK cell proliferation and phenotyping during direct interaction with primary and immortalised CAFs and adjacent normal fibroblasts (ANFs) from various human PDAC patients. The proliferation assay utilized carboxyfluorescein diacetate succinimidyl ester (CFSE), which covalently labels intracellular molecules with a highly fluorescent dye. Upon cell division, the fluorescent dye is equally distributed among daughter cells, resulting in a halving of fluorescence intensity with each division (Quah & Parish, 2010). Interestingly, my investigation yielded contrasting findings; an observation that fibroblasts do not affect the proliferation of T and NK cells if they are stimulated. Instead, fibroblasts can enhance the proliferation of T and NK cells when they are not stimulated. Additionally, my work undertook deep phenotyping of both T and NK cells in direct co-culture with ANF and CAF, offering novel insights.

4.2 Results

4.2.1 Effect of fibroblasts on T and NK cells proliferation and IFN-γ production

The gating strategy for proliferated T and NK cells, stained with CFSE after co-culture with adjacent normal fibroblasts (ANF) and cancer-associated fibroblasts (CAF), is depicted in figures 4.1a and 4.3a. Initially, T and NK cells were gated based on forward scatter (FSC) and side scatter (SSC). Subsequently, viability dye (BV570) was used to exclude dead cells. Figure 4.2 presents the percentage of proliferated T cells in unstimulated and stimulated conditions. Interestingly, the co-culture of non-stimulated T cells with ANF and CAF increases their proliferative capacity (from 1.1% to 2.8%) (Figure 4.2b), while the co-culture of stimulated T cells with ANF and CAF does not significantly affect the proliferation rate (Figure 4.2a). The same effect has been observed with NK cells as depicted in figure 4.4. The co-culture of non-stimulated NK cells with ANF and CAF increases their proliferative capacity (from 7.5% to 18% and 14% respectively) (Figure 4.4b), while the co-culture of stimulated NK cells with ANF and CAF does not significantly affect the proliferation rate (Figure 4.4a). The effect of immortalized fibroblasts on the function of T and NK cells was investigated, as shown in figures 4.5 and 4.6. Moreover, when comparing the effect of ANF and CAF on T cells, I observed that there is no difference between CAF and ANF.

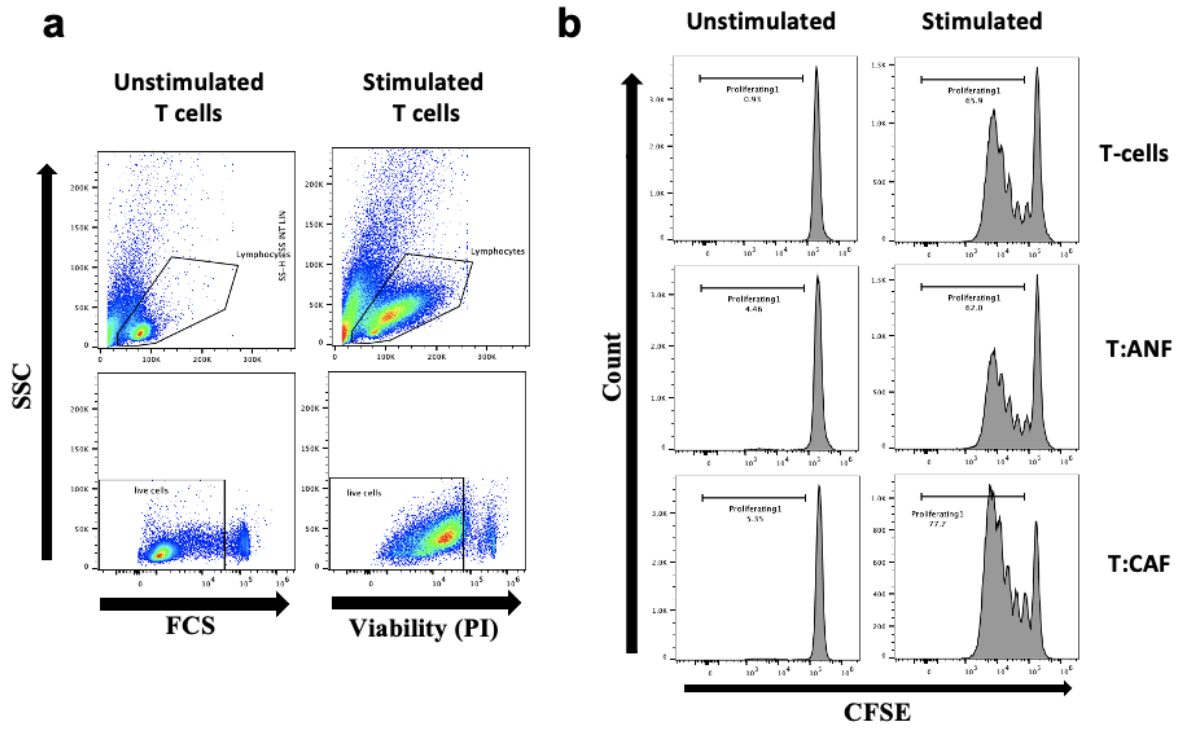


Figure 4.1. Comparison in T cells proliferation ability between T cells co-cultured with primary ANFs and CAFs using CFSE assay (direct contact).
a. Flow cytometry gating strategy of unstimulated versus stimulated total T cells. **b.** Examples of Flow cytometry histograms to compare the CFSE profile between T cells co-cultured with ANF and CAF in both unstimulated and stimulated conditions. The gates indicate the T cells population that has gone through proliferation. It was used in later comparison.

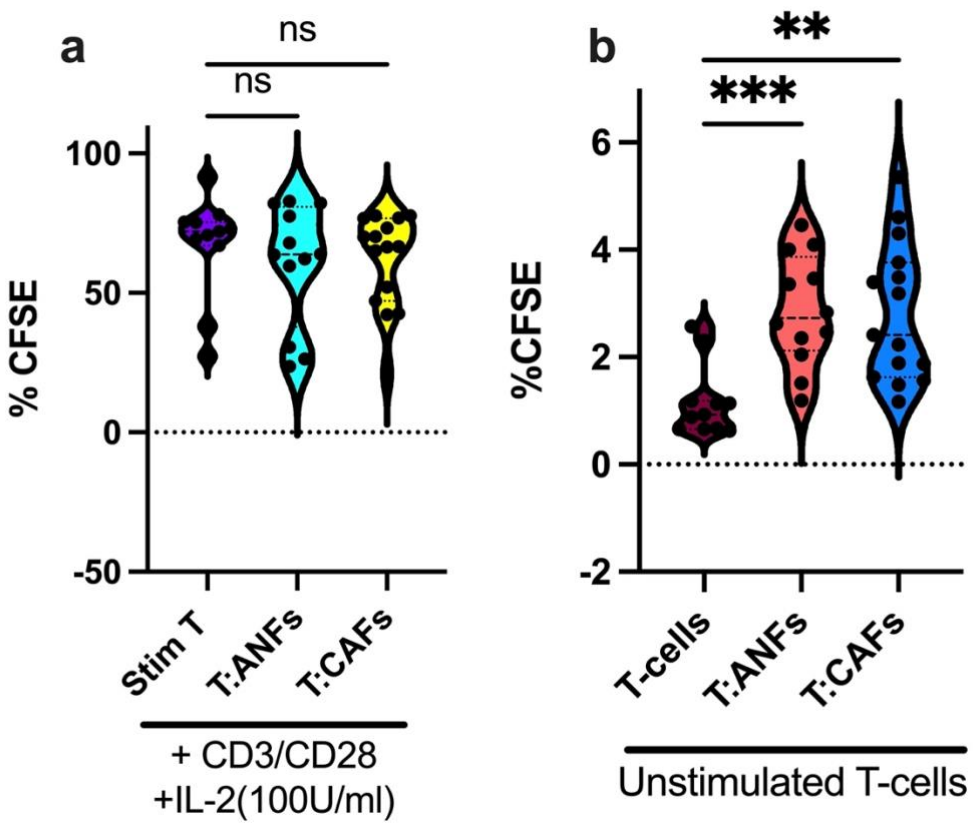


Figure 4.2. Comparison of T cell proliferation ability between T cell co-cultured with primary ANFs and CAFs using CFSE assay (direct contact).
Violin plots to compare the percentage of T cells that has gone through at least one cycle of proliferation between T cells co-cultured with ANFs and CAFs. Each dot in CAF and ANF panel represents a PDAC patient donor. Three healthy donors PBMCs, 12 PDAC donors for ANFs and 15 PDAC donors for CAFs were used in the experiment. The comparison was carried out both in stimulated T cell **(a)** and Unstimulated T cells **(b).** Statistical analysis was carried out using One-way ANOVA test followed by Dunn's test with * ≤0.05; ** ≤0.01.

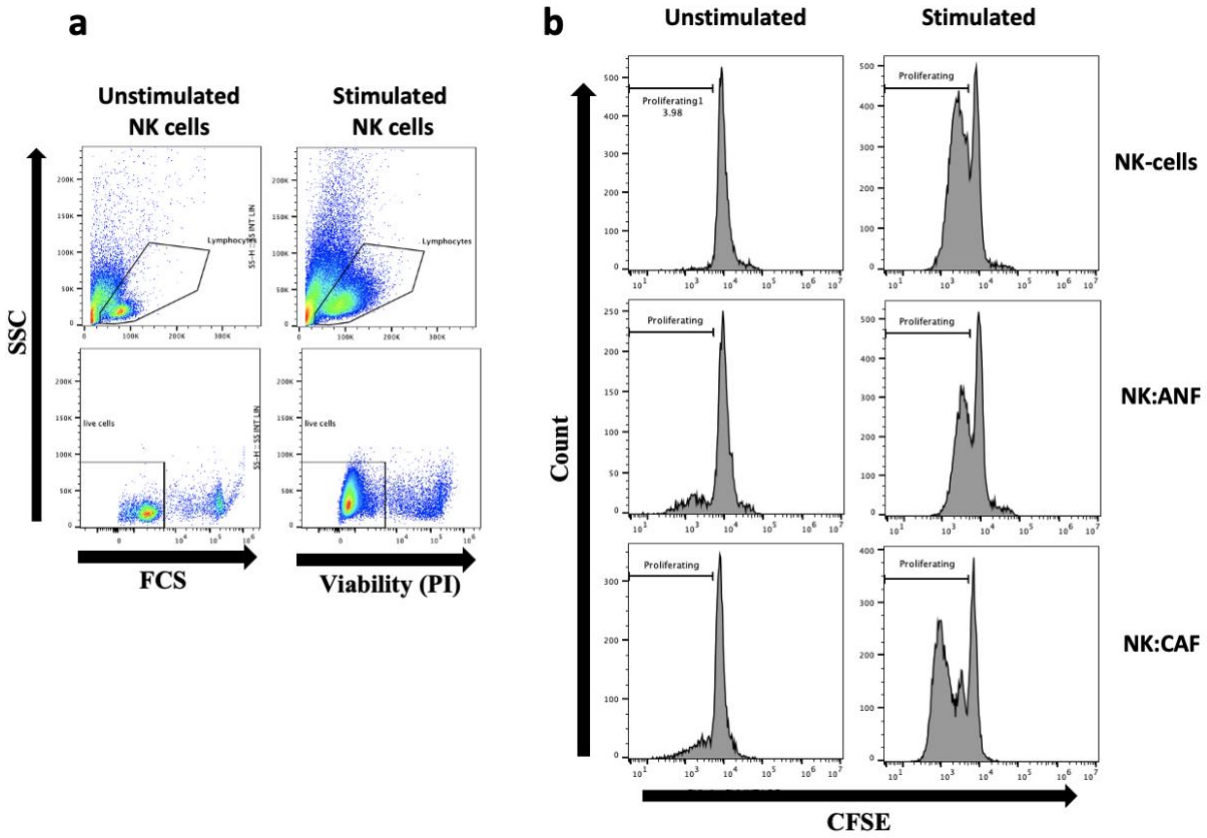


Figure 4.3. Comparison in NK cells proliferation ability between NK cells co-cultured with primary ANFs and CAFs using CFSE assay (direct contact).
a. Flow cytometry gating strategy of unstimulated versus stimulated total NK cells. **b.** Examples of Flow cytometry histograms to compare the CFSE profile between NK cells co-cultured with ANF and CAF in both unstimulated and stimulated conditions. The gates indicate the NK cells population that has gone through proliferation. It was used in later comparison.

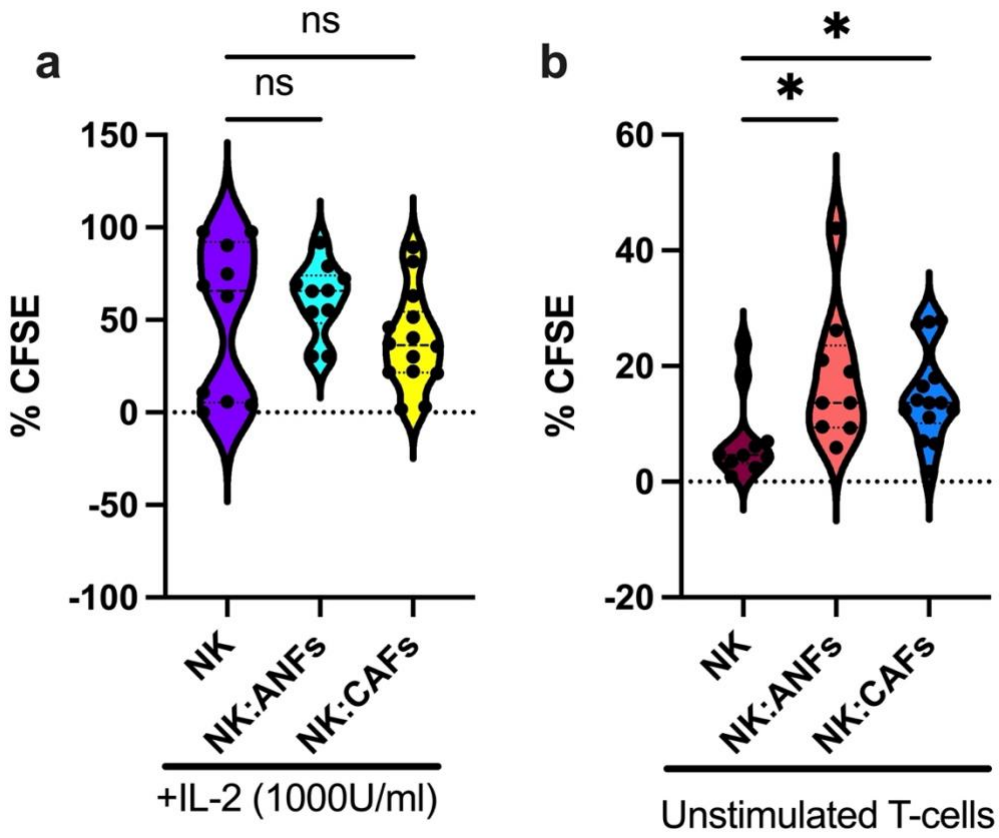


Figure 4.4. Comparison in NK cell proliferation ability between NK cell co-cultured with primary ANFs and CAFs using CFSE assay (direct contact).
Violin plots to compare the percentage of NK cells that has gone through at least one cycle of proliferation between NK cells co-cultured with ANFs and CAFs. Each dot in CAF and ANF panel represents a PDAC patient donor. Three healthy donors PBMCs, 12 PDAC donors for ANFs and 15 PDAC donors for CAFs were used in the experiment. The comparison was carried out both in stimulated NK cell **(a)** and Unstimulated NK cells **(b).** Statistical analysis was carried out using One-way ANOVA test followed by Dunn's test with* ≤0.05; ** ≤0.01.

The experimental protocol followed was consistent with the previous section in figures 4.5a and 4.6a, flow cytometry histograms illustrate the percentage of CFSE in co-cultured T and NK cells with immortalized fibroblasts. Co-culturing non-stimulated T cells with immortalized ANF and CAF led to an increase in their proliferative capacity (from 0.32% to 2%) (Figure 4.5c). However, the proliferation rate of stimulated T cells remained largely unaffected under the same conditions (from 78 % to 77%) (Figure 4.5b). Similar results were observed with NK cells in figure 4.6, where co-culture with non-stimulated NK cells increased their proliferative capacity (from 1.7 to 11.5%) (Figure 4.6c), while co-culture with stimulated NK cells did not significantly impact proliferation rates (from 80% to 78%) (Figure 4.6b).

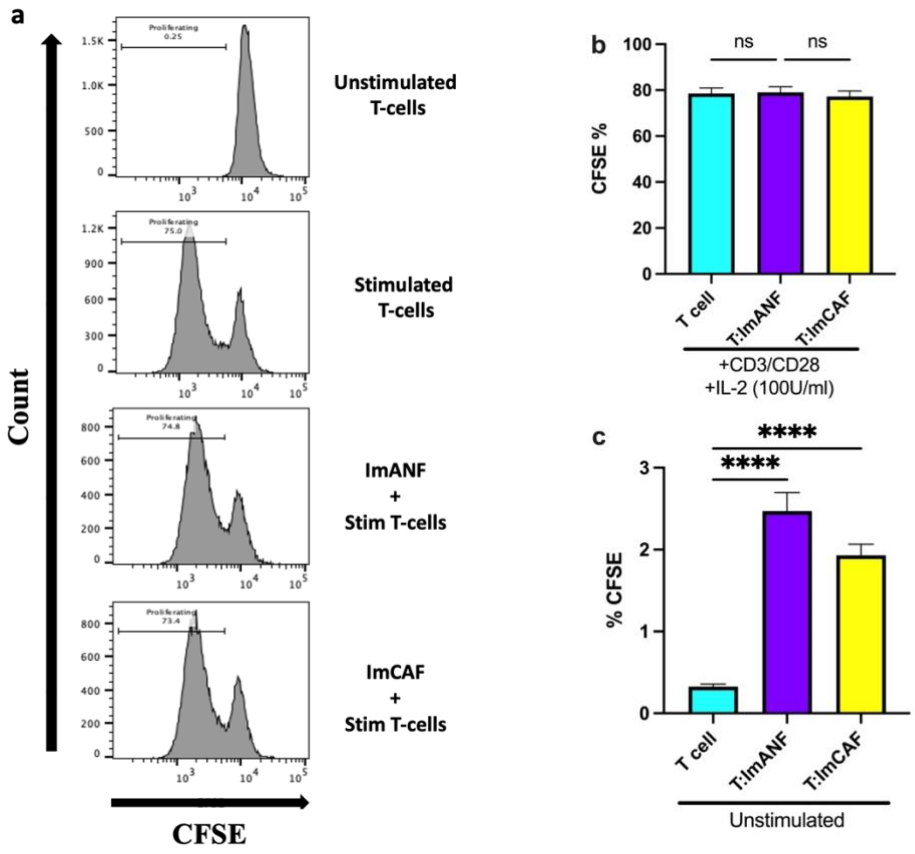


Figure 4.5. Comparison of T cells proliferation ability between T cells co-cultured with immortalised ANF (ImANF) and CAF (ImCAF) cells using CFSE assay (direct contact).

a. Examples of Flow cytometry histograms comparing the percentage of CFSE between co-cultured T cells with Immortalised fibroblasts, ImANF and ImCAF in both unstimulated and stimulated conditions. **b & c**. The percentage of T cell population that has gone through at least one cycle were compared between ImANF and ImCAF co-cultured with T cells in Stimulation and Non-stimulation conditions respectively. 4 donors were used in this experiment all together. Statistical analysis was carried out using One-way ANOVA test followed by Dunnett multiple comparisons test with * ≤0.05; ** ≤0.01.

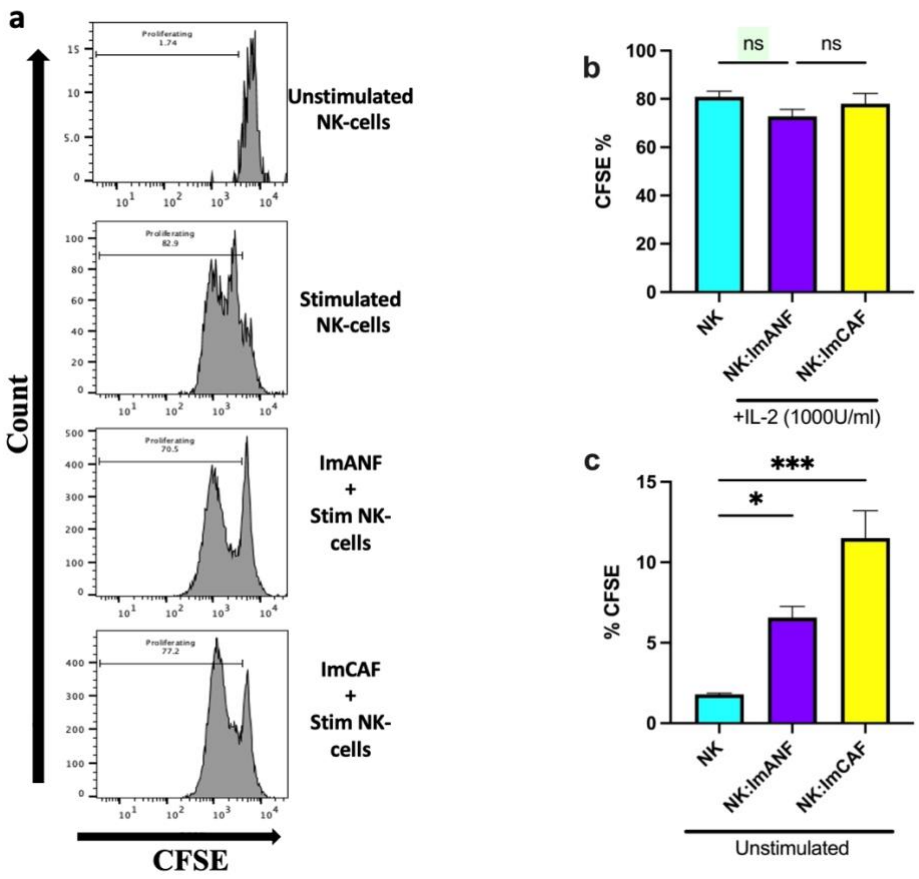


Figure 4.6. Comparison in NK cell proliferation activity between NK cell co-cultured with immortalised ANF (ImANF) and CAF (ImCAF) cells from 4 different PDAC donors was made by CFSE assay (direct contact).

a. Flow cytometry histograms comparing the percentage of CFSE between co-cultured NK cells with Immortalised fibroblasts, ImANF and ImCAF in both unstimulated and stimulated conditions. **b & c**. Comparison in NK cell proliferation percentage between ImANF and ImCAF co-cultured with Stimulated and Unstimulated NK cells respectively. Statistical analysis was carried out using One-way ANOVA test followed by Dunnett multiple comparison test with * ≤0.05; ** ≤0.01.

To explore whether the stimulation of the T and NK proliferation depends on the cell-to-cell contact, the experiments with conditioned media were carried out. Fibroblasts are believed to secrete cytokine and chemokine molecules that influence the function of T and NK cells (Koppensteiner et al., 2022). To investigate this, conditioned media from both primary and immortalized fibroblasts was collected. Fibroblasts were cultured in serum-deprived fresh medium for 48 hours, after which the conditioned media were collected and added to T and NK cells. Upon addition of both primary and immortalized ANF and CAF conditioned medium to stimulated T cells, an increase in their proliferation capacity was observed compared to non-treated T cells (from 65% to 86%), as shown in figures 4.7b and 4.7c. Similar effects were observed with NK cells, where an increase in proliferation capacity was seen compared to non-treated NK cells (from 32% to 58%), as depicted in figures 4.8b and 4.8c.

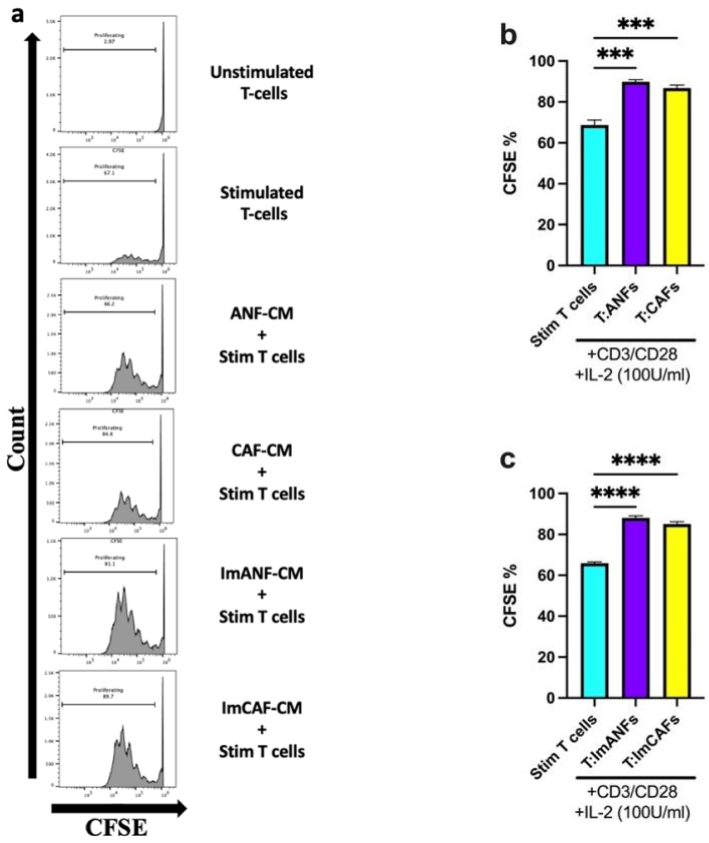


Figure 4.7. T cell proliferation can be enhanced by primary (ANF & CAF) and Immortalised (ImANF & ImCAF) Conditioned media (CM).
CAFs and ANFs were cultured in serum starved medium for 48hours before the conditioned media is harvested. The conditioned media from the cultured primary and immortalised fibroblasts derived from 3 different individuals were collected and used in the T cells stimulation experiment. T cell proliferation was measured using CFSE profile by flow cytometry. Examples of Flow cytometry histograms **(a)** to show the CFSE profile of CD3/CD28/IL-2 stimulated T cells co-cultured with different fibroblasts. Bar charts to show the cumulative data comparing the percentage of proliferated T cells (Lower CFSE population) between stimulated T cells co-cultured with primary **(b)** and Immortalised fibroblasts **(c).** Statistical analysis was carried out using One-way ANOVA test followed by Sidak's multiple comparisons test with * ≤0.05; ** ≤0.01.

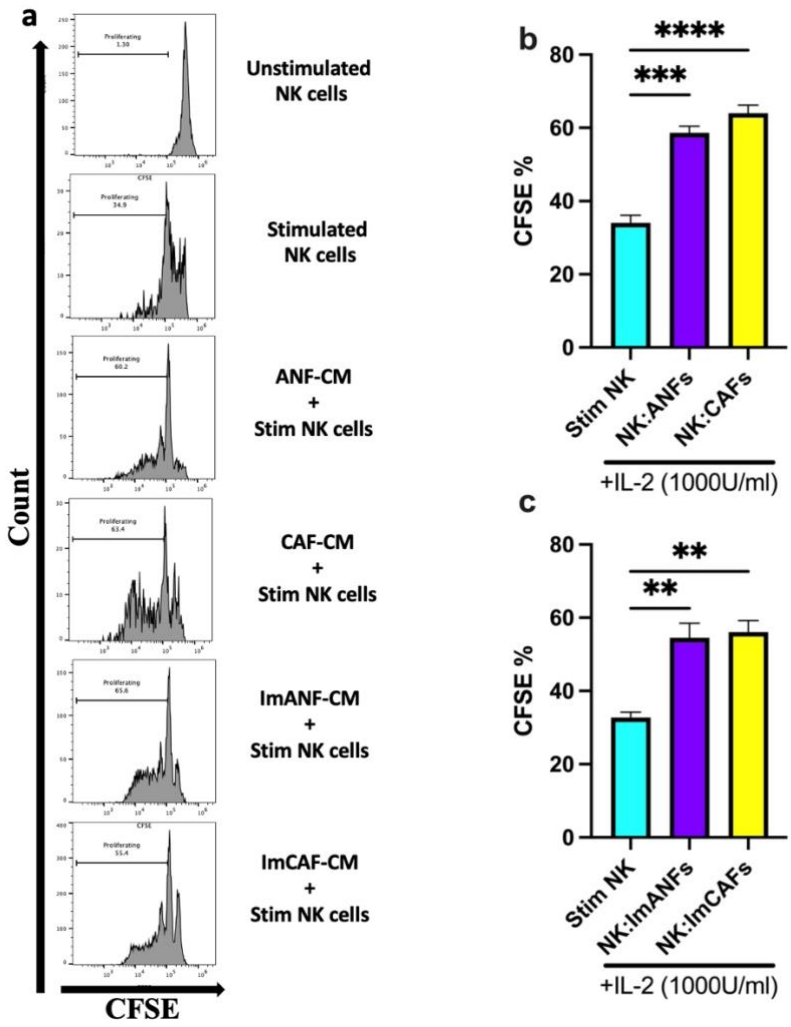


Figure 4.8. Increased NK cell proliferation by primary (ANF & CAF) and Immortalised (ImANF & ImCAF) Conditioned media (CM).

CAFs and ANFs were cultured in serum- starved medium for 48hours. The conditioned media from the cultured primary and immortalised fibroblasts derived from 3 different individuals were collected and added to stimulated NK cells. CFSE were then measured for NK cell proliferation using flow cytometry. Flow cytometry histograms **(a)** and cumulative data **(b)** comparing the percentage of CFSE between co-cultured NK cells with primary and Immortalised fibroblasts. Statistical analysis was carried out using One-way ANOVA test followed by Sidak's multiple comparisons test with * ≤0.05; ** ≤0.01.

Due to an increase in T cell proliferation when adding fibroblast, I was interested in investigating IFN-γ secretion by stimulated T cells when co-cultured with both primary and immortalized ANF and CAF. The two cancer cell lines, PANC-1 and CF-Panc, were used as controls (Figure 4.9). When co-culturing T cells with primary fibroblasts (Figure 4.9a), there was an increase in the level of IFN-γ secreted by stimulated T cells although this did not reach statistical significance. However, when comparing T cells co-cultured with fibroblasts (ANF and CAF) to T cells co-cultured with cancer cell lines (PANC-1 and CF-Panc), a decrease in IFN-γ production was observed with the cancer cell line, which may indicate the potential role of fibroblasts in shaping the tumour microenvironment (Figure 4.9a). When comparing IFN-γ levels from co-cultured stimulated T cells with immortalized fibroblasts (ImANFs and ImCAFs), an increase in IFN-γ compared to stimulated T cells alone was observed. A similar effect was seen when comparing immortalized CAF (T:ImCAFs) to cancer cell lines (T:PANC-1 and T:CF-Panc), as evidenced by a decrease in IFN-γ in cancer cell line conditions (Figure 4.9b).

In conclusion, this investigation into the interaction between T and NK cells with primary and immortalized ANF and CAF fibroblasts reveals intriguing dynamics. While fibroblasts fail to impact stimulated T and NK cells, they notably enhance the proliferation of unstimulated counterparts. Critically, treatment with fibroblast-conditioned media elevates the proliferative rate of stimulated T cells. Moreover, fibroblasts induce increased secretion of IFN-γ by T cells. However, further research is imperative to elucidate the underlying mechanisms driving these observations and to discern their broader implications in tumour microenvironments.

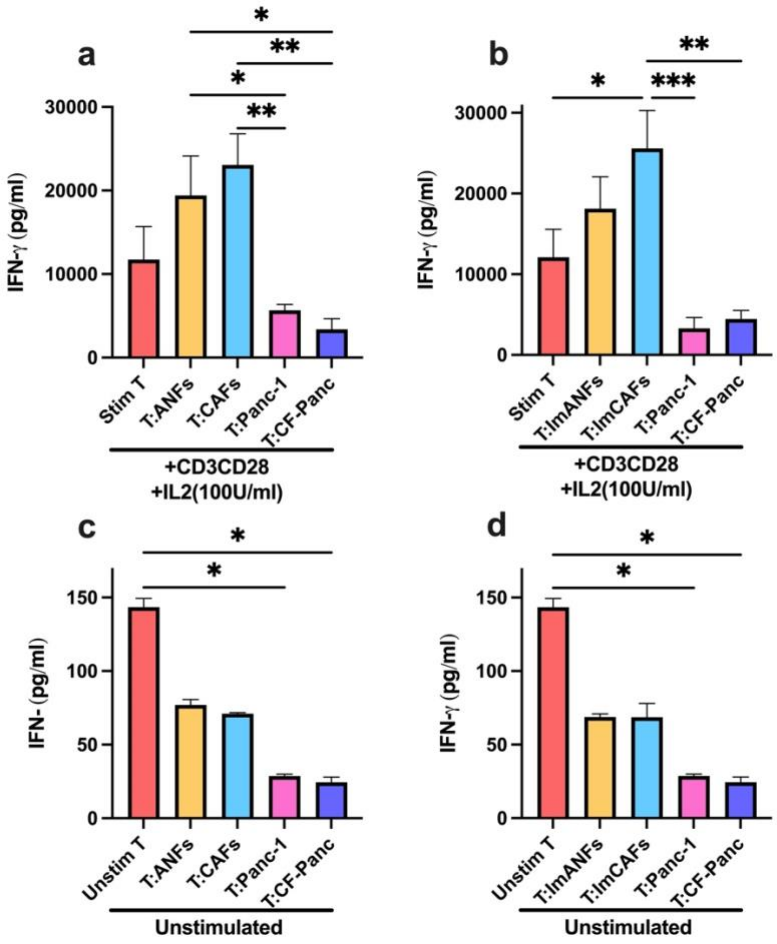


Figure 4.9. IFN-γ production from unstimulated and stimulated T cells culture with conditioned media (CM) from primary and immortalised fibroblasts.
The conditioned media from the cultured primary and immortalised fibroblasts were derived from three different PDAC patients and T cells were isolated from PBMCs of one healthy donor. Stimulated **(a & b)** and Unstimulated **(c & d)** T cells were cultured in primary (ANFs-CM, CAFs-CM) and immortalised (ImANFs-CM, ImCAFs-CM) fibroblasts and two other PDAC cell lines (Panc-1 and CF-Panc) conditioned media for 5 days. Then the supernatants were harvested, and IFN-γ concentration was measured using enzyme-linked immunosorbent assay (ELISA). Statistical analysis was carried out using One-way ANOVA test followed by Dunn's multiple comparison test with* ≤0.05; ** ≤0.01.

4.2.2 Effect of fibroblasts on T cells phenotyping

This section provides information of the effects of fibroblasts on T and NK cell phenotyping, highlighting the complexities of their interplay and their implications for cancer immunotherapy. Figure 4.10 illustrates the gating strategy employed for CD4+ and CD8+ T cells. Initially, unstimulated, and stimulated T cells were gated based on forward scatter (FSC) and side scatter (SSC). Subsequently, viability dye (PI) was utilized to exclude dead cells, and CD3 (AF700) was used to gate T cell lymphocytes, followed by CD4/APC-Cy7 and CD8/perCP-Cy5.5 markers to delineate CD4 and CD8 T cell populations.

Figure 4.11 displays the percentage (Figure 4.11a & b) and Mean Fluorescence Intensity (MFI) (Figure 4.11c & d) of CD4+ and CD8+ T cells in stimulated conditions. Co-culture of T cells with ANF and CAF decreases the percentage of CD4+ T cells compared to T cells alone (from 58.4 % to 51.9%) (Figure 4.11a). No significant effect has been observed with CD8+ T cells (Figure 4.11b). T cells in contact with CAF reduce the MFI of CD4+ T cells compared to T cells alone (from 74669 to 54723), with no significant difference when co-culturing T cells with ANF (Figure 4.11c). No significant effect has been observed with CD8+ T cells (Figure 4.11d).

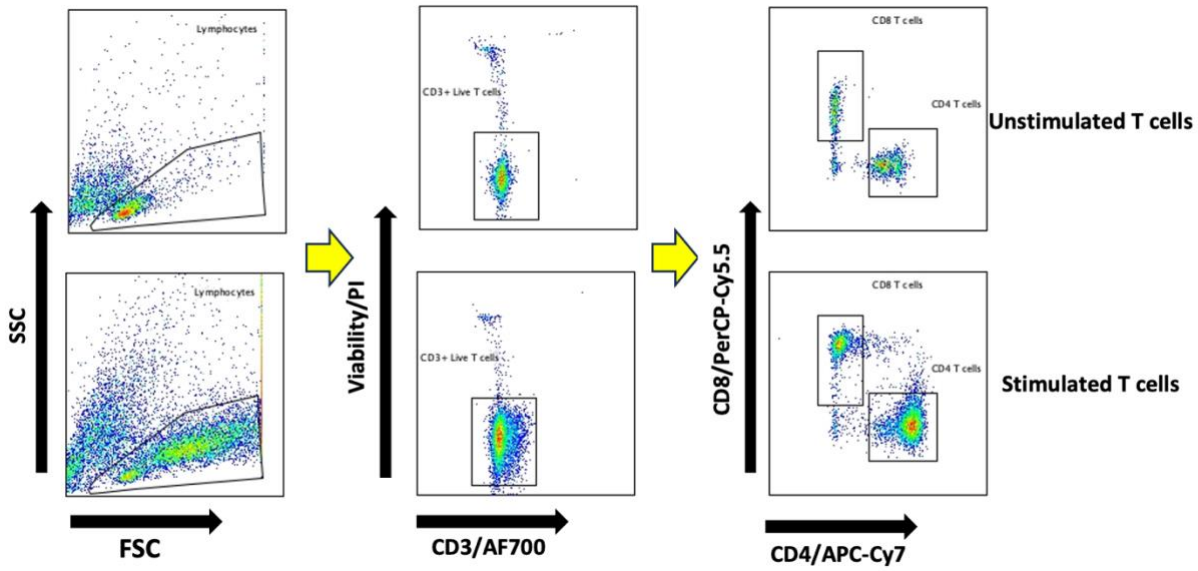


Figure 4.10. Flow cytometry gating strategy of unstimulated versus stimulated T cells.

T cells were co-cultured with ANF and CAF from PDAC patients and stained with flow cytometry panel including Viability dye (PI), CD3/AF700, CD4/APC-Cy7 and CD8/perCP-Cy5.5. Data was collected using flow cytometry then analysed using FlowJo software. At first the lymphocytes were gated according to FS and SS. Then the whole T cells were gated as CD3 positive but PI negative (live cells). At last, the CD4 T cells and CD8 T cells were identified based on CD4 and CD8 expression.

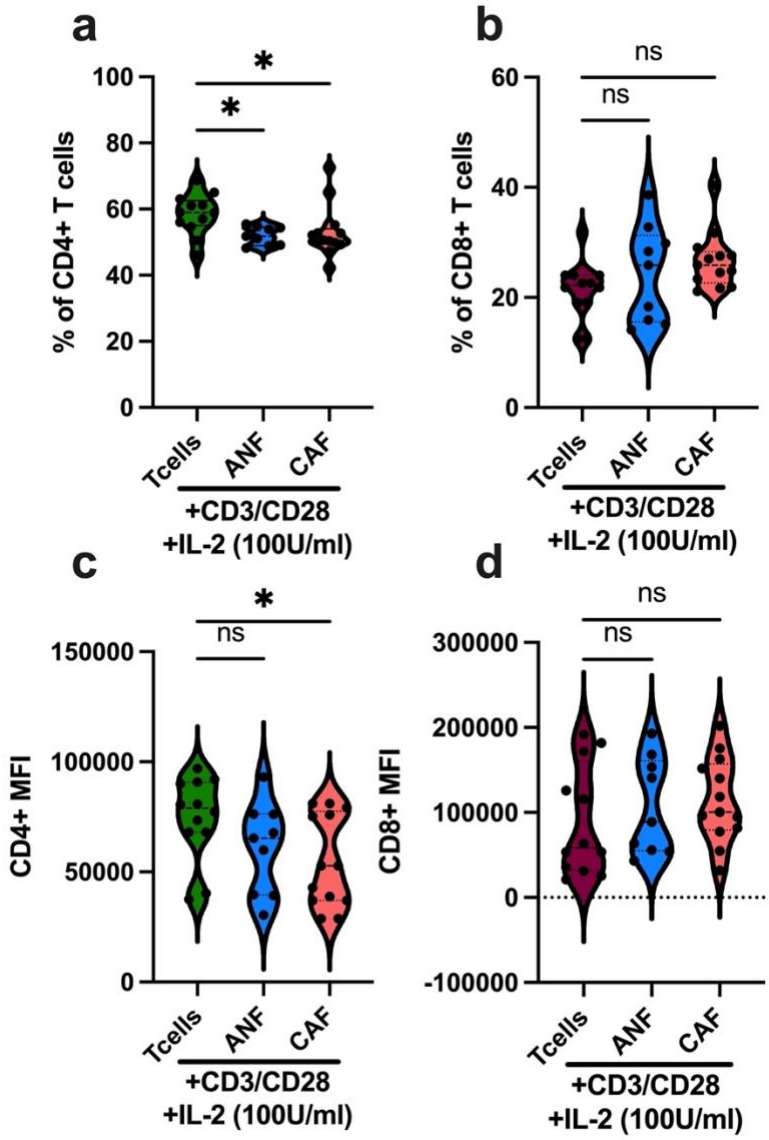


Figure 4.11. The effect of co-culture with primary ANF and CAF on the percentage of stimulated CD4+ and CD8+ T cells and mean fluorescence intensity (MFI) of CD4 and CD8.

a & b. Violin plots to compare the percentage of CD4+ and CD8+ T cell (top). **c & d.** MFI of CD4 and CD8 expression between T cell co-cultured with ANFs and CAFs (bottom). Each CAF and ANF point represent a PDAC donor, providing insights into the differential effects on T cell phenotypes in the context of the tumour microenvironment. Statistical analysis was carried out using One-way ANOVA test followed by Kruskal -Wallis multiple comparison test with* ≤0.05; ** ≤0.01.

My investigation extended to assessing the expression of T cell activation molecules, including CD69, NKG2D, DNAM-1, as well as inhibitory molecules such as PD-1. CD69 expression is known to be promptly upregulated upon activation in most leukocytes, serving as a marker for activated lymphocytes and NK cells (Cibrian & Sanchez-Madrid, 2017). NKG2D, an activating receptor primarily found on cytotoxic immune cells, typically binds to ligands induced in response to stressors like infection or cancer (Huifang Liu, 2019). Although CD4+ T cells generally do not express NKG2D post-activation, certain pathological conditions such as Crohn's disease and cytomegalovirus infection may induce its expression in humans (Wensveen et al., 2018). DNAM-1, expressed on NK cells, CD8+ T cells, CD4+ T cells, and monocytes in humans, plays a role in various innate and adaptive immune responses, including leukocyte migration, activation, expansion, and effector functions of T cells and NK cells (Gilfillan et al., 2008).

Flow cytometry histograms in figures 4.12 and 4.14 depict the examples of the expression pattern of all the mentioned molecules in CD4+ and CD8+ T cells, respectively. Figure 4.13 reveals intriguing findings regarding the expression of CD69, DNAM-1, and NKG2D on CD4+ T cells when co-cultured with ANF and CAF compared to stimulated T cells alone. There is a notable increase in CD69 expression on CD4+ T cells, both in terms of percentage (from 78% to 99%) and MFI (from 1695 to 3310), in the presence of both ANF and CAF (Figure 4.13a and b). However, no significant effect is observed in the expression of DNAM-1 (Figure 4.13c and d). Interestingly, the expression level of NKG2D is elevated on CD4+ T cells when co-cultured with ANF and CAF, demonstrated by both percentage and MFI (Figure 4.13e and f). Notably, a similar elevated effect is noted on PD-1 expression on CD4+ T cells when co-cultured with CAF alone both in terms of percentage (from 36% to 60%) and the MFI level (from

23342 to 42662), while no significant effect is seen with ANF (Figure 4.13g and h). These results prompt further investigation into the differential effects of fibroblasts on specific T cell activation and inhibitory markers, shedding light on the complex interplay within the tumour microenvironment. The findings from figure 4.15 provide valuable insights into how co-culturing with ANF and CAF affects the expression of key molecules in CD8+ T cells. The increase in CD69 expression, both in terms of percentage (from 87% to 97%) and MFI (from 2120 to 4231), suggests that fibroblasts may play a role in activating CD8+ T cells (Figure 4.15a and b). Fibroblasts decrease CD69 in activated lymphocytes and CD3 in resting lymphocytes (Vancheri et al., 2005). Conversely, the lack of significant changes in DNAM-1 expression, at both percentage and MFI levels, suggests that this molecule may not be influenced by the presence of fibroblasts under these experimental conditions (Figure 4.15c and d). However, the upregulation of NKG2D expression, particularly in the presence of CAF, highlights a potential mechanism by which fibroblasts may modulate CD8+ T cell function (Figure 4.15e and f). The notable impact of CAF (MFI: from 22514 to 42662) on PD-1 expression raises questions about the specific signals driving this phenomenon and its potential implications for T cell activation or exhaustion and immune evasion within the tumour microenvironment (Figure 4.15g and h).

When comparing ANF to CAF in the presence of stimulated T cells, I found that the MFI of NKG2D on CD8+ T cells was higher when cultured with CAF, increasing from 2340 to 3270. Additionally, the percentage of PD1 significantly increased on CD8+ T cells when cultured with CAF, rising from 30% to 45% compared to ANF, with no significant changes observed in other markers on both CD4+ and CD8+ T cells.

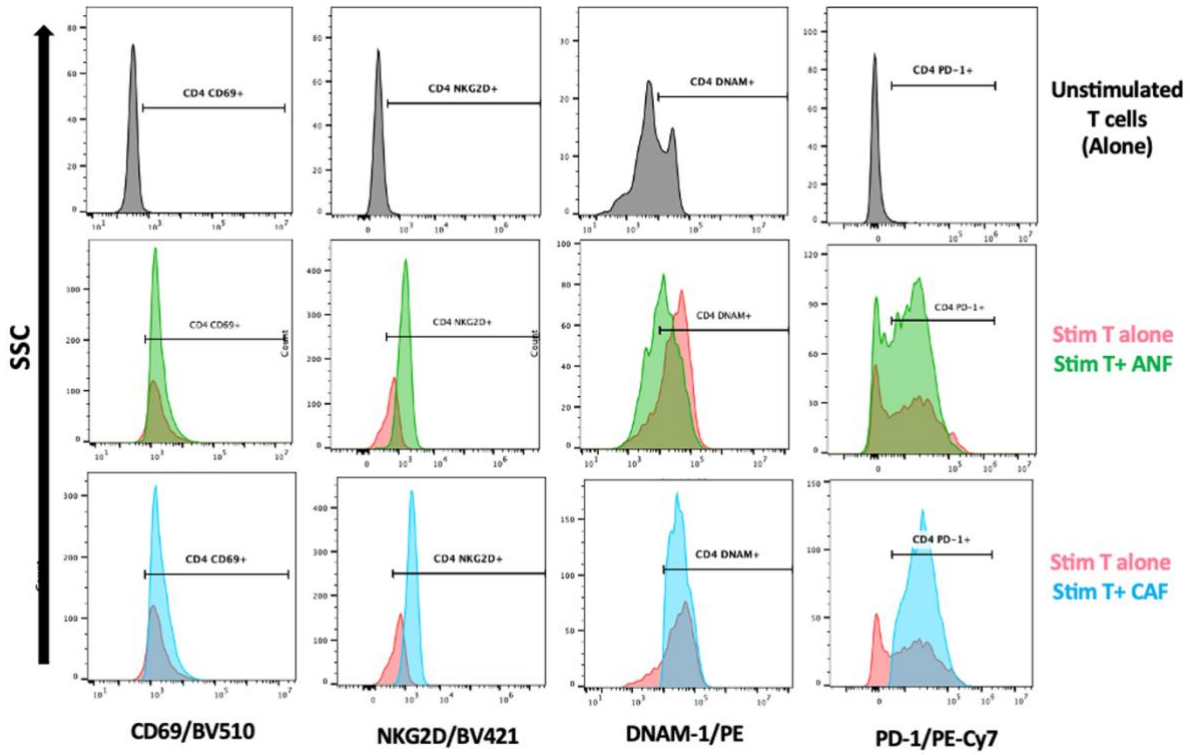


Figure 4.12. Flow cytometry histograms comparing the percentage of co-stimulatory (CD69, NKG2D and DNAM1) and inhibitory (PD-1) molecules expression in CD4+ T cells between those co-cultured with ANF and CAF.
Control histograms depict cultured unstimulated T cell alone. T cells were co-cultured with ANF and CAF from PDAC patients for 4 days and subsequently stained using a flow cytometry panel which included CD69/BV510, NKG2D/BV421, DNAM-1/PE and PD-1/PE-Cy7.

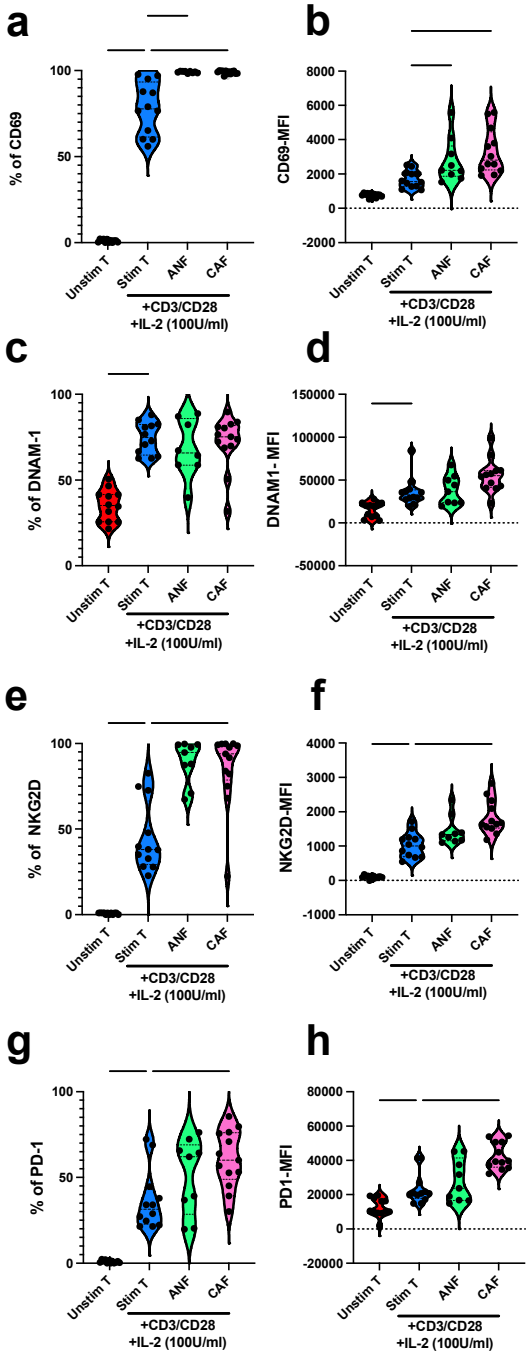


Figure 4.13. The effect of co-culture with primary ANF and CAF on the percentage and mean fluorescence intensity (MFI) of stimulated CD4+ T cells marked by activating and inhibitory molecules.

a, c, e & g. Violin plots to compare the percentage of CD4+ T cell activating (CD69, DNAM-1 and NKG2D) and inhibitory marker PD-1 (left). **b, d, f & h**. MFI between stimulated T cell co-cultured with ANFs and CAFs (right). Each CAF and ANF point represent a PDAC donor. Statistical analysis was carried out using One-way ANOVA test followed by Kruskal -Wallis multiple comparison test with* ≤0.05; ** ≤0.01.

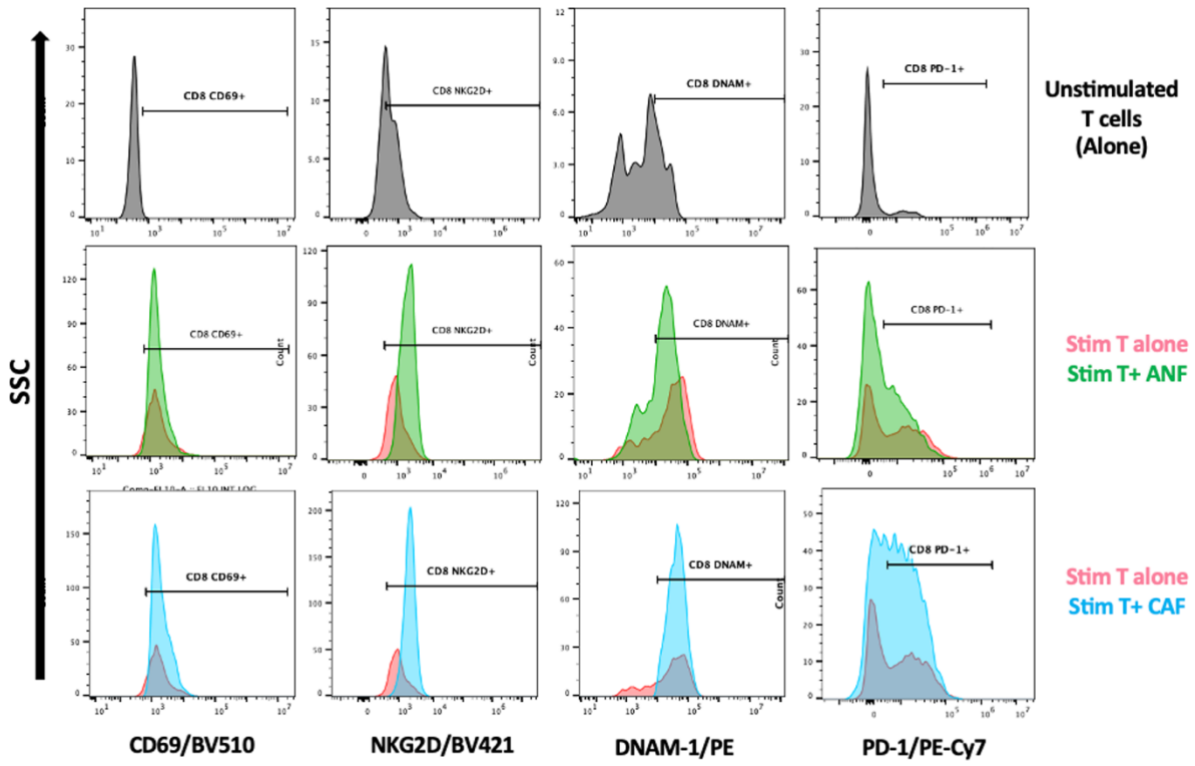


Figure 4.14. Flow cytometry histograms comparing the percentage of co-stimulatory (CD69, NKG2D and DNAM1) and inhibitory (PD-1) molecules expression in CD8+ T cells between those co-cultured with ANF and CAF.
Control histograms depict cultured unstimulated T cell alone. T cells were co-cultured with ANF and CAF from PDAC patients for 4 days and subsequently stained using a flow cytometry panel which included CD69/BV510, NKG2D/BV421, DNAM-1/PE and PD-1/PE-Cy7.

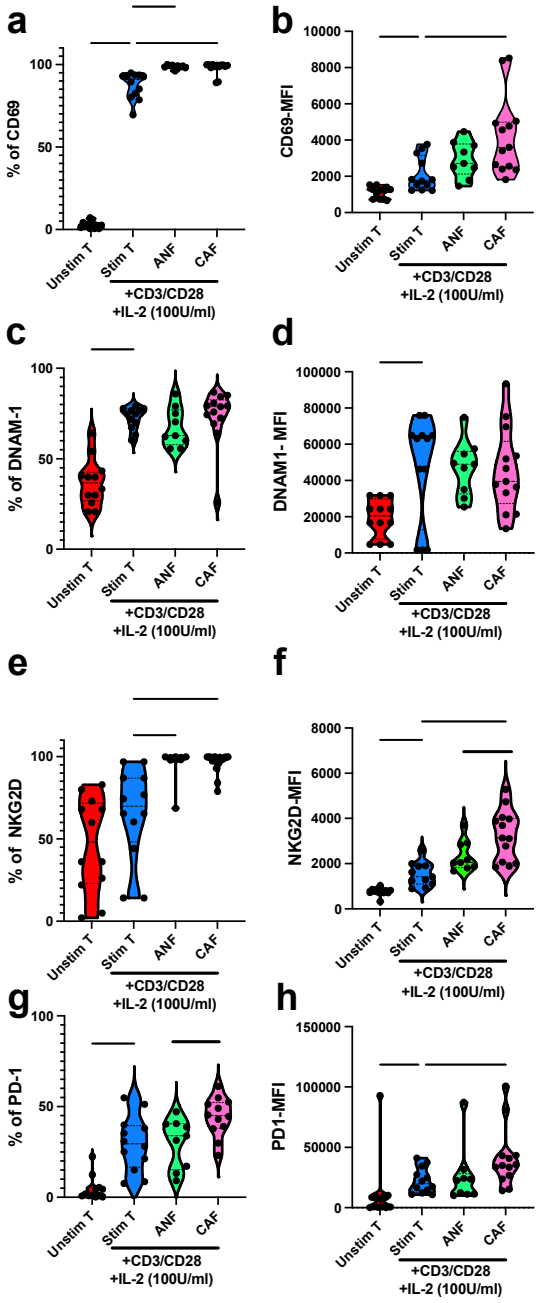


Figure 4.15. The effect of co-culture with primary ANF and CAF on the percentage and mean fluorescence intensity (MFI) of stimulated CD8+ T cells marked by activating and inhibitory molecules.

a, c, e & g. Violin plots to compare the percentage of CD8+ T cell activating (CD69, DNAM-1 and NKG2D) and inhibitory marker PD-1 (left). **b, d, f & h**. MFI between stimulated T cell co-cultured with ANFs and CAFs (right). Each CAF and ANF point represent a PDAC donor. Statistical analysis was carried out using One-way ANOVA test followed by Kruskal -Wallis multiple comparison test with* ≤0.05; ** ≤0.01.

The findings presented in figures 4.16 to 4.18 shed light on the impact of co-culturing fibroblast with unstimulated T cells. Figure 4.16 reveals a noteworthy decrease in CD4+ T cells when co-cultured with CAF, evidenced by both percentage (from 61.27% to 50.19%) and MFI (from 40245 to 31754) measurements (Figure 4.16a and b). Conversely, no significant difference is observed with ANF (Figure 4.16a and b). Interestingly, figure 4.16 demonstrates a significant increase in unstimulated CD8+ T cells, indicated by both percentage and MFI, when co-cultured with CAF (Figure 4.16c and d). However, this effect is not observed when they are cultured with ANF compared to unstimulated T cells alone (Figure 4.16c and d). These findings suggest a complex interplay between T cell subtypes and fibroblasts, with potential implications for immune modulation within the tumour microenvironment.

The expression of CD69, DNAM-1, NKG2D, and PD-1 was assessed on unstimulated CD4+ T cells when co-cultured with ANF and CAF. Figure 4.17 demonstrates a significant increase in CD69 expression on CD4+ T cells, both in terms of percentage (From 0.96% to 34.82%) and MFI from (755.8 to 1080), in the presence of both ANF and CAF (Figure 4.17a and b). However, no significant effect was observed in the expression of DNAM-1 on CD4+ T cells at the percentage level (From 35.05% to 41.30%) (Figure 4.17c), although an increase in MFI (from 16430 to 26662) was noted when cultured with both ANF and CAF (Figure 4.17d). Interestingly, the expression level of NKG2D was elevated on CD4+ T cells when co-cultured with ANF and CAF, shown by both percentage (From 0.7271% to 11.85%) and MFI (from 106.5 to 900) (Figure 4.17e and f). Notably, a similar effect was observed in PD-1 expression on CD4+ T cells when co-cultured with both ANF and CAF at the percentage level (Figure 4.17g), while no significant effect was seen with ANF at the MFI (Figure 4.17h).

The analysis of unstimulated CD8+ T cells, depicted in figure 4.18, revealed an increase in CD69 expression on unstimulated CD8+ T cells in the presence of both ANF and CAF, as indicated by the percentage (Figure 4.18a). Additionally, MFI of CD69 expression showed an increase on unstimulated CD8+ T cells in the presence of CAF, with no significant effect observed in the presence of ANF (Figure 4.18b). Regarding the activation marker DNAM-1, there was no significant effect observed in terms of both percentage and MFI (Figure 4.18c and d). Notably, NKG2D expression increased on unstimulated CD8+ T cells when cultured with both ANF and CAF, as demonstrated by both percentage and MFI (Figure 4.18e and f). Finally, the expression of the inhibitory molecule PD-1 on unstimulated CD8+ T cells increased significantly in the presence of CAF, while no significant effect was observed in the presence of ANF at the percentage level (Figure 4.18g). However, this effect was significantly increased with both ANF and CAF at the MFI level (Figure 4.18h).

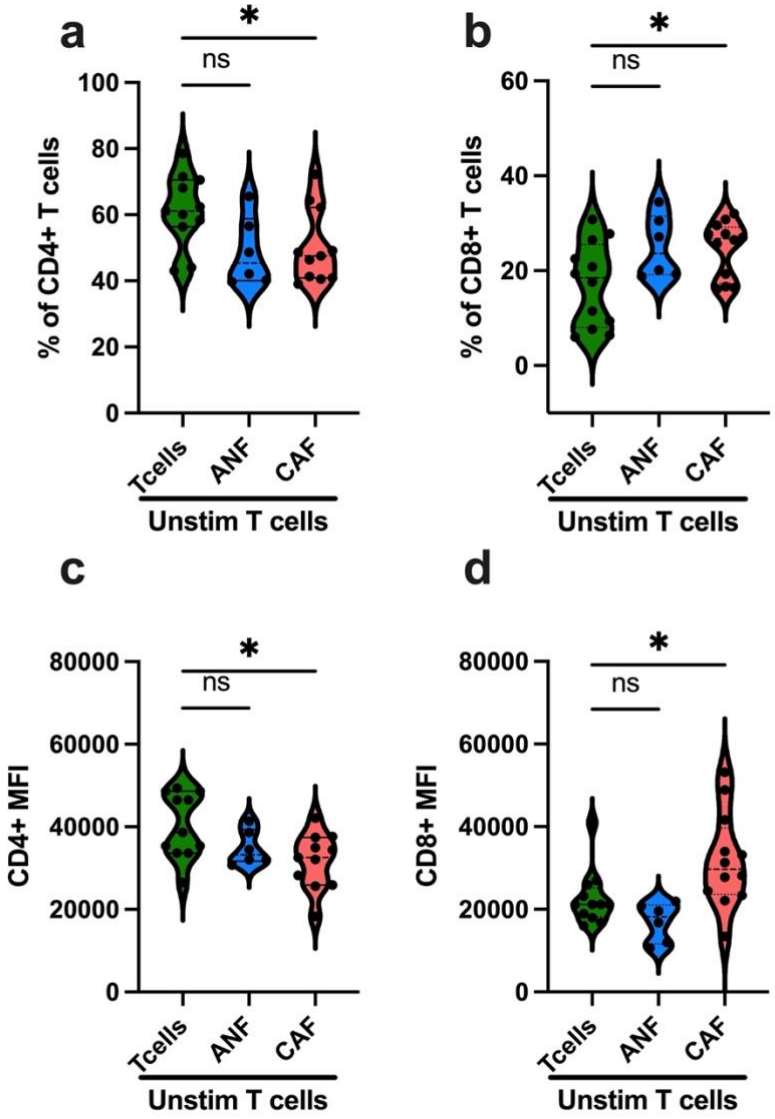


Figure 4.16. The effect of co-culture with primary ANF and CAF on the percentage of unstimulated CD4+ and CD8+ T cells and mean fluorescence intensity (MFI) of CD4 and CD8.

a & b. Violin plots to compare the percentage of CD4+ and CD8+ T cell (top). **c & d.** MFI of CD4 and CD8 expression between unstimulated T cell co-cultured with ANFs and CAFs (bottom). Each CAF and ANF point represent a PDAC donor, providing insights into the differential effects on T cell phenotypes in the context of the tumour microenvironment. Statistical analysis was carried out using One-way ANOVA test followed by Kruskal -Wallis multiple comparison test with* ≤0.05; ** ≤0.01.

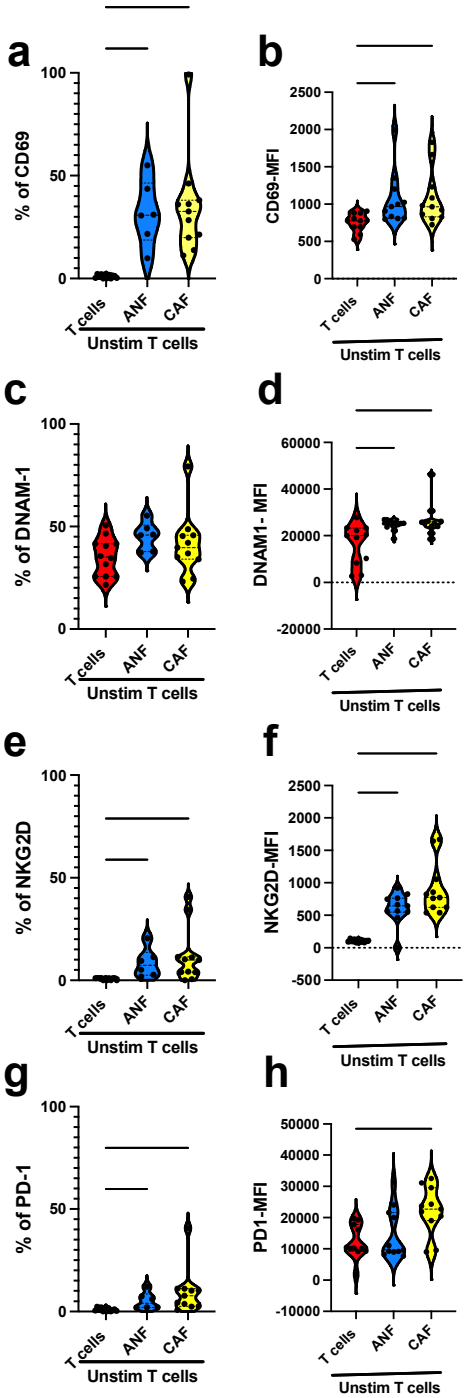


Figure 4.17. The effect of co-culture with primary ANF and CAF on the percentage and mean fluorescence intensity (MFI) of unstimulated CD4+ T cells marked by activating and inhibitory molecules.

a, c, e & g. Violin plots to compare the percentage of CD4+ T cell activating (CD69, DNAM-1 and NKG2D) and inhibitory marker PD-1 (left). **b, d, f & h.** MFI between unstimulated T cell co-cultured with ANFs and CAFs (right). Each CAF and ANF point represent a PDAC donor. Statistical analysis was carried out using One-way ANOVA test followed by Kruskal -Wallis multiple comparison test with* ≤0.05; ** ≤0.01.

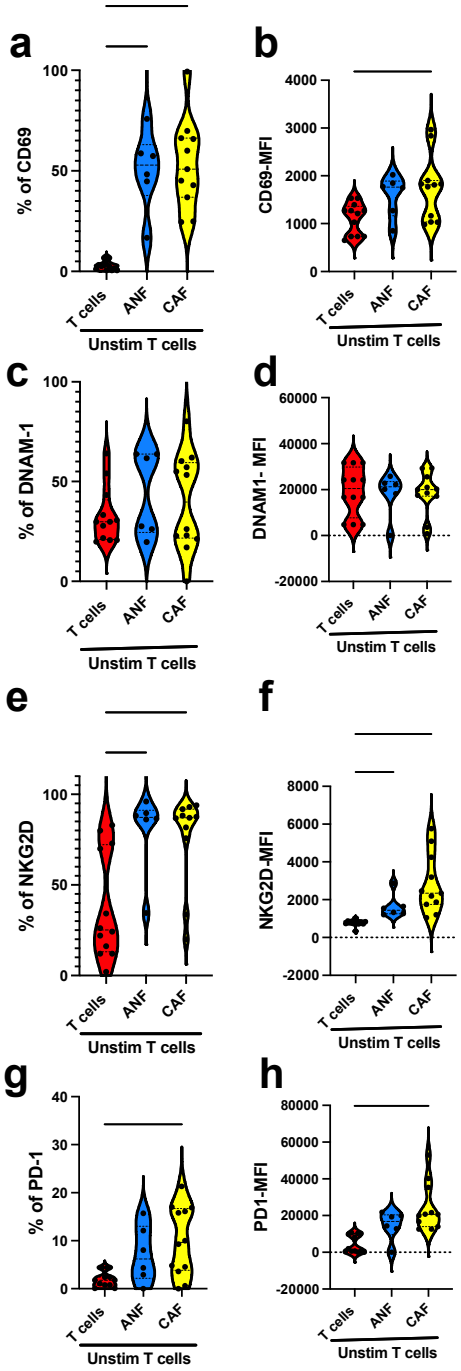
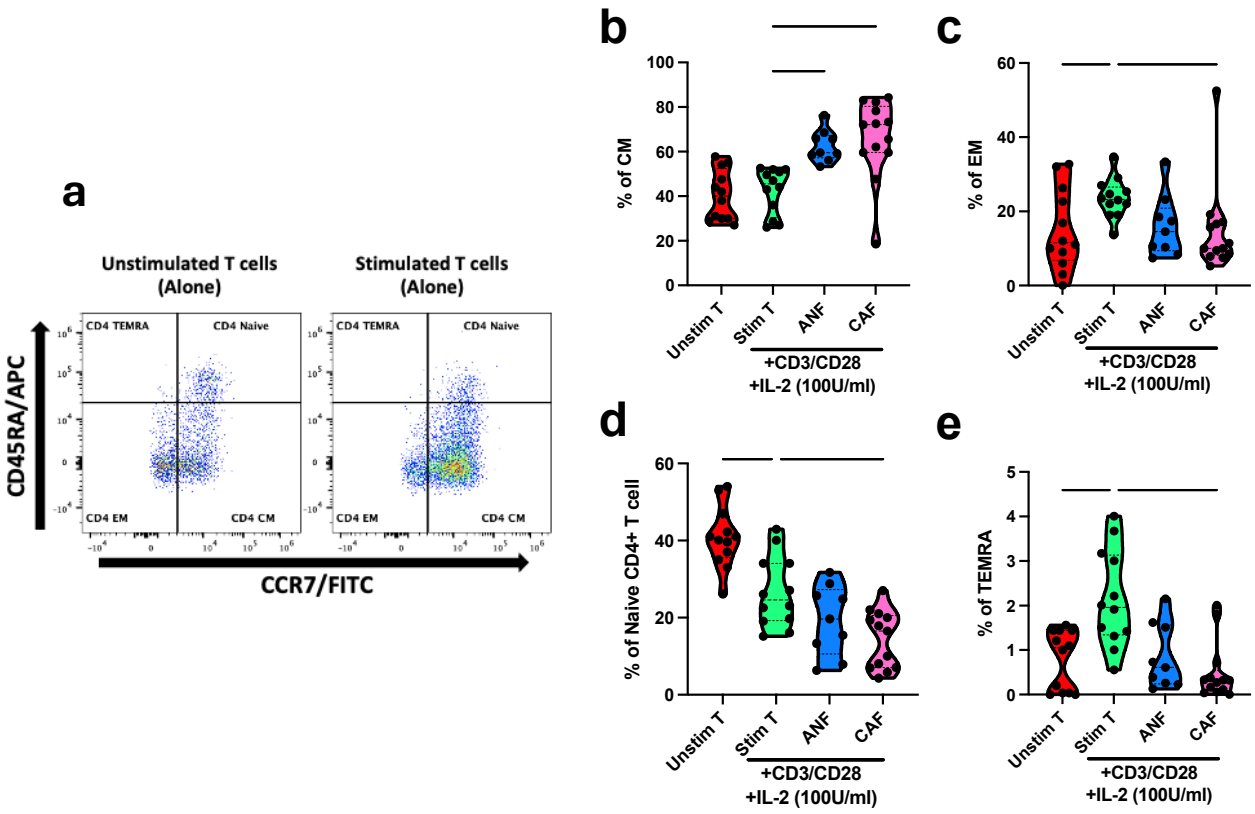


Figure 4.18. The effect of co-culture with primary ANF and CAF on the percentage and mean fluorescence intensity (MFI) of unstimulated CD8+ T cells marked by activating and inhibitory molecules.

a, c, e & g. Violin plots to compare the percentage of CD8+ T cell activating (CD69, DNAM-1 and NKG2D) and inhibitory marker PD-1 (left). **b, d, f & h.** MFI between unstimulated T cell co-cultured with ANFs and CAFs (right). Each CAF and ANF point represent a PDAC donor. Statistical analysis was carried out using One-way ANOVA test followed by Kruskal -Wallis multiple comparison test with* ≤0.05; ** ≤0.01.

The percentage of CD4+ and CD8+ T cell subtypes when co-cultured with ANF and CAF fibroblasts was investigated next, as shown in figures 4.19 and 4.20. Figure 4.19a and figure 4.20a illustrates the gating strategy of different T cell subpopulations, including central memory (CM), effector memory (EM), Naïve, and Temra, using CD45RA and CCR7 markers. Interestingly, ANF and CAF increased the central memory population (CM) on CD4+ T cells compared to stimulated T cells alone (Figure 4.19b). However, concerning effector memory (EM), a decrease was observed with CAF, while no significant effect was seen with ANF on CD4+ T cells (Figure 4.19c). A similar trend was noted with the naïve CD4+ T cell population, where a decreased percentage was observed with co-culturing with CAF, but no significant effect was observed with ANF on CD4+ T cells (Figure 4.19d). Moreover, the Temra population was also decreased in the presence of CAF compared to stimulated T cells alone (from 2.1% to 0.4%), with no effect observed with ANF (Figure 4.19e). The CD8+ T cell population analysis in Figure 4.20 demonstrates an increase in the central memory (CM) subset on CD8+ T cells when co-cultured with both ANF and CAF compared to stimulated T cells alone (from 13.7 to 51.7%) (Figure 4.20b). However, there is a decrease in the effector memory (EM) subset on CD8+ T cells with both ANF and CAF (Figure 4.20c). Similarly, the analysis of the naïve CD8+ T cell population reveals a decreased percentage on CD8+ T cells when co-cultured with CAF, while no significant effect is observed with ANF (Figure 4.20d). Additionally, the Temra population shows a decrease in the presence of both ANF and CAF compared to stimulated T cells alone (Figure 4.20e). These findings suggest a nuanced role for ANF and CAF in modulating the memory and effector functions of CD8 T cells, with potential implications for immune responses in the tumour microenvironment.

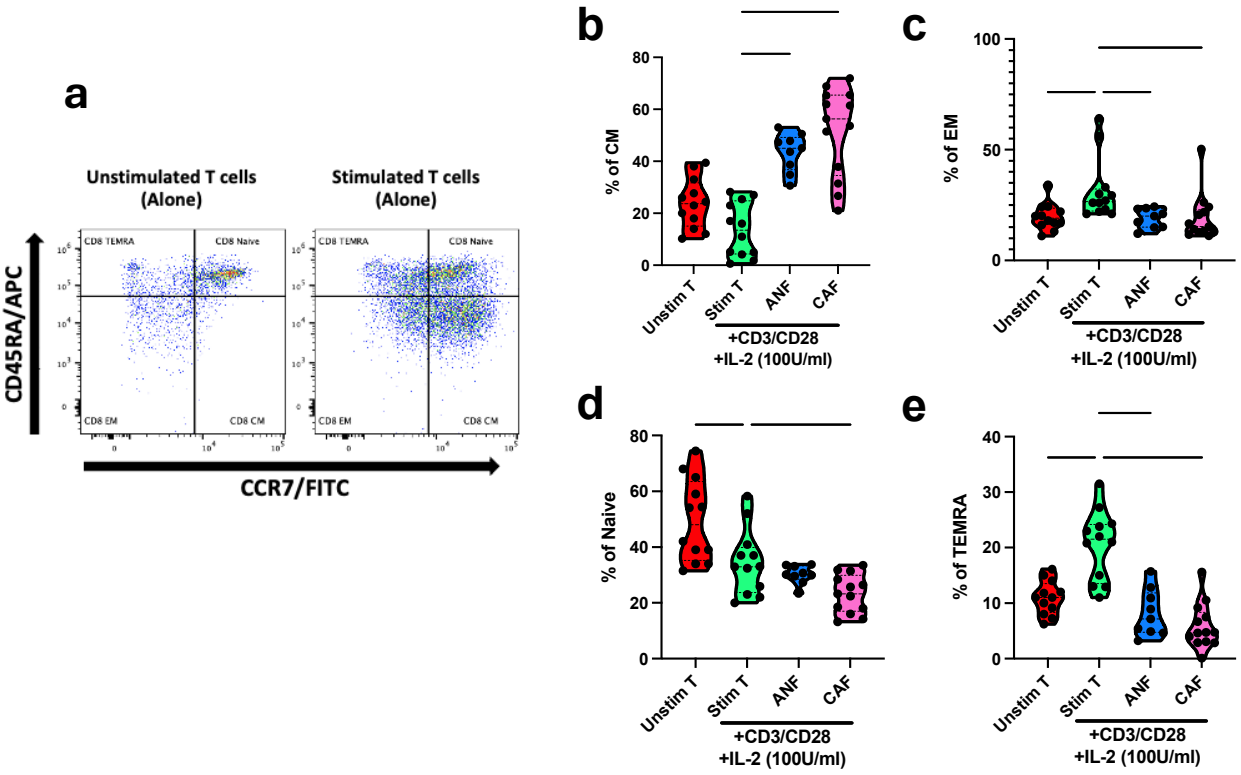


f

Statistical comparison on CD4+ T cells of	CM	EM	Naive	TEMRA
T to ANF	0.007	ns	ns	ns
T to CAF	0.0005	0.006	0.04	0.001
ANF to CAF	ns	ns	ns	ns

Figure 4.19. The effect of co-culture with primary ANF and CAF on the percentage of stimulated CD4+ T cells subtypes, central memory (CM), effector memory (EM), Naïve and Temra.

a. Flow cytometry gating strategy of unstimulated versus stimulated T cells. T cells were co-cultured with ANF and CAF from PDAC patients and stained with flow cytometry panel including CD45RA/APC and CCR7/FITC, CD4+ population were identified based on CD45RA/APC and CCR7/FITC expression. Data was collected using flow cytometry then analysed using FlowJo software. b, c, d & e. Violin plots to compare the percentage of CD4+ T cell between T cell co-cultured with ANFs and CAFs. Each CAF and ANF point represent a PDAC donor**. f.** Statistical comparison results, detailing the differences between groups based on the specified experimental conditions and statistical analyses conducted. Statistical analysis was carried out using One-way ANOVA test followed by Kruskal -Wallis multiple comparison test with* ≤0.05; ** ≤0.01.



f

Statistical comparison on CD8+ T cells of	CM	EM	Naive	TEMRA
T to ANF	<0.0001	0.03	ns	<0.0001
T to CAF	<0.0001	0.001	0.04	<0.0001
ANF to CAF	ns	ns	ns	ns

Figure 4.20. The effect of co-culture with primary ANF and CAF on the percentage of stimulated CD8+ T cells subtypes, central memory (CM), effector memory (EM), Naïve and Temra.

a. Flow cytometry gating strategy of unstimulated versus stimulated T cells. T cells were co-cultured with ANF and CAF from PDAC patients and stained with flow cytometry panel including CD45RA/APC and CCR7/FITC, CD8+ population were identified based on CD45RA/APC and CCR7/FITC expression. Data was collected using flow cytometry then analysed using FlowJo software**. b, c, d & e.** Violin plots to compare the percentage of CD8+ T cell between T cell co-cultured with ANFs and CAFs. Each CAF and ANF point represent a PDAC donor. **f.** Statistical comparison results, detailing the differences between groups based on the specified experimental conditions and statistical analyses conducted. Statistical analysis was carried out using One-way ANOVA test followed by Kruskal -Wallis multiple comparison test with* ≤0.05; ** ≤0.01.

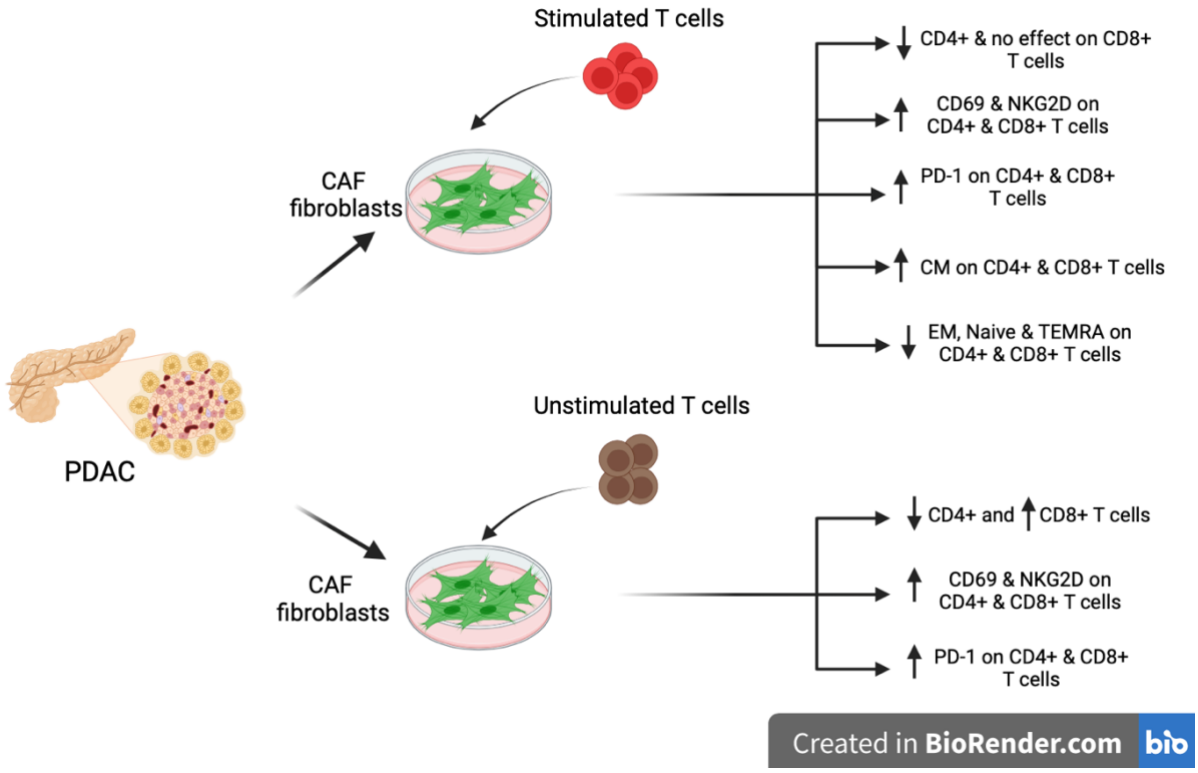


Figure 4.21. Graphical Abstract- Role of CAFs in modulating T cell responses within the PDAC-TME.

Stimulated T Cells: When stimulated T cells are co-cultured with CAFs, there is a notable decrease in CD4+ T cell counts, with no impact on CD8+ T cells. Activation markers CD69 and NKG2D are upregulated on both CD4+ and CD8+ T cells, indicating increased activation and cytotoxic potential. Additionally, PD-1 expression increases, suggesting enhanced T cell activation and/or exhaustion. Central memory (CM) T cells are upregulated, while effector memory (EM), naïve, and TEMRA (terminally differentiated effector memory) T cells are downregulated, pointing towards an altered memory T cell landscape favouring CM T cells. Unstimulated T Cells: In contrast, co-culturing unstimulated T cells with CAFs results in a decrease in CD4+ and an increase in CD8+ T cell populations. There is an upregulation of CD69 and NKG2D, along with an increase in PD-1 expression on both T cell subsets, indicating increased activation and potential exhaustion. Overall, the graphical abstract highlights the immunosuppressive role of CAFs in modulating T cell responses within the PDAC tumour microenvironment, promoting an environment that potentially supports tumour progression.

4.2.3 Effect of fibroblasts on NK cells phenotyping

Understanding the interplay between CAFs and natural killer (NK) cells is crucial in deciphering tumour immune responses. CAFs, prevalent in the tumour microenvironment, exhibit diverse effects on NK cell function and phenotype. This interaction is pivotal in shaping the anti-tumour immune response, influencing tumour progression, and therapeutic outcomes. NK cells, armed with cytotoxic and regulatory functions, play a pivotal role in immune surveillance against tumours. However, the intricate crosstalk between CAFs and NK cells can modulate NK cell activation, phenotype, and ultimately impact tumour immune evasion. Hence, elucidating the influence of CAFs on NK cell phenotyping holds significant therapeutic implications in cancer immunotherapy. Little is known about fibroblasts and NK. Studies on fibroblasts derived from melanoma, hepatocellular, and colorectal carcinoma demonstrate that CAFs can downregulate NK activating receptors like NKp30, NKp44, and NKG2D. This suppression, facilitated by prostaglandin E2 (PGE2) and/or indoleamine-2,3-dioxygenase (IDO) secretion, reduces NK cell cytotoxicity against tumour cells (Linda Ziani, 2017; Mirna Balsamo, 2009; Zhang et al., 2019). This section elucidates the impact of fibroblasts on NK cell phenotyping, underscoring the intricate dynamics of their interaction and their relevance in cancer immunotherapy.

Figure 4.21 delineates the gating strategy applied to NK cells. Initially, both unstimulated and stimulated NK cells were gated based on forward scatter (FSC) and side scatter (SSC). Subsequently, Viability dye (PI) was employed to exclude dead cells, and CD3/AF700 was utilized to gate NK cell lymphocytes (CD3 negative population), followed by CD3/AF700 and CD56/PE-Cy7 to distinguish $CD56^{bright}$ and $CD56^{dim}$ NK cell subsets. Figure 4.22 illustrates the impact of ANF and CAF on the

proportion of $CD56^{bright}$ and $CD56^{dim}$ NK cell subsets. In stimulated NK cells with IL-2 (1000U/ml) (Figure 4.22a), the percentage of $CD56^{bright}$ cells increased compared to the control (NK alone), while a decrease was observed in the dim population when co-cultured with ANF or CAF. In the unstimulated NK cells shown in figure 4.22b, no significant effect was observed when comparing $CD56^{bright}$ or $CD56^{dim}$ populations in the presence or absence of ANF or CAF.

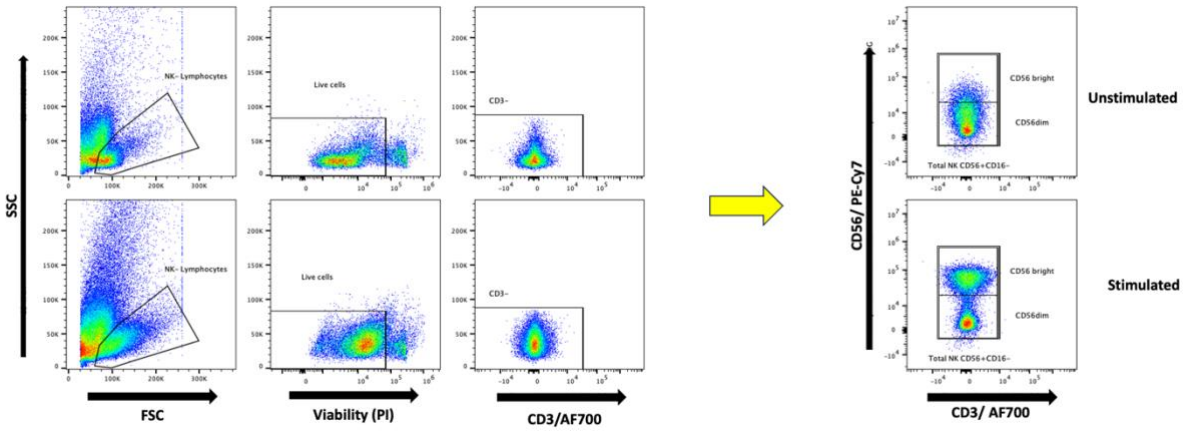


Figure 4.22. Flow cytometry gating strategy of unstimulated versus stimulated NK cells.

NK cells were co-cultured with ANF and CAF from PDAC patients and stained with flow cytometry panel including Viability dye (PI), CD3/AF700, CD4/APC-Cy7 and CD56/PE-Cy7. Data was collected using flow cytometry then analysed using FlowJo software. At first the lymphocytes were gated according to FSC and SSC. Then the NK cells were gated as PI and CD3 negative. At last, the $CD56^{bright}$ and $CD56^{dim}$ NK cells were identified based CD56 expression.

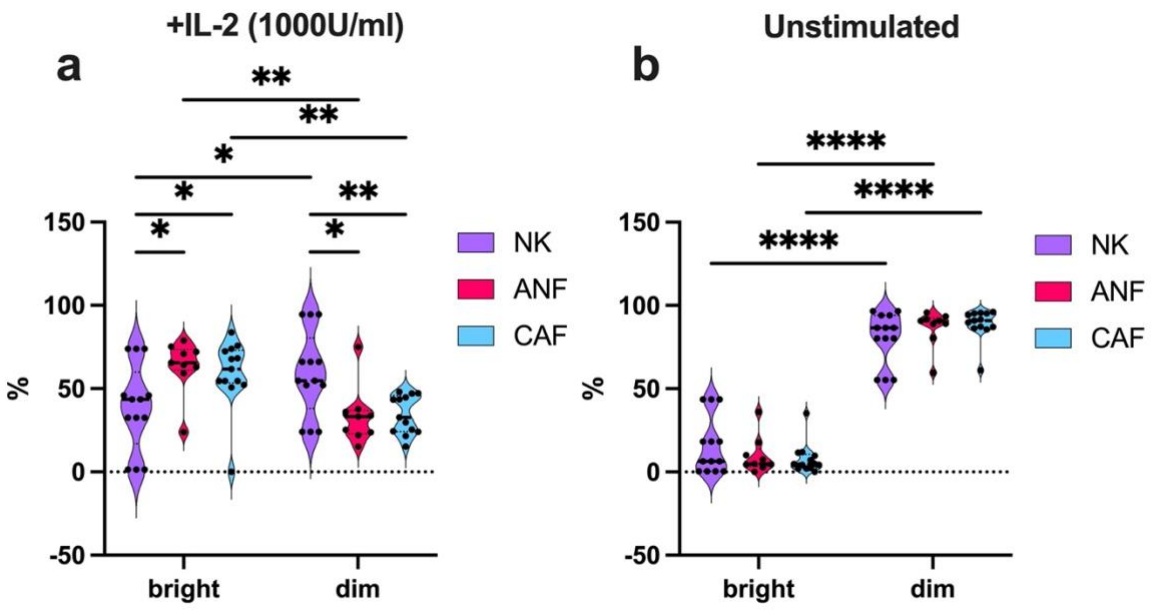


Figure 4.23. The effect of co-culture with primary ANF and CAF on the percentage of CD56^{bright} and CD56^{dim} unstimulated and stimulated NK cells.
a & b. Violin plots to compare the percentage of CD56^{bright} and CD56^{dim} expression between stimulated **(a)** and unstimulated NK cells **(b)** co-cultured with ANFs and CAFs. NK cells were stimulated using 1000U/l of IL-2. Each CAF and ANF point represent a PDAC donor, providing insights into the differential effects on NK cell phenotypes in the context of the tumour microenvironment. Statistical analysis was carried out using One-way ANOVA test followed by Kruskal -Wallis multiple comparison test with * ≤0.05; ** ≤0.01.

Figure 4.23 presents the gating methodology utilized to distinguish various NK cell populations, including CD16−CD56+, CD16+CD56+, CD16+CD56−, and CD16-CD56-. This involved the use of CD16/APC-Cy7 and CD56/PE-Cy7 markers to identify these four subpopulations. Figure 4.24 presents compelling insights into the impact of co-culturing stimulated NK cells with ANF and CAF on the expression of NK cell populations. When comparing unstimulated conditions to stimulated conditions, we found that the stimulated conditions increased the expression of CD16+CD56+ compared to non-stimulated conditions and decrease in the expression of CD16-CD56- in both conditions, stimulated and unstimulated, with no significant differences on CD16−CD56+ and CD16+CD56−.

Regarding the stimulation of NK cells, the data reveal a non-significant alteration in the percentage of CD16−CD56+ on NK cells when co-cultured with both ANF and CAF (Figure 4.24a). Conversely, the percentage of CD16+CD56+ significantly increases in the presence of both ANF and CAF (Figure 4.24b). Notably, there is no significant change in the percentage of CD16+CD56− NK cells when co-cultured with ANF and CAF compared to NK cells cultured alone (from 28.04 to 27.26) (Figure 4.24c). Intriguingly, co-culture with ANF leads to a significant decrease in the percentage of CD16−CD56− on NK cells (from 46.27 to 28.75), while no significant difference is observed with CAF co-culture (Figure 4.24d). In the other hands, when coculturing unstimulated NK cells with ANF and CAF fibroblasts, a non-significant alteration in the percentage of CD16−CD56+ (from 2.5 to 2.4) and of CD16+CD56+ (from 2.3 to 1.2) on NK cells when co-cultured with both ANF and CAF was found (Figure 4.25a & b). Conversely, the expression of CD16+CD56− NK cells significantly increase in the presence of both ANF and CAF (from 34 to 60%) (Figure 4.25c) and a decrease of CD16-CD56− NK cells (from 60 to 36%) when co-cultured with ANF and CAF

compared to NK cells cultured alone (Figure 4.25d). These findings shed light on the complex interplay between NK cells and the tumour microenvironment, suggesting differential effects of ANF and CAF tissues on NK cell phenotype.

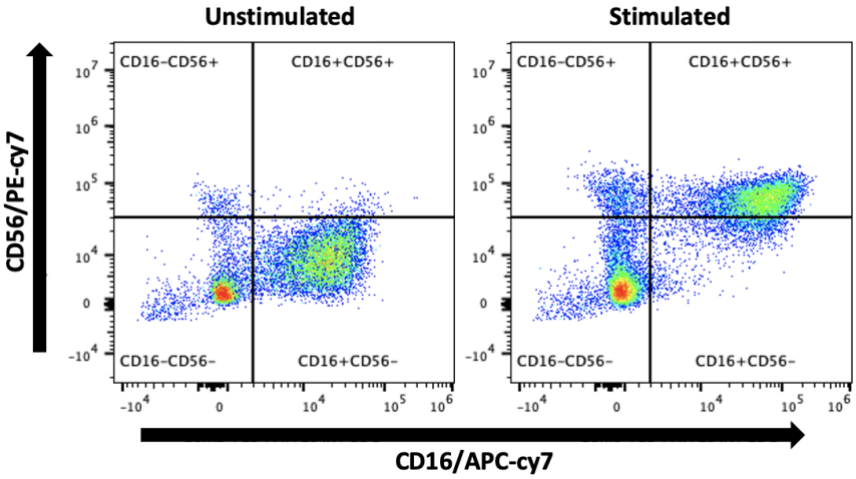


Figure 4.24. Flow cytometry gating strategy of unstimulated versus stimulated NK cells to identify.

The NK cells were cultured with ANF and CAF obtained from PDAC patients. Subsequently, the cells were stained with a flow cytometry panel comprising CD16/APC-Cy7 and CD56/PE-Cy7. Identification of NK cell populations were based on the expression of CD45RA/APC and CD16/APC-Cy-7. Flow cytometry data was collected and analysed using FlowJo software, revealing four subpopulations: CD16−CD56+, CD16+CD56+, CD16+CD56−, and CD16-CD56-.

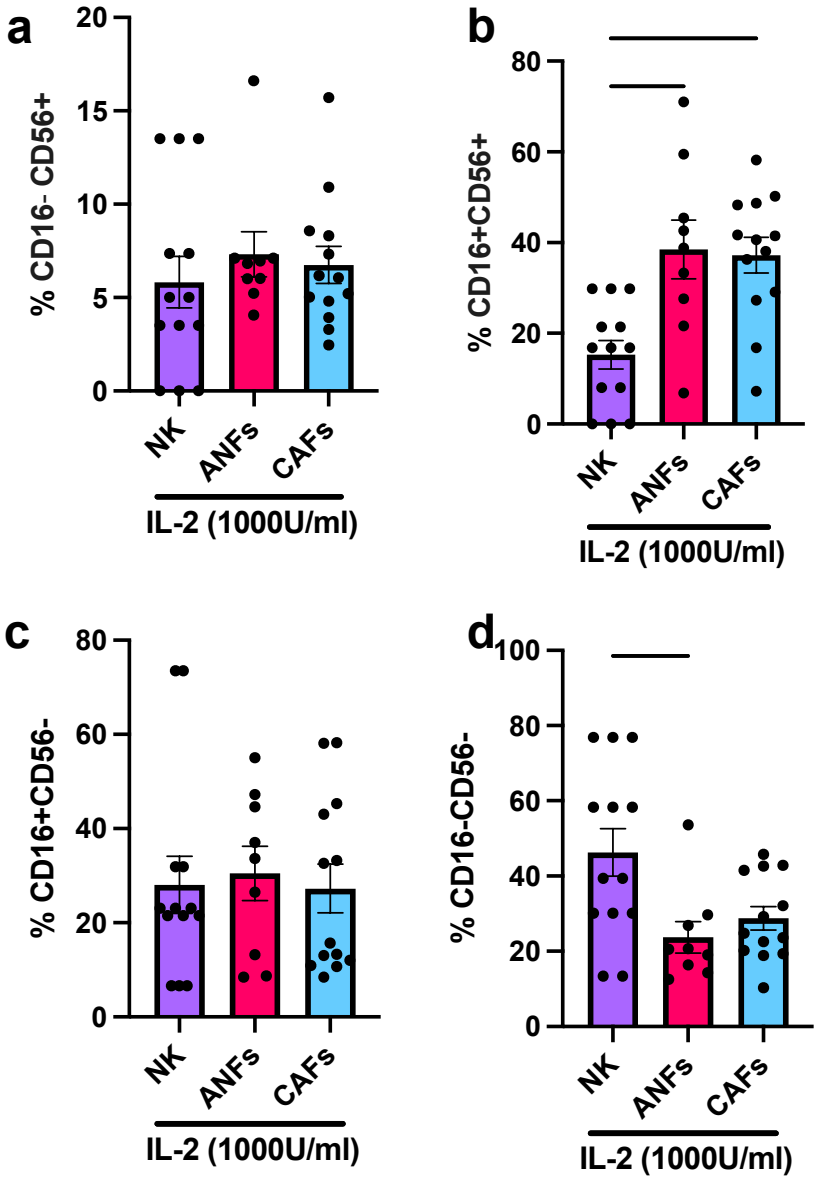


Figure 4.25. The effect of co-culture with primary ANF and CAF on the percentage of stimulated total NK cell subpopulations.
Bar plots were generated to compare the percentage of NK cell subpopulations, including CD16−CD56+ **(a),** CD16+CD56+ **(b),** CD16+CD56− **(c),** and CD16-CD56- **(d),** between stimulated NK cells co-cultured with ANFs and CAFs. Stimulation of NK cells were achieved using 1000U/l of IL-2. Each data point for CAFs and ANFs represents a PDAC donor, offering insights into the varying effects on NK cell phenotypes within the tumour microenvironment. Statistical analysis was carried out using One-way ANOVA test followed by Kruskal -Wallis multiple comparison test with * ≤0.05; ** ≤0.01.

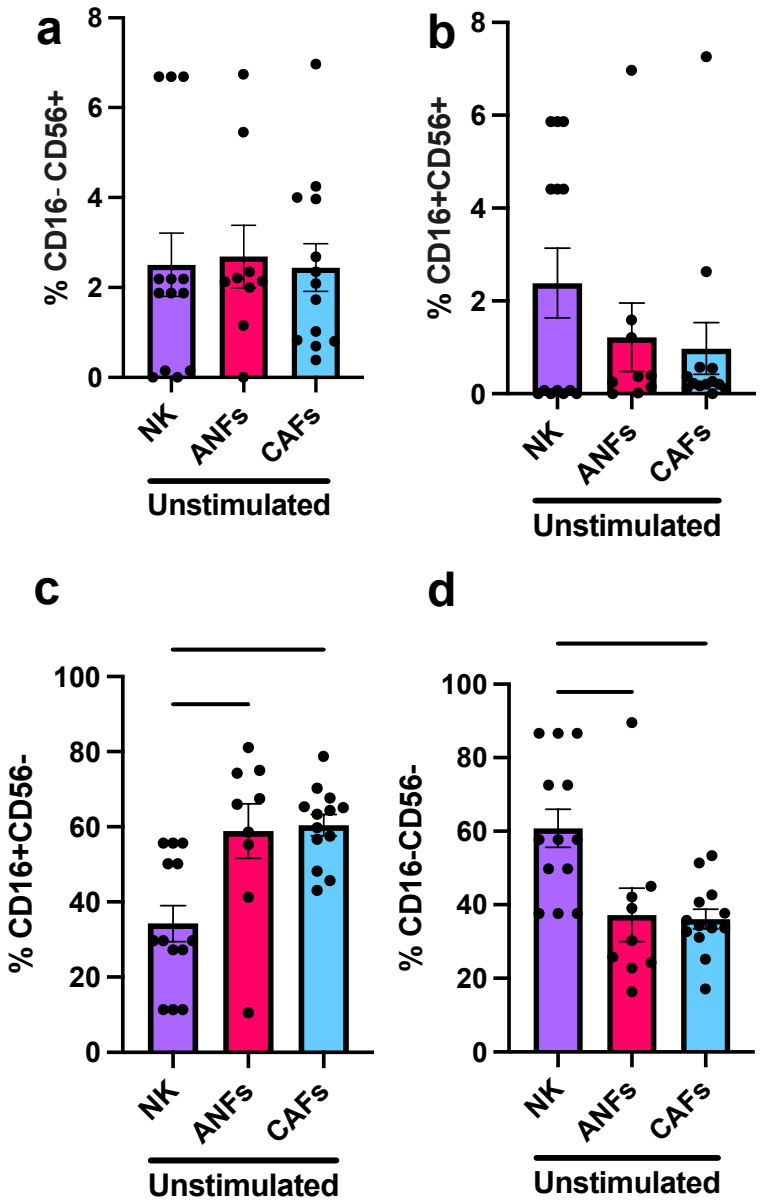


Figure 4.26. The effect of co-culture with primary ANF and CAF on the percentage of unstimulated NK cells subtypes.

Dot plots to compare the percentage of each unstimulated NK subpopulation co-cultured with ANFs and CAFs. Studied NK subtypes are: CD16-CD56+ **(a),** CD16+CD56+ **(b),** CD16+CD56- **(c),** CD16-CD56- **(d).** Each CAF and ANF point represent a PDAC donor, providing insights into the differential effects on NK cell phenotypes in the context of the tumour microenvironment. Significance was calculated with One-way ANOVA. Asterisk indicates p-value of <0.05.

For the stimulated NK cells, figure 4.26 presents an analysis of various activation markers within the total natural killer (NK) cell population, including CD69, DNAM-1, KIRs, NKG2D, and NKp46. Both the percentage and mean fluorescence intensity (MFI) data indicate a non-significant effect on the expression of CD69 and DNAM-1 (Figure 4.26a, b, c, and d). The MFI data demonstrate an increase in KIRs expression (Figure 4.26f), although there is no significant difference at the percentage level (Figure 4.26e). Co-culturing NK cells with ANF and CAF does not lead to significant differences in the expression of NKG2D and NKp46 (Figure 4.26g, h, i, and j). Figure 4.27 illustrates my investigation into the expression of activation molecules on unstimulated natural killer (NK) cells. Both the percentage and mean fluorescence intensity (MFI) data reveal no significant effect on CD69 and DNAM-1 expression (Figure 4.27a, b, c, and d). While the MFI data indicate an increase in KIRs expression when co-cultured with both ANF and CAF (Figure 4.27f), there is no significant difference at the percentage level (Figure 4.27e). Co-culturing NK cells with ANF and CAF does not result in significant differences in NKG2D expression (Figure 4.27g, h). Notably, the percentage of NKp46 increases on total NK cells when co-cultured with ANF and CAF, with no significant difference observed in MFI expression.

In summary, co-culture of stimulated NK cells with CAF fibroblasts results in alterations in NK cell subpopulations, with an increase in $CD56^{bright}$ and a decrease in $CD56^{dim}$ cells. This co-culture also affects NK cell population by increasing CD16+CD56+ and decreasing CD16-CD56- NK cell populations. However, no significant changes are observed in NK cell activation markers except for elevated KIRs. On the other hand, co-culture of unstimulated NK cells with CAF fibroblasts leads to a decrease in $CD56^{dim}$ and an increase in $CD56^{bright}$ cells, along with changes in NK populations by increasing CD16+CD56- and decreasing CD16-CD56- and increased expression of

both KIRs and NKp46. While these findings shed light on the interactions between NK cells and CAFs, further studies are warranted to elucidate the underlying mechanisms and potential limitations, such as the specific signalling pathways involved and the generalizability of findings across different experimental setups or patient populations. Additionally, exploring the functional implications of these observed changes will enhance our understanding of the role of CAFs in modulating NK cell behaviour within the tumour microenvironment.

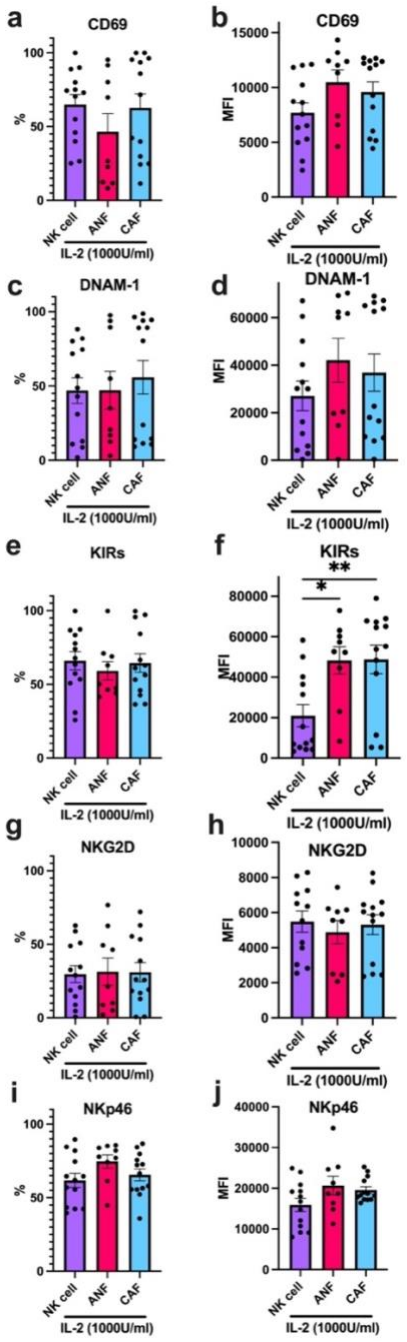


Figure 4.27. The effect of co-culture with primary ANF and CAF on the percentage of stimulated total NK cell markers.

a, c, e, g & i. Bar plots to compare the percentage of total NK cell activating (CD69, DNAM-1 and NKG2D) and inhibitory marker PD-1 (left). **b, d, f, h & j.** MFI between Stimulated NK cell co-cultured with ANFs and CAFs (right). Each data point for CAFs and ANFs represents a PDAC donor, offering insights into the varying effects on NK cell phenotypes within the tumour microenvironment. Statistical analysis was carried out using One-way ANOVA test followed by Kruskal -Wallis multiple comparison test with * ≤0.05; ** ≤0.01.

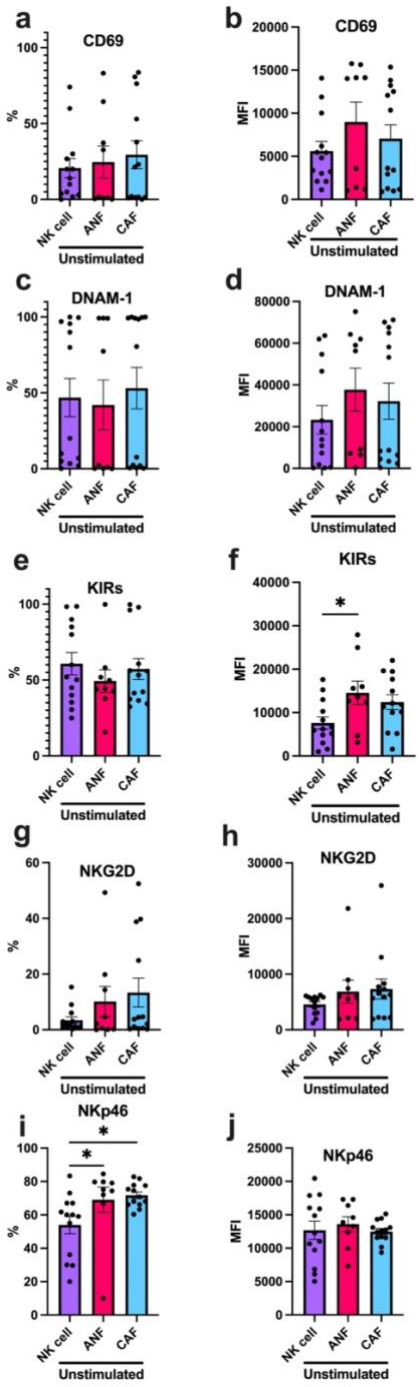


Figure 4.28. The effect of co-culture with primary ANF and CAF on the percentage of unstimulated total NK cell markers.

a, c, e, g & i. Bar plots to compare the percentage of total NK cell activating (CD69, DNAM-1 and NKG2D) and inhibitory marker PD-1 (left). **b, d, f, h & j.** MFI between unstimulated NK cell co-cultured with ANFs and CAFs (right). Each data point for CAFs and ANFs represents a PDAC donor, offering insights into the varying effects on NK cell phenotypes within the tumour microenvironment. Statistical analysis was carried out using One-way ANOVA test followed by Kruskal -Wallis multiple comparison test with * ≤0.05; ** ≤0.01.

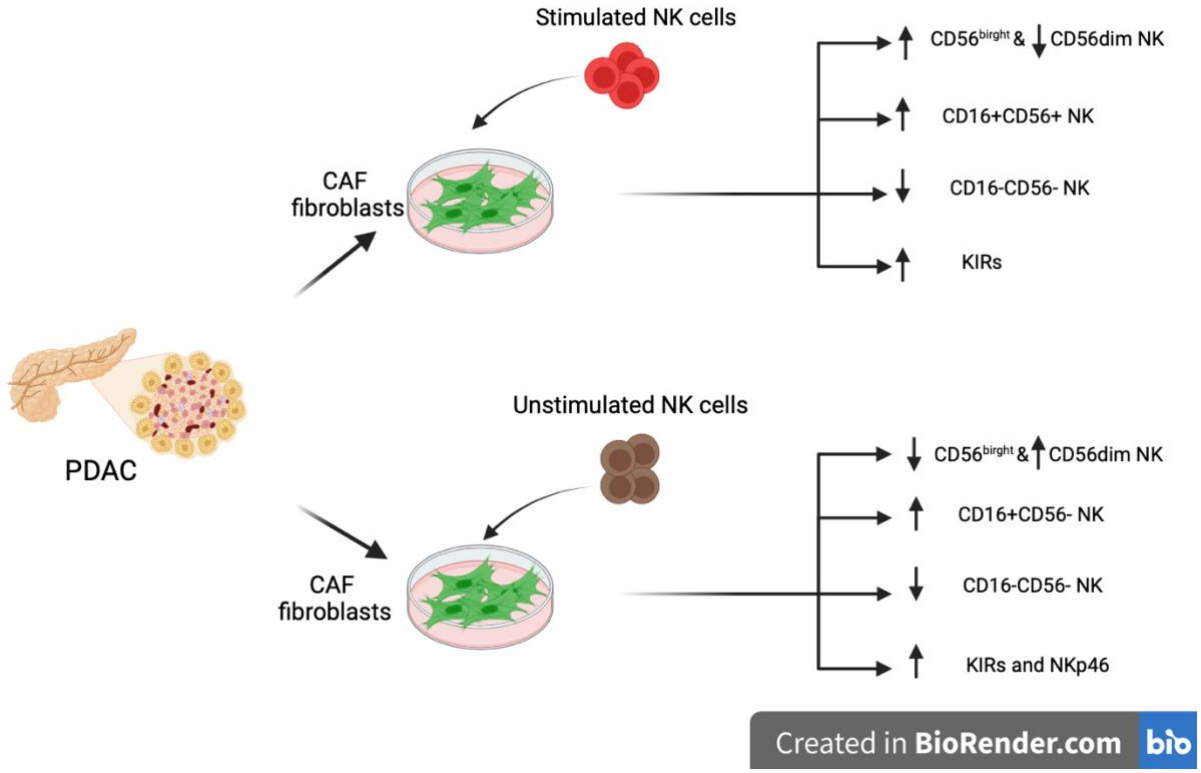


Figure 4.29. Graphical Abstract- Role of CAFs in modulating NK cell responses within the PDAC-TME.

Stimulated NK Cells: When stimulated NK cells are co-cultured with CAFs, there is an increase in $CD56^{bright}$ NK cells and a decrease in $CD56^{dim}$ NK cells. CD16+CD56+ NK cells are upregulated, indicating enhanced cytotoxic potential, while CD16-CD56- NK cells are downregulated. Additionally, killer immunoglobulin-like receptors (KIRs) are upregulated, which can affect NK cell education and function. Unstimulated NK Cells: For unstimulated NK cells co-cultured with CAFs, there is a decrease in $CD56^{bright}$ NK cells and an increase in $CD56^{dim}$ NK cells. CD16+CD56- NK cells are upregulated, suggesting an increase in mature cytotoxic NK cells, while CD16-CD56- NK cells are downregulated. Both KIRs and NKp46 are upregulated, indicating potential changes in NK cell activation and recognition capabilities. Overall, the abstract highlights how CAFs modulate NK cell subsets, potentially shifting the balance between different NK cell phenotypes and affecting their functional properties within the PDAC tumour microenvironment.

4.3 Discussion

NK and T cells are crucial in the immune system (Humphrey, 2023). Recent research highlights the interaction between NK and T cells and CAFs. This chapter explores how CAFs influence T and NK cell responses, either enhancing or inhibiting anti-cancer immunity. While conflicting evidence exists regarding the role of CAFs in tumorigenesis, recent studies highlight bidirectional signalling between T cells and CAFs, emphasizing its significance in shaping the immune landscape of tumours (Kato et al., 2018; Shibuya et al., 2014).

1. Proliferation of T/NK affected by CAF

1.1 Primary CAF

In the first section of my results, activated T cells' proliferation is not significantly affected by ANFs or CAFs, which contrasts with findings by Gorchs and her colleagues indicating that CAFs inhibit T cell proliferation in PDAC (Gorchs et al., 2019). Takahashi's team noted that CAFs express PD-L1 and PD-L2, which suppress T cells through PD-1 binding (Takahashi et al., 2015). Variability in study designs and CAF heterogeneity might explain these differences (Zhang et al., 2022). However, in unstimulated conditions, co-culture with ANF and CAF significantly increased T cell proliferation, suggesting a contact-dependent mechanism possibly mediated by the secretion of cytokines and chemokines by fibroblasts in the conditioned medium.

NK cells are essential for innate immune responses, targeting and eliminating compromised cells (Vivier et al., 2008). Our findings show that ANF and CAF do not affect NK cell proliferation when stimulated. However, in the absence of stimulation, both ANF and CAF co-culture led to a notable increase in NK cell proliferation. This

result contrasts with studies on pancreatic stellate cells (PSCs), which suggest PSCs suppress NK cell function via immunosuppressive factors like TGF-β, IL-10, IL-6, IL-23, and IL-1β (Konjevic et al., 2019). CAFs' impact on NK cells in the tumour microenvironment (TME) is not fully understood. CAFs can secrete cytokines and chemokines affecting various immune cells, including NK cells. For instance, endometrial cancer studies showed CAFs more effectively suppress NK cell cytotoxicity than normal fibroblasts (Inoue et al., 2016). Similarly, in NSCLC, CAFs exhibit reduced proliferation rates (Yang et al., 2020). Fibroblasts secrete cytokines like CXCL12, IL-6, and CCL5, contributing to immune modulation (Lavie et al., 2022). The increased proliferation of T and NK cells in the absence of stimulation suggests these cells may acquire cytotoxic functions, enhancing their ability to target cancer cells. However, my study did not differentiate between CAF subtypes, which may influence the results. CAFs include inflammatory CAFs (iCAFs) and myofibroblast CAFs (myCAFs), each playing unique roles in the TME (Biffi et al., 2019; Elyada et al., 2019). In addition, PBMCs from healthy donors and ANF/CAFs from PDAC patients were used, creating an MHC mismatch. This mismatch could affect our findings and does not fully replicate the PDAC tumour immune environment. Future studies using autologous PBMCs and CAFs from PDAC patients, alongside investigating MHC matching, could further clarify CAFs' immunomodulatory effects.

1.2 Immortalized CAF

Whilst I was able to confirm my findings using immortalized fibroblasts, it is important to consider the inherent heterogeneity and plasticity of fibroblasts. These cells can undergo phenotypic changes after a few passages, potentially altering their functional characteristics (Baranyi et al., 2019; Elena Neumann & Jurgen Steinmeyer, 2010). The

decision to use immortalized fibroblasts was aimed at comparing and validating their effects with primary cells at early passages. Interestingly, similar results were observed in terms of the increased proliferation of T and NK cells when co-cultured with primary or immortalised cells, suggesting that our fibroblasts maintained their phenotype and genotype integrity within passage 1 to passage 8. However, it is essential to acknowledge that even within this early passage range, subtle changes in fibroblast behaviour could occur, potentially influencing the observed outcomes. Thus, further studies exploring the stability of fibroblast characteristics over extended passages would provide valuable insights into their utility as experimental models in immunological research.

1.3 conditioned media

As mentioned earlier, fibroblasts secrete cytokines and chemokines that affect the surrounded cells for that reason, conditioned media (CM) was collected and added it to T and NK cells and then their proliferative capacity in the presence of fibroblasts CM was evaluated. The results show that CAF increase T and NK cell proliferation which might be due to the secretion cytokines and chemokines capable of modulating the behaviour of neighbouring cells, the exact composition and concentration of these factors in the CM were not delineated in this study. Consequently, the specific mediators responsible for the observed increase in T and NK cell proliferation remain unidentified, a task slated for future investigation.

2. Functionality of T cells affected by CAF.

Transitioning to the focus to T cell secretion, the levels of interferon-gamma (IFN-γ) produced by T cells was assessed. My findings revealed that CAFs enhanced IFN-γ

production in stimulated T cells. However, intriguingly, this effect was attenuated in the presence of cancer cell lines, namely Panc-1 and CF-Panc. This observation raises questions regarding the interplay between CAFs and cancer cells in modulating T cell activation. While the decreased IFN-γ production in the presence of Panc-1 and CF-Panc suggests a potential suppression of T cell function by cancer cells, further investigations are warranted to elucidate the underlying mechanisms. Interferon-gamma (IFN-γ) is a cytokine crucial for triggering and regulating various immune responses, primarily originating from activated T cells and natural killer (NK) cells. Its involvement in antitumour immune reactions is well-documented (G. Tau, 1999)

3. Phenotype of T/NK cell affected by CAF

3.1 proportion of CD4 and CD8 T cells

In section 2 of the results, a notable decrease in CD4+ T cell levels with CAF presence was found, irrespective of stimulation, while CD8+ T cell levels remained unchanged upon stimulation but increased under unstimulated conditions. Contradictory findings from studies like Elyada and her colleagues suggest that antigen-presenting CAFs (apCAFs) activate CD4+ T cells antigen-specifically, hinting at the heterogeneity and diverse roles of CAF subtypes (Elyada et al., 2019). Studies propose that apCAFs may induce T cell anergy or differentiation into regulatory T cells (Tregs) via MHC-II expression (Elyada et al., 2019; Vaish et al., 2021). Huang and his colleagues reported that mesothelial-origin apCAFs induce naive CD4+ T cells into Tregs antigen-specifically, highlighting fibroblast-T cell subset interplay (Huang et al., 2019). Myofibroblast CAFs (MyCAFs) in PDAC mouse models suppress immune surveillance by increasing CD4+Foxp3+ Tregs, leading to poor survival outcomes (Hosein et al., 2019; Ozdemir et al., 2014). My findings on CD8+ T cells contrast with reports of

activated pancreatic stellate cells (PSCs) reducing CD8+ T cell infiltration and activity in the stromal region (Ene-Obong et al., 2013). CAFs expressing high levels of FAP and α-SMA have been linked to CD8+ T cell exclusion from the tumour microenvironment (Gorchs et al., 2019). Studies on CAF-rich oesophageal cancer showed CD8+ T cells predominantly in peritumoral regions, unlike in CAF-low tumours where CD8+ T cells are more evenly distributed (Kato et al., 2018; Ozdemir et al., 2014). These discrepancies highlight the complex roles of stromal and immune cells in modulating T cell responses within the tumour microenvironment, warranting further investigation.

3.2 T cell activation

My results also indicated that ANF and CAF increase the expression of activation markers CD69 and NKG2D on both CD4+ and CD8+ T cells under stimulated conditions, with no significant effect on DNAM-1 expression. CD69 is an early activation marker for lymphocytes and NK cells (Cibrian & Sanchez-Madrid, 2017), and NKG2D is an activating receptor found on cytotoxic immune cells, binding stress-induced ligands (Huifang Liu, 2019). Although CD4+ T cells typically do not express NKG2D post-activation, certain pathological conditions can induce its expression (Wensveen et al., 2018). DNAM-1 is involved in various immune responses, including leukocyte migration and T cell and NK cell effector functions (Gilfillan et al., 2008). Fibroblasts in human lung cancer have been implicated in downregulating CD69 expression (Vancheri et al., 2005), whereas Fanconi anemia fibroblasts and T cells exhibit increased NKG2D ligand levels (Casado et al., 2022). Blocking NKG2D reduces NK and CD8+ T cell degranulation towards senescent fibroblasts (Pereira et al., 2019). The results suggest that fibroblasts within the co-culture environment likely trigger signalling pathways that promote the activation and potentially the functional

activity of T cells. One hypothesis is that fibroblasts activate T cells through mechanisms such as antigen recognition, T cell receptor (TCR) engagement, and co-stimulation. These processes initiate intracellular signalling cascades, leading to changes in gene expression and cellular responses necessary for T cell activation. Additionally, fibroblasts may induce T cell clonal expansion, resulting in the proliferation of antigen-specific T cell clones, thereby increasing the pool of T cells capable of responding to the antigen.

3.3 Checkpoint receptor

PD-1, a protein on T cells, regulates immune responses and has two ligands, PD-L1 and PD-L2 (Zhang, 2017). The PD-1/PD-Ls interaction inhibits T cell function and promotes Tregs, facilitating cancer immune evasion (Yanyan Han, 2020). ANF and CAF increase PD-1 expression on both stimulated and unstimulated CD4+ and CD8+ T cells. This upregulation may indicate T cell exhaustion or activation. Higher PD-1 expression with CAF suggests that CAF express PD-1 ligands, contributing to immune dysfunction. This engagement is linked to T cell exhaustion and reduced anti-tumour responses, underscoring PD-1 as a therapeutic target for checkpoint blockade therapy. Further research is needed to understand fibroblast, T cell, and PD-1/PD-L1 axis interactions and their impact on immune suppression in the tumour microenvironment.

3.4 T cell subsets

Both ANF and CAF increase the proportion of central memory (CM) CD4+ and CD8+ T cells while reducing effector memory (EM), naive, and terminally differentiated effector memory (TEMRA) subsets under stimulated conditions. ANF had no significant effect on T cell differentiation. Other studies, like Gorchs et al., showed CAF

maintaining naive T cell phenotypes and reducing effector memory differentiation through soluble factors. My methodology, focusing on CD4+ and CD8+ T cell subtypes, differed from that of Gorchs et al who used whole PBMCs, which could explain the variations. More research is needed to explore fibroblast effects on T cell subtypes and functionality.

Questions arise regarding the fate of these activated T or NK cells. Do they effectively migrate to the tumour site to exert their anti-tumour effects, or do other regulatory mechanisms inhibit their functions within the tumour microenvironment? Are activated T cells associated with exhaustion phenotype or T cell activation and differentiation? Addressing these questions is crucial to understanding the role of fibroblasts in modulating T cell responses and optimizing therapeutic strategies targeting the tumour-immune microenvironment. Further research is needed to unravel the complex interplay between fibroblasts and T cells in the context of cancer immunotherapy.

3.5 NK cells subsets

NK cells are classified into $CD56^{dim}$ and $CD56^{bright}$ subsets based on CD56 expression, with $CD56^{dim}$ NK cells being highly cytotoxic and $CD56^{bright}$ NK cells primarily producing cytokines (Megan A. Cooper, 2001). In PDAC patients, NK cells show compromised function, suggesting potential benefits from therapies enhancing NK cell activity (K. Funa, 1984). Within the pancreatic tumour microenvironment, NK cells exhibit reduced cytotoxicity and a regulatory phenotype characterized by IL-10 expression, indicating immune evasion roles (Marcon et al., 2020). My study revealed that under stimulated conditions both activated ANF and CAF increase the proportion of $CD56^{bright}$ NK cells while decreasing $CD56^{dim}$ NK cells, suggesting an immunomodulatory effect of fibroblasts. The study also showed an increase in

cytotoxic NK cells (CD16+CD56+) and CD16-CD56- NK cells in co-culture with ANF and CAF, highlighting the potential of fibroblasts to enhance immune responses through cytotoxic mechanisms. However, there was no significant effect on regulatory NK cells (CD16-CD56+) and defective NK cells (CD16+CD56-), suggesting selective influence on NK cell subsets. The role of each fibroblast subtype in modulating NK cell phenotype and function requires further characterization.

3.6 KIR expression

My study showed significant upregulation of KIRs in stimulated NK cells co-cultured with ANF and CAF, indicating fibroblast modulation of NK cell activity. KIRs regulate NK cell maturation and activation, influencing immune responses in various contexts (Campbell & Purdy, 2011). In unstimulated NK cells, KIR expression increased with ANF and CAF presence, while other activating receptors remained unchanged. This contrasts with studies on melanoma, hepatocellular, and colorectal carcinoma fibroblasts, which suppress NK activating receptors through PGE2 and/or IDO secretion (Linda Ziani, 2017; Mirna Balsamo, 2009; Zhang et al., 2019). Additionally, the production of IL-6 by iCAF indicates their involvement in immune suppression by inhibiting NK cell function. Furthermore, the attraction of NK cells to cells secreting CXCL12 may divert them from PDAC cells to FAP+ CAFs, implicating FAP+ CAFs in immune evasion. Further research is needed to elucidate the mechanisms of fibroblast-NK cell interactions and their impact on antitumour immunity.

4.4 Conclusion

This chapter highlights the complex interactions between CAFs and T and NK cells within the tumour microenvironment. The findings demonstrate that CAFs significantly influence immune cell functions, including proliferation, activation, and cytotoxicity. CAFs modulate receptor and signaling molecule expression on T and NK cells, impacting their effector functions. These insights emphasize the dynamic interplay between stromal components and immune cells, shaping the tumour immune landscape. Further research into these interactions promises to reveal novel therapeutic strategies targeting the tumour microenvironment to enhance antitumour immunity.

Chapter 5: Adhesion and migration of lymphocytes to Cancer Associated Fibroblasts

5.1 Introduction

Fibroblasts can have substantial impact on the functional activity and migration of immune cells (McGettrick, Buckley, Ed Rainger, et al., 2010) and as such I next went on to assess how fibroblasts from pancreatic tissue acted to influence the migration of lymphoid cells. My focus was on the relative impact of inflammatory CAFs (iCAF) and myo-fibroblastic CAFs (myCAF) on lymphocyte adhesion and migration using a co-culture system. By differentially inducing myCAF with TGF-β and iCAF with IFN-γ/TNF-α, I aimed to decipher how different fibroblast phenotypes modulate lymphocyte behaviour, potentially offering new insights into stromal-immune interplay within the tumour microenvironment.

Leukocyte recruitment is a complex process comprising at least five major stages, any of which can be impeded to halt the migration process (Schwarz, 2010) (Figure 1). Activation of endothelial cells at sites of inflammation induces expression of cellular adhesion molecules, including selectins, in response to local release of cytokines(Granger DN, 2010; Schwarz, 2010). The engagement between endothelial E- and P-selectins and their ligands on leukocytes leads to a change in leukocyte velocity upon binding to the endothelial cell surface, initiating a rolling motion along the vascular wall (Granger DN, 2010; Schwarz, 2010). This initial phase of leukocyte-venular endothelium interactions involves tethering (capture) and rolling, characterized by low affinity interactions. Subsequent reinforcement occurs upon leukocyte activation, mediated by both chemokine-dependent and chemokine-independent mechanisms. This activation ultimately results in the firm attachment of leukocytes to the endothelium, where they become stationary. Subsequently, the leukocytes can migrate into the interstitium by passing through the spaces between adjacent endothelial cells (Granger DN, 2010; Schwarz, 2010).

The multistep adhesion cascade is a highly coordinated process that regulates leukocyte recruitment to sites of inflammation. It begins with the selectin family of adhesion molecules, which mediate the initial tethering and rolling of leukocytes on the endothelial surface under shear stress. Selectins, such as L-selectin on leukocytes and P- and E-selectins on activated endothelial cells, facilitate transient and labile interactions, allowing leukocytes to roll along the vessel wall. This rolling slows the leukocytes and positions them for the next steps in the cascade (Ley et al., 2007; Springer, 1994).

A critical step in firm leukocyte adhesion is the activation of integrins, driven by chemokines and their receptors. Chemokines bind to G-protein-coupled receptors (GPCRs) on leukocytes, triggering "inside-out" signalling pathways. This leads to conformational changes in integrins, transitioning them from a low-affinity bent state to a high-affinity extended state. Integrins like LFA-1 (αLβ2) and VLA-4 (α4β1) can then bind tightly to their ligands, such as ICAM-1 and VCAM-1, expressed on endothelial cells. Chemokines also regulate integrin clustering and spatial organization, ensuring firm adhesion and leukocyte arrest. This interplay between chemokines, GPCRs, and integrins enables efficient leukocyte recruitment and migration, highlighting their pivotal role in immune surveillance and inflammatory responses (Ley et al., 2007; Springer, 1994) The multistep adhesion cascade is a highly coordinated process that regulates leukocyte recruitment to sites of inflammation. It begins with the selectin family of adhesion molecules, which mediate the initial tethering and rolling of leukocytes on the endothelial surface under shear stress. Selectins, such as L-selectin on leukocytes and P- and E-selectins on activated endothelial cells, facilitate transient and labile interactions, allowing leukocytes to roll

along the vessel wall. This rolling slows the leukocytes and positions them for the next steps in the cascade (Ley et al., 2007; Springer, 1994).

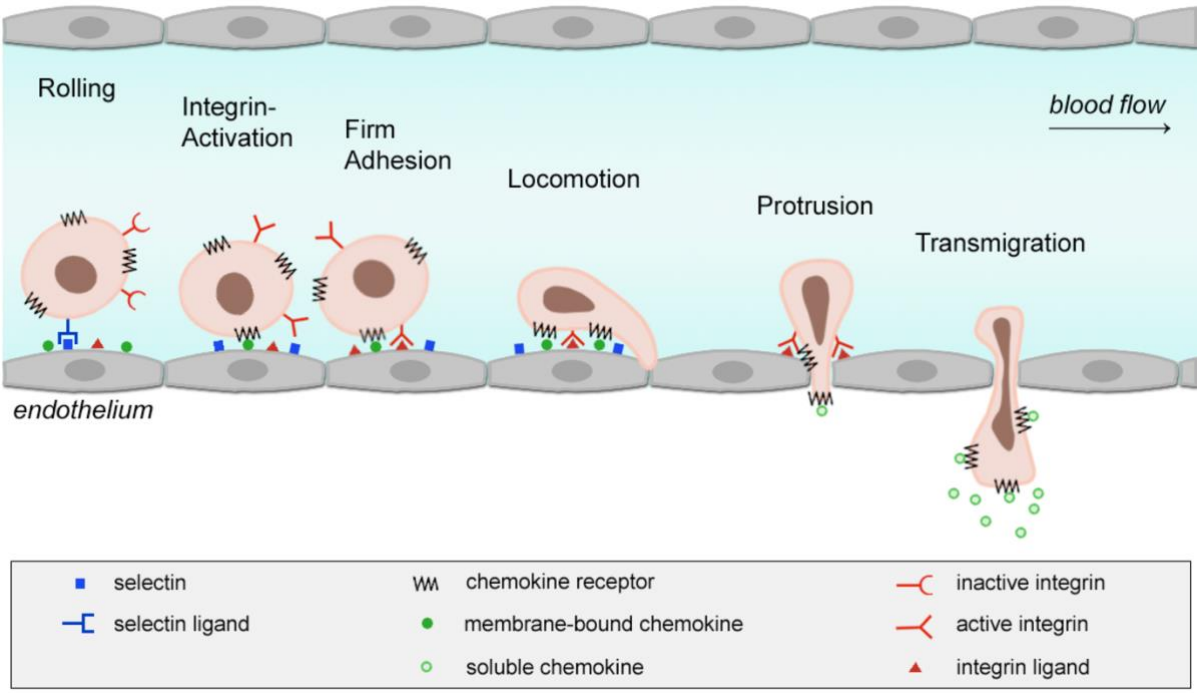


Figure 5.1. Sequential Events in Leukocyte Extravasation.
Activated leukocytes initially interact with selectins expressed on cytokine-activated endothelial cells, initiating a rolling motion. Subsequent activation of integrins results in a conformational change. Integrins, along with adhesion molecules and chemokine receptors, then bind to their respective ligands on the endothelial cell surface, facilitating firm adhesion. Following firm adhesion, leukocytes navigate along the endothelial cell surface in search of a suitable site for transmigration (Schwarz, 2010).

To conduct these studies, I employed two static assay methods, the pseudo-emperipolesis assay (where cells migrate under rather than through other cell types), and transwell assays (Bradfield et al., 2003; Jeffery et al., 2013; McGettrick, Buckley, Ed Rainger, et al., 2010; McGettrick, Buckley, Filer, et al., 2010). Emperipolesis is a term that describes a cell completely engulfing another cell and comes from the Greek (em—within; peri—around; p olemai—to roam). In my thesis pseudo-emperipolesis refers to a cell that is trapped underneath another cell (in this case a fibroblast) but is not engulfed. While transwell systems assess migration through porous membranes and away from cells, simulating physiological conditions, pseudo-emperipolesis mimics immune cell migration across and underneath host cells (Figure 5.2).

Both methodologies offer unique insights into cellular behaviours, enriching understanding of adhesion and migration mechanisms in diverse biological contexts. Static assays, providing a controlled environment, play a crucial role in precise monitoring and analysis of cellular interactions particularly in stromal-immune crosstalk (McGettrick, Buckley, Ed Rainger, et al., 2010; Munir et al., 2015). In the pseudo-emperipolesis assay (Figure 5.2A), non-adherent cells were removed by washing with M199/BSA, leaving behind adhered cells on the fibroblast surface. Adhered cells include bright and grey phase cells. Adhered cells were tallied from both phases, while migrated cells were counted based on their appearance in the dark phase (Figure 5.3). First, using a live cell imaging microscope, adherent cells were quantified by digitizing images at 1-second intervals from recordings made at key time points. Cells were categorized into three phases: (a) Bright phase, representing total peripheral blood lymphocytes (PBLs) adhered to the fibroblast surface with distorted outlines and slow migration; (b) Grey phase, representing additional adherent cells;

and (c) Dark phase, representing migrated cells located beneath fibroblasts, characterized by distorted shapes from prior adherence (Figure 5.3).

In the transwell assay, I collected both the non-adhered fraction and migrated fractions (Figure 5.2B). Both fractions were stained with counting beads to quantify the number of cells that migrated through the porous membrane. Additionally, this also allowed me to quantify the number of adhered cells, which were defined as the total cell count added minus the migrated and non-adhered fractions (McGettrick, Buckley, Ed Rainger, et al., 2010). However, for lymphocyte phenotyping, I focused solely on the migrated fraction within the transwell assay when assessing T cell and NK cells. The three sections in this chapter focus on different aspects of lymphocyte interaction and migration when cultured with adjacent normal fibroblasts (ANF) and cancer associated fibroblasts (CAF) from PDAC patients. One aim was to explore the optimization of the incubation period for lymphocyte adhesion and migration when co-cultured with ANF and CAF in section 1. Additionally, the relative impact of unstimulated or stimulated ANF and CAF on lymphocyte adhesion and migration was assessed in section 2. Furthermore, the influence of ANF and CAF on the phenotype of migrated T cell lymphocytes was investigated in section 3. Lastly, section 4 will focus on examining how ANF and CAF impact the phenotype of migrated NK cell lymphocytes.

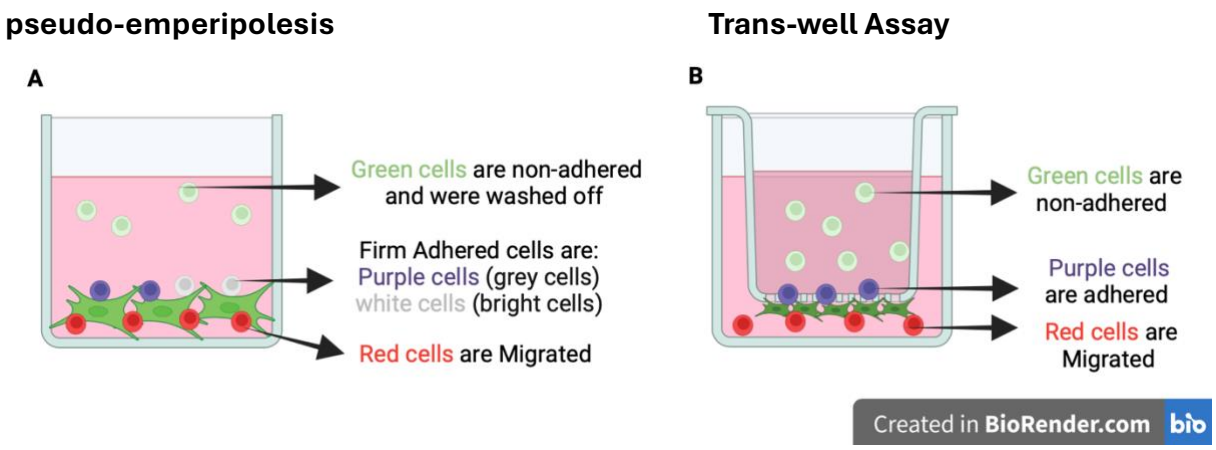


Figure 5.2. Illustration of the principles of the Pseudo-emperipolesis and Transwell Assays.

In both the pseudo-emperipolesis assay (A) and the transwell assay (B), non-adherent cells are represented as green cells, while transmigrated cells are indicated by red cells. In the pseudo-emperipolesis assay, firm adhesion is represented by both purple and white cells, where grey or bright phenotype indicates relative degree of adhesion. Conversely, in the transwell assay, adhered cells on the fibroblast surface are depicted as purple cells.

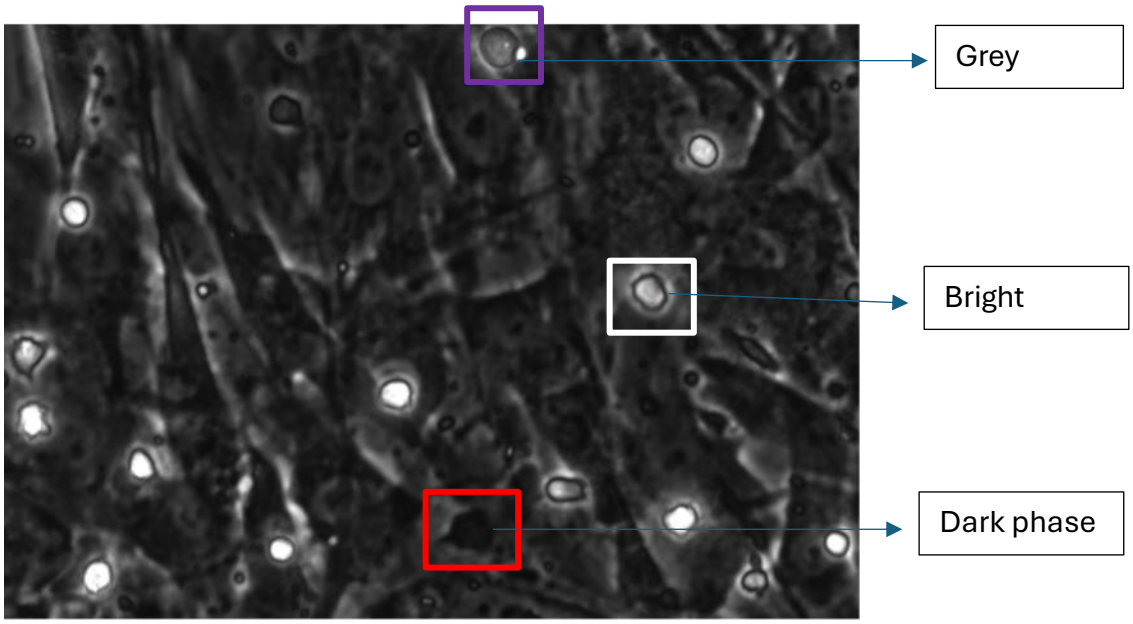


Figure 5.3. illustration of Pseudo-emperipolesis counting strategy.
Adhered cells were counted as the aggregate of those observed in both the bright (White box) and grey phases (purple box), while migrated cells were identified and counted based on their appearance in the dark phase (Red box).

5.2 Results

5.2.1 The impact of incubation period on functional behaviour of lymphocytes in co-culture with fibroblasts

Initially I explored the influence of variation in the incubation period and fibroblast subtype on the profile of lymphocyte migration using the pseudo-emperipolesis assay. Migration was assessed at an early point of 20-minutes and then at 1, 2, 3 and 24 hours. The relative levels of lymphocyte total adhesion, firm adhesion, and transmigration was determined. This initial analysis set the foundation for understanding the dynamic interplay between incubation time and specific fibroblast populations and laid the groundwork for subsequent detailed examinations of their impact on lymphocyte behaviour.

Initially I assessed the total number of adhered cells, which represented the aggregate of all visible cells and was represented as cells per square millimetre (per 10^6 cells applied) (Figure 5.4). This value increased incrementally over time when lymphocytes were cultured with normal fibroblasts (Figure 5.4). However, during incubation with CAF a peak value was seen at 2 hours ($p = 0.001$) following by a subsequent trend towards a decline, potentially representing some detachment and loss of fibroblasts during extended culture. A notable finding was that the number of adhered cells was substantially higher at 2 hours ($p = 0.0007$) when incubated with CAF compared to ANF and is of interest given the potential role of CAF in guiding lymphocyte recruitment within the tumour microenvironment (Figure 5.4).

I next assessed the relative distribution of these adhered cells as either firmly adhered or transmigrated. All cells started out as firmly adhered at 20 minutes ($p = 0.01$) but this then decreased with a parallel increase in transmigration ($p = 0.01$) (Figure 5.5). Importantly, this process was higher at 2 hours showing that, not only do CAF lead to adherence of more cells at 2 hours but that these also transmigrate ($p = 0.001$) (Figure 5.5). A trend towards reduced firm adhesion (i.e., phase bright) (Figure 5.5A) and increased transmigrated lymphocytes (Figure 5.5B) within 1 hour was observed with both ANF and CAF. For ANF, firm adhesion decreased from 97% to 89% while migration increased from 3% to 11% ($p = 0.009$). For CAF, firm adhesion dropped from 87% to 72% and migration increased from 13% to 28% ($p = 0.01$), with CAF showing a more pronounced effect. Fibroblasts from inflamed tissue can induce enhanced lymphocyte adhesion and this may reflect what I was observing with CAF (Lally et al., 2005; McGettrick et al., 2012). Overall, these results show that transmigration is low in the first 20 minutes but increases significantly over 2 hours. CAFs have a greater impact on total lymphocyte adhesion than ANFs, with reduced firm adhesion and increased transmigration within 1 hour. These findings highlight the crucial role of CAFs in lymphocyte behaviour, emphasizing the need to consider CAF-related factors in experimental design and interpretations.

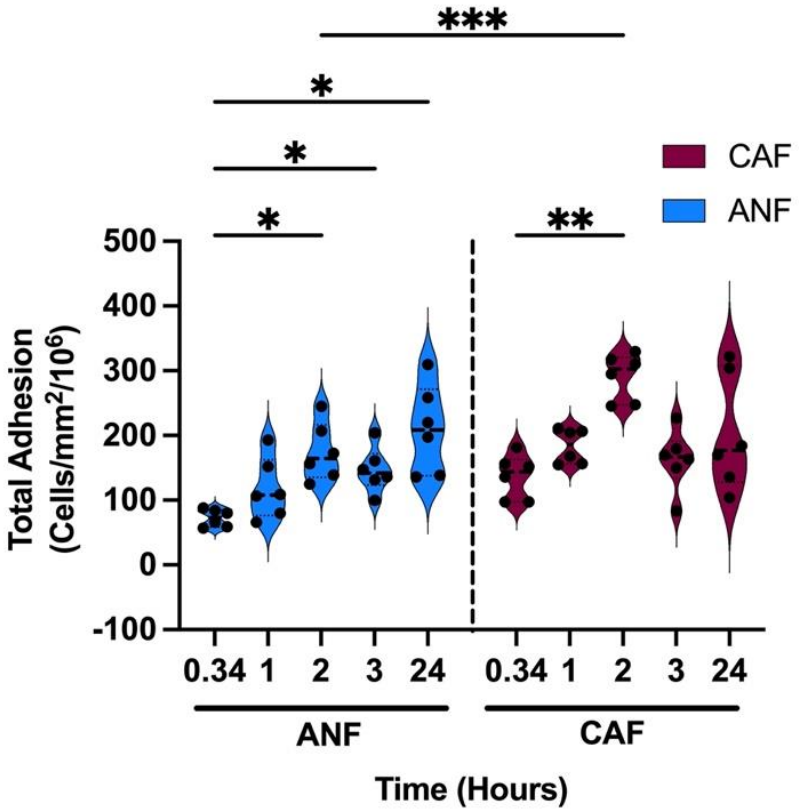


Figure 5.4. Kinetics of adhesion of lymphocytes to fibroblast subsets during co-culture using Pseudo-emperipolesis assay.

Lymphocytes were co-cultured with CAF or ANF fibroblasts for up to 24 hours and sampled at a range of timepoints (0.34, 1, 2, 3 and 24 hours). Cells were visualised using live cell imagine microscope and the total adhesion of lymphocytes to fibroblasts was expressed as number of cells/$mm^2/10^6$. Data are mean ± S.D., n=6 independent experiments using 6 different PBLs from healthy donors for each fibroblast. ANOVA showed a significant effect of times ($p<0.0001$) and of fibroblast type ($p<0.01$) on total adhesion. *<0.05 **<0.01, ***<0.001 by Tukey's multiple comparisons test.

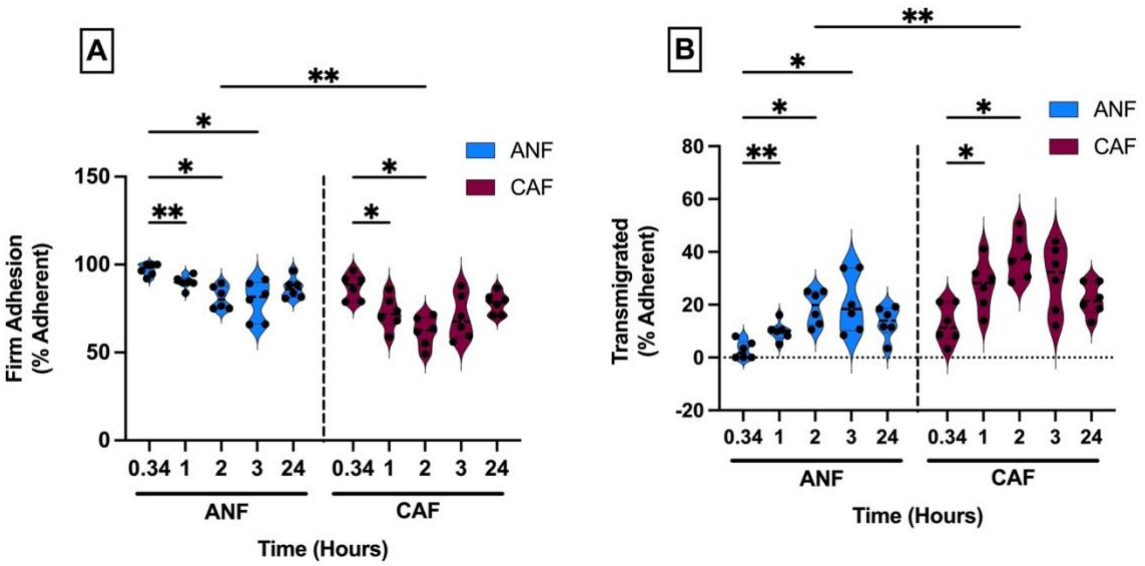


Figure 5.5. Kinetics of adhesion of lymphocytes to fibroblast subsets during co-culture using Pseudo-emperipolesis assay.

Lymphocytes were co-cultured with resting CAF or ANF fibroblasts for up to 24 hours and samples at a range of timepoints (0.34, 1, 2, 3 and 24 hours). Cells were visualised using live cell imagine microscope and the firm adhesion (i.e. phase bright) **(A)** and transmigration **(B)** were expressed as percentage of total cells that adhered. Data are mean ± S.D., n=6 independent experiments using 6 different PBLs from healthy donors for each fibroblast. ANOVA showed a significant effect of times ($p<0.0001$), and of fibroblast type ($p<0.0006$), on both firm adhesion and migration, *<0.05, **<0.01 by Tukey's multiple comparisons test.

5.2.2 The impact of stimulated fibroblasts on functional behaviour of lymphocytes in co-cultures.

Pseudo-emperipolesis assays were next conducted on CAF and ANF following cytokine stimulation with TGF-β or IFN-γ/TNF-α to induce myCAF or iCAF phenotype respectively (Biffi et al., 2019; Elyada et al., 2019). Additionally, a combination of stimulations was explored to mimic the complex signalling environment within the tumour microenvironment. By studying the impact of these stimuli individually, and in combination, I hoped to gain a more comprehensive understanding of the responses and interactions between fibroblasts under conditions that simulate the complexities of the tumour microenvironment (Belle & DeNardo, 2019; Lavie et al., 2022; Zhang et al., 2022).

I selected 20 minutes and 2 hours to use as the incubation periods for these studies due to my prior findings that highlighted the critical impact of CAF on lymphocyte behaviour within a 2-hour timeframe. By focusing on these intervals, I aimed to capture the early (20 minutes) and sustained effect (2 hours) on migration associated with cytokine-induced fibroblasts as assessed by total adhesion, firm adhesion, and transmigration.

Interestingly, total adhesion at the early timepoint of 20 minutes was increased with the use of unmanipulated CAF in this experiment, whilst I had previously seen this only at 2 hours. However, the induction of myCAF with the use of TGF-β attenuated this effect (Figure 5.6A). Interestingly, ANF remained unaffected by TGF-β stimulation at both time points, as did CAF after a 2-hour incubation period (Figure 5.6B).

In contrast, the addition of IFN-γ/TNF-α to CAF markedly increased the percentage of total adhesion ($p = 0.01$) compared to untreated CAF at both time points (Figure 5.6A and B). Additionally, this treatment elevated total adhesion in CAF compared to ANF at the initial 20 mins ($p = 0.01$), although no significant difference was observed after a 2-hour incubation (Figure 5.6A and B). Notably, treating CAF with the combination of both cytokines TGF-β, and IFN-γ/TNF-α, decreased this effect compared to CAF treated with IFN-γ/TNF-α alone at both time points (20 mins and 2 hour) ($p = 0.01$), indicating a complex interplay between cytokines (Figure 5.6A). Interestingly, no significant differences emerged between CAF and ANF in the initial 20 minutes and 2 hours when the fibroblasts had been treated with these cytokines. These data indicate that iCAF and myCAF fibroblast subtypes exert distinct influences on lymphocyte migration whilst cytokines have somewhat less impact on the functional properties of ANF.

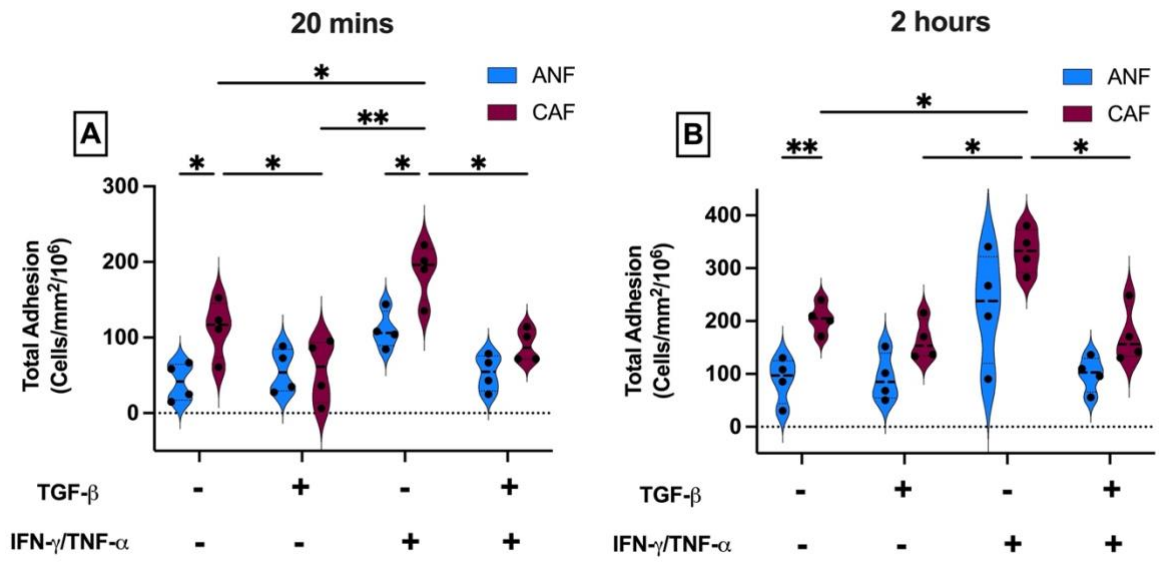


Figure 5.6. Effect of cytokine-stimulated CAF and ANF on lymphocyte total adhesion in co-culture at two-point times using Pseudo-emperipolesis assay. Fibroblasts were treated without (unstimulated) or with TGF-β, or IFN-γ/TNF-α, alone or in combination for 24 hours prior to co-culturing with lymphocytes from healthy donors prior to assessment of total adhesion at 20 mins **(A)** and 2 hours **(B).** Cells were visualised using live cell imagine microscope and the total adhesion was expressed as number of cells/mm^2/10^6. Data are mean ± S.D., n=4 independent experiments using 4 different PBLs from healthy donors for each fibroblast. In A and B, ANOVA showed a significant effect of fibroblasts ($p<0.003$), and of stimulants ($p<0.0001$). *<0.05 **<0.01 by Tukey's multiple comparisons test.

Following measurement of total adhesion, I next assessed relative firm adhesion and migration. Within the initial 20-minute incubation period, treatment of CAF with IFN-γ/TNF-α led to a significant decrease in firm adhesion (Figure 5.7A) and an increase in transmigration (Figure 5.7C) compared to ANF. Firm adhesion and transmigration remained unaffected by TGF-β alone or in combination for both ANF and CAF within this period (Figure 5.7A and 5.7C). At the 2-hour time point a distinct pattern emerged. Here, CAF stimulated with TGF-β exhibited a significant increase in the percentage of firm adhesion from 70% to 87% ($p = 0.007$) (Figure 5.7B) and a decrease of transmigrated lymphocytes from 29% to 13% ($p = 0.007$) (Figure 5.7D) compared to untreated CAF. Conversely, the addition of IFN-γ/TNF-α to CAF resulted in a decrease in firm adhesion from 70% to 51% ($p = 0.03$). This treatment also led to an increase in transmigration from 29% to 46% for CAF compared to the untreated control ($p = 0.03$) and ANF ($p = 0.01$) (Figure 5.7B and 5.7D). Notably, the combination of both treatments, TGF-β, and IFN-γ/TNF-α, increased firm adhesion from 51% to 89% ($p = 0.03$) and reduced the percentage of transmigrated lymphocytes from 46% to 15% when cultured with CAF compared to IFN-γ/TNF-α treatment alone ($p = 0.03$) (Figure 5.7B and D).

Therefore, TGF-β shows an opposing effect on lymphocyte adhesion and migration: Instead of facilitating these processes, it appears to hinder lymphocytes from adhering to surfaces and migrating, suggesting a regulatory role and an antagonistic effect on inflammatory cytokine-simulated migration. Importantly, no significant effect was noticed when comparing CAF to ANF for both firm adhesion and transmigration within 2 hours incubation period when treating the cells with TGF-β either alone or in combination with IFN-γ/TNF-α (Figure 5.7B and 5.7D).

These data indicate that stromal iCAF and myCAF fibroblasts differentially support the adhesion and migration of lymphocytes.

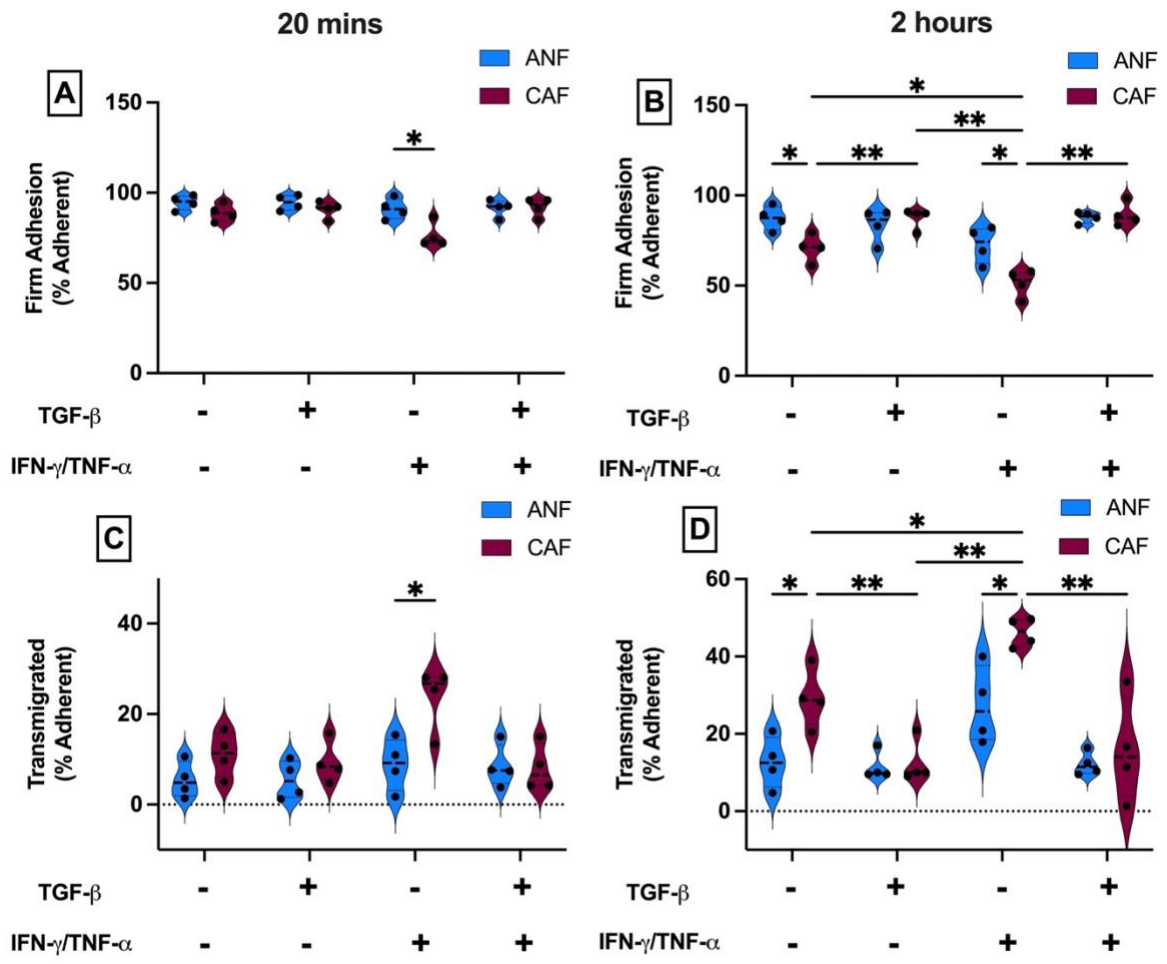


Figure 5.7. Effect of stimulated CAFs and ANFs on lymphocyte firm adhesion and transmigration in co-culture at two-point times using Pseudo-emperipolesis assay.

Fibroblasts were treated without (unstimulated) or with TGF-β, or IFN-γ/TNF-α, alone or in combination for 24 hours prior to co-culturing with lymphocytes from healthy donors for firm adhesion **(A and B)** and transmigration **(C and D)** at two time points 20mins **(A and C)** and 2 hours **(B and D).** The cells were visualised using live cell imagine microscope and the firm adhesion and transmigration were expressed as percentage of the total number of adherent cells. Data are mean ± S.D., n=4 independent experiments using 4 different PBLs from healthy donors for each fibroblast. In all, ANOVA showed a significant effect of fibroblasts ($p<0.02$), and of stimulants ($p<0.0001$) on both firm adhesion and transmigration. *<0.05 **<0.01 by Tukey's multiple comparisons test.

To validate the pseudo-emperipolesis findings, a transwell assay was performed, assessing adhered and migrated cell numbers via counting beads on flow cytometry. A detailed gating strategy, depicted in figure 5.8, was implemented to ensure precise analysis and confirmation of observed patterns in subsequent experiments.

In the transwell assay, lymphocyte adhesion and migration were unaffected by cytokines within a 6-hour incubation for both ANF and CAF (Figure 5.9A and 5.9C). However, within a 24-hour incubation, untreated CAF significantly decreased adhesion from 31% to 21% and increased lymphocytes migration from 20% to 28% compared to ANF ($p = 0.01$) (Figure 5.9B and 5.9D). TGF-β stimulation of CAF decreased lymphocyte adhesion compared to ANF, from 33% to 14% ($p = 0.001$). In contrast, IFN-γ/TNF-α pre-treatment of CAF increased lymphocyte adhesion compared to TGF-β treated CAF, from 14% to 39% ($p = 0.03$) (Figure 5.9B and 5.9D). Regarding migration, TGF-β stimulation of CAF decreased lymphocyte migration compared to untreated CAF, from 28% to 18% ($p = 0.02$). However, IFN-γ/TNF-α pre-treatment increased lymphocyte migration compared to TGF-β treatment, from 18% to 37% ($p = 0.01$), and compared to untreated CAF, from 28% to 37% ($p = 0.02$) (Figure 5.9B and 5.9D). A similar effect was observed with ANF (Figure 5.9B and 5.9D). Combined cytokine treatment of CAF reduced lymphocyte adhesion from 39% to 14% compared to IFN-γ/TNF-α alone within 24 hours, indicating a complex cytokine interplay (Figure 5.9B and 5.9D). Notably, significant differences between ANF and CAF were observed for untreated conditions and IFN-γ/TNF-α treatment, with no impact of TGF-β or the combination (Figure 5.9B and 5D).

In conclusion, my findings reveal the impact of distinct fibroblast phenotypes on lymphocyte migratory behaviour. Induction of myCAF with TGF-β and iCAF with IFN-γ/TNF-α resulted in contrasting effects, with TGF-β diminishing and IFN-γ/TNF-α heightening adhesion and migration in CAF. The combined treatment suggested an antagonistic role of TGF-β in hindering lymphocytes from adhering to surfaces and migrating, suggesting its potential to counteract the enhanced effect induced by IFN-γ/TNF-α in CAF within the TME.

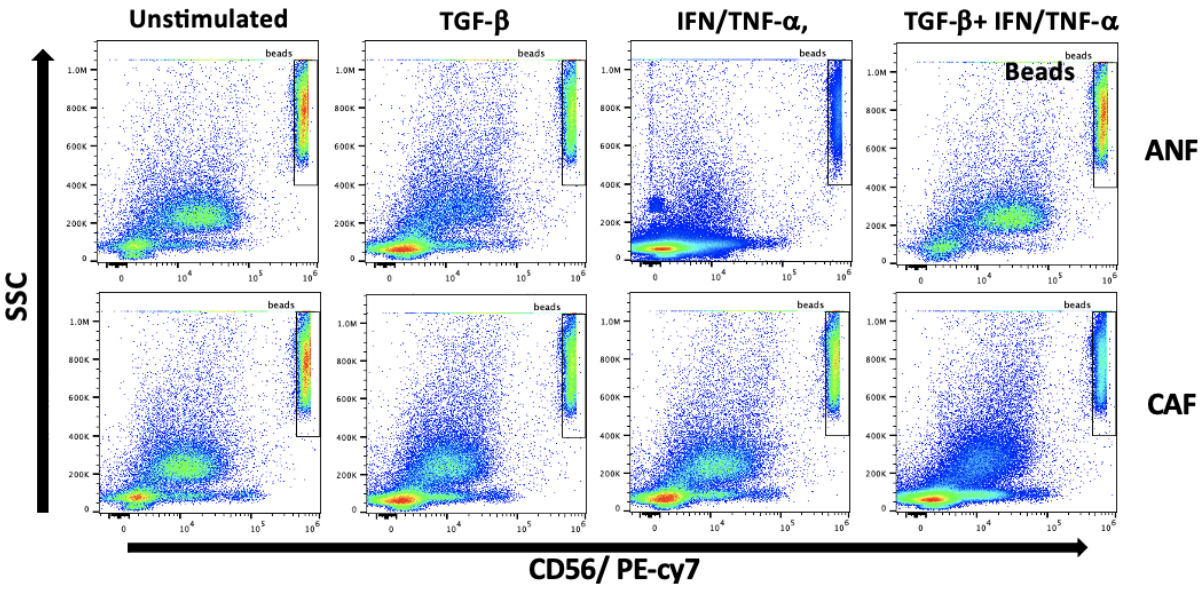


Figure 5.8. Representative gating strategy of lymphocyte number using CountBright™ Absolute counting beads.

Fibroblasts were cultured on opposing sides of 12-well transwell inserts, incubated overnight, and subsequently treated without (unstimulated) or with TGF-β, or IFN-γ/TNF-α, alone or in combination for 24 hours prior to co-culturing with lymphocytes from healthy donors for 6 and 24 hours. The adhered and migrated cells were mixed with the CountBright™ and assayed via flow cytometry. During acquisition, the event gate was set to 5000 beads, which normalized the acquisition volume between samples and allowed for accurate, absolute counts of lymphocytes.

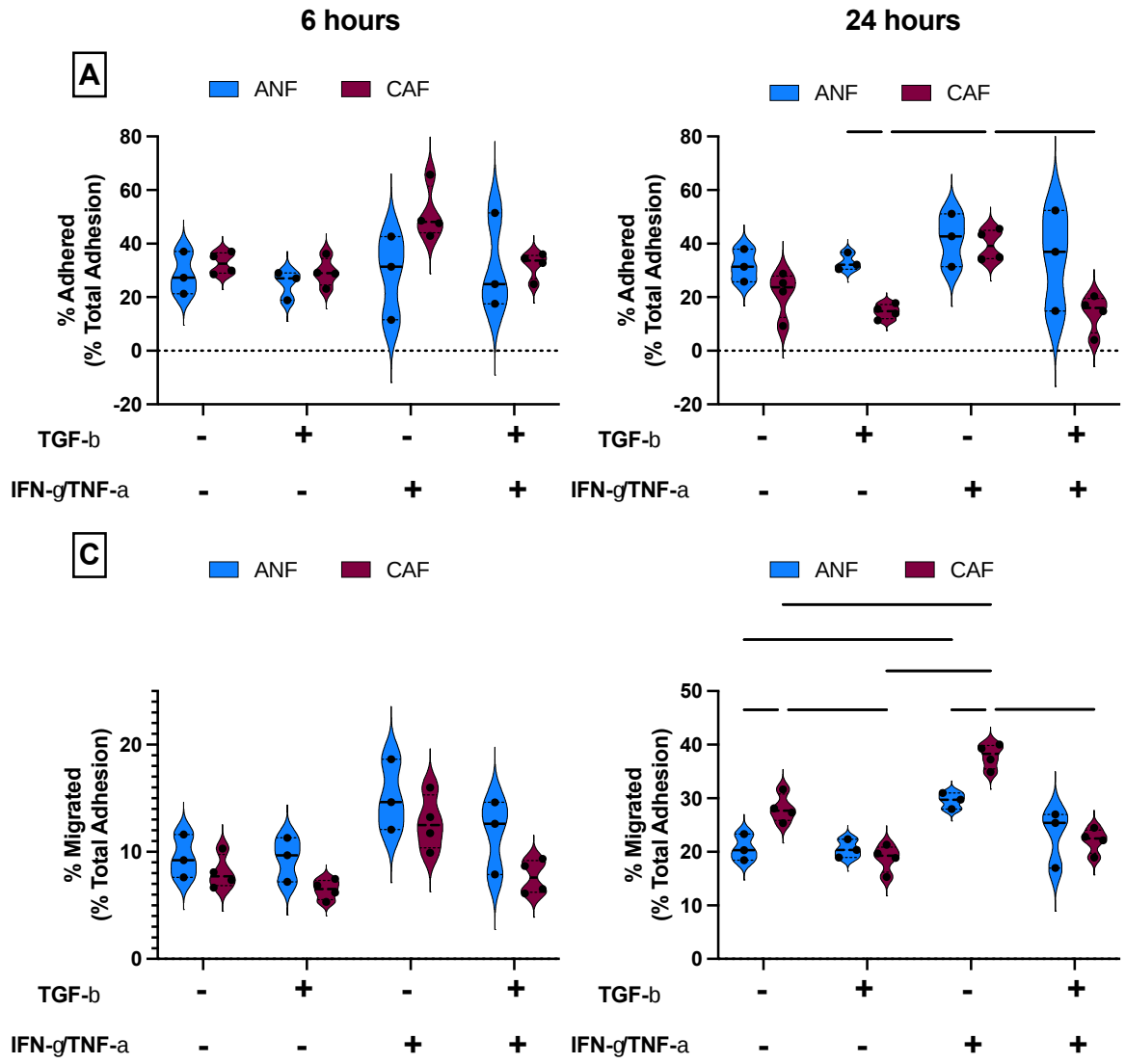


Figure 5.9. Effect of stimulated CAFs and ANFs on lymphocyte adhesion and migration in co-culture at two-point times using Transwell assay.
Fibroblasts were cultured on opposing sides of 12-well transwell inserts, incubated overnight, and subsequently treated without (unstimulated) or with TGF-β, or IFN-γ/TNF-α, alone or in combination for 24 hours prior to co-culturing with lymphocytes from healthy donors for 6 hours **(A and C)** or 24 hours **(B and D).** Adherent **(A and B)** and migrated **(C and D)** cells were counted via flow cytometry using counting beads and expressed as percentage of total cells that adhered. Data are mean ± S.D., from 3 to 4 independent experiments using 3 different PBLs donors for ANFs and 4 PBLs for CAFs fibroblast. In all, ANOVA showed a significant effect of fibroblasts ($p<0.02$), and stimulants ($p<0.0001$) on cell behaviour at both time points. *<0.05 **<0.01 by Tukey's multiple comparisons test.

5.2.3 How do ANF and CAF influence the phenotype of adhered and migrated T cell lymphocytes in the absence of close contact?

In my next phase of work, I aimed to investigate the potential role of stimulated pancreatic fibroblasts in facilitating the migration of CD4 and CD8 T cell subsets. Previous research has established the supportive role of fibroblasts in the spontaneous migration of lymphocytes (Bradfield et al., 2003; Jeffery et al., 2013). To specifically explore the interaction between pancreatic ANF and CAF fibroblasts and T cell subsets, I conducted an indirect contact assay using transwell system at two distinct time points, 6 and 24 hours. The subsequent analysis involved the gating of CD4+ and CD8+ T cells, as illustrated in figure 5.10. Through these experiments, I sought to elucidate the influence of unstimulated or stimulated ANF and CAF on the adhesion and migration dynamics of both CD4+ and CD8+ T cell subsets. Additionally, I examined the expression of additional memory T cell subsets as well as the activation and inhibition markers CD69 and PD1.

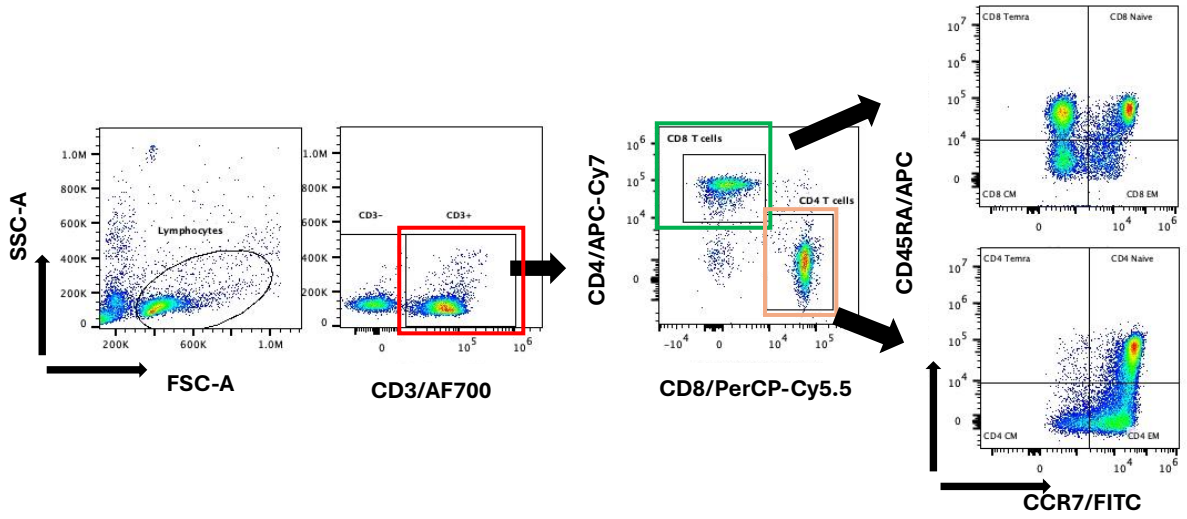


Figure 5.10. Flow cytometry gating strategy of T cell subsets.
Lymphocytes were co-cultured with ANF and CAF from PDAC patients and stained with flow cytometry panel including Viability dye (PI), CD3/AF700, CD4/APC-Cy7 and CD8/perCP-Cy5.5. CD4+ and CD8+ T cell populations were identified based on CD45RA/APC and CCR7/FITC expression. Data was collected using flow cytometry then analysed using FlowJo software. At first the lymphocytes were gated according to FS and SS. Then the whole T cells were gated as CD3 positive but PI negative (live cells). At last, the CD4 T cells and CD8 T cells were identified based on CD4 and CD8 expression. $CD45RA^{+}CCR7^{+}$ (naïve), $CD45RA^{-}CCR7^{+}$ (central memory), $CD45RA^{-}CCR7^{-}$ (effector memory), $CD45RA^{+}CDR7^{-}$ (terminally differentiated) on CD4+ and $CD8^{+}$ T-cells.

I initially evaluated the migratory behaviour of CD4+ and CD8+ T cells and this revealed a distinct pattern in response to varied treatments. During the 6-hour incubation period I observed a non-significant impact of stimulated ANF and CAF fibroblasts with both TGF-β and IFN-γ/TNF-α on CD4+ lymphocyte migration compared to the unstimulated fibroblast control (Figure 5-11A). However, within 24 hours, a significant effect was clearly evident from CAF fibroblasts stimulated with both TGF-β ($p = 0.03$) and IFN-γ/TNF-α ($p = 0.01$) on the migration of CD4+ T cell population compared to the unstimulated fibroblast control (Figure 5-11B). In particular, this was suppressed by TGF-β treatment but increased following prior incubation with IFN-γ/TNF-α. As such the duration of the incubation period plays a crucial role in influencing the migration of CD4+ T cells. TGF-β-treated CAF elicited a reduction in CD4+ T cell migration within 24 hours from an average of 30% to 17% ($p = 0.03$) (Figure 5-11B) and CD8+ T cell migration within 6 hours from an average of 25% to 17% ($p = 0.04$) (Figure 5-12A), with no further impact on the latter after 24 hours, as compared to the control condition. Treatment of CAF with IFN-γ/TNF-α resulted in an elevated migration of CD4+ ($p = 0.01$) and CD8+ T cells ($p = 0.04$) within 6 hours surpassing ANF (Figure 5-11A and 5-12A) and sustained heightened migration within 24 hours (Figure 5-11B and 5-12B). Additionally, IFN-γ/TNF-α treatment CAF increased the migration of CD4+ with an average of 40% and CD8+ T cells with an average of 44% compared to ANF (27% for CD4+ and 34% for CD8+), TGF-β treated CAF (17% for CD4+ and 34% for CD8+), and untreated CAF within 24 hours (30% for CD4+ and 33% for CD8+) (Figure 5-11B and 5-12B). Notably, this combination of cytokine pre-incubation with CAF led to a reduction in the migration of CD4+ T cells to an average of 20% compared to 30% with untreated CAF ($p = 0.02$) and 39% with IFN-γ/TNF-α treated CAF ($p = 0.0007$) within 24 hours (Figure 5-11B). Moreover, the

migration of CD8+ T cells decreased when CAF were treated with the combination cytokines compared to IFN-γ/TNF-α treatment within both 6 ($p = 0.04$) and 24 hours ($p = 0.02$) (Figure 5-12A and 5-12B). These findings highlight that iCAF (IFN-γ/TNF-α) significantly enhances CD4+ and CD8+ T cell migration within the pancreatic TME compared to myCAF (TGF-β), likely due to specific chemokines and cytokines that favour CD8+ T cell adhesion and overall T cell migration.

My next objective was to uncover the influence of ANF and CAF subtypes on the phenotype of the CD4+ and CD8+ T cell subsets that underwent migration. This aspect remains largely unexplored in existing literature, making my study a novel contribution in this area. Figures 5-13 to 5-16 display relative levels of different T cell memory subsets, namely naïve, central memory (CM), effector memory (EM), and terminally differentiated (TEMRA), residing within CD4 and CD8 T cell populations. I assessed these at the two time points, 6 and 24 hours.

I initially focussed on migration of naive T cells. Here there was a trend towards increased migration of CD4+ T cells in the presence of CAF whilst no effects were observed in relation to migration of the CD8+ subset (Fig 5.13). Furthermore, it was of interest that TGF-β treatment was particularly notable in relation to enhancing the migration of CD4+ naive T cells at 24 hours, with 62% migration compared to 30% in the presence of ANF ($p = 0.01$) (Figure 5-13B).

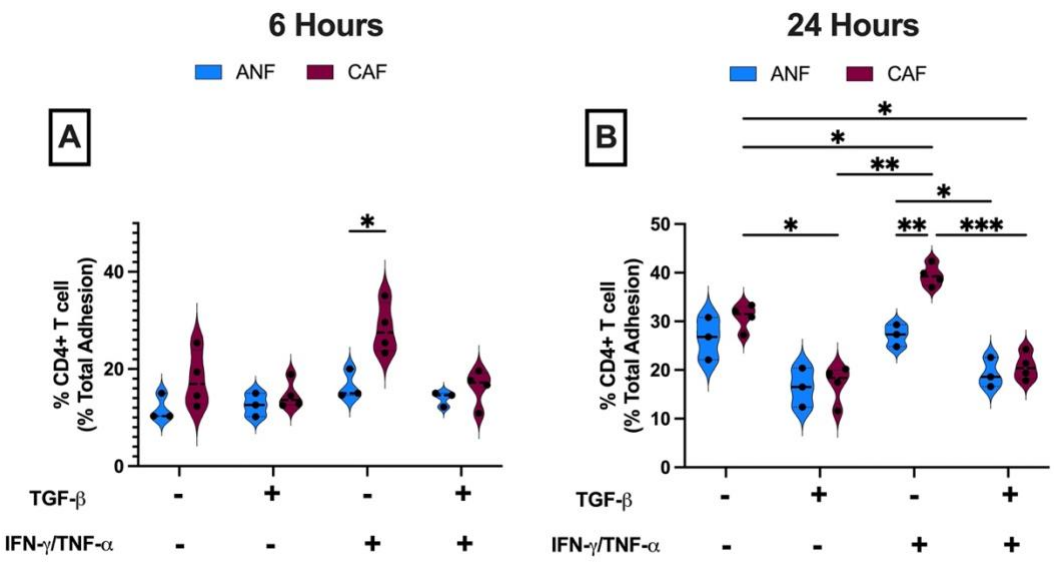


Figure 5.11. Effect of stimulated CAFs and ANFs on CD4+ T cell migration in co-culture at two-point times using Transwell assay.

Fibroblasts were cultured on opposing sides of 12-well transwell inserts, incubated overnight, and subsequently treated without (unstimulated) or with TGF-β, or IFN-γ/TNF-α, alone or in combination for 24 hours prior to co-culturing with lymphocytes from healthy donors for 6 hours **(A)** or 24 hours **(B).** CD4+ T-cell migration was assessed by flow cytometry and expressed as a percentage of cells added. Data are mean ± S.D., from 3 to 4 independent experiments using 3 different PBLs donors for ANFs and 4 PBLs for CAFs fibroblast. In all, ANOVA showed a significant effect of fibroblasts ($p<0.0001$), and stimulants ($p<0.0001$) on cell behaviour at both time points. *<0.05 **<0.01, ***<0.0001 by Tukey's multiple comparisons test.

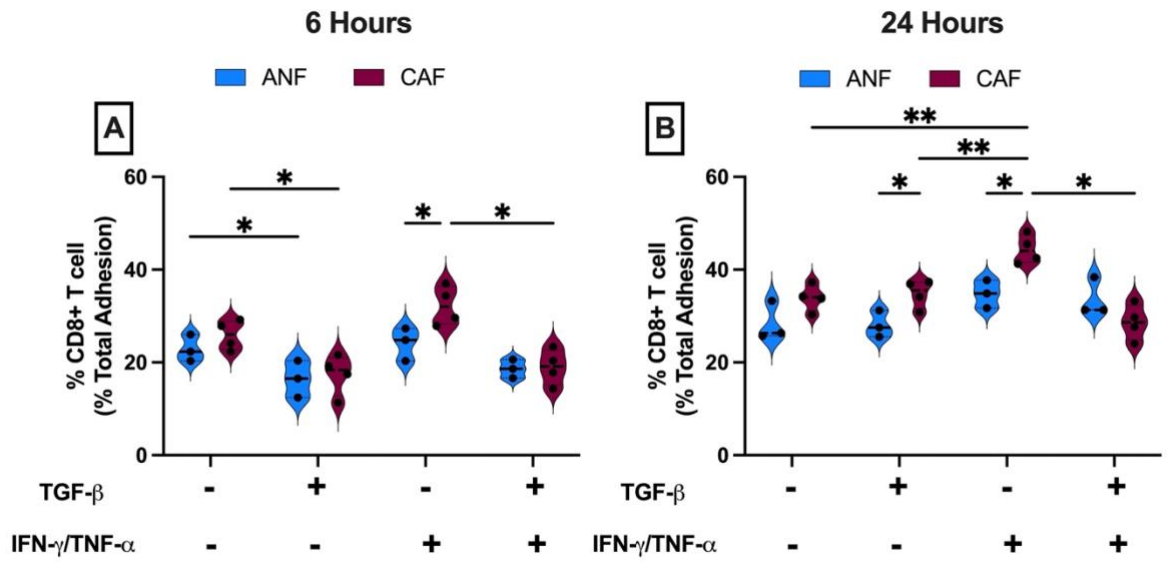


Figure 5.12. Effect of stimulated CAFs and ANFs on CD8+ T cell migration in co-culture at two-point times using Transwell assay.

Fibroblasts were cultured on opposing sides of 12-well transwell inserts, incubated overnight, and subsequently treated without (unstimulated) or with TGF-β, or IFN-γ/TNF-α, alone or in combination for 24 hours prior to co-culturing with lymphocytes from healthy donors for 6 hours **(A)** or 24 hours **(B).** CD8+ T-cell migration was assessed by flow cytometry and expressed as a percentage of cells added. Data are mean ± S.D., from 3 to 4 independent experiments using 3 different PBLs donors for ANFs and 4 PBLs for CAFs fibroblast. In all, ANOVA showed a significant effect of fibroblasts ($p<0.0001$), and stimulants ($p<0.0001$) on cell behaviour at both time points. *<0.05 **<0.01 by Tukey's multiple comparisons test.

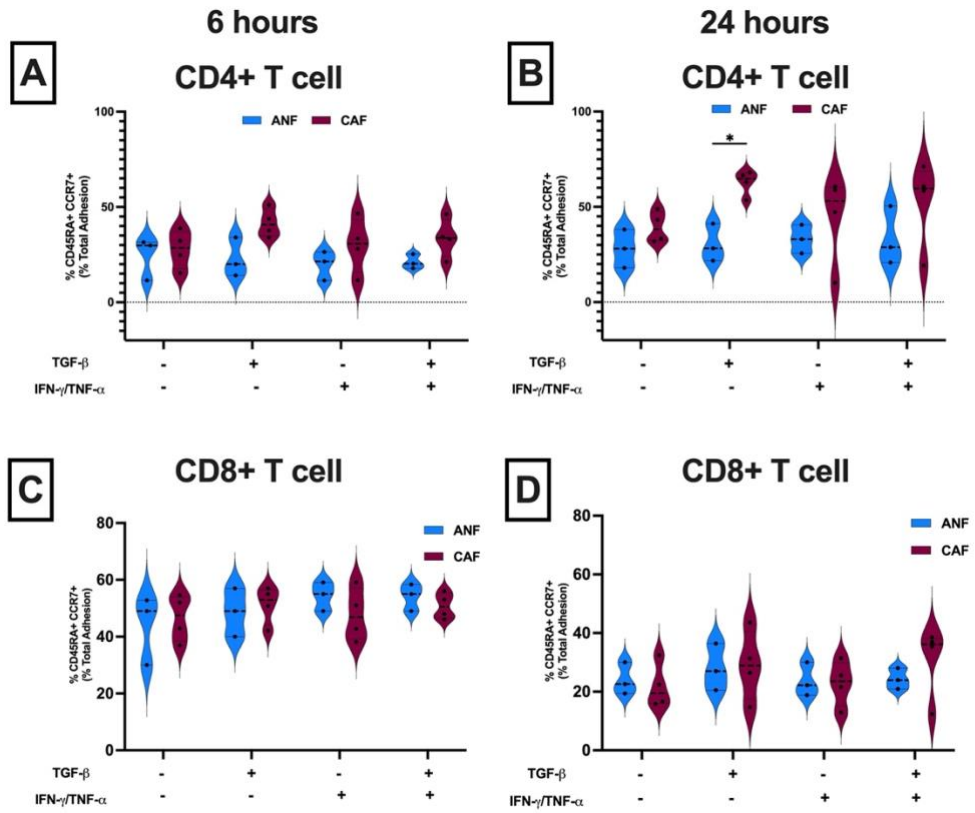


Figure 5.13. Effect of stimulated CAFs and ANFs on the migration of naïve CD4+ and CD8+ T cell subset (CD45RA+CCR7+) in co-culture at two-point times using Transwell assay.

Fibroblasts were cultured on opposing sides of 12-well transwell inserts, incubated overnight, and subsequently treated without (unstimulated) or with TGF-β, or IFN-γ/TNF-α, alone or in combination for 24 hours prior to co-culturing with lymphocytes from healthy donors for 6 hours **(A and C)** or 24 hours **(B and D).** CD4+ and CD8+ T-cells subsets were assessed by flow cytometry and expressed as a percentage of CD3+ T cells. Data are mean ± S.D., from 3 to 4 independent experiments using 3 different PBLs donors for ANFs and 4 PBLs for CAFs fibroblast. In all, ANOVA showed a significant effect of fibroblasts and non-significant effect of stimulants on cell behaviour at both time points. *p<0.05 by Tukey's multiple comparisons test.

When examining central memory (CM) CD4+ T cells there were relatively few differences between ANF or CAF or in relation to the impact of cytokine pre-incubation. In general, there appeared to be somewhat increased migration with the use of ANF although this was not statistically significant of note, the use of TGF-β led to a sharp increase in migration at 24 hours but only with the use of ANF (33% vs 8%; $p = 0.007$) (Figure 5-14B). This effect was partially attenuated with the inclusion of IFN-γ/TNF-α coincubation. A similar effect showing relative impairment of central memory cells across both endothelial cell (EnC) mono- and co-cultures has been seen in arthritis (Jeffery et al., 2013).

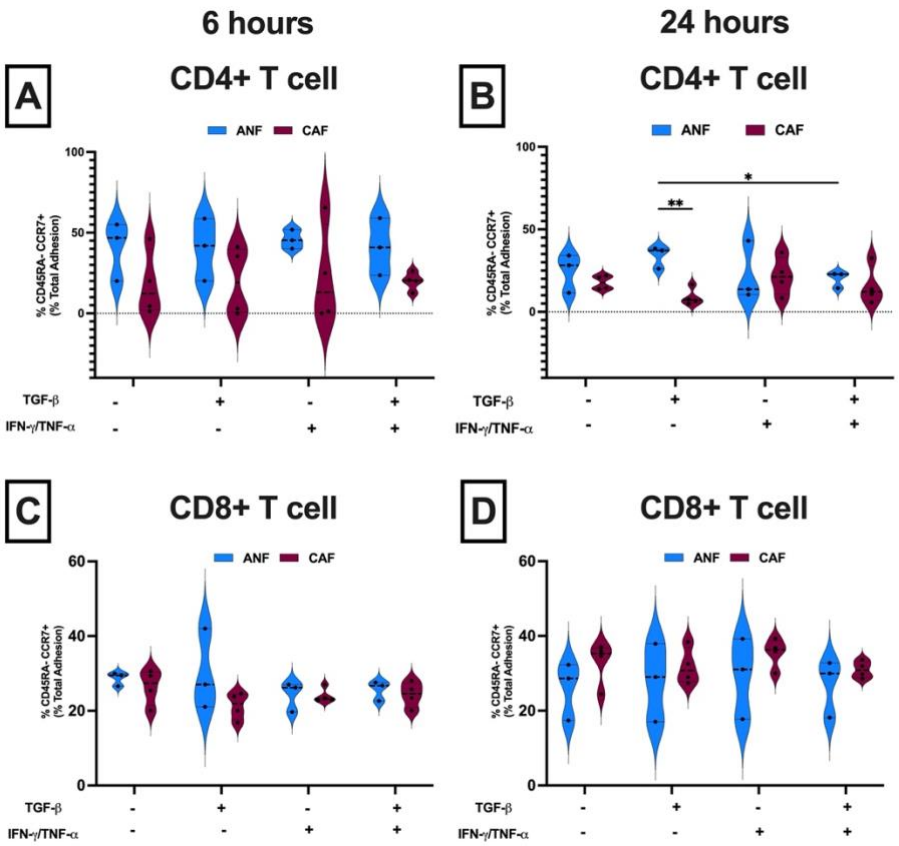


Figure 5.14. Effect of stimulated CAFs and ANFs on the migration of central memory (CM) CD4+ and CD8+ T cell subset (CD45RA−CCR7+) in co-culture at two-point times using Transwell assay.

Fibroblasts were cultured on opposing sides of 12-well transwell inserts, incubated overnight, and subsequently treated without (unstimulated) or with TGF-β, or IFN-γ/TNF-α, alone or in combination for 24 hours prior to co-culturing with lymphocytes from healthy donors for 6 hours **(A and C)** or 24 hours **(B and C).** CD4+ and CD8+ T-cells subsets were assessed by flow cytometry and expressed as a percentage of cells added. Data are mean ± S.D., from 3 to 4 independent experiments using 3 different PBLs donors for ANFs and 4 PBLs for CAFs fibroblast. In all, ANOVA showed a non-significant effect of fibroblasts and of stimulants on cell behaviour at both time points. *p<0.05 and **<0.01 by Tukey's multiple comparisons test.

Effector memory (EM) CD4+ T cell migration appeared increased within 6 hours with the use of CAF although no clear cytokine-mediated effect was seen. These differences had largely resolved after 24 hours. A similar profile was broadly observed for CD8+ subsets and the use of inflammatory cytokines enhanced migration at the late timepoint when applied to CAF subsets (9.5% vs 6% untreated ($p=0.03$) and 5.9% with TGF-β ($p=0.04$); (Figure 5-15A and 5-15B).

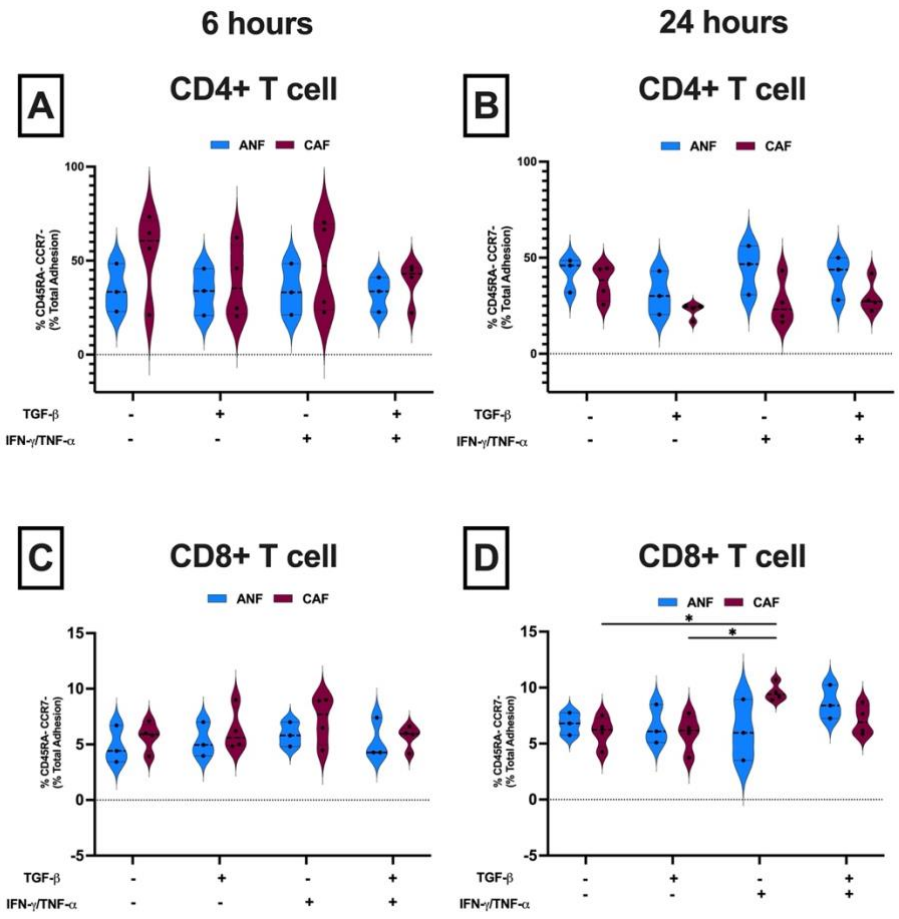


Figure 5.15. Effect of stimulated CAFs and ANFs on the migration of effector memory (EM) CD4+ and CD8+ T cell subset ($CD45RA^{-}CCR7^{-}$) in co-culture at two-point times using Transwell assay.

Fibroblasts were cultured on opposing sides of 12-well transwell inserts, incubated overnight, and subsequently treated without (unstimulated) or with TGF-β, or IFN-γ/TNF-α, alone or in combination for 24 hours prior to co-culturing with lymphocytes from healthy donors for 6 hours **(A and C)** or 24 hours **(B and D).** CD4+ and CD8+ T-cells subsets were assessed by flow cytometry and expressed as a percentage of cells added. Data are mean ± S.D., from 3 to 4 independent experiments using 3 different PBLs donors for ANFs and 4 PBLs for CAFs fibroblast. In all, ANOVA showed a significant effect of stimulants on cell behaviour at both time points. *$p<0.05$ by Tukey's multiple comparisons test.

Finally, I then assessed the relative migration of terminally differentiated (TEMRA) T cells which are antigen-experienced T cells that have re-expressed the CD45RA isoform of CD45R.

Strikingly, CD4+ TEMRA cells migrated very poorly across fibroblasts although at 24 hours this was partially enhanced in the presence of IFN-γ/TNF-α. (Koppensteiner et al., 2022; McGettrick et al., 2009).

Migration was enhanced for CD8+ EMRA T cells although again there were no differences observed in comparisons of ANF/CAF subsets or in relation to cytokine pre-incubation. Of note, a prior study in kidney transplant recipients has shown that TEMRA CD8+ T cells exhibit heightened migratory properties, potentially regulated through response to CXCL12 (Mao et al., 2021).

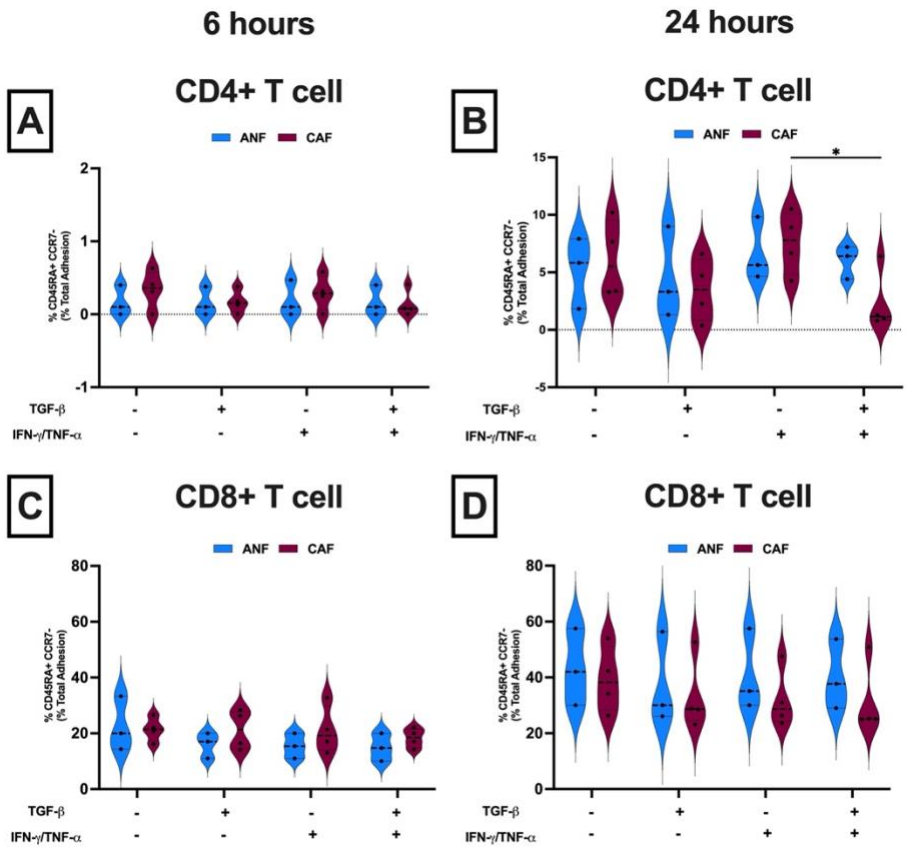


Figure 5.16. Effect of stimulated CAFs and ANFs on the migration of TEMRA CD4+ and CD8+ T cell subset (CD45RA^{+}CDR7^{-}) in co-culture at two-point times using Transwell assay.

Fibroblasts were cultured on opposing sides of 12-well transwell inserts, incubated overnight, and subsequently treated without (unstimulated) or with TGF-β, or IFN-γ/TNF-α, alone or in combination for 24 hours prior to co-culturing with lymphocytes from healthy donors for 6 hours **(A and C)** or 24 hours **(B and D).** CD4+ and CD8+ T-cells subsets were assessed by flow cytometry and expressed as a percentage of cells added. Data are mean ± S.D., from 3 to 4 independent experiments using 3 different PBLs donors for ANFs and 4 PBLs for CAFs fibroblast. In all, ANOVA showed a non-significant effect of fibroblasts and a significant effect of stimulants ($p<0.02$) on cell behaviour at both time points. *$p<0.05$ by Tukey's multiple comparisons test.

Following this thorough analysis of CD4+ and CD8+ T cell migration in response to various stimuli, I extended these investigations to scrutinize the expression of the crucial checkpoint and activation marker PD-1, as well as the early activation marker CD69 on migrated T cells. The evaluation of these key markers serves as a pivotal link in unravelling the complex modulation of immune checkpoints and activation states in the context of pancreatic fibroblast interactions.

In relation to PD-1, all forms of cytokine stimulation acted to increased PD-1 expression at 24 hours. Notably, this effect was observed only with the CAF population. Furthermore, whilst IFN-γ/TNF-α slightly increased expression at 6 hours, at 24 hours the increase was most notable in the presence of single or dual incubation with TGF-β (myCAF induction). In particular, PD-1 was expressed on 52% of CD4+ T cells within 24 hours compared to 42% untreated ($p = 0.01$).

Effects of CD8+ T cells were more modest, but again PD-1 expression was enhanced by TGF-β incubation at 24 hours. PD-1 can be induced on activated T cells, and it remains possible that the modest increase in expression at 24 hours represent a subset of T cells that have been activated within the culture system. However, it is unlikely that these conditions facilitate engagement with cognate peptide and I such it is likely that the patterns observed reflect some differential recruitment of T cells in relation to PD-1 expression.

In order to assess the potential activation of T cells within my culture system I next went on to assess the expression of the activation marker CD69 on populations of migrated cells. For CD4+ T cells a trend was observed towards increased expression within CAF co-cultures at 6 hours. A similar pattern was present at the later timepoint and here combinatorial cytokine treatment marginally suppressed Ki-67 expression (Yanyan Han, 2020). Overall, these data reveal that TGF-β-treated CAFs significantly

increase PD-1 expression on migrated CD4+ and CD8+ T cells, while IFN-γ/TNF-α increases PD-1 only on CD4+ T cells. These cytokine treatments also have modest effects in relation to relative impact of T cell migration dependent on CD69 expression.

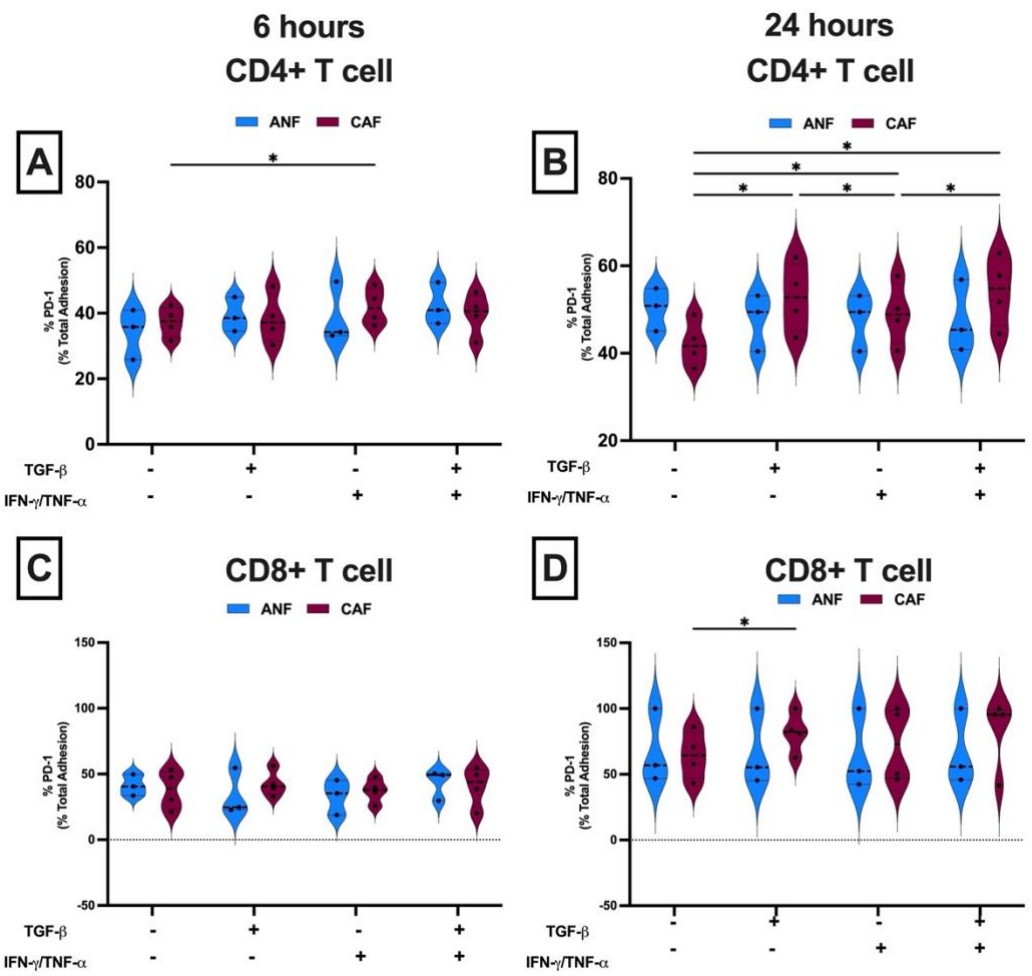


Figure 5.17. Effect of stimulated CAFs and ANFs on the expression of PD-1 on CD4+ and CD8+ T cell in co-culture at two-point times using Transwell assay. Fibroblasts were cultured on opposing sides of 12-well transwell inserts, incubated overnight, and subsequently treated without (unstimulated) or with TGF-β, or IFN-γ/TNF-α, alone or in combination for 24 hours prior to co-culturing with lymphocytes from healthy donors for 6 hours **(A and C)** or 24 hours **(B and D).** Inhibitory marker PD-1 was quantified by flow cytometry on migrated CD4+ and CD8+ T cells and expressed as a percentage of cells added. Data are mean ± S.D., from 3 to 4 independent experiments using 3 different PBLs donors for ANFs and 4 PBLs for CAFs fibroblast. In all, ANOVA showed a non-significant effect of fibroblasts and a significant of stimulants ($p<0.003$). *$p<0.05$ by Tukey's multiple comparisons test.

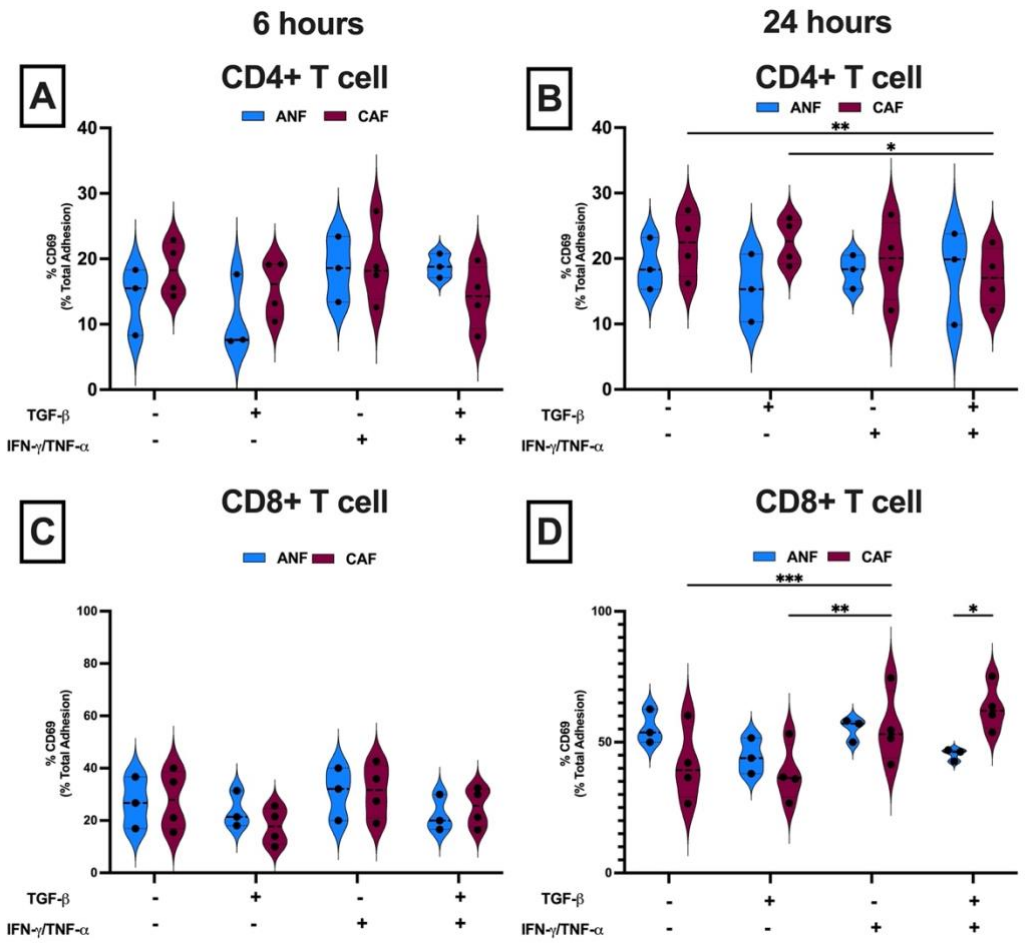


Figure 5.18. Effect of stimulated CAFs and ANFs on the expression of CD69 on CD4+ and CD8+ T cell in co-culture at two-point times using Transwell assay. Fibroblasts were cultured on opposing sides of 12-well transwell inserts, incubated overnight, and subsequently treated without (unstimulated) or with TGF-β, or IFN-γ/TNF- α, alone or in combination for 24 hours prior to co-culturing with lymphocytes from healthy donors for 6 hours **(A and C)** or 24 hours **(B and D).** Activation marker CD69 was quantified by flow cytometry on migrated CD4+ and CD8+ T cells and expressed as a percentage of cells added. Data are mean ± S.D., from 3 to 4 independent experiments using 3 different PBLs donors for ANFs and 4 PBLs for CAFs fibroblast. In all, ANOVA showed a non-significant effect of fibroblasts and a significant of stimulants ($p<0.0009$). *<0.05 **<0.01, ***<0.0001, by Tukey's multiple comparisons test.

5.2.4 Impact of ANF and CAF on adherence and migration of NK cell subsets

Natural Killer (NK) cells are crucial players in the immune defence against cancer, yet the intricacies of their interaction with fibroblasts remain relatively unexplored.

To address this knowledge gap, I investigated the impact of ANF and CAF on relative migration of NK cell subsets. Employing $CD3^{neg}CD56^{pos}$ as markers for both adhered and migrated NK cells, as depicted in Figure 5-19, I aimed to unravel the dynamics of this crosstalk. This exploration promises insights into the regulatory role of fibroblasts on NK cells, offering potential avenues for advancing cancer immunotherapies.

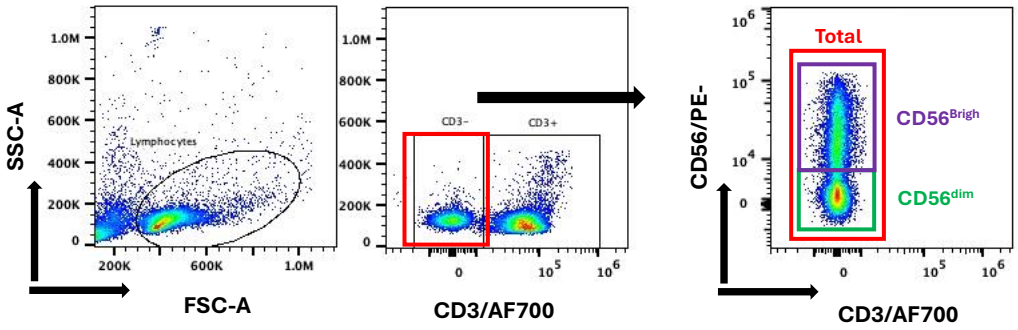


Figure 5.19. Flow cytometry gating strategy of total NK cell and its subsets: $CD56^{Bright}$ and $CD56^{dim}$ from CD3- lymphocytes population.

Fibroblasts were cultured on opposing sides of 12-well transwell inserts, incubated overnight, and subsequently treated without (unstimulated) or with TGF-β, or IFN-γ/TNF-α, alone or in combination for 24 hours prior to co-culturing with lymphocytes from healthy donors for 6 and 24 hours. The adhered and migrated NK cells were gated using $CD3^{neg}CD56^{pos}$ as markers by flow cytometry.

In initial studies I assessed the impact of cytokine pre-treatment of CAF on relative migration of $CD56^{Bright}$ and $CD56^{dim}$ Natural Killer (NK) cell populations. Within the initial 6 hours, no significant effect was observed on both $CD56^{Bright}$ and $CD56^{dim}$ NK cells with all stimulation conditions for both ANF and CAF. However, the migration of $CD56^{Bright}$ cells decreased when CAF were treated with TGF-β (34%) compared to the untreated condition (51%) within 24 hours ($p = 0.04$), with no observed effect on ANF (Figure 5-20B). Interestingly, migrated $CD56^{Bright}$ remained unaffected by cytokine stimulation for ANF at both investigated time points (Figure 5-20A and 5-20B).

In contrast, relative migration of $CD56^{dim}$ cells was increased when CAF were treated with TGF-β (62%) compared to untreated CAF (35%) within 24 hours ($p = 0.01$), with no impact observed for ANF (Figure 5-20D). Migrated $CD56^{dim}$ for both ANF and CAF remained unaffected by other cytokine stimulations within 24 hours and by all cytokines within 6 hours (Figure 5-20C and 5-20D).

These findings intricately highlight the differential effects of TGF-β cytokine treatment on the migration dynamics of $CD56^{Bright}$ and $CD56^{dim}$ NK cell subsets. The data support a potential role for myCAF in stimulating the migration of $CD56^{dim}$ NK cells. However, the non-significant outcomes for some cytokine combination studies underscores the necessity for further investigations and larger-scale studies to unravel the intricate regulatory mechanisms governing NK cell behaviours in the tumour microenvironment.

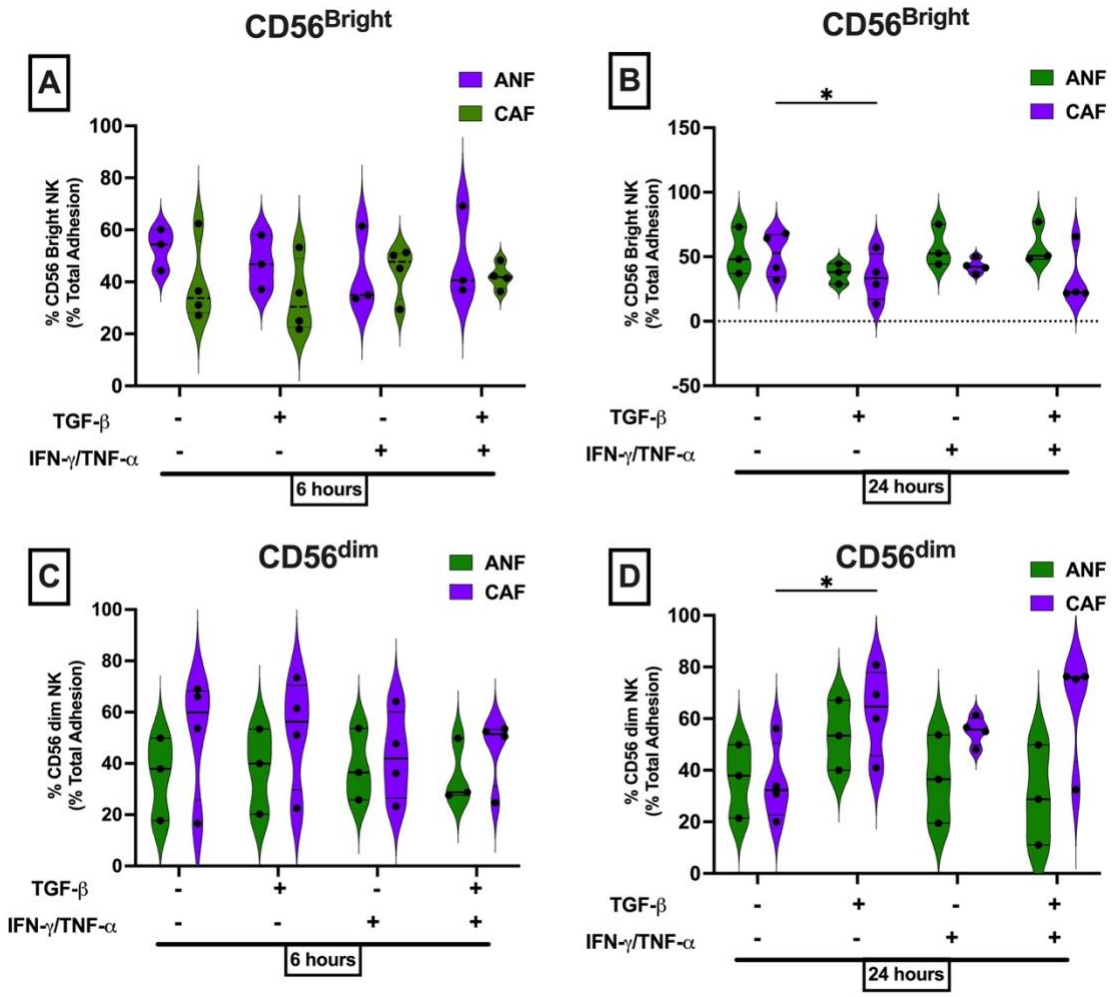


Figure 5.20. Effect of stimulated CAFs and ANFs on migrated CD56^{Bright} and CD56^{dim} NK cell at two-point times using Transwell assay.

Fibroblasts were cultured on opposing sides of 12-well transwell inserts, incubated overnight, and subsequently treated without (unstimulated) or with TGF-β, or IFN-γ/TNF-α, alone or in combination for 24 hours prior to co-culturing with lymphocytes from healthy donors for 6 hours **(A and C)** or 24 hours **(B and D).** CD56^{Bright} **(A, B)** and CD56^{dim} **(C, D)** phenotyping was assessed by flow cytometry and expressed as a percentage of cells added. Data are mean ± S.D., from 3 to 4 independent experiments using 3 different PBLs donors for ANFs and 4 PBLs for CAFs fibroblast. In all, ANOVA showed a significant effect of fibroblasts and incubation period ($p<0.01$), and of stimulants ($p<0.03$) on cell behaviour. *$p<0.05$ by Tukey's multiple comparisons test.

I next expanded the exploration to assess the expression profiles of PD-1 and CD69 on total NK cells following migration.

Expression of PD-1 was quite high on NK cells, with a notable bimodal pattern of expression. However, no differences were observed following cytokine treatment of fibroblasts (Figures 5-21A). Similarly, pre-treatment of fibroblasts did not have any impact on CD69 expression (Figures 5-21) on ANF or CAF (Figure 5-21).

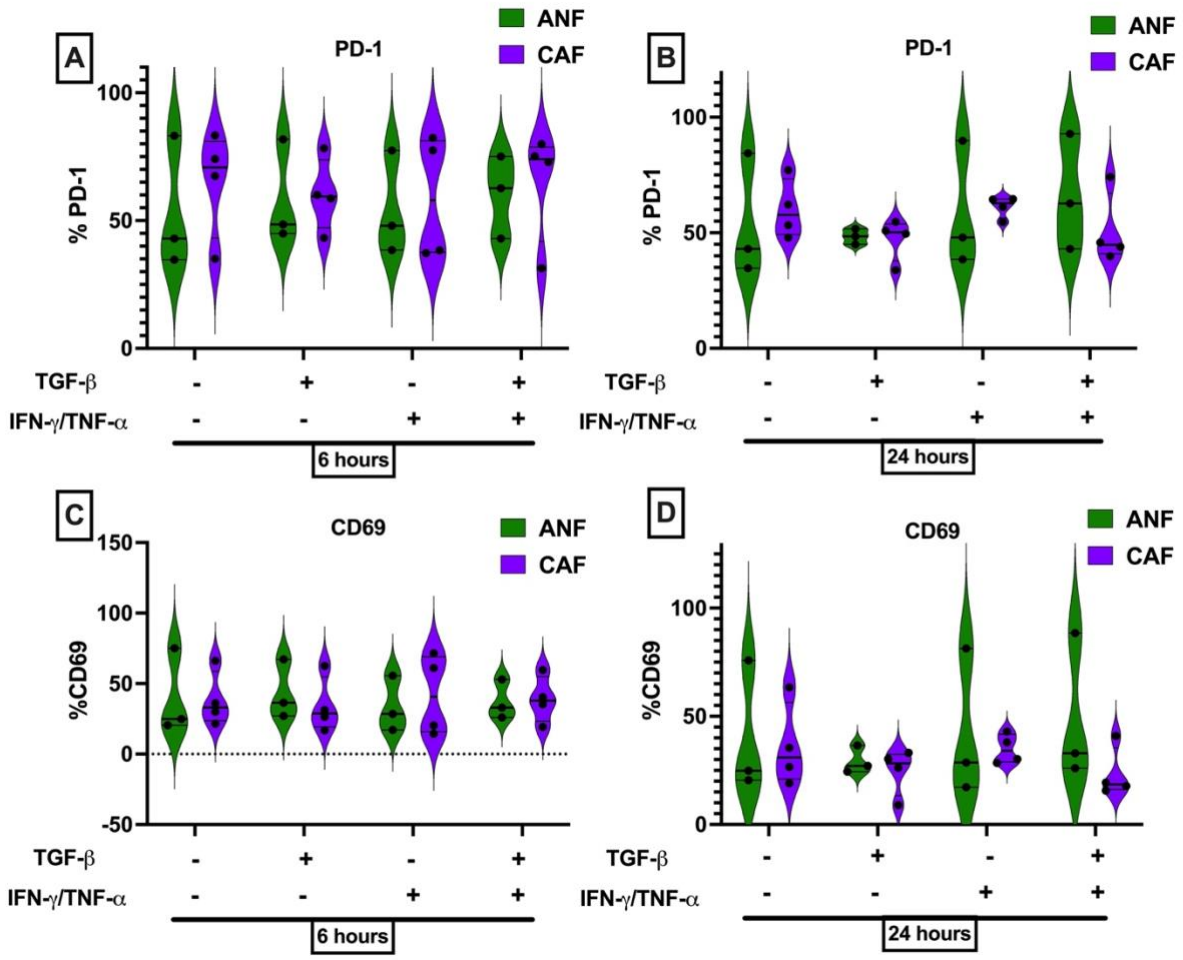


Figure 5.21. Effect of stimulated CAFs and ANFs on migrated Total NK cell examining the expression of inhibitory molecule PD-1 and co-stimulatory molecule CD69 at two-point times using Transwell assay.

Fibroblasts were cultured on opposing sides of 12-well transwell inserts, incubated overnight, and subsequently treated without (unstimulated) or with TGF-β, or IFN-γ/TNF-α, alone or in combination for 24 hours prior to co-culturing with lymphocytes from healthy donors for 6 hours **(A and C)** or 24 hours **(B and D).** expression of PD-1 **(A, B)** and CD69 **(C, D)** on migrated total NK-cell was assessed by flow cytometry and expressed as a percentage of cells added. Data are mean ± S.D., from 3 to 4 independent experiments using 3 different PBLs donors for ANFs and 4 PBLs for CAFs fibroblast. In all, ANOVA showed a non-significant effect of fibroblasts and of stimulants on cell behaviour. ns<0.1 by Tukey's multiple comparisons test.

5.2.5 Spatial determination and impact of fibroblast transcriptome in PDAC

In order to complement my migration studies, I next related it to ongoing studies within the laboratory that were addressing the spatial transcriptomic and single-cell RNA sequencing (scRNA-Seq) landscape of CAFs. A major aim of this work was to assess the relative impact of proximity to tumours on CAF phenotype (Croft et al., 2023).

My migration assays had shown that iCAF encourage lymphocyte migration, whereas myCAF reduce it. I hypothesised that this could be attributed to the location of each fibroblast subtype within the tumour, and subsequent impact on the expression and secretion of specific molecules, chemokines, and cytokines. Furthermore, our paper showed that tumour-proximal fibroblasts were characterized by a predominant presence of myCAFs, exhibiting robust expression of podoplanin (Croft et al., 2023). Conversely, tumour-distal subsets were enriched with iCAFs and exhibited differential expression of complement components (Croft et al., 2023). These findings underscore the remarkable transcriptional heterogeneity within CAF populations, which is intricately influenced by their spatial relationship with tumour lesions.

In Figure 5.22, I plotted the normalized expression of various markers, including fibroblast markers *THY1* and *PDPN*, cytokines *IL11* and *IL6,* and chemokines *CXCL9* and *CXCL10,* as well as adhesion molecules from the integrin family such as *ITGAX* (integrin/CD11c), *ITGB8* (Integrin beta8), *ITGAM* (Integrin alpha M), *ITGAV* (Integrin alpha V), and *ITGB2* (Integrin beta2), using NanoString data. These were analysed in the spatially defined tumour-proximal (T-P) and tumour-distant (T-D) regions. Integrins play a crucial biological role as the primary receptors utilized by animal cells to interact with the extracellular matrix (ECM). In cancer, dysregulated integrin signalling can contribute to tumour progression by promoting cell adhesion, invasion, and

metastasis, highlighting the significance of integrins as potential therapeutic targets in cancer treatment (Alberts B, 2002). The findings revealed that T-P fibroblasts exhibit heightened expression of *CXCL9* and *CXCL10* in comparison to T-D fibroblasts (Figure 5.22). Conversely, T-P fibroblasts showed decreased expression levels of IL-6 compared to T-D fibroblasts. Upon examining adhesion molecules of the integrin family, an elevated expression of *ITGAX* and *ITGAV* in T-P fibroblasts relative to T-D fibroblasts was observed. Conversely, T-D fibroblasts displayed increased expression of I*TGB8* compared to T-P fibroblasts (Figure 5.22).

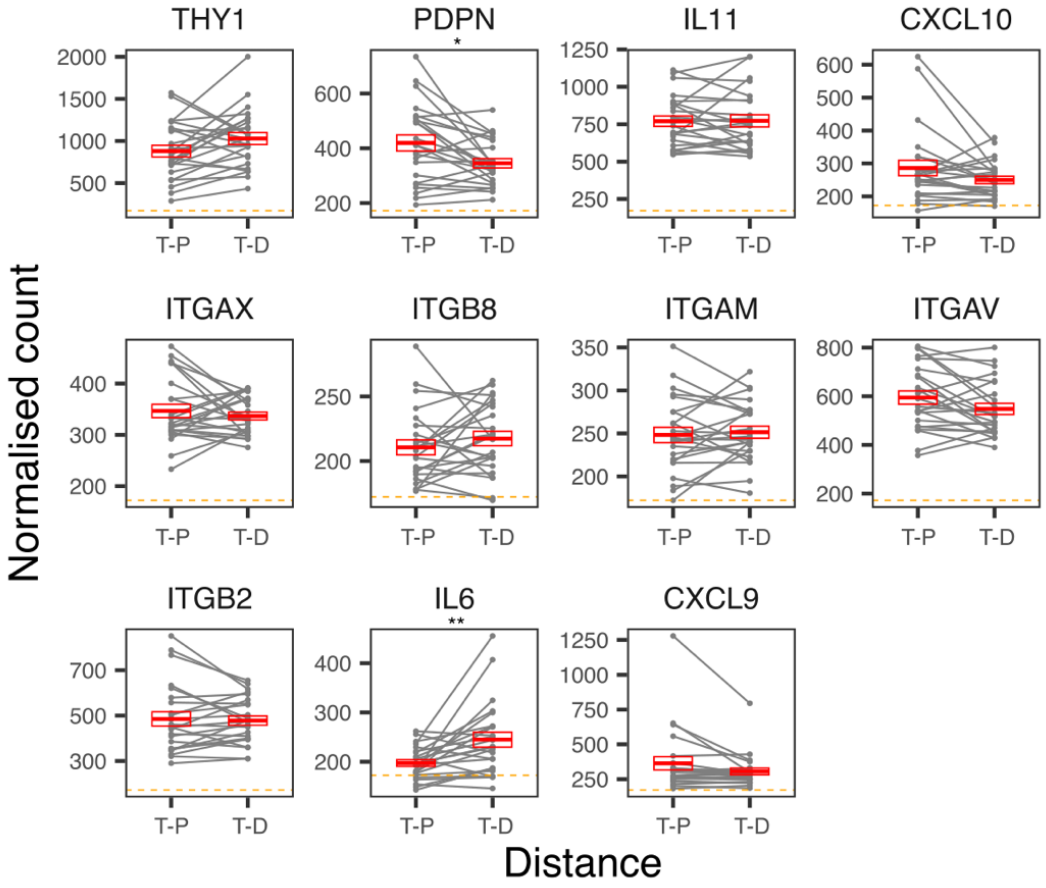


Figure 5.22. Identification of gene expression data from spatially defined stromal two regions within the PDAC tumour microenvironment using NanoString GeoMx DSP.

PDAC FFPE tissues underwent staining and profiling using NanoString GeoMx Digital Spatial RNA immunofluorescent antibody. Slides were also stained with a panel of photocleavable RNA probes. Custom regions of interest (ROI) were delineated based on these markers to define specific domains, including tumour-proximal stroma and tumour-distant stroma areas. Quantification was performed for fibroblast markers *THY1* and *PDPN*, cytokines such as *IL11* and *IL6*, and chemokines including *CXCL9* and *CXCL10*, as well as adhesion molecules of the integrin family, including *ITGAX* (Integrin/CD11c), *ITGB8* (Integrin beta8), *ITGAM* (Integrin alpha M), *ITGAV* (Integrin alpha V), and *ITGB2* (Integrin beta2). Statistical significance (by paired Wilcoxon test) between tumour-proximal (T-P) and tumour-distant (T-D) regions is indicated. A dashed yellow line represents the mean background signal from negative probes, confirming that the signal for the probes of interest exceeds background levels. Mean +/- SE of mean shown in red.

In figure 5.23, the expression profiles of inflammation, extracellular matrix (ECM), and adhesion-related genes across tumour-proximal (T-P), tumour-distant (T-D), and Unknown fibroblast populations was examined. Chronic inflammation, sustained by persistent triggers or failures in control mechanisms, fosters conditions ripe for cancer development (Greten & Grivennikov, 2019; Singh et al., 2019). Here I observed that T-P fibroblasts (Figure 5.23) were enriched for specific inflammation markers, including *CXCL14, CXCL8, CXCL10,* and *CXCL2,* as well as ECM molecules primarily from the collagen family, such as *COL27A1, COL4A5, COL10A1, COL24A1, COL9A1* and *COL12A1,* and the actin marker α-SMA (*ACTA2).* Moreover, they exhibited a broad range of adhesion molecules, including various integrin family members like ITGA8, *ITGA2, ITGA11, ITGA1,* and *ITGB1.* T-D fibroblasts, on the other hand, demonstrated enrichment for distinct inflammation markers such as *CCL2, CXCL9, IL6, CXCL12, IL11*, and *LIF*. Their ECM profile included collagen family members like *COL6A3, COL6A2, COL6A1, COL8A1, COL18A1, COL15A1, COL9A3, COL6A6, COL28A1, COL4A4, COL5A3,* as well as genes for hyaluronic synthase (*HAS1*) and fibulin (*FBLN2*). Furthermore, T-D fibroblasts expressed adhesion molecules from the integrin alpha and beta families, including *ITGBL1, ITGB4, ITGA5, ITGA2B, ITGB3, ITGA9,* and *ITGAL.* Finally, unknown fibroblasts exhibited expression of inflammation, ECM, and adhesion molecules, with markers such as *CXCL1, CXCR4, LIF, COL21A1, COL19A1, COL13A1,* among others, and integrin alpha and beta members as adhesion molecules.

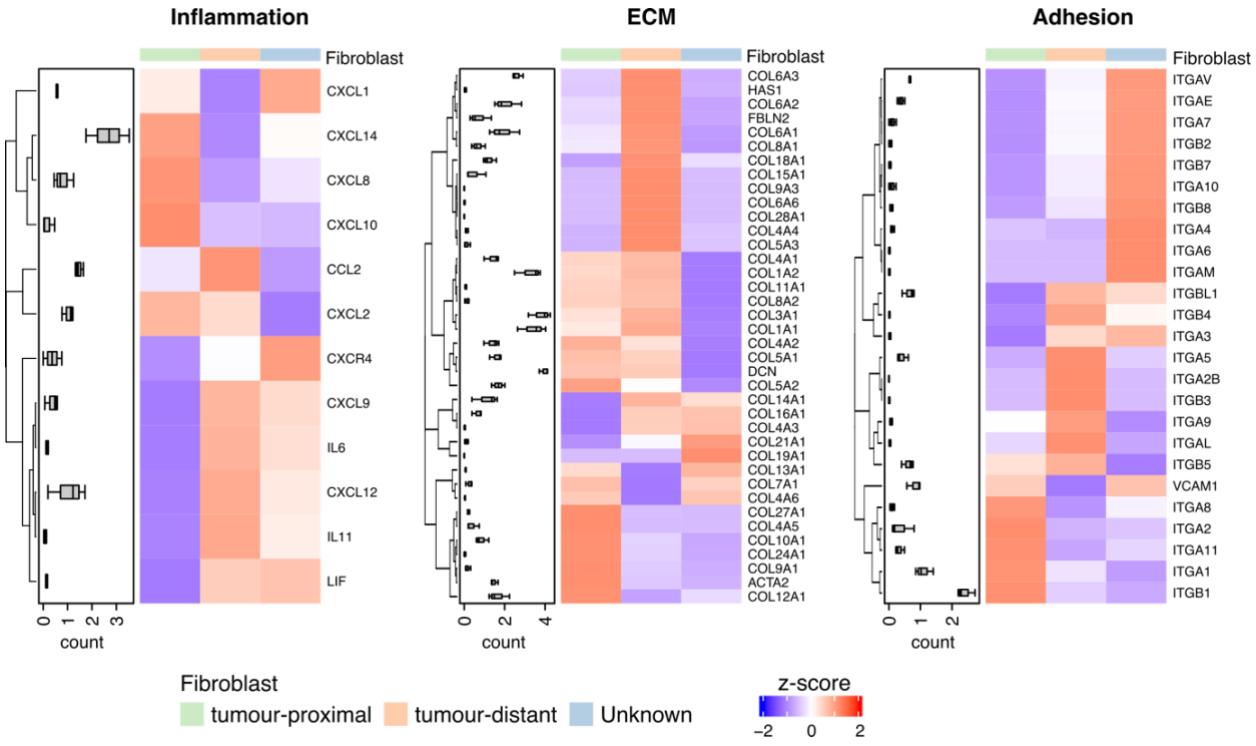


Figure 5.23. Proximal, Distal, and unknown Fibroblast populations identified in PDAC single cell transcriptome data.

The expression patterns of inflammation, extracellular matrix (ECM), and adhesion-related genes in tumour-proximal, tumour-distant, and Unknown fibroblast populations. Boxplots adjacent to each heatmap depict the normalized gene expression count distribution. The heatmap colour indicates the z-score, reflecting standard deviations from the mean across all fibroblast clusters.

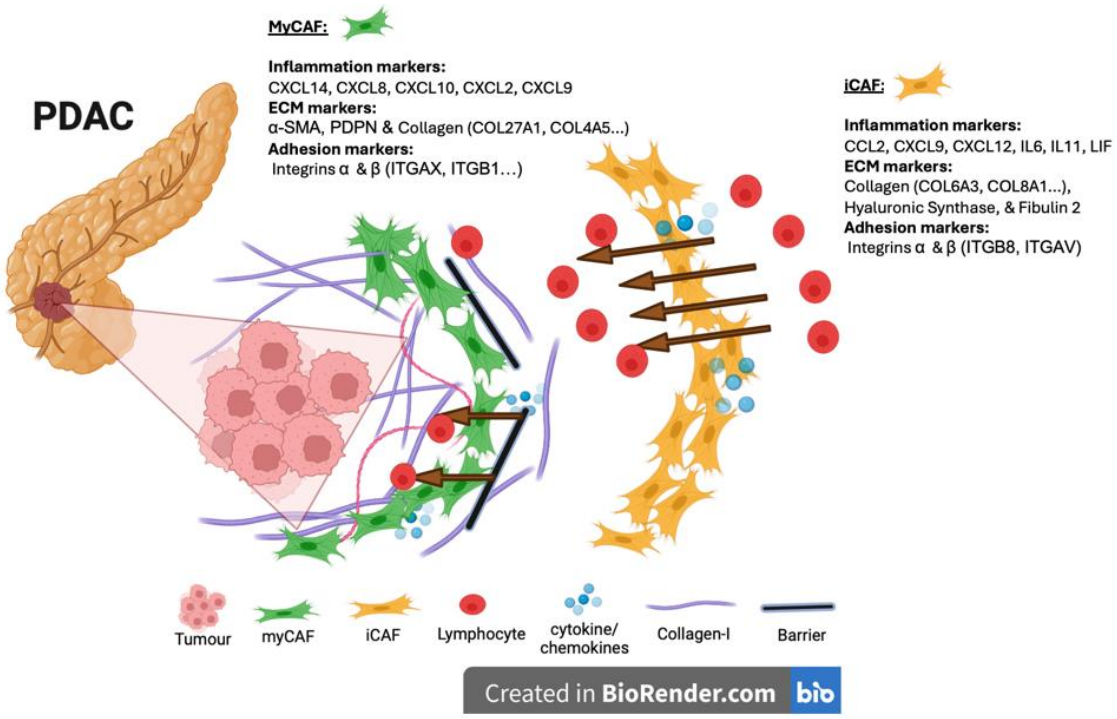


Figure 5.24. Graphical Abstract-Dynamic interplay of iCAF and myCAF within the PDAC-TME.

The iCAF subset, characterized by strong cytokine secretion, contrasts with the myCAF subset expressing α-SMA, PDPN, and engaging in TGF-β signalling. Their spatial organizations differ, with myCAF surrounding tumour ducts proximally, engaging in juxtracrine interactions, while iCAF reside at greater distances in the stroma, interacting with various cell types through inflammatory cytokines (Belle & DeNardo, 2019; Elyada et al., 2019; Croft et al., 2023). Our NanoString data revealed that myCAF express inflammation markers such as *CXCL14, CXCL8, CXCL10*, and *CXCL2*, alongside ECM markers including α-SMA, podoplanin (*PDPN*), and collagen (*COL27A1, COL4A5*). Additionally, myCAF express adhesion molecules such as integrins α (*ITGAX*) and β (*ITGB1*), promoting cancer progression. Conversely, cells farther away (iCAF) produce immune-related proteins, characterized by the high level of secretion of cytokines such as *CCL2, CXCL9, CXCL12, IL6, IL11,* and *LIF*. They also express ECM markers including collagen (*COL6A3, COL8A1*), hyaluronic synthase, and fibulin 2, along with adhesion molecules like integrins α (*ITGAV*) and β (*ITGB8*). The spatial distribution of each fibroblast subtype and their unique molecular profiles contribute to their identification. This supports my hypothesis that iCAF promotes lymphocyte migration while myCAF inhibits it. CAF can change in response to TGF-β and IFN-γ/TNF-α, releasing factors that either impede or facilitate lymphocyte adhesion and migration. Specifically, iCAF facilitates migration by secreting molecules unhindered by physical barriers, unlike myCAF. It is likely that myCAF actively remodel the extracellular matrix (ECM) and adhesion molecules such as integrins, creating an environment conducive to lymphocyte adhesion and migration.

5.3 Discussion

The pivotal role of stromal cells in facilitating leucocyte migration, as highlighted by (McGettrick et al., 2012), underscores their significance in the context of pancreatic cancer. Specifically, cancer-associated fibroblasts (CAFs) emerge as crucial determinants of disease progression. This chapter of my thesis delves into a relatively uncharted territory, exploring the intricate dynamics between stromal cells, leucocyte migration, and their implications in pancreatic cancer. My investigation assessed the nuanced effects of distinct CAF subsets, namely myCAF and iCAF, on lymphocyte behaviour, offering valuable insights for tailored immunotherapeutic strategies.

My observations indicate that incubation period has an important impact on lymphocyte migration in ANF and CAF co-cultures and suggests that temporal kinetics are an important determinant of cellular interactions and immune responses within the tumour microenvironment. At the current time is it unclear if local tissue concentrations of key chemokines and cytokines are stable within the PDAC environment or may fluctuate due to local factors. Soluble mediators, potentially enhanced by the close juxtaposition of cells, are key determinants of fibroblast phenotype (McGettrick, Buckley, Filer, et al., 2010). Additionally, an increase of adhesion and migration of lymphocytes to CAF rather than to ANF was seen within 2 hours. This underscores a unique phenotypic profile of CAF compared to ANF and this feature is likely to have an important impact on regulating the immune response to PDAC tumours.

The observation that unstimulated ANF and CAF both support lymphocyte adhesion and migration suggests that fibroblasts, regardless of their origin, have a baseline capacity to interact with lymphocytes. This interaction is likely to support immune surveillance and response against infection and cancer cells. Indeed, the efficiency of

lymphocyte adhesion and migration within the relatively short time frame of 2 hours indicates that fibroblasts are primed to engage with lymphocytes rapidly. This priming likely involves the expression of adhesion molecules and secretion of cytokines and chemokines by fibroblasts, which facilitate the recruitment and activation of lymphocytes. Research conducted by Bradfield et al. reveals that fibroblast-like synoviocytes (FLS) from patients with rheumatoid arthritis exhibit a heightened migratory capacity for T cells influenced by the augmented secretion of chemokines and cytokines, particularly SDF-1 (CXCL12) and vascular cell adhesion molecule 1 (VCAM-1; CD106) (Bradfield et al., 2003). Activation of specific fibroblast subtypes (iCAF and myCAF) leads to distinct changes in lymphocyte behaviour, indicating that different fibroblast states within the tumour stroma can selectively modulate immune cell infiltration and function, affecting tumour progression and immune evasion. CAF populations are very heterogeneous within the PDAC microenvironment (Elyada et al., 2019) and relative proximity to tumour is one important determinant in this regard. Myofibroblast CAF (myCAF) express α-SMA and are localised close to tumour (Croft et al., 2023) whilst inflammatory CAF (iCAF) are more distantly positioned and may play an important role in supporting immune responses (Belle & DeNardo, 2019; Elyada et al., 2019). The substantial reduction in total adhesion and migration of lymphocytes over myCAFs at 20 minutes and 2 hours suggests that myCAFs may create a less conducive environment for lymphocyte movement compared to other fibroblast phenotypes. However, there is an increase in firm adhesion within 2 hours, indicating that lymphocytes that do adhere to myCAFs exhibit stronger adherence. This could be due to changes in the expression of adhesion molecules or extracellular matrix components by myCAFs. The relatively limited impact of TGF-β-treated ANFs on total adhesion suggests that these fibroblasts may not significantly alter lymphocyte

behaviour compared to untreated ANFs within the short time frame studied. The induction of the iCAF phenotype increases lymphocyte adhesion and migration at 20 minutes and 2 hours, accompanied by a decrease in firm adhesion. This suggests that iCAFs create a more permissive environment for lymphocyte movement compared to other fibroblast phenotypes. The observed impact of cytokine incubation on ANF populations was less pronounced, indicating that ANFs may not respond as robustly to cytokine stimulation compared to CAFs. TGF-β is a strongly immunosuppressive cytokine and plays a complex role in tumour development, acting both to suppress the expansion of pre-malignant cells whilst also promoting a tumour-enhancing microenvironment at later stages of malignancy (Batlle & Massague, 2019) Whilst TGF-β has been established as a suppressor of chemokine secretion, often characterized as an anti-inflammatory cytokine due to its ability to reduce lymphocyte activation and proliferation, its promotion of mesenchymal cell types, particularly fibroblasts, highlights its involvement in the later phases of inflammation when tissue repair and regeneration become paramount (J P Cai, 1992; P. HILLYER, 2003).

The observation that myCAF are relatively less effective at supporting migration of CD4+ and CD8+ T cells compared to iCAF highlights the diverse roles fibroblast subtypes can play on lymphoid migration. As such, the therapeutic targeting of specific fibroblast subtypes potentially act to either suppress or enhance particular T cell populations within the tumour, providing insights into potential novel immunotherapeutic strategies. The combined administration of TGF-β and TNF-α/IFN-γ leading to a decrease in both CD4+ and CD8+ T cell migration underscores the complexity of cytokine interactions and their potential to modulate immune responses in the tumour microenvironment. TGF-β, known for its pleiotropic nature, emerges as

a key contributor to immunosuppression, signifying myCAF' involvement in disabling the cytotoxic activity of T cells, thereby promoting immune evasion and restricting T cell infiltration into the tumour (Gorchs & Kaipe, 2021). Notably, studies by Principe and his colleagues revealed that inhibiting TGF-β not only reduced CAF activation, leading to diminished fibrosis, but also increased T cell infiltration (Principe et al., 2019).

The increase in effector memory (EM) cells with iCAF stimulation suggests a potential role for iCAFs in promoting a robust and sustained immune response, which could be beneficial in anti-tumour immunity. Conversely, the impact of TGF-β-stimulated myCAFs on T cell differentiation within the pancreatic TME underscores the complex influence of myCAFs in modulating immune responses, potentially contributing to immune evasion or suppression by altering T cell phenotypes. Functional assays have reported that CAFs increase the proportion of FoxP3+CD4+ regulatory T cells (Tregs), potentially promoting the differentiation of induced Tregs (iTregs) and mediating immunosuppression (Gorchs et al., 2019). Moreover, exposure of stimulated T cells to CAFs results in a significant reduction in differentiation into EM and central memory (CM) T cells, with a larger pool of T cells remaining in their naïve state, as well as the induction of Tregs via CAF-secreted TGF-β (Kinoshita et al., 2013). Inhibition of TGF-β in PDAC mouse models, combined with gemcitabine, leads to alterations in Treg phenotype markers, reducing Treg-mediated suppression of CD8+ T cells and potentially enhancing anti-tumour immunity (Gorchs et al., 2019; Kondo et al., 2021).

The observed increase in PD1 expression on both adhered and migrated CD4+ and CD8+ T cells when interacting with myCAFs, and notable increase in adhered CD4+

T cells when cocultured with iCAFs after 24 hours, suggests a potential role of myCAFs in promoting T cell exhaustion or tolerance. PD1 is a known marker of T cell exhaustion, indicating reduced effector function and increased susceptibility to immune evasion by cancer cells. The unchanged expression of CD69, a marker of T cell activation, on adhered and migrated CD4+ and CD8+ T cells when interacting with iCAFs and myCAFs, suggests potential issues with activation signals or the induction of T cell tolerance or exhaustion. Pancreatic CAFs are known to express immune checkpoints, and their overexpression correlates with poor prognosis. Inhibition of TGF-β has been shown to reduce CAF activation, enhancing T cell infiltration, and improving PD1 and PD-L1 treatment efficacy (Gorchs et al., 2019; Gorchs & Kaipe, 2021; Hu et al., 2019). Studies in melanoma CAFs and conditioned media support the notion that CAFs can modulate early T cell activation markers and cytotoxicity, emphasizing the complexity of CAF-T cell interactions in the tumour microenvironment (Baker et al., 2021; Koppensteiner et al., 2022). Moreover, the employment of two distinct time points, 6 hours, and 24 hours, in the study provides a broader window to observe changes in T cell activation and exhaustion, shedding light on the dynamic interplay between fibroblasts and T cells within the tumour microenvironment over time.

NK cells are a type of cytotoxic lymphocyte critical for the innate immune response against virally infected cells and tumours cells. The observed decrease in CD56bright natural killer (NK) cells and increase in CD56dim NK cell population in response to myCAFs from tumour tissues suggests a modulation of NK cell composition within the TME. CD56bright NK cells are associated with cytokine production and immunomodulation, while CD56dim NK cells are more cytotoxic. This shift in NK cell

subsets may reflect an altered immune landscape influenced by the presence of myCAFs in tumour tissues. Importantly, no such effects were observed with myCAFs derived from normal tissues, indicating a tumour-specific interaction between myCAFs and NK cell subsets. This modulation of NK cell composition by myCAFs could have implications for the anti-tumour immune response within the TME. Existing literature highlights the significant role of TGF-β as a major suppressor of NK cell functions (Linda Ziani, 2017; Yang et al., 2020; Zhang et al., 2019). Activated CAF have been shown to diminish NK cell cytotoxicity, reducing the expression of IFN-γ, perforin, granzyme B, and several activating NK cell receptors in in vitro co-culture experiments involving pancreatic stellate cells (PSCs) or colorectal fibroblasts with NK cells (Li et al., 2013; Zhang et al., 2019). Recent research has also demonstrated that NK cells exhibit migratory behaviours towards cells secreting CXCL12, potentially supporting the hypothesis that myCAFs play a role in immune evasion by redirecting NK cell migration (Malchiodi & Weiner, 2021). This mechanism could enhance the migration and differentiation of NK cells, considering the well-established fact that CAFs secrete CXCL12. Limited research exists on this topic, and our study is the first to explore this aspect comprehensively. Interestingly, our data revealed no significant impact on the expression levels of PD-1 and CD69 on NK cells under the investigated conditions. This suggests that the cytokine stimulations applied did not significantly alter the activation status or migratory behaviour of the total NK cell population. However, the absence of conclusive results may stem from the limited number of experiments conducted and the diverse sources of fibroblasts utilized.

The integration of spatially defined transcription signatures with NanoString and single-cell RNA-Seq data has illuminated the distinct gene profiles of proximal and

distal stromal cells within the tumour microenvironment (TME). Tumour-proximal populations exhibit characteristics consistent with myCAFs, displaying elevated expression of α-SMA and extracellular matrix (ECM) molecules such as integrins and collagen markers. Conversely, more distal fibroblasts demonstrate an inflammatory profile marked by upregulated cytokines and chemokines, including CCL2, CXCL9, CXCL12, IL6, IL11, and LIF, corroborating previous research (Biffi et al., 2019; Elyada et al., 2019; Ohlund et al., 2017). Notably, myCAF markers, including the pro-tumorigenic chemokine CXCL14, are prominently expressed in these populations, suggesting their potential role in shaping the TME. Furthermore, the heightened expression of α-SMA, collagen, and integrins implies the formation of a robust barrier hindering lymphocyte migration.

Distinct from myCAFs, iCAFs exhibit a unique transcriptomic profile characterized by the expression of inflammatory and chemotactic mediators, including IL-6, IL-11, LIF, CCL2, and CXCL12. Spatial analysis reveals that iCAFs are often spatially separated from myCAFs and cancer cells, secreting inflammatory mediators such as IL6, IL11, and LIF driven by IL1 signalling, thus contributing to tumour growth and survival (Biffi & Tuveson, 2021). The heterogeneity within the CAF population is further emphasized by research on intrahepatic cholangiocarcinoma, highlighting the significant contribution of FAP+ CAFs in CCL2 secretion (Timperi & Romano, 2023). Elayda and her colleagues observed that mouse iCAFs exhibit similarities to their human counterparts, expressing higher levels of the hyaluronan synthase Has1 and specific collagens suggesting their involvement in extracellular matrix (ECM) deposition (Elyada et al., 2019). Our study extends understanding by revealing fibulin-2 (FBLN2) expression in iCAFs, marking a novel finding. FBLN2, a secreted glycoprotein of the

ECM, plays crucial roles in tissue development and remodelling, influencing processes like cell adhesion, migration, and angiogenesis (Takako Sasaki, 1996; H. Zhang et al., 2020).

5.4 Conclusion

The intricate interplay between stromal cells, particularly cancer-associated fibroblasts, and immune cells within the pancreatic tumour microenvironment (TME) plays a pivotal role in tumour progression and immune evasion. My investigation sheds light on the diverse effects of distinct CAF subsets, myCAFs, and iCAFs, on lymphocyte behaviour, offering valuable insights for tailored immunotherapeutic strategies. The observed alterations in T cell differentiation and NK cell composition suggest a complex modulation of immune responses by CAFs, with potential implications for anti-tumour immunity. Further understanding of these interactions could pave the way for the development of novel therapeutic approaches targeting the stromal compartment to enhance immune-mediated tumour clearance.

5.5 Limitations

The limitations identified in this study pose challenges to drawing definitive conclusions and supporting robust interpretations of data. The prolonged cell culture process, although essential, introduced the risk of cellular senescence, potentially undermining the reliability of findings. Additionally, the stringent passage limit imposed on fibroblasts limited cell availability for experimentation, thereby impeding the comprehensiveness of our analyses and hindering my ability to draw firm conclusions. The variability in cell number and functionality among lymphocyte donors further complicates the ability to obtain consistent results. Moreover, the lack of matched fibroblasts between ANF and CAF introduces another layer of uncertainty, potentially affecting the accuracy of findings. To mitigate these limitations and bolster the robustness of the conclusions, future studies could focus on optimizing cell culture protocols to minimize senescence and maximize cell availability. Exploring alternative experimental approaches or technologies requiring fewer cells could also enhance the reliability of our data and provide more conclusive answers to our research questions. These considerations underscore the ongoing need for optimization and refinement in future research endeavours to ensure the validity and reliability of the conclusions.

Summative discussion

This thesis, a journey through the TME in PDAC, unfolded across three interconnected chapters, each building on the last to unravel the complex roles of fibroblasts and their interactions with immune cells. These chapters weave a cohesive narrative, exploring how fibroblasts shape the TME, influence immune responses, and ultimately impact PDAC progression and therapeutic outcomes.

Chapter 3: The Foundation - Fibroblasts in the TME

Chapter 3 lays the groundwork by delving into the intricate cellular composition of the PDAC microenvironment, with a particular focus on the role of fibroblasts. PDAC is notorious for its dense fibrous stroma, which is largely composed of cancer-associated fibroblasts. These cells are not mere bystanders but active participants in tumour progression and resistance to therapy. The chapter sets out to achieve three primary objectives: characterizing the cellular makeup of PDAC, differentiating between inflammatory CAFs (iCAFs) and myofibroblastic CAFs (myCAFs), and examining how these fibroblasts respond to chemotherapy.

The study reveals that the TME in PDAC is highly heterogeneous, with a dynamic interplay between fibroblasts, endothelial cells, and immune cells. This heterogeneity is influenced by genetic mutations, epigenetic changes, and external factors such as hypoxia and immune responses. A significant finding is the inverse relationship between the abundance of endothelial and immune cells versus fibroblasts in tumour tissues compared to adjacent normal regions. This balance, or imbalance, within the

TME is crucial for understanding how PDAC progresses and how it responds to treatment.

A key focus of this chapter is the differentiation between two CAF subtypes: iCAFs and myCAFs. iCAFs are characterized by a pro-inflammatory phenotype and are more prevalent in tumour tissues, while myCAFs are associated with normal adjacent tissues. The study suggests that chemotherapy, a standard treatment for PDAC, may induce a shift in the TME, increasing the proportion of iCAFs. This shift could promote a more inflammatory and potentially resistant microenvironment, complicating the therapeutic landscape. The potential of fibroblast markers as biomarkers for predicting treatment outcomes is also emphasized, laying the foundation for subsequent exploration of immune cell interactions within the TME.

Chapter 4: Immune Cell Interactions - The Role of CAFs

Building on the fibroblast-focused foundation laid in Chapter 3, Chapter 4 shifts the focus to the interactions between CAFs and immune cells, particularly T cells and natural killer (NK) cells. T cells are central to the adaptive immune response, while NK cells play a crucial role in innate immunity. The chapter investigates how CAFs modulate these immune responses, either enhancing or suppressing anti-tumour immunity.

One of the key findings was that while primary CAFs do not significantly inhibit T cell proliferation following their activation, they do enhance proliferation in unstimulated conditions. This contrasts with previous studies that reported CAF-mediated suppression of T cell proliferation, highlighting the variability and complexity of CAF functions. Similarly, NK cell proliferation is not affected by CAFs when stimulated, but

there is a marked increase under unstimulated conditions. This suggests a potential enhancement of NK cell cytotoxic functions, which could be harnessed for therapeutic purposes. The mechanisms are unclear but could include secretion of cytokines from the fibroblasts.

Interferon-gamma (IFN-γ) is a critical cytokine in anti-tumour immunity, and I was interested to observe that CAFs enhance IFN-γ production in stimulated T cells whilst this effect is attenuated in the presence of PDAC cancer cells. As such this profile is rather different to what was observed in relation to T cell proliferation and reveals an interesting dissonance in the functional impact from CAF. It also suggests that cancer cells within the TME may suppress T cell function, potentially contributing to immune evasion.

In terms of T cell phenotype, CAFs decrease CD4+ T cell levels while leaving CD8+ T cell levels unchanged under stimulated conditions. CD8+ T cells are generally considered as the most important mediators in tumour-specific immunity whilst CD4+ pools may comprise an immune suppression regulatory element. As such these data again indicate a potential supportive role in immune function. I

Additionally, CAFs increase the expression of activation markers on T cells, such as CD69 and NKG2D, which are also critical for initiating immune responses. These findings underscore potential for supporting and enhancing selective CAF-immune cell interactions in cancer therapy.

Chapter 5: Spatial and Temporal Dynamics - Lymphocyte Behaviour in the TME

In addition to assessment of the phenotype and function of CAF, I was also able to undertake studies into their impact on the migration of lymphoid cells using *in vitro*

models. This was of particular interest given the specialised nature of this experimental technology that is not available in many research centres.

I focussed on the interactions between distinct CAF subtypes (iCAFs and myCAFs) and lymphoid subsets, particularly their impact on lymphocyte migration and adhesion. This chapter builds on the findings of the previous chapters by examining how different fibroblast states within the tumour stroma selectively modulate immune cell behaviour, influencing both tumour progression and immune evasion.

A key observation from this chapter was that lymphocytes exhibit increased adhesion and migration in the presence of CAFs compared to ANFs. This suggests that CAFs create a more conducive environment for immune cell infiltration. The study also reveals that different CAF subtypes have distinct effects on lymphocyte behaviour. In particular, when I used cytokines to polarize CAF towards a myCAF or iCAF phenotype I observed a reciprocal influence on lymphoid migration. Notably, myCAF were generally inhibitory to migration whilst iCAF accelerated the rate and degree of transmigration.

myCAFs, characterized by α-SMA expression and located closer to the tumour, thus appear to create a less conducive environment for lymphocyte movement, potentially hindering immune cell infiltration into the tumour. In contrast, iCAFs, with their pro-inflammatory profile and distal location, support greater lymphocyte adhesion and migration, indicating their role in promoting immune responses within the TME.

The chapter also addressed the temporal dynamics of lymphocyte-CAF interactions, revealing that the incubation period significantly impacts lymphocyte migration and adhesion and highlighting a dynamic nature of immune cell interactions within the TME. The findings suggest that by selectively targeting myCAFs or iCAFs, it may be possible to modulate specific T cell populations within the tumour, offering new

avenues for immunotherapy. The chapter also underscores the need for further research into the spatial dynamics of the TME and the transcriptional profiles of different stromal cells, which could lead to the development of more effective cancer treatments.

Connecting the Dots

Taken together, my work presents a narrative that highlights the central role of fibroblasts in shaping the TME and influencing immune cell behaviour in PDAC. Chapter 3 lays the foundation by exploring the heterogeneity of fibroblasts within the TME and their response to chemotherapy. This sets the stage for Chapter 4, which delves into the complex interactions between CAFs and immune cells, revealing how these interactions can either promote or inhibit anti-tumour immunity. Finally, Chapter 5 builds on these findings by examining the impact of different CAF subtypes on lymphocyte behaviour, offering insights into how the spatial and temporal dynamics of the TME influence immune cell infiltration and function.

As research continues to unravel the complexities of the TME, these insights will be crucial for developing more effective treatments that can overcome the challenges of immune evasion and resistance in PDAC.

Limitations

Inevitably, ambitious studies of primary human cancer tissue can carry some limitations in relation to delivery and interpretation. I was able to obtain a significant number of primary samples for my studies in chapter 3 but access to a greater number

would have allowed me to gain greater statistical power to assess the variation in stromal phenotype between CAF and ANF populations. The cohort of neo-adjuvant samples was also somewhat limited although this was a valuable assessment of how this therapy may act to temporarily 'normalise' stromal populations.

The studies on CAF-lymphoid interactions could be extended by increasing the combinatorial admixture of CAF subsets with different T cell and NK populations. The substantial heterogeneity of CAF is such that this work is challenging and is also modulated by the impact that experimental culture conditions can have on fibroblast phenotype. Nevertheless, this sort of work is essential to establish the underlying selective forces that drive the selection of different CAF subsets.

Potential areas for future investigation

Whilst my research has uncovered a range of interesting insights into the potential functional impact of fibroblast subsets within PDAC it is inevitable that this raises a number of questions for future investigation.

In chapter 3 I was able to characterise expression of a range of canonical stromal proteins on fibroblasts from fresh tumour. However, the challenge with gating expression of specific proteins on flow cytometry was such that I was not able to analyse the multiparametric co-expression of these markers and gain deeper insight into the major clusters of CAF in primary tumours. scRNA-Seq analysis of PDAC fibroblasts has been undertaken by several groups but it is still important to assess protein expression as the dynamic range of protein expression is greater than RNA levels. Furthermore, the correlation between RNA and protein expression is not absolute. Newly emerging technologies that may be able to address this challenge

could include the use of spatial proteomic analysis which allows staining for expression of many different protein molecules on a single slide. This technology would also provide architectural information on the location of fibroblasts subsets in relation to the tumour.

In relation to my CAF-lymphocyte co-culture experiments it will be valuable, in future work, to assess how a variety of different CAF subpopulations vary in relation to inhibitory or activation potential. In particular, the significant variation in expression of inflammatory proteins such as complement C3 and CD90, which were preferentially expressed on myCAF subsets, would be expected to be reflected in differential impact on modulation of lymphoid populations. Furthermore, I would also be interested to extend my functional analyses, potentially using approaches such as RNA-Seq to assess the global impact of CAF-coculture on lymphoid profile. This may uncover differential signalling mechanisms and potentially identify biochemical mechanisms by which CAF support or inhibit PDAC survival.

Another area that would be of interest is to delineate the specific ligand-receptor interactions between CAF and lymphocytes that lead to functional modulation. One approach to this would be through the use of antibodies to block candidate target molecules on each cell subtype.

The migration studies were ambitious in their nature and revealed clear outcomes. Future ambitious innovations here might include the use of flow technologies to assess the impact of shear forces and videography technology to assess lymphoid cell migration.

References

Alberts B, J. A., Lewis J, et al. (2002). *Integrins*. Garland Science. https://www.ncbi.nlm.nih.gov/books/NBK26867/#

Astarita, J. L., Acton, S. E., & Turley, S. J. (2012). Podoplanin: emerging functions in development, the immune system, and cancer. *Front Immunol*, *3*, 283. https://doi.org/10.3389/fimmu.2012.00283

Axelrod, M. L., Cook, R. S., Johnson, D. B., & Balko, J. M. (2019). Biological Consequences of MHC-II Expression by Tumor Cells in Cancer. *Clin Cancer Res*, *25*(8), 2392-2402. https://doi.org/10.1158/1078-0432.CCR-18-3200

Backx, E., Coolens, K., Van Den Bossche, J.-L., Houbracken, I., Espinet, E., & Rooman, I. (2022). On the Origin of Pancreatic Cancer: Molecular Tumor Subtypes in Perspective of Exocrine Cell Plasticity. *Cellular and Molecular Gastroenterology and Hepatology*, *13*(4), 1243-1253. https://doi.org/10.1016/j.jcmgh.2021.11.010

Baker, A. T., Abuwarwar, M. H., Poly, L., Wilkins, S., & Fletcher, A. L. (2021). Cancer-Associated Fibroblasts and T Cells: From Mechanisms to Outcomes. *J Immunol*, *206*(2), 310-320. https://doi.org/10.4049/jimmunol.2001203

Baranyi, U., Winter, B., Gugerell, A., Hegedus, B., Brostjan, C., Laufer, G., & Messner, B. (2019). Primary Human Fibroblasts in Culture Switch to a Myofibroblast-Like Phenotype Independently of TGF Beta. *Cells*, *8*(7). https://doi.org/10.3390/cells8070721

Barth, P. J., Ebrahimsade, S., Ramaswamy, A., & Moll, R. (2002). CD34+ fibrocytes in invasive ductal carcinoma, ductal carcinoma in situ, and benign breast lesions. *Virchows Arch*, *440*(3), 298-303. https://doi.org/10.1007/s004280100530

Bartok, B., & Firestein, G. S. (2010). Fibroblast-like synoviocytes: key effector cells in rheumatoid arthritis. *Immunol Rev*, *233*(1), 233-255. https://doi.org/10.1111/j.0105-2896.2009.00859.x

Bastos, A. G. P., Carvalho, B., Silva, R., Leitao, D., Linhares, P., Vaz, R., & Lima, J. (2022). Endoglin (CD105) and proliferation index in recurrent glioblastoma treated with anti-angiogenic therapy. *Front Oncol*, *12*, 910196. https://doi.org/10.3389/fonc.2022.910196

Batlle, E., & Massague, J. (2019). Transforming Growth Factor-beta Signaling in Immunity and Cancer. *Immunity*, *50*(4), 924-940. https://doi.org/10.1016/j.immuni.2019.03.024

Belkin, A. M., & Retta, S. F. (1998). beta1D integrin inhibits cell cycle progression in normal myoblasts and fibroblasts. *J Biol Chem*, *273*(24), 15234-15240. https://doi.org/10.1074/jbc.273.24.15234

Belle, J. I., & DeNardo, D. G. (2019). A Single-Cell Window into Pancreas Cancer Fibroblast Heterogeneity. *Cancer Discov*, *9*(8), 1001-1002. https://doi.org/10.1158/2159-8290.CD-19-0576

Biffi, G., Oni, T. E., Spielman, B., Hao, Y., Elyada, E., Park, Y., Preall, J., & Tuveson, D. A. (2019). IL1-Induced JAK/STAT Signaling Is Antagonized by TGFbeta to Shape CAF Heterogeneity in Pancreatic Ductal Adenocarcinoma. *Cancer Discov*, *9*(2), 282-301. https://doi.org/10.1158/2159-8290.CD-18-0710

Biffi, G., & Tuveson, D. A. (2021). Diversity and Biology of Cancer-Associated Fibroblasts. *Physiol Rev*, *101*(1), 147-176. https://doi.org/10.1152/physrev.00048.2019

Blair, A. B., Kim, V. M., Muth, S. T., Saung, M. T., Lokker, N., Blouw, B., Armstrong, T. D., Jaffee, E. M., Tsujikawa, T., Coussens, L. M., He, J., Burkhart, R. A., Wolfgang, C. L., & Zheng, L. (2019). Dissecting the Stromal Signaling and Regulation of Myeloid Cells and Memory Effector T Cells in Pancreatic Cancer. *Clin Cancer Res*, *25*(17), 5351-5363. https://doi.org/10.1158/1078-0432.CCR-18-4192

Board, R., & Jayson, G. C. (2005). Platelet-derived growth factor receptor (PDGFR): a target for anticancer therapeutics. *Drug Resist Updat*, *8*(1-2), 75-83. https://doi.org/10.1016/j.drup.2005.03.004

Bockorny, B., Semenisty, V., Macarulla, T., Borazanci, E., Wolpin, B. M., Stemmer, S. M., Golan, T., Geva, R., Borad, M. J., Pedersen, K. S., Park, J. O., Ramirez, R. A., Abad, D. G., Feliu, J., Munoz, A., Ponz-Sarvise, M., Peled, A., Lustig, T. M., Bohana-Kashtan, O., . . . Hidalgo, M. (2020). BL-8040, a CXCR4 antagonist, in combination with pembrolizumab and chemotherapy for pancreatic cancer: the COMBAT trial. *Nat Med*, *26*(6), 878-885. https://doi.org/10.1038/s41591-020-0880-x

Bradfield, P. F., Amft, N., Vernon-Wilson, E., Exley, A. E., Parsonage, G., Rainger, G. E., Nash, G. B., Thomas, A. M., Simmons, D. L., Salmon, M., & Buckley, C. D. (2003). Rheumatoid fibroblast-like synoviocytes overexpress the chemokine stromal cell-derived factor 1 (CXCL12), which supports distinct patterns and rates of CD4+ and CD8+ T cell migration within synovial tissue. *Arthritis Rheum*, *48*(9), 2472-2482. https://doi.org/10.1002/art.11219

Bradley, J. E., Ramirez, G., & Hagood, J. S. (2009). Roles and regulation of Thy-1, a context-dependent modulator of cell phenotype. *Biofactors*, *35*(3), 258-265. https://doi.org/10.1002/biof.41

By Akio Yamakage, K. K., Edwin A. Smith, E. Carwile LeRoy, and Maria Trojanowska. (1992). Selective Upregulation of Platelet-derived Growth
Factor c~Receptors by Transforming Growth Factor/~
in Scleroder Fibroblasts. *J. Exp. Med*

Campbell, K. S., & Purdy, A. K. (2011). Structure/function of human killer cell immunoglobulin-like receptors: lessons from polymorphisms, evolution, crystal structures and mutations. *Immunology*, *132*(3), 315-325. https://doi.org/10.1111/j.1365-2567.2010.03398.x

Carstens, J. L., Correa de Sampaio, P., Yang, D., Barua, S., Wang, H., Rao, A., Allison, J. P., LeBleu, V. S., & Kalluri, R. (2017). Spatial computation of intratumoral T cells correlates with survival of patients with pancreatic cancer. *Nat Commun*, *8*, 15095. https://doi.org/10.1038/ncomms15095

Casado, J. A., Valeri, A., Sanchez-Dominguez, R., Vela, P., Lopez, A., Navarro, S., Alberquilla, O., Hanenberg, H., Pujol, R., Segovia, J. C., Minguillon, J., Surralles, J., de Heredia, C. D., Sevilla, J., Rio, P., & Bueren, J. A. (2022). Upregulation of NKG2D ligands impairs hematopoietic stem cell function in Fanconi anemia. *J Clin Invest*, *132*(15). https://doi.org/10.1172/JCI142842

Chang, S. K., Kohlgruber, A. C., Mizoguchi, F., Michelet, X., Wolf, B. J., Wei, K., Lee, P. Y., Lynch, L., Duquette, D., Ceperuelo-Mallafre, V., Banks, A. S., & Brenner, M. B. (2017). Stromal cell cadherin-11 regulates adipose tissue inflammation and diabetes. *J Clin Invest*, *127*(9), 3300-3312. https://doi.org/10.1172/JCI86881

Chang, S. K., Noss, E. H., Chen, M., Gu, Z., Townsend, K., Grenha, R., Leon, L., Lee, S. Y., Lee, D. M., & Brenner, M. B. (2011). Cadherin-11 regulates fibroblast

inflammation. *Proc Natl Acad Sci U S A*, *108*(20), 8402-8407. https://doi.org/10.1073/pnas.1019437108

Chang, Y., Li, H., & Guo, Z. (2014). Mesenchymal stem cell-like properties in fibroblasts. *Cell Physiol Biochem*, *34*(3), 703-714. https://doi.org/10.1159/000363035

Chaponnier, B. H. G. C. J. J. T. G. G. a. C. (2001). Alpha-Smooth Muscle Actin Expression Upregulates Fibroblast Contractile Activity. *Molecular Biology of the Cell*, *Vol. 12, 2730–2741*.

Chen, H., Yang, W. W., Wen, Q. T., Xu, L., & Chen, M. (2009). TGF-beta induces fibroblast activation protein expression; fibroblast activation protein expression increases the proliferation, adhesion, and migration of HO-8910PM [corrected]. *Exp Mol Pathol*, *87*(3), 189-194. https://doi.org/10.1016/j.yexmp.2009.09.001

Chen, K., Wang, Q., Li, M., Guo, H., Liu, W., Wang, F., Tian, X., & Yang, Y. (2021). Single-cell RNA-seq reveals dynamic change in tumor microenvironment during pancreatic ductal adenocarcinoma malignant progression. *EBioMedicine*, *66*, 103315. https://doi.org/10.1016/j.ebiom.2021.103315

Chen, Y., Kim, J., Yang, S., Wang, H., Wu, C. J., Sugimoto, H., LeBleu, V. S., & Kalluri, R. (2021). Type I collagen deletion in alphaSMA(+) myofibroblasts augments immune suppression and accelerates progression of pancreatic cancer. *Cancer Cell*, *39*(4), 548-565 e546. https://doi.org/10.1016/j.ccell.2021.02.007

Cibrian, D., & Sanchez-Madrid, F. (2017). CD69: from activation marker to metabolic gatekeeper. *Eur J Immunol*, *47*(6), 946-953. https://doi.org/10.1002/eji.201646837

Collisson, E. A., Sadanandam, A., Olson, P., Gibb, W. J., Truitt, M., Gu, S., Cooc, J., Weinkle, J., Kim, G. E., Jakkula, L., Feiler, H. S., Ko, A. H., Olshen, A. B., Danenberg, K. L., Tempero, M. A., Spellman, P. T., Hanahan, D., & Gray, J. W. (2011). Subtypes of pancreatic ductal adenocarcinoma and their differing responses to therapy. *Nat Med*, *17*(4), 500-503. https://doi.org/10.1038/nm.2344

Contreras, O., Cruz-Soca, M., Theret, M., Soliman, H., Tung, L. W., Groppa, E., Rossi, F. M., & Brandan, E. (2019). Cross-talk between TGF-beta and PDGFRalpha signaling pathways regulates the fate of stromal fibro-adipogenic progenitors. *J Cell Sci*, *132*(19). https://doi.org/10.1242/jcs.232157

Costa, A., Kieffer, Y., Scholer-Dahirel, A., Pelon, F., Bourachot, B., Cardon, M., Sirven, P., Magagna, I., Fuhrmann, L., Bernard, C., Bonneau, C., Kondratova, M., Kuperstein, I., Zinovyev, A., Givel, A. M., Parrini, M. C., Soumelis, V., Vincent-Salomon, A., & Mechta-Grigoriou, F. (2018). Fibroblast Heterogeneity and Immunosuppressive Environment in Human Breast Cancer. *Cancer Cell*, *33*(3), 463-479 e410. https://doi.org/10.1016/j.ccell.2018.01.011

Croft, A. P., Campos, J., Jansen, K., Turner, J. D., Marshall, J., Attar, M., Savary, L., Wehmeyer, C., Naylor, A. J., Kemble, S., Begum, J., Durholz, K., Perlman, H., Barone, F., McGettrick, H. M., Fearon, D. T., Wei, K., Raychaudhuri, S., Korsunsky, I., . . . Buckley, C. D. (2019). Distinct fibroblast subsets drive inflammation and damage in arthritis. *Nature*, *570*(7760), 246-251. https://doi.org/10.1038/s41586-019-1263-7

Croft, W., Pearce, H., Margielewska-Davies, S., Lim, L., Nicol, S. M., Zayou, F., Blakeway, D., Marcon, F., Powell-Brett, S., Mahon, B., Merard, R., Zuo, J., Middleton, G., Roberts, K., Brown, R. M., & Moss, P. (2023). https://doi.org/10.1101/2023.01.20.524883

Davidson, S., Efremova, M., Riedel, A., Mahata, B., Pramanik, J., Huuhtanen, J., Kar, G., Vento-Tormo, R., Hagai, T., Chen, X., Haniffa, M. A., Shields, J. D., & Teichmann, S. A. (2020). Single-Cell RNA Sequencing Reveals a Dynamic Stromal Niche That Supports Tumor Growth. *Cell Rep*, *31*(7), 107628. https://doi.org/10.1016/j.celrep.2020.107628

Desbois, M., Udyavar, A. R., Ryner, L., Kozlowski, C., Guan, Y., Durrbaum, M., Lu, S., Fortin, J. P., Koeppen, H., Ziai, J., Chang, C. W., Keerthivasan, S., Plante, M., Bourgon, R., Bais, C., Hegde, P., Daemen, A., Turley, S., & Wang, Y. (2020). Integrated digital pathology and transcriptome analysis identifies molecular mediators of T-cell exclusion in ovarian cancer. *Nat Commun*, *11*(1), 5583. https://doi.org/10.1038/s41467-020-19408-2

Dick, M. K. (2020). https://www.ncbi.nlm.nih.gov/books/NBK279364/

Dick, M. K. (2022). *StatPearls* https://www.ncbi.nlm.nih.gov/books/NBK541065/

Eibl, M. E. a. G. (2014). Risk factors for pancreatic cancer: underlying mechanisms and potential targets. *Front Physiol. 2014; 5: 490.* https://www.ncbi.nlm.nih.gov/pmc/articles/PMC4261721/

Elena Neumann, B. R., Anette Knedla, Stephanie Lefèvre, Ingo H Tarner, Joachim Grifka,, & Jurgen Steinmeyer, J. S., Steffen Gay and Ulf Müller-Ladner (2010). Cell culture and passaging alters gene expression pattern and proliferation rate in rheumatoid arthritis synovial fibroblasts. *Arthritis Research & Therapy*

Elyada, E., Bolisetty, M., Laise, P., Flynn, W. F., Courtois, E. T., Burkhart, R. A., Teinor, J. A., Belleau, P., Biffi, G., Lucito, M. S., Sivajothi, S., Armstrong, T. D., Engle, D. D., Yu, K. H., Hao, Y., Wolfgang, C. L., Park, Y., Preall, J., Jaffee, E. M., . . . Tuveson, D. A. (2019). Cross-Species Single-Cell Analysis of Pancreatic Ductal Adenocarcinoma Reveals Antigen-Presenting Cancer-Associated Fibroblasts. *Cancer Discov*, *9*(8), 1102-1123. https://doi.org/10.1158/2159-8290.CD-19-0094

Ene-Obong, A., Clear, A. J., Watt, J., Wang, J., Fatah, R., Riches, J. C., Marshall, J. F., Chin-Aleong, J., Chelala, C., Gribben, J. G., Ramsay, A. G., & Kocher, H. M. (2013). Activated pancreatic stellate cells sequester CD8+ T cells to reduce their infiltration of the juxtatumoral compartment of pancreatic ductal adenocarcinoma. *Gastroenterology*, *145*(5), 1121-1132. https://doi.org/10.1053/j.gastro.2013.07.025

Falcomata, C., Barthel, S., Schneider, G., Rad, R., Schmidt-Supprian, M., & Saur, D. (2023). Context-Specific Determinants of the Immunosuppressive Tumor Microenvironment in Pancreatic Cancer. *Cancer Discov*, *13*(2), 278-297. https://doi.org/10.1158/2159-8290.CD-22-0876

Farr, L., Ghosh, S., & Moonah, S. (2020). Role of MIF Cytokine/CD74 Receptor Pathway in Protecting Against Injury and Promoting Repair. *Front Immunol*, *11*, 1273. https://doi.org/10.3389/fimmu.2020.01273

FARSHAD NASSIRI, M. D. C., BERND W. SCHEITHAUER, FABIO ROTONDO, ALESSANDRA FAZIO, GEORGE M. YOUSEF, LUIS V. SYRO4, KALMAN KOVACS and RICARDO V. LLOYD. (2011). Endoglin (CD105): A Review of its Role in Angiogenesis and Tumor Diagnosis, Progression and Therapy. *ANTICANCER RESEARCH*.

Fearon, D. T. (2014). The carcinoma-associated fibroblast expressing fibroblast activation protein and escape from immune surveillance. *Cancer Immunol Res*, *2*(3), 187-193. https://doi.org/10.1158/2326-6066.CIR-14-0002

Feig, C., Jones, J. O., Kraman, M., Wells, R. J., Deonarine, A., Chan, D. S., Connell, C. M., Roberts, E. W., Zhao, Q., Caballero, O. L., Teichmann, S. A., Janowitz,

T., Jodrell, D. I., Tuveson, D. A., & Fearon, D. T. (2013). Targeting CXCL12 from FAP-expressing carcinoma-associated fibroblasts synergizes with anti-PD-L1 immunotherapy in pancreatic cancer. *Proc Natl Acad Sci U S A*, *110*(50), 20212-20217. https://doi.org/10.1073/pnas.1320318110

Filer, A., Ward, L. S. C., Kemble, S., Davies, C. S., Munir, H., Rogers, R., Raza, K., Buckley, C. D., Nash, G. B., & McGettrick, H. M. (2017). Identification of a transitional fibroblast function in very early rheumatoid arthritis. *Ann Rheum Dis*, *76*(12), 2105-2112. https://doi.org/10.1136/annrheumdis-2017-211286

Fincham, R. E. A., Delvecchio, F. R., Goulart, M. R., Yeong, J. P. S., & Kocher, H. M. (2021). Natural killer cells in pancreatic cancer stroma. *World J Gastroenterol*, *27*(24), 3483-3501. https://doi.org/10.3748/wjg.v27.i24.3483

Fitzgerald, A. A., & Weiner, L. M. (2020). The role of fibroblast activation protein in health and malignancy. *Cancer Metastasis Rev*, *39*(3), 783-803. https://doi.org/10.1007/s10555-020-09909-3

Ford, K., Hanley, C. J., Mellone, M., Szyndralewiez, C., Heitz, F., Wiesel, P., Wood, O., Machado, M., Lopez, M. A., Ganesan, A. P., Wang, C., Chakravarthy, A., Fenton, T. R., King, E. V., Vijayanand, P., Ottensmeier, C. H., Al-Shamkhani, A., Savelyeva, N., & Thomas, G. J. (2020). NOX4 Inhibition Potentiates Immunotherapy by Overcoming Cancer-Associated Fibroblast-Mediated CD8 T-cell Exclusion from Tumors. *Cancer Res*, *80*(9), 1846-1860. https://doi.org/10.1158/0008-5472.CAN-19-3158

Friedman, G., Levi-Galibov, O., David, E., Bornstein, C., Giladi, A., Dadiani, M., Mayo, A., Halperin, C., Pevsner-Fischer, M., Lavon, H., Nevo, R., Stein, Y., Ali, H. R., Caldas, C., Nili-Gal-Yam, E., Alon, U., Amit, I., & Scherz-Shouval, R. (2020). Cancer-associated fibroblast compositions change with breast-cancer progression linking S100A4 and PDPN ratios with clinical outcome
. https://doi.org/10.1101/2020.01.12.903039

G. Tau, P. R. (1999). Biologic functions of the IFN-γ receptors. *Allergy*, *54*(12), 1233-1251. https://doi.org/10.1034/j.1398-9995.1999.00099.x.

Gao, Z., Sasaoka, T., Fujimori, T., Oya, T., Ishii, Y., Sabit, H., Kawaguchi, M., Kurotaki, Y., Naito, M., Wada, T., Ishizawa, S., Kobayashi, M., Nabeshima, Y., & Sasahara, M. (2005). Deletion of the PDGFR-beta gene affects key fibroblast functions important for wound healing. *J Biol Chem*, *280*(10), 9375-9389. https://doi.org/10.1074/jbc.M413081200

Gilfillan, S., Chan, C. J., Cella, M., Haynes, N. M., Rapaport, A. S., Boles, K. S., Andrews, D. M., Smyth, M. J., & Colonna, M. (2008). DNAM-1 promotes activation of cytotoxic lymphocytes by nonprofessional antigen-presenting cells and tumors. *J Exp Med*, *205*(13), 2965-2973. https://doi.org/10.1084/jem.20081752

Giorello, M. B., Martinez, L. M., Borzone, F. R., Padin, M. D. R., Mora, M. F., Sevic, I., Alaniz, L., Calcagno, M. L., Garcia-Rivello, H., Wernicke, A., Labovsky, V., & Chasseing, N. A. (2023). CD105 expression in cancer-associated fibroblasts: a biomarker for bone metastasis in early invasive ductal breast cancer patients. *Front Cell Dev Biol*, *11*, 1250869. https://doi.org/10.3389/fcell.2023.1250869

Givel, A. M., Kieffer, Y., Scholer-Dahirel, A., Sirven, P., Cardon, M., Pelon, F., Magagna, I., Gentric, G., Costa, A., Bonneau, C., Mieulet, V., Vincent-Salomon, A., & Mechta-Grigoriou, F. (2018). miR200-regulated CXCL12beta promotes fibroblast heterogeneity and immunosuppression in ovarian cancers. *Nat Commun*, *9*(1), 1056. https://doi.org/10.1038/s41467-018-03348-z

Gonzalez, H., Hagerling, C., & Werb, Z. (2018). Roles of the immune system in cancer: from tumor initiation to metastatic progression. *Genes Dev*, *32*(19-20), 1267-1284. https://doi.org/10.1101/gad.314617.118

Gorchs, L., Fernandez Moro, C., Bankhead, P., Kern, K. P., Sadeak, I., Meng, Q., Rangelova, E., & Kaipe, H. (2019). Human Pancreatic Carcinoma-Associated Fibroblasts Promote Expression of Co-inhibitory Markers on CD4(+) and CD8(+) T-Cells. *Front Immunol*, *10*, 847. https://doi.org/10.3389/fimmu.2019.00847

Gorchs, L., & Kaipe, H. (2021). Interactions between Cancer-Associated Fibroblasts and T Cells in the Pancreatic Tumor Microenvironment and the Role of Chemokines. *Cancers (Basel)*, *13*(12). https://doi.org/10.3390/cancers13122995

Goulart, M. R., Stasinos, K., Fincham, R. E. A., Delvecchio, F. R., & Kocher, H. M. (2021). T cells in pancreatic cancer stroma. *World J Gastroenterol*, *27*(46), 7956-7968. https://doi.org/10.3748/wjg.v27.i46.7956

Granger DN, S. E. (2010). *Inflammation andthe Microcirculation*.

Green, J., Endale, M., Auer, H., & Perl, A. K. (2016). Diversity of Interstitial Lung Fibroblasts Is Regulated by Platelet-Derived Growth Factor Receptor alpha Kinase Activity. *Am J Respir Cell Mol Biol*, *54*(4), 532-545. https://doi.org/10.1165/rcmb.2015-0095OC

Greten, F. R., & Grivennikov, S. I. (2019). Inflammation and Cancer: Triggers, Mechanisms, and Consequences. *Immunity*, *51*(1), 27-41. https://doi.org/10.1016/j.immuni.2019.06.025

Guo, J., Xie, K., & Zheng, S. (2016). Molecular Biomarkers of Pancreatic Intraepithelial Neoplasia and Their Implications in Early Diagnosis and Therapeutic Intervention of Pancreatic Cancer. *International Journal of Biological Sciences*, *12*(3), 292-301. https://doi.org/10.7150/ijbs.14995

Haeryfar, S. M., & Hoskin, D. W. (2004). Thy-1: more than a mouse pan-T cell marker. *J Immunol*, *173*(6), 3581-3588. https://doi.org/10.4049/jimmunol.173.6.3581

Han, C., Liu, T., & Yin, R. (2020). Biomarkers for cancer-associated fibroblasts. *Biomarker Research*, *8*(1). https://doi.org/10.1186/s40364-020-00245-w

Hartmann, N., Giese, N. A., Giese, T., Poschke, I., Offringa, R., Werner, J., & Ryschich, E. (2014). Prevailing role of contact guidance in intrastromal T-cell trapping in human pancreatic cancer. *Clin Cancer Res*, *20*(13), 3422-3433. https://doi.org/10.1158/1078-0432.CCR-13-2972

Hewitt, K. J., Shamis, Y., Knight, E., Smith, A., Maione, A., Alt-Holland, A., Sheridan, S. D., Haggarty, S. J., & Garlick, J. A. (2012). PDGFRbeta expression and function in fibroblasts derived from pluripotent cells is linked to DNA demethylation. *J Cell Sci*, *125*(Pt 9), 2276-2287. https://doi.org/10.1242/jcs.099192

Hong, W. C., Lee, D. E., Kang, H. W., Kim, M. J., Kim, M., Kim, J. H., Fang, S., Kim, H. J., & Park, J. S. (2023). CD74 Promotes a Pro-Inflammatory Tumor Microenvironment by Inducing S100A8 and S100A9 Secretion in Pancreatic Cancer. *Int J Mol Sci*, *24*(16). https://doi.org/10.3390/ijms241612993

Hosein, A. N., Huang, H., Wang, Z., Parmar, K., Du, W., Huang, J., Maitra, A., Olson, E., Verma, U., & Brekken, R. A. (2019). Cellular heterogeneity during mouse pancreatic ductal adenocarcinoma progression at single-cell resolution. *JCI Insight*, *5*(16). https://doi.org/10.1172/jci.insight.129212

Hu, Y., Chen, W., Yan, Z., Ma, J., Zhu, F., & Huo, J. (2019). Prognostic value of PD-L1 expression in patients with pancreatic cancer: A PRISMA-compliant meta-

analysis. *Medicine (Baltimore)*, *98*(3), e14006. https://doi.org/10.1097/MD.0000000000014006

Huang, H., Wang, Z., Zhang, Y., Pradhan, R. N., Ganguly, D., Chandra, R., Murimwa, G., Wright, S., Gu, X., Maddipati, R., Muller, S., Turley, S. J., & Brekken, R. A. (2022). Mesothelial cell-derived antigen-presenting cancer-associated fibroblasts induce expansion of regulatory T cells in pancreatic cancer. *Cancer Cell*, *40*(6), 656-673 e657. https://doi.org/10.1016/j.ccell.2022.04.011

Huang, Q., Huang, M., Meng, F., & Sun, R. (2019). Activated pancreatic stellate cells inhibit NK cell function in the human pancreatic cancer microenvironment. *Cell Mol Immunol*, *16*(1), 87-89. https://doi.org/10.1038/s41423-018-0014-2

Huber, M., Brehm, C. U., Gress, T. M., Buchholz, M., Alashkar Alhamwe, B., von Strandmann, E. P., Slater, E. P., Bartsch, J. W., Bauer, C., & Lauth, M. (2020). The Immune Microenvironment in Pancreatic Cancer. *Int J Mol Sci*, *21*(19). https://doi.org/10.3390/ijms21197307

Huifang Liu, S. W., Jing Xin, Jing Wang, Cuiping Yao, Zhenxi Zhang (2019). Role of NKG2D and its ligands in cancer immunotherapy. *Am J Cancer Res*.

Humphrey, J. H. a. P., Samuel Scott. (2023). <immune system -- Britannica Online Encyclopedia.pdf>. https://www.britannica.com/science/immune-system

Hur, C., Tramontano, A. C., Dowling, E. C., Brooks, G. A., Jeon, A., Brugge, W. R., Gazelle, G. S., Kong, C. Y., & Pandharipande, P. V. (2016). Early Pancreatic Ductal Adenocarcinoma Survival Is Dependent on Size. *Pancreas*, *45*(7), 1062-1066. https://doi.org/10.1097/mpa.0000000000000587

Hutton, C., Heider, F., Blanco-Gomez, A., Banyard, A., Kononov, A., Zhang, X., Karim, S., Paulus-Hock, V., Watt, D., Steele, N., Kemp, S., Hogg, E. K. J., Kelly, J., Jackstadt, R. F., Lopes, F., Menotti, M., Chisholm, L., Lamarca, A., Valle, J., . . . Jorgensen, C. (2021). Single-cell analysis defines a pancreatic fibroblast lineage that supports anti-tumor immunity. *Cancer Cell*, *39*(9), 1227-1244 e1220. https://doi.org/10.1016/j.ccell.2021.06.017

Inoue, T., Adachi, K., Kawana, K., Taguchi, A., Nagamatsu, T., Fujimoto, A., Tomio, K., Yamashita, A., Eguchi, S., Nishida, H., Nakamura, H., Sato, M., Yoshida, M., Arimoto, T., Wada-Hiraike, O., Oda, K., Osuga, Y., & Fujii, T. (2016). Cancer-associated fibroblast suppresses killing activity of natural killer cells through downregulation of poliovirus receptor (PVR/CD155), a ligand of activating NK receptor. *Int J Oncol*, *49*(4), 1297-1304. https://doi.org/10.3892/ijo.2016.3631

Iwasa, S., Jin, X., Okada, K., Mitsumata, M., & Ooi, A. (2003). Increased expression of seprase, a membrane-type serine protease, is associated with lymph node metastasis in human colorectal cancer. *Cancer Lett*, *199*(1), 91-98. https://doi.org/10.1016/s0304-3835(03)00315-x

J P Cai, V. F., J R Taylor, Y H Chin. (1992). Transforming growth factor-beta differentially regulates the adhesiveness of normal and psoriatic dermal microvascular endothelial cells for peripheral blood mononuclear cells. https://pubmed.ncbi.nlm.nih.gov/1548425/

J P Thiery, D. C. (1999). Epithelial cell plasticity in development and tumor progression. *Cancer and Metastasis Reviews*. https://doi.org/10.1023/a:1006256219004

James C. Bonner, A. B., Pamela M. Lindroos, and Alvaro R. Osornio-Vargas (1995). Transforming Growth Factor {31 Downregulates the Platelet-derived Growth Factor a-Receptor Subtype on Human Lung Fibroblasts In Vitro. *AMERICAN JOURNAL OF RESPIRATORY CELL AND MOLECULAR BIOLOGY*.

Jeffery, H. C., Buckley, C. D., Moss, P., Rainger, G. E., Nash, G. B., & McGettrick, H. M. (2013). Analysis of the effects of stromal cells on the migration of lymphocytes into and through inflamed tissue using 3-D culture models. *J Immunol Methods*, *400-401*, 45-57. https://doi.org/10.1016/j.jim.2013.10.004

Jiang, H., Hegde, S., Knolhoff, B. L., Zhu, Y., Herndon, J. M., Meyer, M. A., Nywening, T. M., Hawkins, W. G., Shapiro, I. M., Weaver, D. T., Pachter, J. A., Wang-Gillam, A., & DeNardo, D. G. (2016). Targeting focal adhesion kinase renders pancreatic cancers responsive to checkpoint immunotherapy. *Nat Med*, *22*(8), 851-860. https://doi.org/10.1038/nm.4123

Jing, Y., Yang, Y., Hao, F., Song, Y., Zhang, X., Zhang, Y., Huang, X., Hu, Q., & Ni, Y. (2018). Higher Ki67 expression in fibroblast like cells at invasive front indicates better clinical outcomes in oral squamous cell carcinoma patients. *Biosci Rep*, *38*(6). https://doi.org/10.1042/BSR20181271

K. Funa, B. N., G.Jacobsson & G.V.Alm. (1984). Decreased natural kiler celactivity and interferon
production by leucocytes in patients with adenocarcinoma of
thepancreas.

Kalluri, R., & Neilson, E. G. (2003). Epithelial-mesenchymal transition and its implications for fibrosis. *Journal of Clinical Investigation*, *112*(12), 1776-1784. https://doi.org/10.1172/jci200320530

Kalluri, R., & Zeisberg, M. (2006). Fibroblasts in cancer. *Nat Rev Cancer*, *6*(5), 392-401. https://doi.org/10.1038/nrc1877

Kato, T., Noma, K., Ohara, T., Kashima, H., Katsura, Y., Sato, H., Komoto, S., Katsube, R., Ninomiya, T., Tazawa, H., Shirakawa, Y., & Fujiwara, T. (2018). Cancer-Associated Fibroblasts Affect Intratumoral CD8(+) and FoxP3(+) T Cells Via IL6 in the Tumor Microenvironment. *Clin Cancer Res*, *24*(19), 4820-4833. https://doi.org/10.1158/1078-0432.CCR-18-0205

Kawase, T., Yasui, Y., Nishina, S., Hara, Y., Yanatori, I., Tomiyama, Y., Nakashima, Y., Yoshida, K., Kishi, F., Nakamura, M., & Hino, K. (2015). Fibroblast activation protein-alpha-expressing fibroblasts promote the progression of pancreatic ductal adenocarcinoma. *BMC Gastroenterol*, *15*, 109. https://doi.org/10.1186/s12876-015-0340-0

Kerdidani, D., Aerakis, E., Verrou, K. M., Angelidis, I., Douka, K., Maniou, M. A., Stamoulis, P., Goudevenou, K., Prados, A., Tzaferis, C., Ntafis, V., Vamvakaris, I., Kaniaris, E., Vachlas, K., Sepsas, E., Koutsopoulos, A., Potaris, K., & Tsoumakidou, M. (2022). Lung tumor MHCII immunity depends on in situ antigen presentation by fibroblasts. *J Exp Med*, *219*(2). https://doi.org/10.1084/jem.20210815

Kim, K. I., Lee, K. H., Kim, T. R., Chun, Y. S., Lee, T. H., & Park, H. K. (2014). Ki-67 as a predictor of response to neoadjuvant chemotherapy in breast cancer patients. *J Breast Cancer*, *17*(1), 40-46. https://doi.org/10.4048/jbc.2014.17.1.40

Kinoshita, T., Ishii, G., Hiraoka, N., Hirayama, S., Yamauchi, C., Aokage, K., Hishida, T., Yoshida, J., Nagai, K., & Ochiai, A. (2013). Forkhead box P3 regulatory T cells coexisting with cancer associated fibroblasts are correlated with a poor outcome in lung adenocarcinoma. *Cancer Sci*, *104*(4), 409-415. https://doi.org/10.1111/cas.12099

Kitano, H., Kageyama, S., Hewitt, S. M., Hayashi, R., Doki, Y., Ozaki, Y., Fujino, S., Takikita, M., Kubo, H., & Fukuoka, J. (2010). Podoplanin expression in cancerous stroma induces lymphangiogenesis and predicts lymphatic spread

and patient survival. *Arch Pathol Lab Med*, *134*(10), 1520-1527. https://doi.org/10.5858/2009-0114-OA.1

Kolev, M., Das, M., Gerber, M., Baver, S., Deschatelets, P., & Markiewski, M. M. (2022). Inside-Out of Complement in Cancer. *Front Immunol*, *13*, 931273. https://doi.org/10.3389/fimmu.2022.931273

Kondo, Y., Suzuki, S., Takahara, T., Ono, S., Goto, M., Miyabe, S., Sugita, Y., Ogawa, T., Ito, H., Satou, A., Tsuzuki, T., Yoshikawa, K., Ueda, R., & Nagao, T. (2021). Improving function of cytotoxic T-lymphocytes by transforming growth factor-beta inhibitor in oral squamous cell carcinoma. *Cancer Sci*, *112*(10), 4037-4049. https://doi.org/10.1111/cas.15081

Konjevic, G. M., Vuletic, A. M., Mirjacic Martinovic, K. M., Larsen, A. K., & Jurisic, V. B. (2019). The role of cytokines in the regulation of NK cells in the tumor environment. *Cytokine*, *117*, 30-40. https://doi.org/10.1016/j.cyto.2019.02.001

Koppensteiner, L., Mathieson, L., O'Connor, R. A., & Akram, A. R. (2022). Cancer Associated Fibroblasts - An Impediment to Effective Anti-Cancer T Cell Immunity. *Front Immunol*, *13*, 887380. https://doi.org/10.3389/fimmu.2022.887380

Koyama, H., Kobayashi, N., Harada, M., Takeoka, M., Kawai, Y., Sano, K., Fujimori, M., Amano, J., Ohhashi, T., Kannagi, R., Kimata, K., Taniguchi, S. I., & Itano, N. (2008). Significance of Tumor-Associated Stroma in Promotion of Intratumoral Lymphangiogenesis. *The American Journal of Pathology*, *172*(1), 179-193. https://doi.org/10.2353/ajpath.2008.070360

Kubouchi, Y., Yurugi, Y., Wakahara, M., Sakabe, T., Haruki, T., Nosaka, K., Miwa, K., Araki, K., Taniguchi, Y., Shiomi, T., Nakamura, H., & Umekita, Y. (2018). Podoplanin expression in cancer-associated fibroblasts predicts unfavourable prognosis in patients with pathological stage IA lung adenocarcinoma. *Histopathology*, *72*(3), 490-499. https://doi.org/10.1111/his.13390

Lally, F., Smith, E., Filer, A., Stone, M. A., Shaw, J. S., Nash, G. B., Buckley, C. D., & Rainger, G. E. (2005). A novel mechanism of neutrophil recruitment in a coculture model of the rheumatoid synovium. *Arthritis Rheum*, *52*(11), 3460-3469. https://doi.org/10.1002/art.21394

Lambin, T., Lafon, C., Drainville, R. A., Pioche, M., & Prat, F. (2022). Locoregional therapies and their effects on the tumoral microenvironment of pancreatic ductal adenocarcinoma. *World Journal of Gastroenterology*, *28*(13), 1288-1303. https://doi.org/10.3748/wjg.v28.i13.1288

Lavie, D., Ben-Shmuel, A., Erez, N., & Scherz-Shouval, R. (2022). Cancer-associated fibroblasts in the single-cell era. *Nat Cancer*, *3*(7), 793-807. https://doi.org/10.1038/s43018-022-00411-z

LeBleu, V. S., & Neilson, E. G. (2020). Origin and functional heterogeneity of fibroblasts. *FASEB J*, *34*(3), 3519-3536. https://doi.org/10.1096/fj.201903188R

Lefevre, S., Knedla, A., Tennie, C., Kampmann, A., Wunrau, C., Dinser, R., Korb, A., Schnaker, E. M., Tarner, I. H., Robbins, P. D., Evans, C. H., Sturz, H., Steinmeyer, J., Gay, S., Scholmerich, J., Pap, T., Muller-Ladner, U., & Neumann, E. (2009). Synovial fibroblasts spread rheumatoid arthritis to unaffected joints. *Nat Med*, *15*(12), 1414-1420. https://doi.org/10.1038/nm.2050

Ley, K., Laudanna, C., Cybulsky, M. I., & Nourshargh, S. (2007). Getting to the site of inflammation: the leukocyte adhesion cascade updated. *Nat Rev Immunol*, *7*(9), 678-689. https://doi.org/10.1038/nri2156

Li, C., Jiang, P., Wei, S., Xu, X., & Wang, J. (2020). Regulatory T cells in tumor microenvironment: new mechanisms, potential therapeutic strategies and future prospects. *Mol Cancer*, *19*(1), 116. https://doi.org/10.1186/s12943-020-01234-1

Li, R., Bernau, K., Sandbo, N., Gu, J., Preissl, S., & Sun, X. (2018). Pdgfra marks a cellular lineage with distinct contributions to myofibroblasts in lung maturation and injury response. *Elife*, *7*. https://doi.org/10.7554/eLife.36865

Li, T., Yi, S., Liu, W., Jia, C., Wang, G., Hua, X., Tai, Y., Zhang, Q., & Chen, G. (2013). Colorectal carcinoma-derived fibroblasts modulate natural killer cell phenotype and antitumor cytotoxicity. *Med Oncol*, *30*(3), 663. https://doi.org/10.1007/s12032-013-0663-z

Linda Ziani, T. B. S.-S., Johanne Gourbeix, Andrea Cavalcanti, Caroline Robert, Gilles Favre, Salem Chouaib, Jerome Thiery (2017). Melanoma-associated fibroblasts decrease tumor cell susceptibility to NK cell-mediated killing through matrix-metalloproteinases secretion. *Oncotarget*.

Liu, Q., Liao, Q., & Zhao, Y. (2017). Chemotherapy and tumor microenvironment of pancreatic cancer. *Cancer Cell Int*, *17*, 68. https://doi.org/10.1186/s12935-017-0437-3

Madsen, C. D. (2021). Pancreatic cancer is suppressed by fibroblast-derived collagen I. *Cancer Cell*, *39*(4), 451-453. https://doi.org/10.1016/j.ccell.2021.02.017

Malchiodi, Z. X., & Weiner, L. M. (2021). Understanding and Targeting Natural Killer Cell-Cancer-Associated Fibroblast Interactions in Pancreatic Ductal Adenocarcinoma. *Cancers (Basel)*, *13*(3). https://doi.org/10.3390/cancers13030405

Mao, X., Xu, J., Wang, W., Liang, C., Hua, J., Liu, J., Zhang, B., Meng, Q., Yu, X., & Shi, S. (2021). Crosstalk between cancer-associated fibroblasts and immune cells in the tumor microenvironment: new findings and future perspectives. *Mol Cancer*, *20*(1), 131. https://doi.org/10.1186/s12943-021-01428-1

Marcon, F., Zuo, J., Pearce, H., Nicol, S., Margielewska-Davies, S., Farhat, M., Mahon, B., Middleton, G., Brown, R., Roberts, K. J., & Moss, P. (2020). NK cells in pancreatic cancer demonstrate impaired cytotoxicity and a regulatory IL-10 phenotype. *Oncoimmunology*, *9*(1), 1845424. https://doi.org/10.1080/2162402X.2020.1845424

Mariathasan, S., Turley, S. J., Nickles, D., Castiglioni, A., Yuen, K., Wang, Y., Kadel, E. E., III, Koeppen, H., Astarita, J. L., Cubas, R., Jhunjhunwala, S., Banchereau, R., Yang, Y., Guan, Y., Chalouni, C., Ziai, J., Senbabaoglu, Y., Santoro, S., Sheinson, D., . . . Powles, T. (2018). TGFbeta attenuates tumour response to PD-L1 blockade by contributing to exclusion of T cells. *Nature*, *554*(7693), 544-548. https://doi.org/10.1038/nature25501

Martinez, C. D. a. G. J. (2010). T cells: the usual subsets.

McGettrick, H. M., Buckley, C. D., Ed Rainger, G., & Nash, G. B. (2010). Influence of stromal cells on lymphocyte adhesion and migration on endothelial cells. *Methods Mol Biol*, *616*, 49-68. https://doi.org/10.1007/978-1-60761-461-6_4

McGettrick, H. M., Buckley, C. D., Filer, A., Rainger, G. E., & Nash, G. B. (2010). Stromal cells differentially regulate neutrophil and lymphocyte recruitment through the endothelium. *Immunology*, *131*(3), 357-370. https://doi.org/10.1111/j.1365-2567.2010.03307.x

McGettrick, H. M., Butler, L. M., Buckley, C. D., Rainger, G. E., & Nash, G. B. (2012). Tissue stroma as a regulator of leukocyte recruitment in inflammation. *J Leukoc Biol*, *91*(3), 385-400. https://doi.org/10.1189/jlb.0911458

McGettrick, H. M., Smith, E., Filer, A., Kissane, S., Salmon, M., Buckley, C. D., Rainger, G. E., & Nash, G. B. (2009). Fibroblasts from different sites may promote or inhibit recruitment of flowing lymphocytes by endothelial cells. *Eur J Immunol*, *39*(1), 113-125. https://doi.org/10.1002/eji.200838232

Megan A. Cooper, T. A. F. a. M. A. C. (2001). The biology of human natural killer-cell subsets.

Merle, N. S., Church, S. E., Fremeaux-Bacchi, V., & Roumenina, L. T. (2015). Complement System Part I - Molecular Mechanisms of Activation and Regulation. *Front Immunol*, *6*, 262. https://doi.org/10.3389/fimmu.2015.00262

Mhaidly, R., & Mechta-Grigoriou, F. (2020). Fibroblast heterogeneity in tumor micro-environment: Role in immunosuppression and new therapies. *Semin Immunol*, *48*, 101417. https://doi.org/10.1016/j.smim.2020.101417

Mirna Balsamo, F. S., Gabriella Pietra, Claudia Manzini, Claudia Cantoni, Monica Boitano, Paola Queirolo, William Vermi, Fabio Facchetti, Alessandro Moretta, Lorenzo Moretta, Maria Cristina Mingari, and Massimo Vitale. (2009). Melanoma-associated fibroblasts modulate NK cell phenotype and antitumor cytotoxicity. *PNAS*.

Morimoto, C., & Schlossman, S. F. (1998). The structure and function of CD26 in the T-cell immune response. *Immunol Rev*, *161*, 55-70. https://doi.org/10.1111/j.1600-065x.1998.tb01571.x

Mota Reyes, C., Demir, E., Cifcibasi, K., Istvanffy, R., Friess, H., & Demir, I. E. (2022). Regulatory T Cells in Pancreatic Cancer: Of Mice and Men. *Cancers (Basel)*, *14*(19). https://doi.org/10.3390/cancers14194582

Moustakas, A., Lohr, J. M., & Heuchel, R. L. (2022). Cellular heterogeneity in pancreatic cancer: the different faces of gremlin action. *Signal Transduct Target Ther*, *7*(1), 364. https://doi.org/10.1038/s41392-022-01203-8

Munir, H., Rainger, G. E., Nash, G. B., & McGettrick, H. (2015). Analyzing the effects of stromal cells on the recruitment of leukocytes from flow. *J Vis Exp*(95), e52480. https://doi.org/10.3791/52480

Murray, E. R., Menezes, S., Henry, J. C., Williams, J. L., Alba-Castellon, L., Baskaran, P., Quetier, I., Desai, A., Marshall, J. J. T., Rosewell, I., Tatari, M., Rajeeve, V., Khan, F., Wang, J., Kotantaki, P., Tyler, E. J., Singh, N., Reader, C. S., Carter, E. P., . . . Cameron, A. J. M. (2022). Disruption of pancreatic stellate cell myofibroblast phenotype promotes pancreatic tumor invasion. *Cell Rep*, *38*(4), 110227. https://doi.org/10.1016/j.celrep.2021.110227

Nielsen, B. R., Ratzer, R., Bornsen, L., von Essen, M. R., Christensen, J. R., & Sellebjerg, F. (2017). Characterization of naive, memory and effector T cells in progressive multiple sclerosis. *J Neuroimmunol*, *310*, 17-25. https://doi.org/10.1016/j.jneuroim.2017.06.001

Noda, S., Hosoya, T., Komiya, Y., Tagawa, Y., Endo, K., Komori, K., Koga, H., Takahara, Y., Sugimoto, K., Sekiya, I., Saito, T., Mizoguchi, F., & Yasuda, S. (2022). CD34(+)THY1(+) synovial fibroblast subset in arthritic joints has high osteoblastic and chondrogenic potentials in vitro. *Arthritis Res Ther*, *24*(1), 45. https://doi.org/10.1186/s13075-022-02736-7

Noda, Y., Tomita, H., Ishihara, T., Tsuboi, Y., Kawai, N., Kawaguchi, M., Kaga, T., Hyodo, F., Hara, A., Kambadakone, A. R., & Matsuo, M. (2022). Prediction of overall survival in patients with pancreatic ductal adenocarcinoma: histogram analysis of ADC value and correlation with pathological intratumoral necrosis. *BMC Medical Imaging*, *22*(1). https://doi.org/10.1186/s12880-022-00751-3

Noor L. et al. (2017). Pancreatic ductal adenocarcinoma epidemiology and risk

assessment: Could we prevent? Possibility for an early diagnosis. https://www.ncbi.nlm.nih.gov/pmc/articles/PMC5774073/

Öhlund, D., Elyada, E., & Tuveson, D. (2014). Fibroblast heterogeneity in the cancer wound. *Journal of Experimental Medicine*, *211*(8), 1503-1523. https://doi.org/10.1084/jem.20140692

Ohlund, D., Handly-Santana, A., Biffi, G., Elyada, E., Almeida, A. S., Ponz-Sarvise, M., Corbo, V., Oni, T. E., Hearn, S. A., Lee, E. J., Chio, II, Hwang, C. I., Tiriac, H., Baker, L. A., Engle, D. D., Feig, C., Kultti, A., Egeblad, M., Fearon, D. T., . . . Tuveson, D. A. (2017). Distinct populations of inflammatory fibroblasts and myofibroblasts in pancreatic cancer. *J Exp Med*, *214*(3), 579-596. https://doi.org/10.1084/jem.20162024

Orth, M., Metzger, P., Gerum, S., Mayerle, J., Schneider, G., Belka, C., Schnurr, M., & Lauber, K. (2019). Pancreatic ductal adenocarcinoma: biological hallmarks, current status, and future perspectives of combined modality treatment approaches. *Radiation Oncology*, *14*(1). https://doi.org/10.1186/s13014-019-1345-6

Ozdemir, B. C., Pentcheva-Hoang, T., Carstens, J. L., Zheng, X., Wu, C. C., Simpson, T. R., Laklai, H., Sugimoto, H., Kahlert, C., Novitskiy, S. V., De Jesus-Acosta, A., Sharma, P., Heidari, P., Mahmood, U., Chin, L., Moses, H. L., Weaver, V. M., Maitra, A., Allison, J. P., . . . Kalluri, R. (2014). Depletion of carcinoma-associated fibroblasts and fibrosis induces immunosuppression and accelerates pancreas cancer with reduced survival. *Cancer Cell*, *25*(6), 719-734. https://doi.org/10.1016/j.ccr.2014.04.005

P. HILLYER, E. M., G. FLYNN & D. MALE (2003). Chemokines, chemokine receptors and adhesion molecules on different human endothelia: discriminating the tissue-specific functions that affect leucocyte migration. https://doi.org/10.1046/j.1365-2249.2003.02323.x

Pandol., S. J. (2010). *The Exocrine Pancreas*. https://www.ncbi.nlm.nih.gov/books/NBK54128/

Pasanen, I., Lehtonen, S., Sormunen, R., Skarp, S., Lehtilahti, E., Pietila, M., Sequeiros, R. B., Lehenkari, P., & Kuvaja, P. (2016). Breast cancer carcinoma-associated fibroblasts differ from breast fibroblasts in immunological and extracellular matrix regulating pathways. *Exp Cell Res*, *344*(1), 53-66. https://doi.org/10.1016/j.yexcr.2016.04.016

Passanha, F. R., Divinagracia, M. L., & LaPointe, V. L. S. (2022). Cadherin-11 Regulates Cell Proliferation via the PDGFRbeta-ERK1/2 Signaling Pathway in Human Mesenchymal Stem Cells. *Stem Cells*, *40*(2), 165-174. https://doi.org/10.1093/stmcls/sxab019

Pelon, F., Bourachot, B., Kieffer, Y., Magagna, I., Mermet-Meillon, F., Bonnet, I., Costa, A., Givel, A. M., Attieh, Y., Barbazan, J., Bonneau, C., Fuhrmann, L., Descroix, S., Vignjevic, D., Silberzan, P., Parrini, M. C., Vincent-Salomon, A., & Mechta-Grigoriou, F. (2020). Cancer-associated fibroblast heterogeneity in axillary lymph nodes drives metastases in breast cancer through complementary mechanisms. *Nat Commun*, *11*(1), 404. https://doi.org/10.1038/s41467-019-14134-w

Pereira, B. I., Devine, O. P., Vukmanovic-Stejic, M., Chambers, E. S., Subramanian, P., Patel, N., Virasami, A., Sebire, N. J., Kinsler, V., Valdovinos, A., LeSaux, C. J., Passos, J. F., Antoniou, A., Rustin, M. H. A., Campisi, J., & Akbar, A. N. (2019). Senescent cells evade immune clearance via HLA-E-mediated NK and

CD8(+) T cell inhibition. *Nat Commun*, *10*(1), 2387. https://doi.org/10.1038/s41467-019-10335-5

Ping, Q., Yan, R., Cheng, X., Wang, W., Zhong, Y., Hou, Z., Shi, Y., Wang, C., & Li, R. (2021). Cancer-associated fibroblasts: overview, progress, challenges, and directions. *Cancer Gene Therapy*, *28*(9), 984-999. https://doi.org/10.1038/s41417-021-00318-4

Plikus, M. V., Wang, X., Sinha, S., Forte, E., Thompson, S. M., Herzog, E. L., Driskell, R. R., Rosenthal, N., Biernaskie, J., & Horsley, V. (2021). Fibroblasts: Origins, definitions, and functions in health and disease. *Cell*, *184*(15), 3852-3872. https://doi.org/10.1016/j.cell.2021.06.024

Principe, D. R., Park, A., Dorman, M. J., Kumar, S., Viswakarma, N., Rubin, J., Torres, C., McKinney, R., Munshi, H. G., Grippo, P. J., & Rana, A. (2019). TGFbeta Blockade Augments PD-1 Inhibition to Promote T-Cell-Mediated Regression of Pancreatic Cancer. *Mol Cancer Ther*, *18*(3), 613-620. https://doi.org/10.1158/1535-7163.MCT-18-0850

Quah, B. J., & Parish, C. R. (2010). The use of carboxyfluorescein diacetate succinimidyl ester (CFSE) to monitor lymphocyte proliferation. *J Vis Exp*(44). https://doi.org/10.3791/2259

Radu, P., Zurzu, M., Paic, V., Bratucu, M., Garofil, D., Tigora, A., Georgescu, V., Prunoiu, V., Pasnicu, C., Popa, F., Surlin, P., Surlin, V., & Strambu, V. (2023). CD34-Structure, Functions and Relationship with Cancer Stem Cells. *Medicina (Kaunas)*, *59*(5). https://doi.org/10.3390/medicina59050938

Rawla, P., Sunkara, T., & Gaduputi, V. (2019). Epidemiology of Pancreatic Cancer: Global Trends, Etiology and Risk Factors. *World Journal of Oncology*, *10*(1), 10-27. https://doi.org/10.14740/wjon1166

Rege, T. A., & Hagood, J. S. (2006). Thy-1 as a regulator of cell-cell and cell-matrix interactions in axon regeneration, apoptosis, adhesion, migration, cancer, and fibrosis. *FASEB J*, *20*(8), 1045-1054. https://doi.org/10.1096/fj.05-5460rev

Ren, B., Cui, M., Yang, G., Wang, H., Feng, M., You, L., & Zhao, Y. (2018). Tumor microenvironment participates in metastasis of pancreatic cancer. *Mol Cancer*, *17*(1), 108. https://doi.org/10.1186/s12943-018-0858-1

Rockey, D. C., Weymouth, N., & Shi, Z. (2013). Smooth muscle alpha actin (Acta2) and myofibroblast function during hepatic wound healing. *PLoS One*, *8*(10), e77166. https://doi.org/10.1371/journal.pone.0077166

Rubin, S. J. S., Sojwal, R. S., Gubatan, J., & Rogalla, S. (2022). The Tumor Immune Microenvironment in Pancreatic Ductal Adenocarcinoma: Neither Hot nor Cold. *Cancers (Basel)*, *14*(17). https://doi.org/10.3390/cancers14174236

Sahai, E., Astsaturov, I., Cukierman, E., DeNardo, D. G., Egeblad, M., Evans, R. M., Fearon, D., Greten, F. R., Hingorani, S. R., Hunter, T., Hynes, R. O., Jain, R. K., Janowitz, T., Jorgensen, C., Kimmelman, A. C., Kolonin, M. G., Maki, R. G., Powers, R. S., Pure, E., . . . Werb, Z. (2020). A framework for advancing our understanding of cancer-associated fibroblasts. *Nat Rev Cancer*, *20*(3), 174-186. https://doi.org/10.1038/s41568-019-0238-1

Sahai, E., Astsaturov, I., Cukierman, E., Denardo, D. G., Egeblad, M., Evans, R. M., Fearon, D., Greten, F. R., Hingorani, S. R., Hunter, T., Hynes, R. O., Jain, R. K., Janowitz, T., Jorgensen, C., Kimmelman, A. C., Kolonin, M. G., Maki, R. G., Powers, R. S., Puré, E., . . . Werb, Z. (2020). A framework for advancing our understanding of cancer-associated fibroblasts. *Nature Reviews Cancer*, *20*(3), 174-186. https://doi.org/10.1038/s41568-019-0238-1

Salmon, H., Franciszkiewicz, K., Damotte, D., Dieu-Nosjean, M. C., Validire, P., Trautmann, A., Mami-Chouaib, F., & Donnadieu, E. (2012). Matrix architecture defines the preferential localization and migration of T cells into the stroma of human lung tumors. *J Clin Invest*, *122*(3), 899-910. https://doi.org/10.1172/JCI45817

Sarantis, P., Koustas, E., Papadimitropoulou, A., Papavassiliou, A. G., & Karamouzis, M. V. (2020). Pancreatic ductal adenocarcinoma: Treatment hurdles, tumor microenvironment and immunotherapy. *World Journal of Gastrointestinal Oncology*, *12*(2), 173-181. https://doi.org/10.4251/wjgo.v12.i2.173

Schroder, B. (2016). The multifaceted roles of the invariant chain CD74--More than just a chaperone. *Biochim Biophys Acta*, *1863*(6 Pt A), 1269-1281. https://doi.org/10.1016/j.bbamcr.2016.03.026

Schwarz, N. (2010). *Requirements for leukocyte transendothelial migration via the transmembrane chemokines CX3CL1 and CXCL16*

Shibuya, K. C., Goel, V. K., Xiong, W., Sham, J. G., Pollack, S. M., Leahy, A. M., Whiting, S. H., Yeh, M. M., Yee, C., Riddell, S. R., & Pillarisetty, V. G. (2014). Pancreatic ductal adenocarcinoma contains an effector and regulatory immune cell infiltrate that is altered by multimodal neoadjuvant treatment. *PLoS One*, *9*(5), e96565. https://doi.org/10.1371/journal.pone.0096565

Shiga, K., Hara, M., Nagasaki, T., Sato, T., Takahashi, H., & Takeyama, H. (2015). Cancer-Associated Fibroblasts: Their Characteristics and Their Roles in Tumor Growth. *Cancers (Basel)*, *7*(4), 2443-2458. https://doi.org/10.3390/cancers7040902

Shook, B. A., Wasko, R. R., Rivera-Gonzalez, G. C., Salazar-Gatzimas, E., Lopez-Giraldez, F., Dash, B. C., Munoz-Rojas, A. R., Aultman, K. D., Zwick, R. K., Lei, V., Arbiser, J. L., Miller-Jensen, K., Clark, D. A., Hsia, H. C., & Horsley, V. (2018). Myofibroblast proliferation and heterogeneity are supported by macrophages during skin repair. *Science*, *362*(6417). https://doi.org/10.1126/science.aar2971

Shu, C., Zha, H., Long, H., Wang, X., Yang, F., Gao, J., Hu, C., Zhou, L., Guo, B., & Zhu, B. (2020). C3a-C3aR signaling promotes breast cancer lung metastasis via modulating carcinoma associated fibroblasts. *J Exp Clin Cancer Res*, *39*(1), 11. https://doi.org/10.1186/s13046-019-1515-2

Simmons, P. J., & Torok-Storb, B. (1991). CD34 expression by stromal precursors in normal human adult bone marrow. *Blood*, *78*(11), 2848-2853. https://doi.org/10.1182/blood.V78.11.2848.2848

Singh, N., Baby, D., Rajguru, J. P., Patil, P. B., Thakkannavar, S. S., & Pujari, V. B. (2019). Inflammation and cancer. *Ann Afr Med*, *18*(3), 121-126. https://doi.org/10.4103/aam.aam_56_18

Springer, T. A. (1994). Traffic Signals for Lymphocyte Recirculation and Leukocyte Emigration: The Multistep Paradigm. *Cell*. https://doi.org/https://doi.org/10.1016/0092-8674(94)90337-9

Sun, H., Zhang, B., & Li, H. (2020). The Roles of Frequently Mutated Genes of Pancreatic Cancer in Regulation of Tumor Microenvironment. *Technol Cancer Res Treat*, *19*, 1533033820920969. https://doi.org/10.1177/1533033820920969

Takahashi, H., Sakakura, K., Kawabata-Iwakawa, R., Rokudai, S., Toyoda, M., Nishiyama, M., & Chikamatsu, K. (2015). Immunosuppressive activity of cancer-associated fibroblasts in head and neck squamous cell carcinoma. *Cancer Immunol Immunother*, *64*(11), 1407-1417. https://doi.org/10.1007/s00262-015-1742-0

Takako Sasaki, H. W., Monika Matzner, Mon-Li Chu, Rupert Timpl. (1996). Expression of fibulin-2 by fibroblasts and deposition with fibronectin into a fibrillar matrix. *Journal of Cell Science*

Thomas Kolodecik, C. S., Munish Ashat, and Edwin C. Thrower. (2014). Risk factors for pancreatic cancer: underlying mechanisms and potential targets. *Front. Physiol.* https://doi.org/ https://doi.org/10.3389/fphys.2013.00415

Timperi, E., & Romano, E. (2023). Stromal circuits involving tumor-associated macrophages and cancer-associated fibroblasts. *Front Immunol*, *14*, 1194642. https://doi.org/10.3389/fimmu.2023.1194642

Togarrati, P. P., Dinglasan, N., Desai, S., Ryan, W. R., & Muench, M. O. (2018). CD29 is highly expressed on epithelial, myoepithelial, and mesenchymal stromal cells of human salivary glands. *Oral Dis*, *24*(4), 561-572. https://doi.org/10.1111/odi.12812

Truffi, M., Sorrentino, L., Monieri, M., Fociani, P., Mazzucchelli, S., Bonzini, M., Zerbi, P., Sampietro, G. M., Di Sabatino, A., & Corsi, F. (2018). Inhibition of Fibroblast Activation Protein Restores a Balanced Extracellular Matrix and Reduces Fibrosis in Crohn's Disease Strictures Ex Vivo. *Inflamm Bowel Dis*, *24*(2), 332-345. https://doi.org/10.1093/ibd/izx008

Ushio, J., Kanno, A., Ikeda, E., Ando, K., Nagai, H., Miwata, T., Kawasaki, Y., Tada, Y., Yokoyama, K., Numao, N., Tamada, K., Lefor, A. K., & Yamamoto, H. (2021). Pancreatic Ductal Adenocarcinoma: Epidemiology and Risk Factors. *Diagnostics*, *11*(3), 562. https://doi.org/10.3390/diagnostics11030562

Vaish, U., Jain, T., Are, A. C., & Dudeja, V. (2021). Cancer-Associated Fibroblasts in Pancreatic Ductal Adenocarcinoma: An Update on Heterogeneity and Therapeutic Targeting. *Int J Mol Sci*, *22*(24). https://doi.org/10.3390/ijms222413408

Vancheri, C., Mastruzzo, C., Trovato-Salinaro, E., Gili, E., Lo Furno, D., Pistorio, M. P., Caruso, M., La Rosa, C., Crimi, C., Failla, M., & Crimi, N. (2005). Interaction between human lung fibroblasts and T-lymphocytes prevents activation of CD4+ cells. *Respir Res*, *6*(1), 103. https://doi.org/10.1186/1465-9921-6-103

Veenstra, V., Garcia-Garijo, A., Van Laarhoven, H., & Bijlsma, M. (2018). Extracellular Influences: Molecular Subclasses and the Microenvironment in Pancreatic Cancer. *Cancers*, *10*(2), 34. https://doi.org/10.3390/cancers10020034

Venning et al. (2021). Deciphering the temporal heterogeneity of cancer-associated fibroblast subpopulations in breast cancer. *Journal of Experimental & clinical cancer research*. https://doi.org/10.1186/s13046-021-01944-4

Vivier, E., Tomasello, E., Baratin, M., Walzer, T., & Ugolini, S. (2008). Functions of natural killer cells. *Nat Immunol*, *9*(5), 503-510. https://doi.org/10.1038/ni1582

Wang, S., Zheng, Y., Yang, F., Zhu, L., Zhu, X. Q., Wang, Z. F., Wu, X. L., Zhou, C. H., Yan, J. Y., Hu, B. Y., Kong, B., Fu, D. L., Bruns, C., Zhao, Y., Qin, L. X., & Dong, Q. Z. (2021). The molecular biology of pancreatic adenocarcinoma: translational challenges and clinical perspectives. *Signal Transduct Target Ther*, *6*(1), 249. https://doi.org/10.1038/s41392-021-00659-4

Wang, Y., Liang, Y., Xu, H., Zhang, X., Mao, T., Cui, J., Yao, J., Wang, Y., Jiao, F., Xiao, X., Hu, J., Xia, Q., Zhang, X., Wang, X., Sun, Y., Fu, D., Shen, L., Xu, X., Xue, J., & Wang, L. (2021). Single-cell analysis of pancreatic ductal adenocarcinoma identifies a novel fibroblast subtype associated with poor prognosis but better immunotherapy response. *Cell Discov*, *7*(1), 36. https://doi.org/10.1038/s41421-021-00271-4

Wang, Y. J., Schug, J., Won, K.-J., Liu, C., Naji, A., Avrahami, D., Golson, M. L., & Kaestner, K. H. (2016). Single-Cell Transcriptomics of the Human Endocrine Pancreas. *Diabetes*, *65*(10), 3028-3038. https://doi.org/10.2337/db16-0405

Wen, X., He, X., Jiao, F., Wang, C., Sun, Y., Ren, X., & Li, Q. (2017). Fibroblast Activation Protein-alpha-Positive Fibroblasts Promote Gastric Cancer Progression and Resistance to Immune Checkpoint Blockade. *Oncol Res*, *25*(4), 629-640. https://doi.org/10.3727/096504016X14768383625385

Wensveen, F. M., Jelencic, V., & Polic, B. (2018). NKG2D: A Master Regulator of Immune Cell Responsiveness. *Front Immunol*, *9*, 441. https://doi.org/10.3389/fimmu.2018.00441

Werba, G., Weissinger, D., Kawaler, E. A., Zhao, E., Kalfakakou, D., Dhara, S., Wang, L., Lim, H. B., Oh, G., Jing, X., Beri, N., Khanna, L., Gonda, T., Oberstein, P., Hajdu, C., Loomis, C., Heguy, A., Sherman, M. H., Lund, A. W., . . . Simeone, D. M. (2023). Single-cell RNA sequencing reveals the effects of chemotherapy on human pancreatic adenocarcinoma and its tumor microenvironment. *Nat Commun*, *14*(1), 797. https://doi.org/10.1038/s41467-023-36296-4

Westhoff, C. C., Jank, P., Jacke, C. O., Albert, U. S., Ebrahimsade, S., Barth, P. J., & Moll, R. (2020). Prognostic relevance of the loss of stromal CD34 positive fibroblasts in invasive lobular carcinoma of the breast. *Virchows Arch*, *477*(5), 717-724. https://doi.org/10.1007/s00428-020-02835-3

Worthen, C. A., Cui, Y., Orringer, J. S., Johnson, T. M., Voorhees, J. J., & Fisher, G. J. (2020). CD26 Identifies a Subpopulation of Fibroblasts that Produce the Majority of Collagen during Wound Healing in Human Skin. *J Invest Dermatol*, *140*(12), 2515-2524 e2513. https://doi.org/10.1016/j.jid.2020.04.010

Xu, S., Li, X., Tang, L., Liu, Z., Yang, K., & Cheng, Q. (2021). CD74 Correlated With Malignancies and Immune Microenvironment in Gliomas. *Front Mol Biosci*, *8*, 706949. https://doi.org/10.3389/fmolb.2021.706949

Yang, C., Cheng, H., Zhang, Y., Fan, K., Luo, G., Fan, Z., Huang, Q., Lu, Y., Jin, K., Wang, Z., Yu, X., & Liu, C. (2018). Anergic natural killer cells educated by tumor cells are associated with a poor prognosis in patients with advanced pancreatic ductal adenocarcinoma. *Cancer Immunol Immunother*, *67*(12), 1815-1823. https://doi.org/10.1007/s00262-018-2235-8

Yang, N., Lode, K., Berzaghi, R., Islam, A., Martinez-Zubiaurre, I., & Hellevik, T. (2020). Irradiated Tumor Fibroblasts Avoid Immune Recognition and Retain Immunosuppressive Functions Over Natural Killer Cells. *Front Immunol*, *11*, 602530. https://doi.org/10.3389/fimmu.2020.602530

Yanyan Han, D. L., Lianhong Li. (2020). PD-1/PD-L1 pathway: current researches in cancer. *Am J Cancer Res*. https://www.ncbi.nlm.nih.gov/pmc/articles/PMC7136921/

Yao, L., Rathnakar, B. H., Kwon, H. R., Sakashita, H., Kim, J. H., Rackley, A., Tomasek, J. J., Berry, W. L., & Olson, L. E. (2022). Temporal control of PDGFRalpha regulates the fibroblast-to-myofibroblast transition in wound healing. *Cell Rep*, *40*(7), 111192. https://doi.org/10.1016/j.celrep.2022.111192

Zeltz, C., Alam, J., Liu, H., Erusappan, P. M., Hoschuetzky, H., Molven, A., Parajuli, H., Cukierman, E., Costea, D. E., Lu, N., & Gullberg, D. (2019). alpha11beta1 Integrin is Induced in a Subset of Cancer-Associated Fibroblasts in Desmoplastic Tumor Stroma and Mediates In Vitro Cell Migration. *Cancers (Basel)*, *11*(6). https://doi.org/10.3390/cancers11060765

Zhang, H., Hui, D., & Fu, X. (2020). Roles of Fibulin-2 in Carcinogenesis. *Med Sci Monit*, *26*, e918099. https://doi.org/10.12659/MSM.918099

Zhang, R., Qi, F., Zhao, F., Li, G., Shao, S., Zhang, X., Yuan, L., & Feng, Y. (2019). Cancer-associated fibroblasts enhance tumor-associated macrophages enrichment and suppress NK cells function in colorectal cancer. *Cell Death Dis*, *10*(4), 273. https://doi.org/10.1038/s41419-019-1435-2

Zhang, T., Ren, Y., Yang, P., Wang, J., & Zhou, H. (2022). Cancer-associated fibroblasts in pancreatic ductal adenocarcinoma. *Cell Death Dis*, *13*(10), 897. https://doi.org/10.1038/s41419-022-05351-1

Zhang, X. (2017). PD-1 and its ligands are important immune checkpoints in cancer. *Oncotarget*. https://doi.org/10.18632/oncotarget.13895

Zhang, Y., Lazarus, J., Steele, N. G., Yan, W., Lee, H. J., Nwosu, Z. C., Halbrook, C. J., Menjivar, R. E., Kemp, S. B., Sirihorachai, V. R., Velez-Delgado, A., Donahue, K., Carpenter, E. S., Brown, K. L., Irizarry-Negron, V., Nevison, A. C., Vinta, A., Anderson, M. A., Crawford, H. C., . . . Pasca di Magliano, M. (2020). Regulatory T-cell Depletion Alters the Tumor Microenvironment and Accelerates Pancreatic Carcinogenesis. *Cancer Discov*, *10*(3), 422-439. https://doi.org/10.1158/2159-8290.CD-19-0958